TAMPEREEN TEKNILLINEN YLIOPISTO
TAMPERE UNIVERSITY OF TECHNOLOGY

Kati Valtonen

Relevance of Laboratory Wear Experiments for the Evaluation of In-Service Performance of Materials

Julkaisu 1587 • Publication 1587

Tampere 2018

Tampereen teknillinen yliopisto. Julkaisu 1587
Tampere University of Technology. Publication 1587

Kati Valtonen

Relevance of Laboratory Wear Experiments for the Evaluation of In-Service Performance of Materials

Thesis for the degree of Doctor of Science in Technology to be presented with due permission for public examination and criticism in Konetalo Building, Auditorium K1702, at Tampere University of Technology, on the 2nd of November 2018, at 12 noon.

Tampereen teknillinen yliopisto - Tampere University of Technology
Tampere 2018

Doctoral candidate: Kati Valtonen
Laboratory of Materials Science
Faculty of Engineering Sciences
Tampere University of Technology
Finland

Supervisor: Professor Veli-Tapani Kuokkala
Laboratory of Materials Science
Faculty of Engineering Sciences
Tampere University of Technology
Finland

Pre-examiners: Professor Mikael Olsson
Steel Forming and Surface Engineering
School of Technology and Business Studies
Dalarna University
Sweden

Dr Daniel Fabijanic
Institute for Frontier Materials
Deakin University
Australia

Opponents: Associate Professor Esa Vuorinen
Department of Engineering Sciences and Mathematics
Luleå University of Technology
Sweden

Dr Daniel Fabijanic
Institute for Frontier Materials
Deakin University
Australia

ISBN 978-952-15-4228-2 (printed)
ISBN 978-952-15-4244-2 (PDF)
ISSN 1459-2045

Abstract

In high-stress abrasion, rocks or minerals are being crushed between two moving bodies. In the mining industry, this kind of wear occurs for example in the haulage and grinding of minerals. Wear of materials causes also significant economic and ecological losses in the mining business, because the replacement of wear parts causes interruptions in the mining operations, and production of new wear parts creates a big carbon footprint for the mines. Therefore, the selection and development of better materials for the demanding wear environments is worth the effort.

Although the results of field wear tests are readily applicable for example for materials selection, such tests are challenging to conduct, overly expensive, and very time consuming. Thus, it is important to create substitutive application oriented wear test methods and research methodologies that produce relevant and repeatable results and are well controllable, unlike the in-service conditions. However, the relevance of the test method should also be somehow traceable and verifiable.

This thesis elucidates the relevance of laboratory wear experiments for the evaluation of the in-service performance of materials. Two cutting edges of underground mining loader buckets and two feed hopper wear plates were tested in the in-service conditions, and their wear rates were recorded using 3D scanning. Moreover, a used wear plate of a dumper truck body and a grooved roller from a hoist system were received for characterization. A novel method for testing impact wear of steels in Arctic conditions was also used and analyzed. The wear conditions in these in-service cases were simulated using various laboratory wear testing systems, the wear surfaces and cross-sections of the test specimens were carefully characterized, and the results of the wear tests and characterizations were correlated with the in-service cases.

There are two common ways to utilize laboratory wear tests, i.e., testing of different materials using the same test method or device, or testing the same material(s) using different test methods. In both cases, however, the fundamental question is, how do the test results compare with the real application under consideration? Another question that affects the outcome of the testing program is, how should the test results be presented to obtain the correct or best possible answer to the set research question? In this work, normalization of the test results using the mass loss of a reference sample proved to be a good methodology, when comparing the wear rates of different steels. Even the small differences between the different test cycles were corrected in this way. However, when different test methods are compared to each other or to the in-service data, the normalization should also take account of the differences in the contact time and the contact area in different cases. In addition to the numerical correlation, it is essential to characterize and compare the wear mechanisms and deformation of materials during wear. Only by combing these two different types of results, the relevance of the used test method can be assessed and confirmed.

Preface

This doctoral study was conducted at Tampere Wear Center, which is part of the Laboratory of Materials Science of Tampere University of Technology. The research was mainly done within the FIMECC DEMAPP – *Demanding applications* and DIMECC BSA – *Breakthrough steels and applications* programs and as part of the DIMECC *Breakthrough Materials Doctoral School*. I gratefully acknowledge the financial support from the Finnish Funding Agency for Innovation (Tekes) and the participating companies. Moreover, the Doctoral programme of the Faculty of Engineering Sciences at Tampere University of Technology is thanked for providing funding for the finalizing stage of the thesis.

I address my sincere gratitude to my supervisor Prof. Veli-Tapani Kuokkala for his smart comments, tireless corrections of the misused prepositions, and patient guidance throughout this study. Without his persistence and encouragement, this thesis would not exist. I am deeply grateful to my marvellous TWC team: Vilma Ratia, Vuokko Heino, Niko Ojala, Juuso Terva, Matti Lindroos, and Ville Oksanen. Your hard work laid the ground for this study and your example inspired me. Also the work of other co-authors Anu Kemppainen, Minnamari Vippola, Kimmo Keltamäki, Peter Andersson, Kenneth Holmberg, Antti Vaajoki, Anssi Laukkanen, Marian Apostol, and Karthik Ram Ramakrishnan is acknowledged; thank you for your collaboration and expertise. I am also thankful for the research assistants, who have assisted me during this study.

During the past 23 years at Tampere University of Technology, I have been privileged to work in the inspiring atmosphere created by my wonderful colleagues. Thank you for your support and company during these years. Without you, the working days and coffee breaks would not have been so enjoyable.

I am grateful to my family and friends for your tireless support and encouragement. Juha and Aino, thank you for being there for me ♥

Tampere, October 2018

Kati Valtonen

Contents

List of symbols and abbreviations

Δm	Mass loss
ΔV	Volume loss
φ	Cutting-to-plasticity ratio
ρ	Density
ψ	Angle between sample normal and normal of the diffracting plane
A	Area
A	Mineral composition, when determining equivalent quartz content
A5	Elongation at fracture with 50 mm sample
AsB	Angle selective back-scatter electron (detector for SEM)
ASB	Adiabatic shear band
CAI	Cerchar abrasivity index
CERCHAR	Test method by Centre d'Etudes et Recherches des Charbonages de France
CPOD	Crushing pin-on-disc
CEV	Carbon equivalent value
d	Lattice plane spacing
DBT	Ductile-to-brittle transition
LHD	Load-haul-dumper
EBSD	Electron backscatter diffraction
EDS	Energy dispersive X-ray spectrometer
EQu	Equivalent quartz content
FEG-SEM	Field emission gun scanning electron microscope
FWHM	Full width at half maximum
HVPI	High-velocity particle impactor
L_c	Parallel length of test pieces
LCPC	Test method by Laboratoires des Ponts et Chaussées
m	Mass
R	Rosiwal abrasiveness
R_m	Ultimate tensile strength
$R_{p0.2}$	Yield strength
RAI	Rock abrasivity index
RT	Room temperature
SEM	Scanning electron microscope
S_q	Root-mean-square height of the surface
S_{sk}	Skewness of the surface
SAW	Submerged arc welding
SE	Secondary electron (detector for SEM)

SEM	Scanning electron microscope
t	Time
UC	Uniaxial crusher
V	Volume
V_{neg}	Negative volume below the surface
V_{pos}	Positive volume above the surface
$WR_{mm/h}$	Wear rate, volume loss over area and time
$WR_{N\%}$	Wear rate, percentage normalization with reference
WR_{ND}	Wear rate, normalized directly with reference

Publications

I. Ratia, V., Valtonen, K., Kemppainen, A., Vippola, M., Kuokkala, V.-T., High-stress abrasion and impact-abrasion testing of wear resistant steels, *Tribology Online 8(2):152-161(2013).*

II. Valtonen, K., Ratia, V., Ojala, N., Kuokkala, V.-T., Comparison of laboratory wear test results with the in-service performance of cutting edges of loader buckets, *Wear 388–389:93-100(2017).*

III. Valtonen, K., Keltamäki, K., Kuokkala, V.-T., High-stress abrasion of wear resistant steels in the cutting edges of loader buckets, *Tribology International 119:707-720 (2018).*

IV. Valtonen, K., Ratia, V., Ramakrishnan, K. R., Apostol, M., Terva, J., Kuokkala, V.-T., Impact wear and mechanical behavior of steels in subzero conditions. *Tribology International 129:476-493(2019).*

V. Oksanen, V., Valtonen, K., Andersson, P., Vaajoki, A., Laukkanen, A., Holmberg, K., Kuokkala, V.-T., Comparison of laboratory rolling-sliding wear tests with in-service wear of nodular cast iron rollers against wire ropes, *Wear 340-341:73-81(2015).*

Author's contribution

In Publication I, Kati Valtonen was a co-author. Vilma Ratia was the main author, and the publication was also published as a part of her thesis [1]. As a supervisor to Vilma Ratia, Kati Valtonen took part in the planning of the experimental part of the work and commented the manuscript. Moreover, in this thesis manuscript, Kati Valtonen further analyzed the laboratory wear tested samples and compared them to an in-service case, i.e., a wear plate of a dumper body, which was not available at the time of the publication of this article.

In Publications II and III, Kati Valtonen was the main researcher and author. She planned the laboratory wear tests, conducted all characterization work, and made the comparison to the in-service cases. Kimmo Keltamäki from Lapland University of Applied Sciences was responsible for the field tests and ATOS scanning.

In Publication IV, Kati Valtonen was the main researcher and author. She took part in the planning of the tests and wrote most of the manuscript. She also conducted the electron microscopy characterization, and most of the optical microscopy characterization. The high-velocity particle impact tests were conducted and analyzed by Vilma Ratia, who participated also in the writing of the manuscript and commented it. The numerical modeling part was made by Karthik Ram Ramakrishnan.

In Publication V, Kati Valtonen was a co-author. Ville Oksanen was the main researcher and author. As his supervisor, Kati Valtonen took part in the planning of the characterization work and writing of the manuscript, especially in the comparison of the laboratory tests to the in-service case. Peter Andersson from VTT Technical Research Centre of Finland was responsible for the twin-disc tests.

Kati Valtonen was the main researcher behind the unpublished results presented in this thesis. She planned the laboratory wear tests, conducted all characterization work, the residual stress measurements, and made the comparison to the in-service cases. The scratch tests were conducted by Matti Lindroos. The feed hopper mine tests were conducted by Jukka Joutsenvaara and Heidi Kalliosalo from Lapland University of Applied Sciences.

In all publications and throughout the thesis work, Prof. Veli-Tapani Kuokkala gave indispensable help by commenting and correcting the manuscripts.

1 Introduction

Wear of materials is interesting, and it is extremely challenging to study such a complex phenomenon where everything affects everything. Especially in mining operations, there are numerous variables that affect the type, mechanisms, and progression of wear, including the processed minerals, their particle size and moving velocity, the contact mode between the minerals and the machinery, the loading energy, temperature, humidity, and so forth. There are, however, huge incentives for in-depth wear research, as the development of new wear resistant materials, as well as efficient and precise materials selection from existing materials for example for the mining environment, can save significant amounts of money and energy. The total energy consumption of global mining activities has been estimated to be over 6% of the total global energy consumption, and the energy spent to overcome friction and to manufacture and replace worn out parts is known to cause over 200 000 M€ costs annually [2].

There are numerous standardized wear tests, and even many more ad-hoc non-standardized laboratory wear tests, in common use. However, the evaluation of the relevance of the laboratory wear experiments for the determination of the in-service performance of materials is largely lacking, especially in the high-stress abrasion and impact wear conditions [3,4]. On the other hand, the simulation of the in-service wear environments in the laboratory-scale is very challenging, even when the actual conditions are known, as a plethora of variables affecting the active wear mechanism(s) and the resulting wear rate must be properly taken into consideration.

Fig. 1.1 visualizes some of the challenges encountered when trying to scale up the results of simple sliding wear tests to the selection of materials for a full-size jaw crusher. If the full-scale field tests are carefully planned and successfully implemented, they give results that are directly utilizable for the in-service use. However, for example in the case of a jaw crusher, it is practically impossible to perform two identical field tests, because inevitably the crushable material and the operational and environmental conditions change. Moreover, it is very expensive to produce full-scale jaws just for testing. In a pilot test plant, it is possible to follow and record the test conditions, but the complex environment is still a challenge; the testing is laborious and expensive, and the wear test may fail due to the failure of some other machine part. Thus, the pilot test plant is a good environment for material testing, when the preselection of materials has been made for example using a miniature test crusher or a small laboratory scale crusher. In the laboratory, it is possible to control the test environment and produce repeatable results with reasonable time and cost. The control of the tests increases, the simpler the test is. However, the applied loads are usually lower than in the in-service use, and there may also be differences in the wear mechanisms. All things considered, the

laboratory-scale wear tests are an important step in the material selection. Nevertheless, it is essential to have a good knowledge on the prevailing wear environment is the in-service conditions, which is then utilized in the planning of the best possible approach for the wear tests.

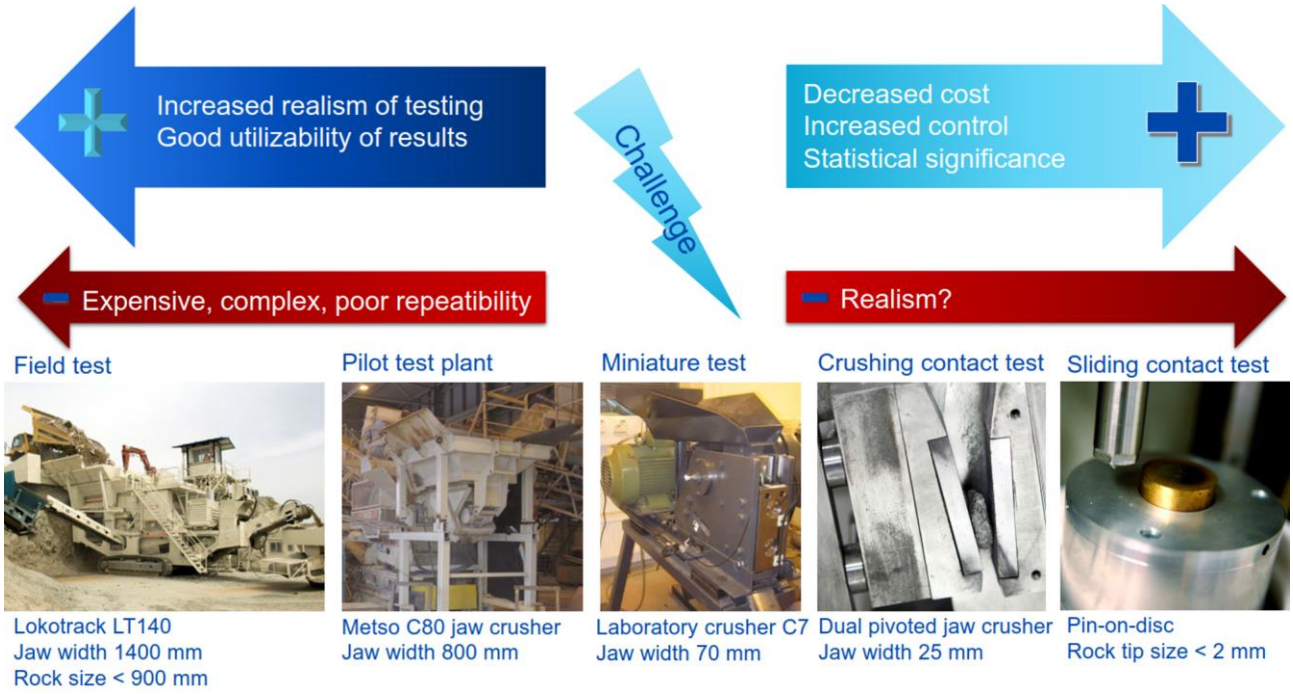

Figure 1.1. Challenges in the scaling of wear tests.

1.1 Background

The materials selection based on laboratory tests needs test methods that simulate the in-service conditions as closely as possible. On the other hand, analysis of the relevance of the laboratory test methods is needed. In this thesis, the wear behavior in various in-service cases is simulated in the laboratory scale using several application oriented wear testing methods, such as the crushing pin-on-disc, the uniaxial crusher, the impeller-tumbler, and the high-speed slurry-pot with a dry abrasive bed. These test methods simulate the harsh high-stress abrasive or impact-abrasive conditions of mining and mineral processing. The wear behavior in the in-service cases is compared to that of the samples wear tested in the laboratory by analyzing the wear rates and by characterizing the wear surfaces and microstructures of the samples.

This thesis is based primarily on the laboratory wear tests and the development of wear testing methods made in the FIMECC DEMAPP – Demanding applications (2009-2014) and in the DIMECC BSA – Breakthrough steels and applications (2014-2017) programs. Both projects were conducted in close collaboration with the Finnish metals and engineering industry. In addition to this thesis, the results of the above-mentioned programs have already been reported in numerous scientific articles, including [2,5-25], which form the foundation for this study as presented in Fig. 1.2.

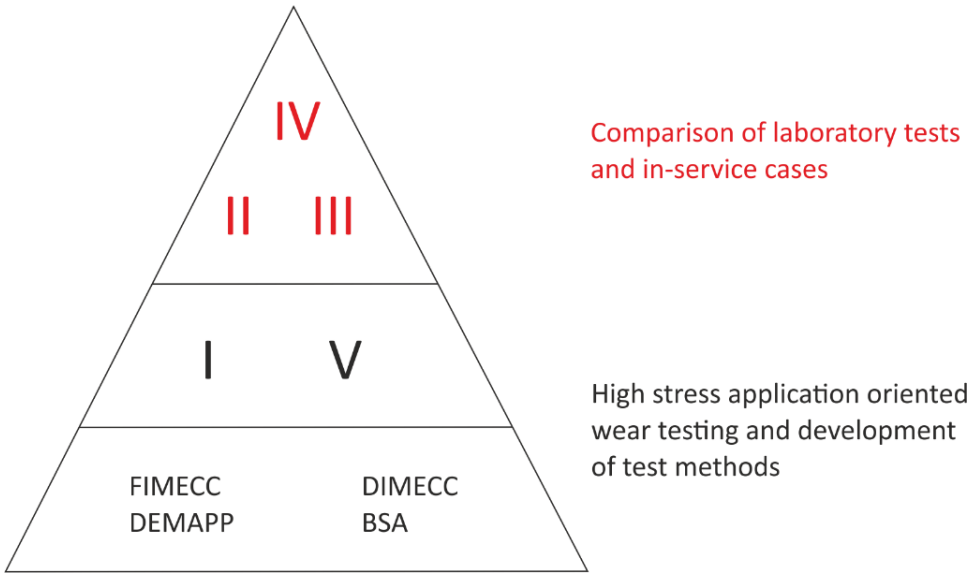

Figure 1.2. Structure of the thesis based on Publications I-V.

1.2 Objectives of the study

The primary motivation for this thesis is the above-mentioned gap between the in-service performance of wear resistant materials and the results and correct choice of laboratory wear experiments for each application. In short, the main target of this work is to obtain a better understanding of the relevance of the laboratory wear tests compared to the in-service performance of materials in high-stress wear conditions.

The three research questions of this thesis are as follows:

- What kind of effects the mechanical properties and the microstructure have on the wear behavior of martensitic wear resistant steels in various wear environments?
- What kind of laboratory wear test methods could be used and how the tests should be planned to assist the materials selection for the selected in-service case studies?
- What kind of research methodologies are best applicable for the evaluation of the relevance of the laboratory wear experiments relative to the in-service behavior and performance of wear resistant steels?

To answer these questions, this study uses a multiscale approach to laboratory wear testing, i.e., tests ranging from single well-defined micrometer scale scratches to tests that yield a more macroscopic and averaged response of materials to the applied wear conditions. Furthermore, the tests are compared to the in-service cases. In addition, laboratory wear experiments and new practices with better correspondence to the in-service cases are being developed especially for mining industry applications. The answers to the research questions, as well as the main scientific contributions of this work, will be presented in Chapter 8, *Concluding remarks*.

2 Wear of materials

Wear is defined in ASTM standard G40 [26] as “iteration of a solid surface by progressive loss or progressive displacement of material due to relative motion between that surface and a contacting substance or substances”. However, wear of materials is just one aspect of tribology, a science that concentrates on all kinds of interactions of surfaces in relative motion, including friction and lubrication. This chapter describes briefly the different categories of wear, and in particular the wear of steels in the abrasive and impact contacts.

The wear of materials may occur by various processes, and there are also many different ways to define and categorize the wear modes. Material can be removed from the surface of a solid body by fracturing, by dissolving it chemically, or by melting [27,28]. Thus, wear can be either a mechanical, chemical, or a thermal process. The actual wear modes and mechanisms causing wear overlap, and that is one of the reasons why there is no unambiguous way to define them. One of the most typical ways is to divide the wear modes into adhesive, abrasive, fatigue, and corrosive wear [27]. On the other hand, ASTM International uses a different approach, which categorizes wear to abrasive and non-abrasive modes, including sliding, rolling, and impact [28]. Erosion is dealt separately, because it involves also fluid or gas motion. Fig. 2.1 illustrates these categories, which are utilized also in this work.

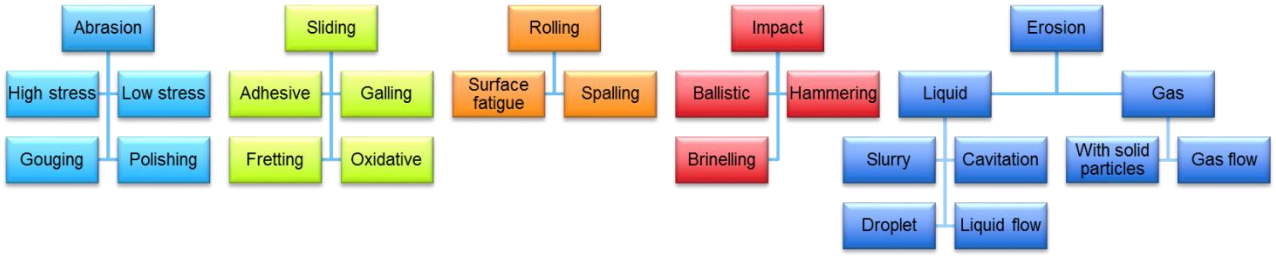

Figure 2.1. Major categories of wear (based on [28]).

2.1 Abrasion

Abrasion is the most common wear mode, where material is removed by moving hard particles or surface asperities. In high-stress abrasion, the stresses are high enough to break the abrasive particles. Sometimes the extreme case of high-stress abrasion is called gouging abrasion. In gouging

abrasion, large and hard particles are grooving the surfaces, such as in rock crushing [29]. The low stress abrasion is more common in mineral handling and agricultural systems [28].

It is also common to divide abrasion into two-body or three-body abrasion [30,31]. In two-body abrasion, the abrading particles are attached to a rigid body, such as an abrasive paper. When two solid parts are moving with loose abrasive particles in the contact with them, it is then called three-body abrasion. The particles in the three-body abrasion are able to roll or slide, and therefore it is not so aggressive mechanism as two-body abrasion [30]. However, it should be noticed that these definitions are not standardized and sometimes misinterpreted or mixed with high-stress and low-stress abrasion. For example, the excavation of rock piles and embedment of abrasives into a softer counterbody are somewhat controversial cases [32].

The wear mechanism defines how material is removed from the surface. Fig. 2.2 [31] enumerates the abrasion wear (micro) mechanisms, including cutting, fatigue by ploughing, fracture, and grain pull-out. In (micro) cutting, wear chips are formed, when the particle moves against the surface at a high attack angle. When the attack angle is low, the particle just ploughs the surface, which then becomes mainly plastically deformed. Only repeated ploughing starts to remove material from the surface by a mechanism, which is often also called micro fatigue. In brittle materials, the surface tends to fracture by the contact with sharp asperities. This may also happen in ductile materials, if the surface is sufficiently work hardened during wear [31]. In hard metals or metal matrix composites with hard carbides, single grains may pull-out during the contact with an abrasive particle, as illustrated in Fig. 2.2.d. This is more probable if the matrix material is already worn out and the particles are thus exposed to wear.

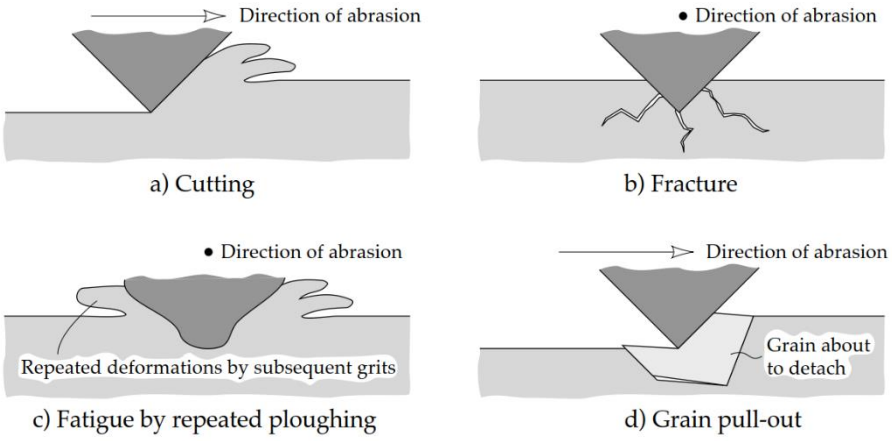

Figure 2.2. Abrasion wear mechanisms [31].

2.2 Impact wear

Impact wear is defined as wear by repetitive collisions of two bodies [26]. The main difference between erosion and impact wear is that in impact wear, the bodies tend to be large and the contact points somewhat defined, whereas in erosion, the eroding particles are small, move with gas or liquid flow, and interact randomly with the target surface. The actual wear mechanism in impact wear depends on the impact energy. At lower impact energies, the mechanism is usually adhesion

or abrasion, when ploughing deforms the material plastically. When the impact energies are higher, surface fatigue leads to cracking and delamination, or even to brittle failure [33].

When the impacting body is a (large) abrasive particle, the term “impact-abrasion” is generally used [34]. However, the term is not strictly defined, and thus impact-abrasion describes both high velocity impacts in ore-crushing hammer mills and lower velocity impacts in grinding mills [34]. Moreover, the abrasive material can be impacted between two solid bodies, or the abrasives can flow freely as in the impeller-tumbler tester, which was utilized also in the present study.

2.3 Wear of steels

Wear of steels in abrasion and impact wear is determined by their ability to deform plastically. Fig. 2.3 [22] illustrates plastic deformation in steels during an abrasive contact. The mechanical properties of the steel, including hardness, change in the wearing area. This effect is called work hardening or strain hardening, which is the result of the multiplication and mutual reactions of dislocations during the deformation process [35]. Wear can also affect the stress states in the surface layer of the material, which can lead to the initiation of cracks.

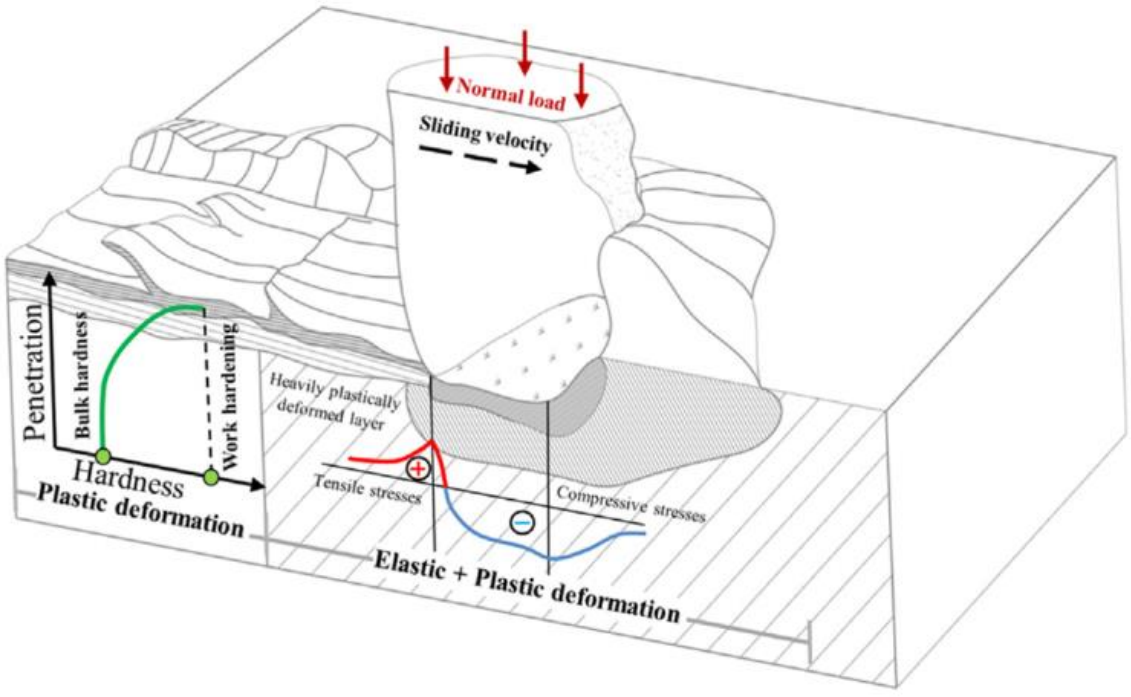

Figure 2.3. Plastic deformation of steel in high-stress abrasive wear [22].

In high-stress abrasive and impact wear, the material is subjected to heavy plastic deformation and relatively high strain rates. When a certain critical strain is exceeded, adiabatic shear bands (ASB) are formed in a thermomechanical process [36]. The high strain rates during the wear contact cause the rise of the surface temperature above the austenite formation temperature. The rapid cooling by the underlying bulk metal and simultaneous severe plastic deformation lead then to the formation of untempered martensite [37–39]. Typically ASBs have a very fine nanostructure and higher strength and hardness than the original bulk material [14]. This type of ASBs are also called

transformed bands or white layers, because they appear white (unetched), when studied with an optical microscope after etching for example with Nital [36,40]. Fig. 2.4 shows an example of the different appearance of transformed bands and deformed bands, the latter of which are seen as darker areas in the etched steel. The hardness of the transformed bands was up to 650 HV and about 420 HV for the deformed bands, when the bulk material hardness was about 350 HV, as reported Boakye-Yiadom and Bassim [40]. They also stated that due to high internal stresses, the transformed bands are also prone to cracking. Thus, the presence of the transformed bands in the microstructure increases the possibility to catastrophic failure during an impact.

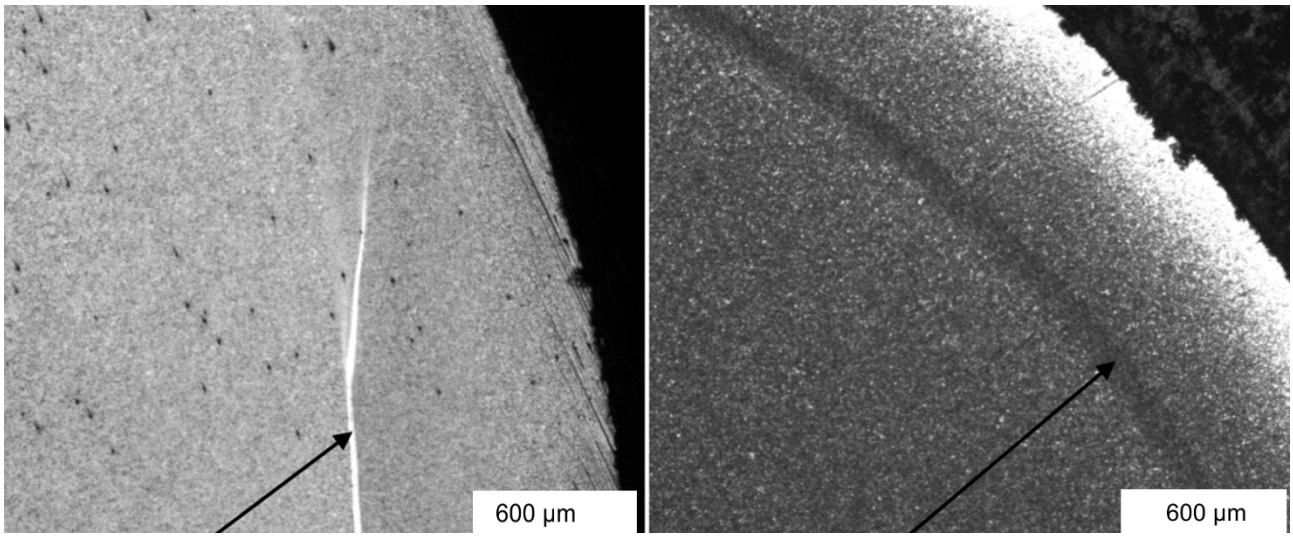

a) *b)*

Figure 2.4. Adiabatic shear bands in AISI 4340 steel samples after direct impact Hopkinson pressure bar tests, a) transformed band and b) deformed band indicated with arrows [40].

In order to clarify the influence of material properties on the formation of ASBs, Pursche and Mayer [41] made an extensive study on quenched and tempered steels. They stated that the temperature-softening characteristic of the steel is the most important material property related to the formation of adiabatic shear bands. Moreover, they showed a clear correlation between the hardness of the studied steels and ASB related failure, indicating that the high strength steels are more prone to form ASBs. A recent study by Lindroos, Laukkanen, and Kuokkala [42] proposed a crystal plasticity approach for the formation of shear bands in a 500 HB grade martensitic steel. They showed that the rolling texture has a marked effect on the formation of shear bands and the related shear softening.

3 Wear testing methods

This chapter presents some of the many methods that are used to simulate high-stress wear conditions for example in mining and tunneling operations. However, the methods used in this thesis are not included in this overview but will presented in Chapter 5.

In the *Standard Guide for Developing and Selecting Wear Tests* [43], ASTM International lists 33 standards related to wear and tribology testing. In addition, ASTM International has published a standard terminology list for wear and erosion [26]. Although the standards enumerate and explain a wide variety of methods, they contain only a limited number of standardized methods that produce high-stress abrasive wear conditions. In this chapter, ASTM G65, *Standard Test Method for Measuring Abrasion Using the Dry Sand/Rubber Wheel Apparatus* [44], ASTM G105 *Standard Test Method for Conducting Wet Sand/Rubber Wheel Abrasion Tests* [45], *Standard Test Method for Determining the High Stress Abrasion Resistance of Hard Materials* [46], and ASTM G81, *Standard Test Method for Jaw Crusher Gouging Abrasion Test* [47] will be discussed.

3.1 Rubber wheel abrasion testers

The rubber wheel abrasion tester with dry silica sand according to ASTM G65 standard [44] is probably the most commonly used wear test method in the world. Fig. 3.1.a illustrates the basic operation principle of the test, showing how a rectangular specimen is pressed with a constant normal force against a rotating rubber coated steel wheel. The rubber liner material is chlorobutyl rubber (Falex Corporation) with Durometer hardness A58-A62 [44]. A hopper feeds a continuous 300-400 g/min flow of silica sand with a nozzle, which is placed between the specimen and the wheel. The silica sand used in the test should be rounded beach quartz sand, AFS 50/70 Test Sand from Ottawa Silica Co. with 212-300 µm particle size [44]. The sand particles are not crushed in the test, and thus the rubber wheel abrasion tester is a low-stress wear testing method [48].

Although the rubber wheel abrasion tester is widely used to test scratching abrasive wear of metals and coatings, the relevance of the results to the in-service performance of materials is not clear. Moreover, its suitability to test novel hard steels or hardmetals is not optimal. The wear testing results may be even totally opposite when compared to the high-stress abrasion test methods, as reported for example by Konyashin and Ries [49] and Hyttel et al. [50]. Petrica et al. [51] concluded that if the load is increased in the testing of hard materials, also the breaking of sand particles increases markedly, which changes the wear mechanism. Budinski and Budinski [48] critized the low

abrasivity of the silica sand used in the test. Moreover, they highlighted the marked effect of rubber quality on the test results. Both the “standard sand” and “standard rubber” are available just from one supplier in the USA. Thus, the shipping costs of the sand outside North America and the acquisition costs of the wheel material can be quite high [48].

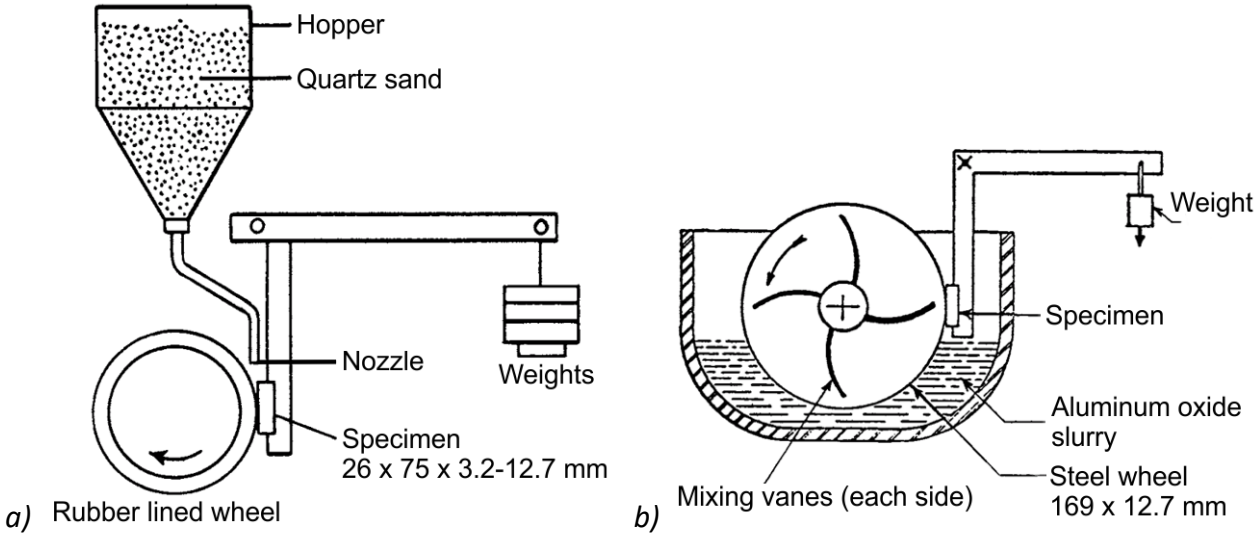

Figure 3.1. Schematics of a) the standardized rubber wheel abrasion tester [44] and b) the high-stress abrasion steel wheel tester [46].

The wet sand version of the rubber wheel abrasion tester is quite similar to the dry sand tester, but it contains also a slurry chamber [45]. The slurry consist of 1.5 kg quartz in 0.94 kg of deionized water. The rotating wheel with paddles rotates the slurry during the tests. The contact between the wheel and the sample is similar as in the dry wheel tester, but the wheel rotates in the opposite direction lifting the wet sand to the contact point. Three wheel materials with Durometer hardness of 50, 60, and 70 are recommended in the standard [45].

For high-stress abrasion testing of harder materials, especially for hard metals, a slurry testing system with a rotating steel wheel is also widely used. Fig. 3.1.b presents a schematic of the system [46] that uses slurry containing 30-mesh (595-707 µm) aluminum oxide mixed with water in the proportion of 4 g/1 cm^3. Konyashin and Ries [52] showed the importance of selecting the correct test method, when they compared the low-stress rubber wheel test with the steel wheel tests of WC-Co hard metals. In the rubber wheel test, wear was found to increase with decreasing amount of the binder phase and with increasing size of the carbides. However, in the steel wheel test, better wear resistance was gained with a low binder content and a large carbide size. In other words, the wear mechanisms in the hard metals turned out to be totally different in these two test methods, leading to quite opposite results.

3.2 Jaw crusher testers

ASTM G81, *Standard Test Method for Jaw Crusher Gouging Abrasion Test* [47], was designed to test the high-stress gouging abrasion resistance of materials. Fig. 3.2 presents the test system, which basically is a small-scale jaw crusher with a feed opening of 100 mm by 150 mm. The minimum jaw

opening during the crushing cycle is set to 3.2 mm. The sample and reference plates are positioned next to each other both in the stationary jaw frame and in the movable jaw frame so that they also oppose each other. A typical size of the samples is 230 mm x 83 mm x 19 mm. The suggested hardness for the reference plate is 269±8 HB, but also other steel grades, such as manganese steels, can be used as a reference. Up to 900 kg of pre-crushed and sieved 25-50 mm morainal rock is fed to the crusher in 225 kg cycles, between which the jaw opening is adjusted. The wear ratio is determined by averaging the mass or volume loss ratios of the stationary and movable jaws [47].

Sare and Constantine [53] criticized the inefficiency of the test procedure and the effect of the variability of the reference material on the determined wear ratio in ASTM G81 tests, especially if manganese steels are used as a reference. They suggested an alternative way to conduct the tests by circulating the positions of the materials in separate tests. According to Sare and Constantine [53], this procedure leads to better results when the gouging abrasive wear performance of several materials is compared. The method is cited also in the updated ASTM G81 standard [47].

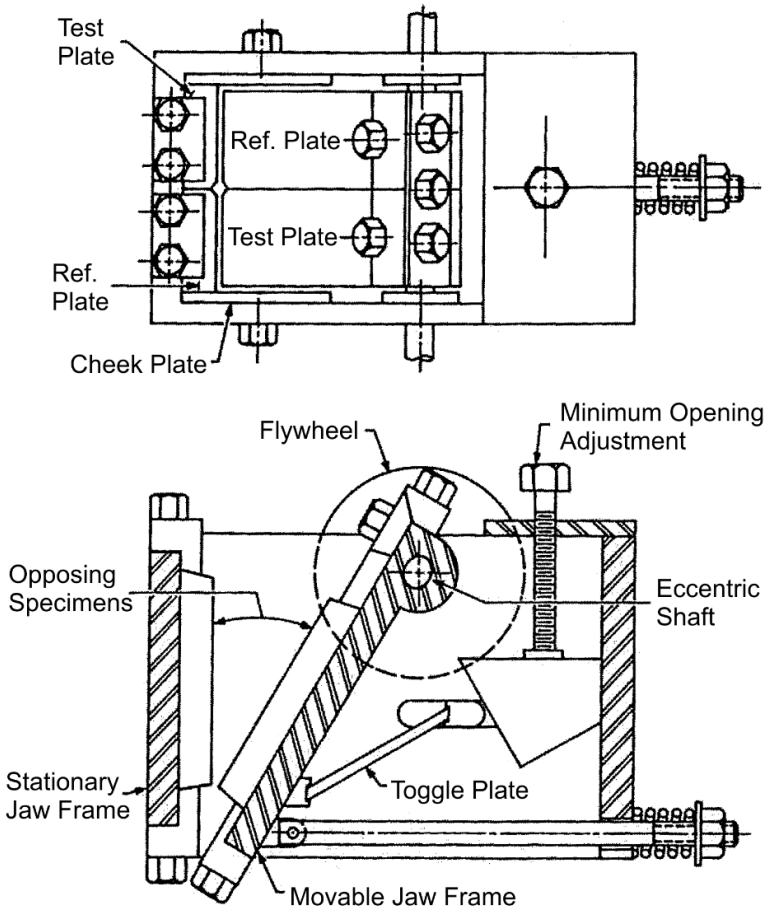

Figure 3.2. Schematic of the jaw crusher construction and the test plate layout for ASTM G81 tests [47].

In the ASTM G81 test, the large amount of rock and the consequently long test time limit its usability. Terva et al. [12] designed a dual pivoted jaw crusher that produces similar wear rates as the ASTM G81 standard system, when comparing the mass loss of the jaws to the amount of the fed gravel (g/kg). Fig. 3.3 shows the construction of the dual pivoted jaw crusher, which also enables monitoring of the crushing events by high-speed cameras when the side plate is made of a transparent polymer. The crushing process is also monitored by the two force sensors that can

record the crushing forces of individual crushing events. The fed abrasive is typically under 14 mm in size, and the rocks are fed one at a time with a vibrating bowl feeder. In one test cycle, the amount of rock is typically 4 kg. The number of needed cycles depends on the axle tilt angle and the tested material. The sample size is 75 mm x 25 mm x 10 mm [11].

The novelty of the dual pivoted jaw crusher is the possibility to control the compression-to-sliding ratio of the crushing event by selecting the tilt angle of the axles between 0° and 90° in 15° steps [11]. Moreover, it is possible to evaluate the effects of the compression and sliding components on the energy consumption during crushing [12].

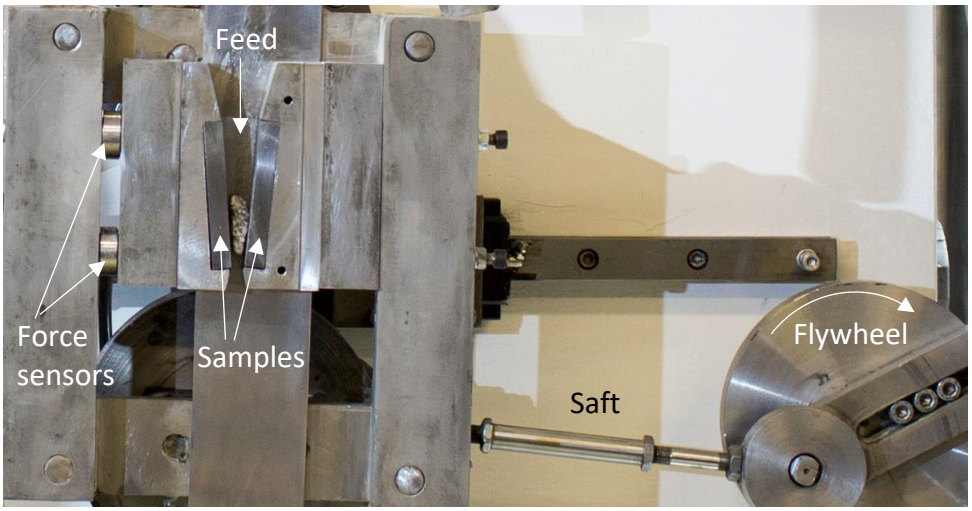

Figure 3.3. Crushing unit of the dual pivoted jaw crusher with the axle tilt angle in the 90° position.

3.3 Impact testers

There are various impact wear testers in common use, but in this chapter only some application oriented wear testing methods related to the mining industry are presented. In mines, the high-stress impact wear causes challenges especially in percussive drilling, in various crushing and grinding stages, and in haulage. Thus, in many cases impact wear is combined with abrasion [54].

The hammer-mill type wear tester [55] was developed to simulate high-stress impact wear in crushing and grinding applications. Fig. 3.4 illustrates the schematic of the system, where two rotating hammers are impacting against a plate specimen. There is also a possibility to feed abrasive material to the contact point. Consequently, the hammer-mill can produce both direct metal-to-metal impact contacts and more impact-abrasive type contacts. By changing the impact velocity from 5.1 to 9.0 m/s, the impact energy can be increased from 21.9 to 66.9 J. The specimen table can be tilted to a selected angle, and it can also be set to a constant x-y movement during the test.

The wear of the balls used in the grinding mills have been modeled, for example, using small laboratory scale ball mills [56,57] or by dropping in-service size grinding balls from a dropping tower [58,59]. Some test systems have also been developed for the evaluation of the impact wear in grinding mill liners [60,61]. In the laboratory scale ball mills, wear is mainly abrasive or impact-

abrasive, and as high energy impacts as in the in-service conditions are not produced [56,57]. On the other hand, with laboratory ball mills it is possible to test the effect of different abrasives or ores unlike with dropping tower tests.

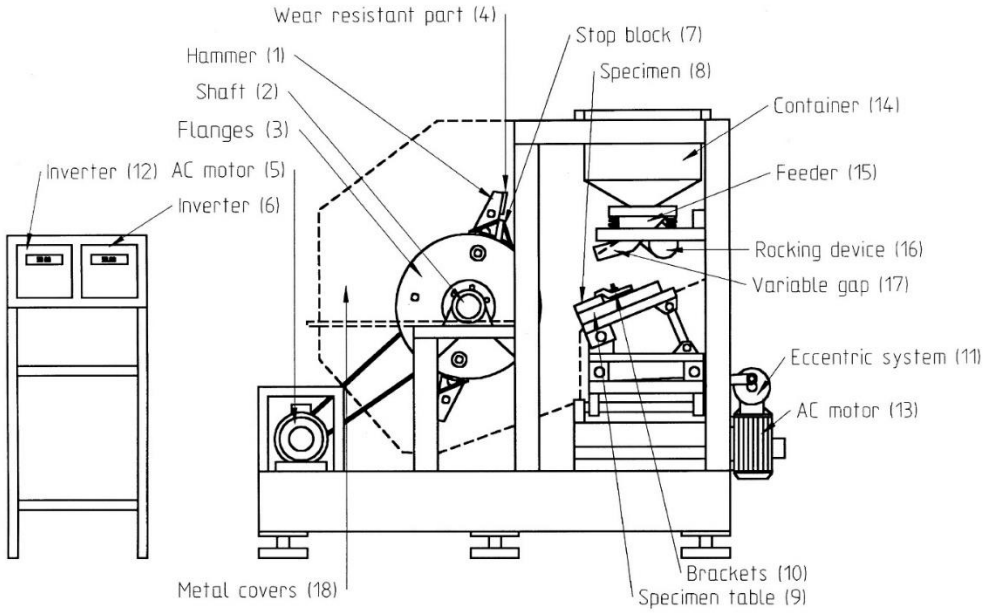

Figure 3.4. A hammer-mill type impact wear tester [55].

Blickensderfer and Tylczak [58,59] designed a 3.5 m tall dropping tower with a conveyer system. In a ball-on-ball dropping test, a 75 mm ball is dropped inside a tube directly on top of 18 balls in a curved tube. The dropping ball moves the balls inside the tube so that the last one of them moves back to the conveyer system. Thus, there is an about 54 J impact energy in the first metal-to-metal contact, but also lower energy contacts throughout the lined balls down to about 5 J. When the test was continued from 10 000 up to 300 000 impacts, surface cracking and spalling were observed randomly distributed on the surfaces of the balls [58,59]. A similar dropping tower was also used for ball-on-block tests, so that it served also as a liner material tester.

Impact testing devices with a cyclically impacting plunger have been used in several studies [10,62–65]. The used impact energy is usually much lower than in the above-mentioned systems, typically ranging from 0.5 J to 6 J. The test systems can be used with or without abrasive particles flowing freely through the contact point.

3.4 Slurry-erosion testers

The slurry transport systems are common in the mining and mineral processing industry for moving ores and tailings with added water [66]. The components in the slurry transport systems are typically subjected to erosion. However, the particle size, flow velocity, and attack angle have a marked effect on the wear behavior of the materials. For example, in slurry tube curves or pump blades, the impact angle is typically high, but in slurry tubes the angle is close to zero [66,67]. In the slurry environment, also the effect of corrosion must be taken into account.

Several different types of slurry erosion testers have been developed for example at the National Research Council Canada (NRC) [66]. However, in those systems, the slurry consists of fine sand particles. A high-speed slurry-pot [6,18] was developed at Tampere Wear Center for testing also larger, up to 10 mm particles, in a slurry. In this system, 2-8 samples are attached to a rotating shaft on four levels, as illustrated in Fig. 3.5. The speed at the sample tip can be adjusted from 1 m/s to 20 m/s. The sample size, shape, and angle are adjustable, which makes the system very versatile. In the present work, the high-speed slurry tester was used as an abrasive testing system with dry gravel, as described in Chapter 5.

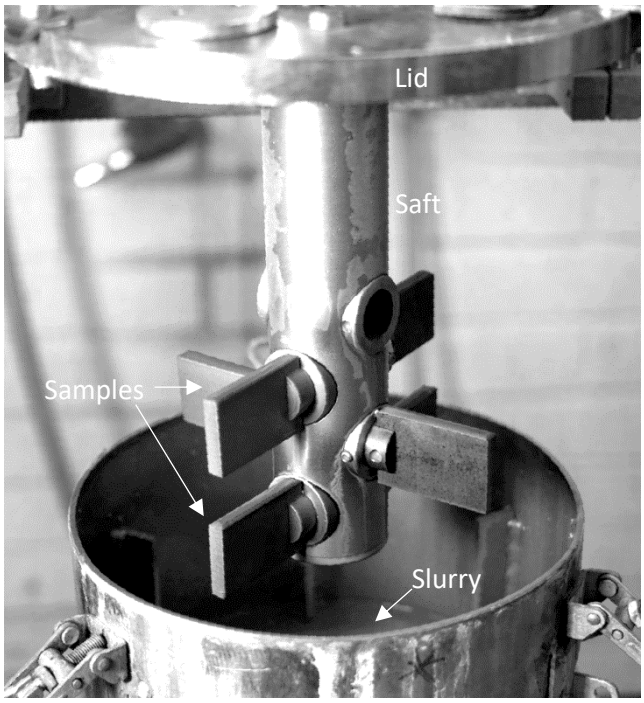

Figure 3.5. High-speed slurry-pot wear tester with 64 x 40 x 10 mm samples.

3.5 Abrasivity testers

The abrasivity of minerals describes their ability to cause abrasive wear. Abrasivity is an important factor especially in the mining and tunneling industries because of its significant impact on the wear rates of the wear parts. The abrasivity of minerals must also be taken into account in the planning of abrasive wear tests that use natural minerals. Pintaude and Bartalini [68] stated that the ASTM G81 jaw crusher method is well suited also for the abrasivity testing of minerals. However, the use of 900 kg of rock is not a very attractive and effective way to determine abrasivity. This chapter presents some of the most common methods used for the abrasivity determination [69].

3.5.1 LCPC

In the LCPC test (Laboratoires des Ponts et Chaussées, Paris) [70,71], the mass loss of a steel impeller, which rotates in a pot filled with gravel at 4500 rpm for 5 min, is measured (Fig. 3.6). The size of the impeller is 50 mm x 25 mm x 5 mm, and thus the speed in the impeller tip is about 11.8 m/s. The abrasiveness value is given as the mass loss of the steel impeller divided by the mass of

the mineral in the test, 500 g, multiplied by 1000. The mineral is sieved to the size of 4-6.3 mm before the test, and the sieving is repeated after the test to determine also the crushability of the mineral. The crushability is given as the percentage of the mass of gravel below 1.6 mm compared to the original mass, i.e., (500g-$m_{1.6}$)/500g*100. The steel impellers are typically made of low hardness 60-75 HRB structural steel [72]. The steel properties have a marked effect on the LCPC test results [72,73], which should be taken into account when comparing the results from different test series or test laboratories.

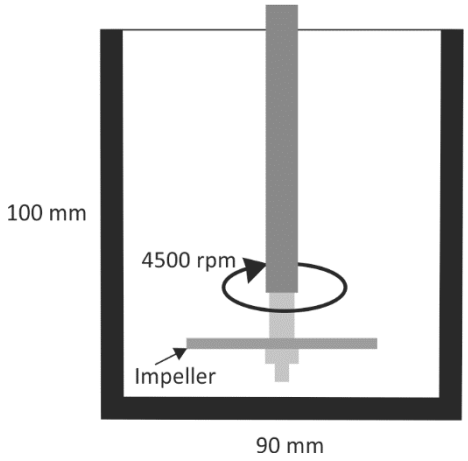

Figure 3.6. Schematic of the LCPC test system.

3.5.2 CERCHAR

ASTM D7625, *Standard Test Method for Laboratory Determination of Abrasiveness of Rock Using the CERCHAR Method* [74], is a commonly used method for the determination of the abrasiveness of rocks especially in the tunneling industry. In the CERCHAR test (Centre d'Etudes et Recherches des Charbonages de France), rock surfaces are scratched with a steel stylus. The smooth rock surfaces are either freshly broken with a hammer, or cut using a diamond saw. The steel styluses with 55±1 HRC hardness and a 90° cone angle are used to scratch the rock surface for a length of 10 mm by a 70 N normal load, typically at the speed of 1 m/s or 10 m/s [75,76]. The Cerchar Abrasivity Index (CAI) is the diameter of the flat plane that is formed on the stylus tip, as illustrated in Fig. 3.7 [77]. At least five scratches are made, and the arithmetic mean value of the flat diameters is given [74].

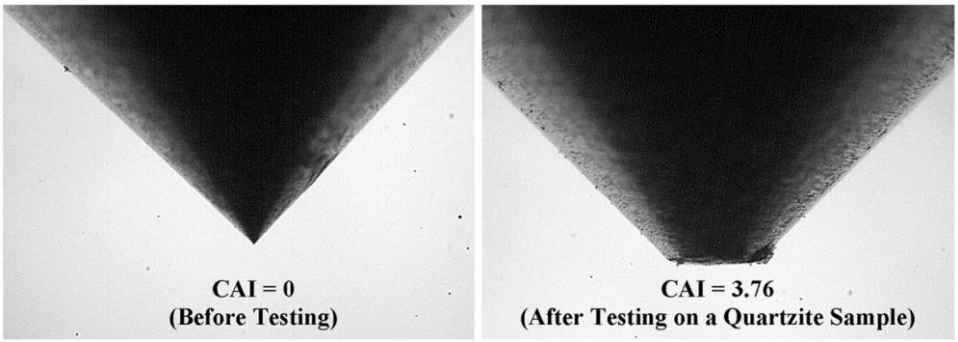

Figure 3.7. Pin (stylus) tip before and after the Cerchar test [77].

Although the CERCHAR test is widely used, there are certain factors that may have an effect on the obtained test results. The measurement of the flat plane from the stylus tip is not as easy as it may seem. Majeed and Abu Bakar [75] reported that the traditional way to determine the area with an optical microscope looking from above gives 17-19% higher values than the measurement done from the side of the stylus (Fig. 3.7), which also gives more accurate results. In addition, Abu Bakar et al. [78] showed that the moisture in the rock typically lowers the CAI value. Moreover, the rock surface quality affects the test results, especially when testing hard rocks [75,76]. In general, the CAI value correlates well with the uniaxial compression strength and hardness of the rock [76].

3.5.3 Equivalent quartz content and rock abrasivity index

For the determination of the equivalent quartz content (EQu), the quartz content of the mineral is analyzed from a thin section by modal analysis or using the x-ray diffractometer. The EQu (%) is then determined as $\Sigma_{i=1-n} A_i \cdot R_i$ [79], where n is the number of minerals, A is the mineral composition (%), and R is the Rosiwal abrasiveness (hardness) (%) for the mineral, which is 120 for quartz [80].

The rock abrasivity index (RAI) is an improved version of EQu. It is determined by multiplying the EQu value by the unconfined compressive strength of the rock [81,82]. Thus, it combines the mineralogical and mechanical properties of the rock.

4 Industrial high-stress wear testing

This chapter concentrates on the high-stress wear and wear testing of metals in the industry. Especially case studies related to the mining industry are introduced and discussed.

4.1 Field testing

Sare and Constantine [3] described various wear problems that arise in the different areas of operation in the mines. They suggested that especially for the materials selection for crushers, chute liners, and bucket teeth, more realistic test methods should be developed because the statistical analysis of field tests in the mines is very difficult. On the other hand, for example for the slurry pumps or drill bits, parallel trial tests in the field can often be arranged, if extra monitoring capabilities and manpower are available. However, as also earlier indicated [2,83], better material selection pays often back the investment in a reasonably short time.

In general, the in-service tests in the industrial environment are difficult to control, and there are many things that can go wrong. Also, conducting a scientific research is not the main concern in the daily operation of factories or mines. Typical factors that can lead to problems are hurry and communication gaps between the test participants, especially because often the tests are performed by outside research institutes. Moreover, it is essential that the contact persons in the industry be committed to the test work. In the worst case, the tested samples may vanish or the test data becomes somehow corrupted. On the other hand, the environment in the mines or factories is so complex that differences between the test samples may arise even though the field test is well planned and executed [84,85]. For example, in mineral handling and haulage, there are notable gradients in the wear of chutes [84], teeth of bucket wheel excavators [84,86], sorting machine bars [85], slurry pumps [87], etc. These kind of gradients in the wear cause challenges in the evaluation of the field test results. Blickensderfer [84] suggests various specimen layouts and attachment setups that help to determine the gradient for concurrent group tests with reference samples. However, fixing of samples next to each other with a perfect fit is often challenging, and misalignment or extensive wear of some samples may change also the wear behavior of the other samples [19].

4.2 Abrasion

Abrasion is the dominating wear mode in mineral excavation, handling, and haulage. Fernandez et al. [86] made an extensive field study for seven weld overlay coatings on the teeth of a bucket wheel excavator, and a comparative study using the ASTM G105 Standard test method for conducting wet sand/rubber wheel abrasion tests [45]. Fig. 4.1 illustrates the wear test results in the laboratory and in the field normalized by the wear resistance of the MR5 coating. The Cr–Nb–V based weld overlay MR3 showed the best wear resistance in both test environments [86]. However, the order of the test results of the other materials was not quite consistent. The used low-stress wear test method probably was not able to produce similar wear mechanisms as observed in the in-service conditions. For example, Dommarco et al. [88] showed that dry rubber wheel abrasion tests produced different wear surfaces for ductile iron samples compared to the teeth of a loader bucket that had been used mainly for excavating quartzite. Moreover, the wear rates (expressed as g/cm^2 h) were at least four times higher in the in-service conditions than in the rubber wheel tests.

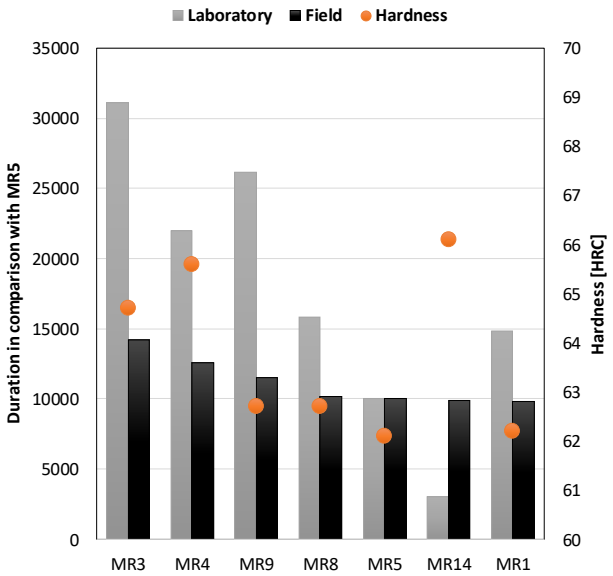

Figure 4.1. Wear resistance of weld overlay coatings in laboratory and field tests normalized by the wear resistance of MR5 based on the reported values of Fernandez et al. [86].

A new material is often not the only solution for a wear problem. Sarkar et al. [89] suggested a welded mesh structure to be used on the underside of excavator buckets. They reported clearly lower wear rates, when using a miniature bucket tester that simulated the movement of a full-size excavator bucket. The mesh structure under the bucket was supposed to change the sliding type of abrasive wear to more rolling type that causes less wear in the bucket. Unfortunately, no characterization of the wear surfaces was published from this study.

Mining is not the only area where soil handling causes wear, and field tests have been made for example to study the wear of agricultural tools, such as ploughshares [90,91]. Bialobrzeska and Kostencki [91] showed that although the rubber wheel tester simulates quite well the low-stress abrasion in the ploughshares, the impacts caused by occasional rocks in the soil should be tested separately. Moreover, the soil abrasivity affects the materials selection. As already mention before, abrasivity of the ground or rock is of special interest when tunnels are excavated using tunnel boring

machines (TBM), as wear of the disc cutters is critical for the progress of the process. Therefore, quite many studies have been published about more practical methods to evaluate the abrasivity of soft ground [92–95], granular ground [96–98], or solid rock [79,99,100] for the needs of the tunneling industry.

Gharahbagh et al. [94] compared the abrasivity of silica sand with different moisture contents and soil conditioning agents using a soil abrasivity tester with three winged propellers rotating in a soil filled pot. Fig. 4.2 shows that the weight loss of the rotating steel parts was much higher with 10-15 % water content compared to dry silica sand. The result was similar when a crushed rock mixture <4.75 mm in size was tested. However, the addition of soil conditioner lowered the wear rates. Apparently, the moist sand or rock mixture cemented to the bottom of the tester, increasing the torque and changing the wear mechanism towards two body abrasive wear [94].

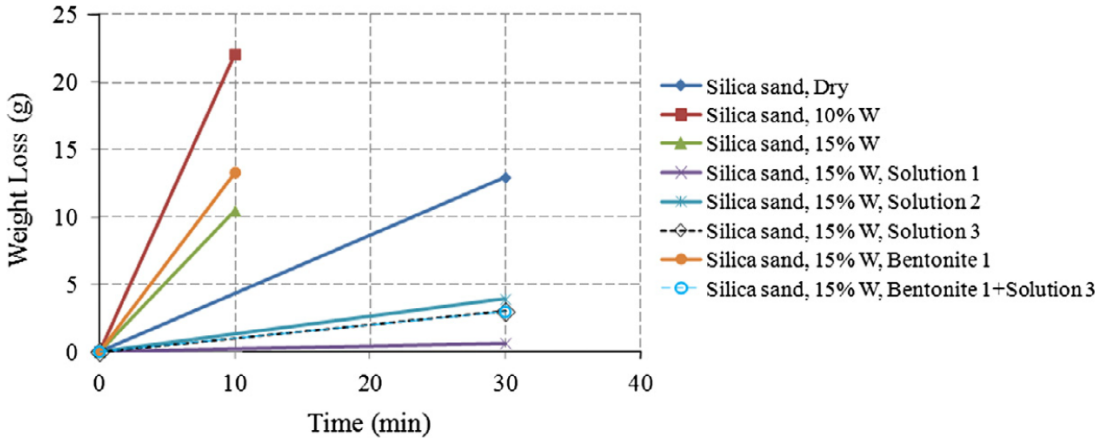

Figure 4.2. Effect of water and soil conditioner on the abrasivity of silica sand [94].

4.3 Impact wear

In the mining industry, the wear parts are subjected to high-stress impact wear or impact-abrasive wear for example in hammer crushers [101], grinding mill liners [102], and during percussive drilling [103,104]. It is quite surprising that rubber wheel abrasion tests are still used to simulate also these conditions. Pereira et al. [102] characterized an in-service pearlitic semi-autogenous (SAG) mill liner. They concluded that large pieces had spalled off from the surface due to the formation of thick white layers. The surface was deformed about 300 µm deep in the in-service samples, but in the rubber wheel tests the deformed surface was only about 3 µm thick, even though the normal load was increased from 20 N to 380 N. Only the wear rate and amount of microcutting increased with the increase of the normal load [102]. Thus, the rubber wheel abrasion was, once again, a too low-stress method for the simulation of a mining wear environment.

Beste and Jacobson [103] studied in detail the deterioration mechanisms of the WC-Co drill-bit inserts in percussive drilling. They suggested that intermixing of the rock layer with WC-Co leads to the formation of an in-situ composite material, the properties of which depend on the drilled rock material. The impacts of the percussive drill to the rock may then crush the brittle composite or even the exposed WC particles.

Wear in the cemented carbide inserts of a drill-bit was simulated using several methods by Tkalich et al. [104]. They used single impact Hopkinson split bar tests against a massive granite block, LCPC tests with cemented carbide pieces attached to the blade, and sliding abrasion tests against loose rock bed on a rotating disc. The wear mechanisms in these tests were compared with full scale drill-bit inserts used in drilling tests. Similar to Beste and Jacobson [103], Tkalich et al. [104] did not find evidence of abrasive wear in the laboratory or in-service tested cemented carbide samples. However, the laboratory tests were not able to produce similar intermixed rock tribofilms as were observed in the in-service drill-bit insert samples. Moreover, the normalized wear rates against the reference material were different.

Heavy impact wear is a challenge also in the recycling industry. Abbasi, Luo and Owens [105] studied the complex wear mechanisms of scrap shear blades. They reported that higher amounts of subsurface adiabatic shear bands were observed in the steel with a lower wear rate, when two martensitic 50 HRC steels used in the actual conditions were compared. The hardness of the deformed layer (ASBs not included) was, however, higher in the steel with a higher wear rate. In the scrap shear blades, the ASBs were formed both on the surface and in the subsurface region, which typically contained cracks. As a consequence, they concluded that spalling and delamination of the cracked layers was the main wear mechanism in the blades [105].

4.4 Wear in the Arctic environment

The exploitation of the Arctic area is getting more intensive, when the current mines are impoverished and the price of the raw materials is increasing. Moreover, in the countries around the Arctic Circle, the temperatures are typically below 0°C during the winter months (Fig. 4.3). The working conditions at subzero temperatures set demands also to the materials. The ductile-to-brittle transition (DBT) at low temperatures is typical for metals with a body-centered cubic microstructure [106]. Therefore, also the wear behavior of the steels can change markedly at subzero temperatures, when their ability for plastic deformation becomes limited.

In the wheel-rail contacts in the Arctic region, the subzero temperatures have been observed to have a marked effect on the wear behavior of materials [107,108]. Ma et al. [107] studied the wheel-rail contact with a twin-disc-type tester in the temperature range of +20°C…-40°C. In the studied pearlitic steel, the highest wear rates and the deepest subsurface cracks were formed at -15°C, which is close to the DBT temperature of the steel. Ma et al. [107] suggested that during the 24 hour test at lower temperatures, the pearlitic lamellae had changed to irregular and short, preventing the crack propagation due to the increased strength.

Lyu, Bergseth and Olofsson [108] reported similar results for a rail steel when using a pin-on-disc tester with or without snow in a contact. They showed that friction and wear were most temperature sensitive close to the DBT temperature of the steel. Moreover, the addition of snow decreased the wear rates, because under the contact pressure snow formed a liquid-like lubrication layer that also promoted the formation of protective hard hematite on the wear surface.

Figure 4.3. Tram line construction worksite in Tampere, in operation at -20 ℃ in Winter 2018.

5 Materials and methods

5.1 Materials

In addition to the wear behavior of selected steels and cast irons, also the role of abrasives used or encountered in various applications was studied in this thesis. The following sub-chapters introduce all the test materials and abrasives (minerals) used in this work, including their compositions and most important properties related to abrasive wear.

5.1.1 Steels

Table 5.1 lists the studied steels and their nominal compositions and typical mechanical properties, including bulk Vickers hardness, yield strength ($R_{p0.2}$), ultimate tensile strength (R_m), elongation (A5), and impact toughness at -40°C (from data sheets). The typical carbon equivalent values (CEV) were determined using CEV = C + Mn/6 + (Cr + Mo + V)/5 + (Ni + Cu)/15. The Vickers hardness values were measured from the polished cross-sections of the samples.

Table 5.1. Typical mechanical properties and nominal compositions of the tested steels.

	S355	**400HB**	**450HB**	**R500HB**	**500HB**	**550HB**	**600HB**
Publication	I, IV	I- IV	I, III	I- IV	III	III	III
Hardness HV10 [kg/mm^2]	162 ± 3	408 ± 20	489 ± 9 (I) 435 ± 6 (III)	508 ± 18	481 ± 18	554 ± 8	609 ± 16
$R_{p0.2}$ [N/mm^2]	355	1000	1200	1250	1300	1400	1650
R_m [N/mm^2]	430-530	1250	1450	1600	1550	1700	2000
A5 [min %]	24	10	8	8	8	7	7
Impact toughness -40°C [J]	40	30	30	30	37	30	20
C [wt%] max.	0.12	0.26	0.26	0.30	0.30	0.37	0.47
Si [wt%] max.	0.03	0.80	0.80	0.80	0.70	0.50	0.70
Mn [wt%] max.	1.5	1.70	1.70	1.7	1.60	1.30	1.4
Cr [wt%] max.	-	1.5	1.5	1.5	1.5	1.14	1.20
Ni [wt%] max.	-	1.0	1.0	1.0	1.5	1.4	2.50
Mo [wt%] max.	-	0.5	0.5	0.5	0.6	0.6	0.70
B [wt%] max.	-	0.005	0.005	0.005	0.005	0.004	0.005
CEV typical	0.28	0.57	0.57	0.66	0.62	0.72	0.61

The studied steels included two different 500HB grade steels, of which R500HB was used as a reference steel throughout the thesis (although the naming practices slightly varied in the Publications). As Fig. 5.1 shows, the microstructures of the wear resistant steels consist mostly of tempered martensite, but may contain also small amounts of retained austenite (<0.5 %) [109] and untempered martensite, which is seen as white unetched grains. The structural steel S355 with a ferritic-pearlitic microstructure was used as a test material in Publications I and IV.

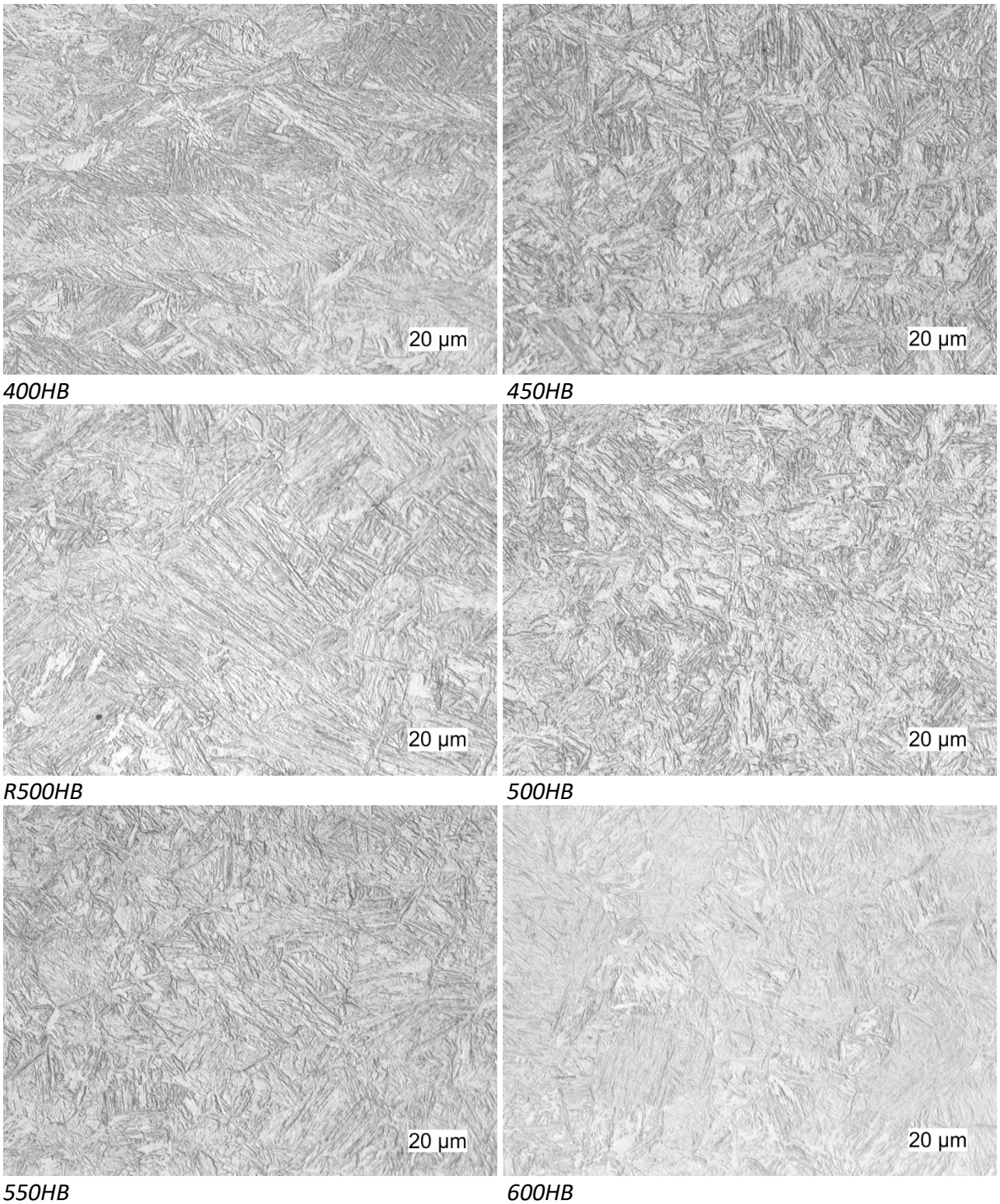

400HB *450HB*

R500HB *500HB*

550HB *600HB*

Figure 5.1. Optical micrographs of the studied wear resistant steels.

5.1.2 Abrasives

Mineral abrasives have a marked role in the high-stress abrasive wear in mining and rock handling. In this study, four crushed rock materials were used as abrasives: chromite, quartzite, and two slightly different granites. The Sorila granite was earlier an 'in-house standard' rock material, but the properties of different batches were found to vary markedly. Thus, it was changed to Kuru granite, which has a finer and more homogenous microstructure. For simulating the conditions in a chromite mine, also chromite ore was used as an abrasive. Quartzite, in turn, was selected because of its high abrasivity and common use in wear testing. Fig 5.2 shows an example of the microstructure of the minerals, and Table 5.2 lists their composition and typical mechanical properties. The abrasivity and crushability values of the minerals were determined by the LCPC test at Metso Ltd [70]. In the LCPC tests, the reference steel was SSAB Laser 250C with a minimum yield strength of 250 MPa. Chromite is easily crushed, because the hard chromite particles are surrounded by silicates, as seen in Fig. 5.2. Therefore, the abrasivity value of chromite is relatively low despite its high hardness.

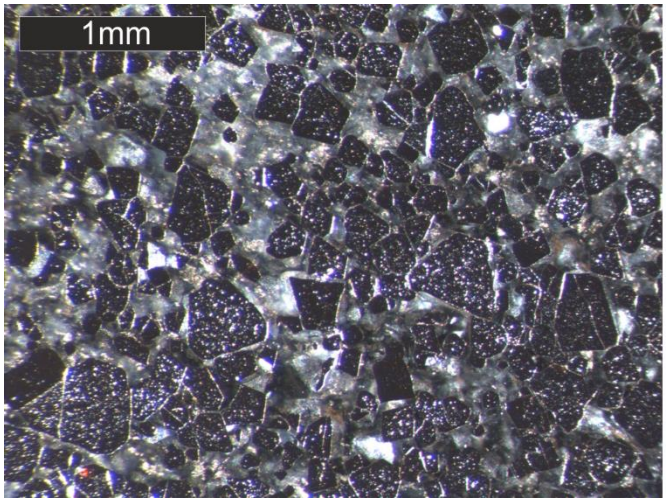

Chromite

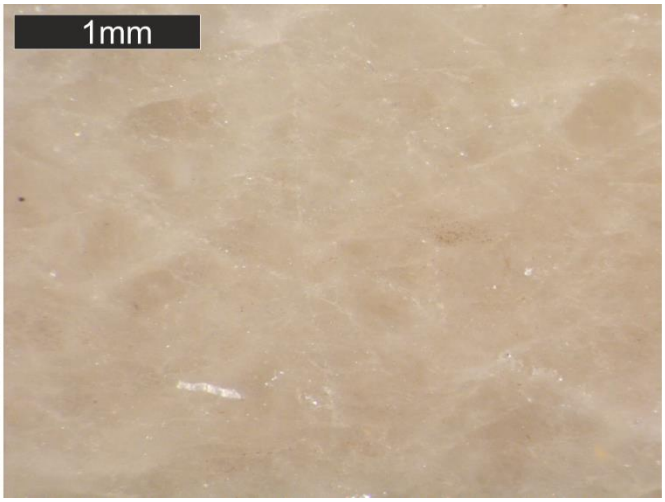

Quartzite

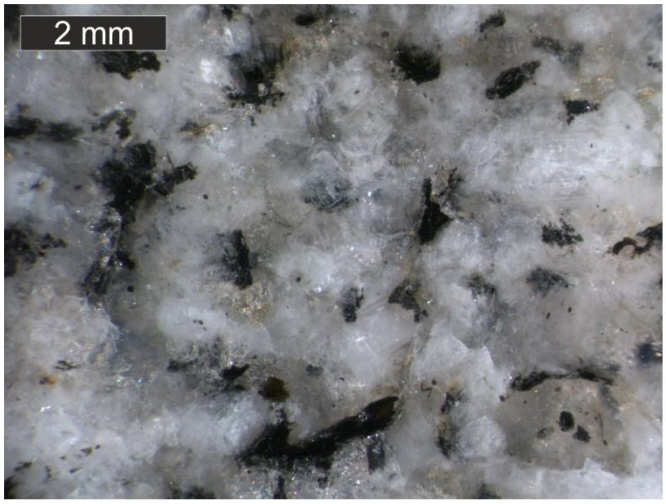

Kuru granite

Sorila granite

Figure 5.2. Stereomicroscope images of the cross-sections of the abrasives used in this study [Publication III].

Table 5.2. Properties and nominal composition of the abrasives used in this study.

	Quartzite	**Chromite**	**Kuru granite**	**Sorila granite**
Publication	III	III	III, unpublished	I, II, III, unpublished
Quarry	Baskarp Svedudden, Sweden	Outokumpu Tornio Works Kemi Mine, Finland	Kuru, Finland	Sorila, Finland
Solid density [t/m^3]	2.65	3.46	2.64	2.72
Crushability [%]	35	79	38	38
Abrasiveness	1940	460	1380	1500
Median hardness HV1 [kg/mm^2]	992 ± 162	1059 ± 97	977 ± 134	955 ± 159
Nominal mineral contents [%]	Quartz 99	Chromite 90 Silicates [110]	Quartz 35 Plagioclase 30 Orthoclase 28 Biotite 3 Diopside 2 Chlorite 1 [111]	Plagioclase 45 Quartz 25 Orthoclase 13 Biotite 10 Amphibole 5 [5]

5.1.3 Nodular cast iron rollers and wire ropes

Nodular cast iron EN-GJS-700-2 was used in the manufacturing of the studied grooved rollers and twin-disc test samples [Publication V]. Table 5.3 lists the mechanical properties of EN-GJS-700-2 according to standard SFS-EN 1563 [112], as well as the measured median hardness values of the cast iron samples. Fig. 5.3 presents a typical microstructure of an unused cast iron roller with (black) spherical graphite precipitates in an almost fully pearlitic iron matrix.

Table 5.3. Standardized mechanical properties of the EN-GJS-700-2 nodular cast iron [112] *and the hardness values measured from the studied samples.*

	EN-GJS-700-2	**Unused roller**	**In-service roller**	**Test roller 10 kN**	**Test roller 15 kN**	**Twin-disc**
Hardness [HBW 1/30]	225-305	285 ± 6	268 ± 7	277 ± 4	277 ± 2	272 ± 5
Rp0.2 [N/mm^2]	400					
Rm [N/mm^2]	700					
A5 [min %]	2					

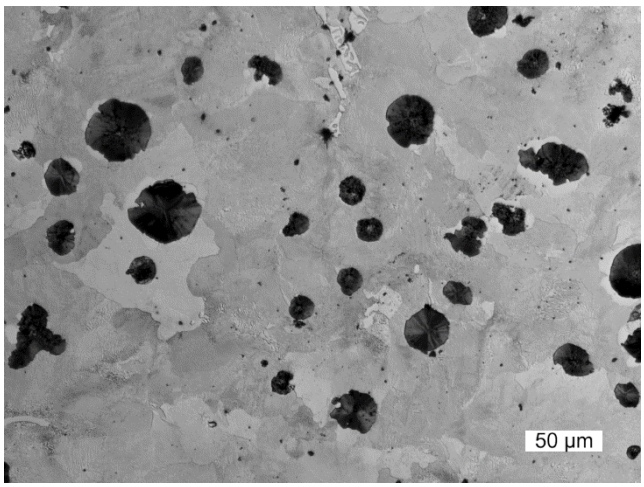

Figure 5.3. Optical micrograph of the microstructure of an unused nodular cast iron roller.

The wire materials used in this study [Publication V] were drawn from an unalloyed pearlitic steel with 0.6 wt.% carbon content. The wire rope used in the roller tests and in the in-service use had 8x19 regular left lay Seale outer strands and a steel wire rope core. The outer diameter of the 2160 N/mm^2 tensile strength grade wire rope was 8 mm. In the twin disc tests, the measured hardness of the single wires was 456$\pm$6 HV_5 and the ultimate tensile strength 1700 N/mm^2.

5.2 Wear testing methods

In order to study the potential of various wear testing methods for the simulation of different in-service cases in the laboratory scale, several application oriented wear testing methods were used and analyzed in this thesis. The wear loss results in the abrasive, impact-abrasive, and erosive tests were obtained by weighting the samples at different stages of the tests.

5.2.1 Crushing pin-on-disc

The crushing pin-on-disc (CPOD) abrasive wear tester was designed to simulate various types of mineral crushers [113]. In this thesis, it was utilized in various case studies, including a wear plate of a dumper body [Publication I], a cutting edge of a mining loader bucket [Publication II], and a wear plate in a feed hopper [unpublished].

The crushing pin-on-disc method is based on the conventional pin-on-disc test, where a cylindrical pin is pressed against a rotating disc. However, in the CPOD system, the pin does not touch the disc at any point, because there is always a layer of loose rock particles between the pin and the disc. In addition, the compression is made cyclically. Fig. 5.4 illustrates the construction and working principle of the CPOD. The compression (crushing) cycle lasts 5 seconds, followed by 2.5 seconds of free rotation with the pin lifted up from the gravel bed. When the disc rotates at 28 rpm, the pin is pressed to the highest point of the abrasive bed in each cycle. The sample holder rotates freely around its axis. Thus, the wear rate is quite similar over the whole wear (pin) surface and the direction of abrasion varies randomly in each cycle.

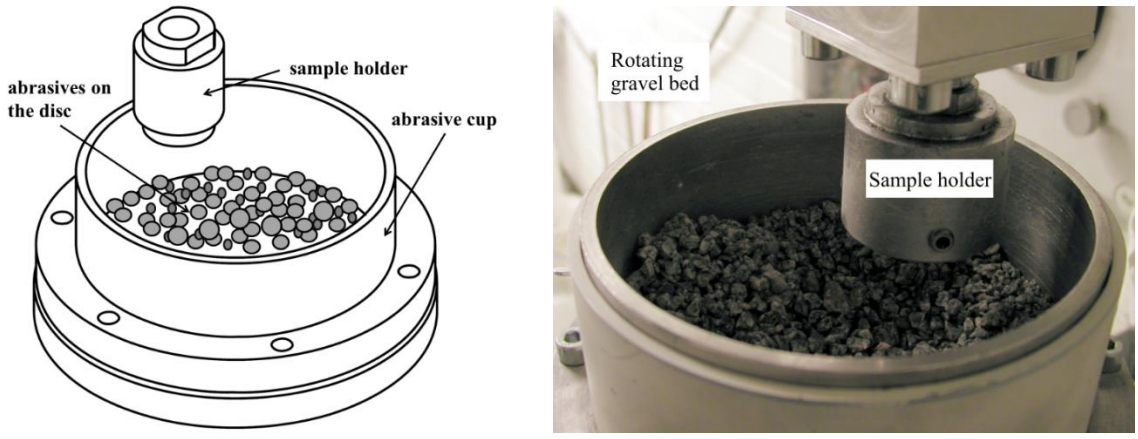

a) *b)*

Figure 5.4. The crushing pin-on-disc system a) schematic [Publication I] and b) photo [Publication II].

The sample pin is a solid cylinder with a 36 mm diameter and a wear area of 1017 mm^2. However, the true contact during each compression cycle area is only 2-3.5%, as determined by Lindroos [114]. Figs. 5.5a and b illustrate the increase in the true contact area during a 20 minute test due to the comminution of the abrasives. The amount of abrasive in each test is 500 g, and the size of the particles is initially 2-10 mm. Fig. 5.6 shows the original particle size distribution and an example of the comminution of the rock during the test. In this thesis, Sorila granite was used as an abrasive in all crushing pin-on-disc tests.

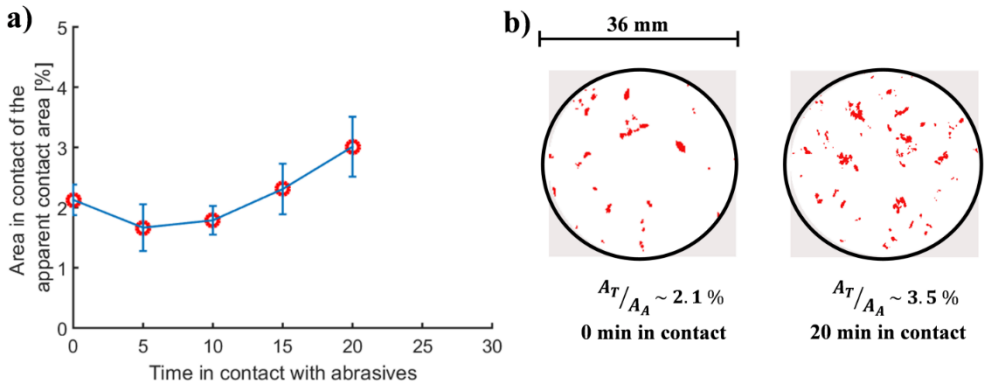

Figure 5.5. a) Change of the true contact area during a CPOD test and b) true contact points recorded with a pressure sensitive paper [114].

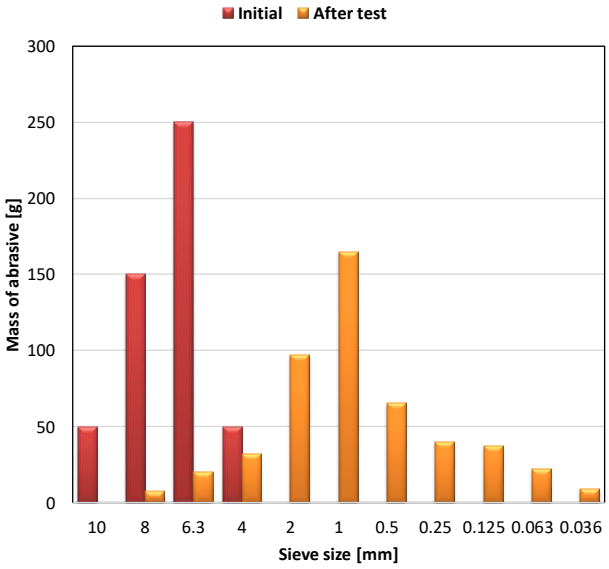

Figure 5.6. Comminution of Sorila granite in a 20 minute test with a 400HB steel pin and a S355 steel disc.

The selection of the disc material is based on the desired wear mechanism. A soft disc material typically leads to higher wear rates, as the abrasive particles embedding to the disc cause increased cutting in the pin sample. In other words, the soft disc with embedded abrasives resembles an ordinary abrasive paper. When the disc material is hard, there is more rolling of the rock in the contact, and the wear rates of the sample pin remain lower [113]. At Tampere Wear Center, two in-house 'standards' for testing of steels have been created; one with a disc material with hardness similar to the pin, and another with the soft S355 steel as the disc material plus a little bit higher

normal force. Both methods were used also in this thesis, as listed in Table 5.4. In order to study steady state wear only, a running-in with 2-4 mm granite was conducted for all specimens before the actual tests.

Table 5.4. Test parameters used in the crushing pin-on-disc tests.

	Publication I	**Publication II**	**Unpublished**	
Case	Dumper truck wear plate	Cutting edge of mining loader bucket	Feed hopper wear plate	
Contact time [min]	20	3 x 20	20	
Wear area [mm^2]	1017	1017	1017	
Pressure [bar]	0.9	1.1	0.9	1.1
Normal force [N]	200	240	200	240
Disc material	Similar to pin	S355	Similar to pin	S355
Abrasive	Sorila granite	Sorila granite	Sorila granite	
Abrasive size [mm]	2-10	2-10	2-10	
Amount of abrasive in one test cycle [g]	500	500	500	
Running-in time [min]	20	15	15	

5.2.2 Uniaxial crusher

In the uniaxial crusher [115], rock is crushed between two metal parts with a high normal force, similar to cone crushers, roll crushers, and high pressure grinding rolls. In this study, the uniaxial crusher method was used to simulate the high loads caused by the piles of rocks in the dumper truck wear plates [Publication I] and in the cutting edges of mining loader buckets [Publication II]. Figure 5.7 presents the principle of the test method. The pre-crushed and sieved rock is first fed into a tilting cup with a supply tube, which also levels up the rock pile when it is retracted. The cylindrical sample is compressed against the rock pile inside the cup using a pneumatic cylinder. The normal force is 23 – 86 kN depending on the set pressure value. Finally, the tilting cup is emptied automatically and the cycle starts again.

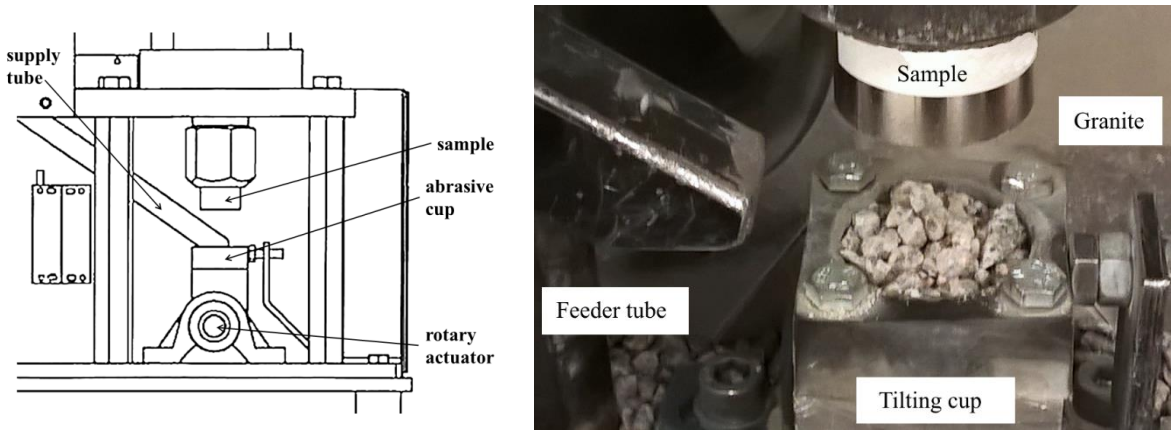

a) *b)*

Figure 5.7. Uniaxial crusher a) a schematic [Publication I] and b) a photo of the crushing area [Publication II].

Table 5.4 lists the uniaxial crusher test parameters used in this study. The tilting cup is made of rubber and the counterpart of a tool steel. In this test method, the properties of the counterpart do not have such a marked effect as in the crushing pin-on-disc tests, because the rock pile is thick and there is practically no horizontal movement of the abrasives. The sample is similar as in the crushing pin-on-disc tests, which facilitates testing of same materials, or even same samples, with different devices.

Table 5.4. Test parameters used in the uniaxial crusher tests.

	Publication I	**Publication II**
Case	Dumper truck wear plate	Cutting edge of mining loader bucket
Contact time [min]		15
Wear area [mm^2]	1017	1017
Pressure [bar]	4	4
Normal force [kN]	53	53
Counterpart	Tool steel	Tool steel
Abrasive	Sorila granite	Sorila granite
Abrasive size [mm]	4-6.3 mm	4-6.3 mm
Running-in	100 compressions	15 min with CPOD

In order to test also the sliding abrasive wear of heavily deformed wear surfaces, a combination test procedure with the crushing pin-on-disc device and the uniaxial crusher was used [Publication II]. The samples were first compressed 500 times with the uniaxial crusher. The deformed surfaces were then tested with the crushing pin-on-disc device using a 20 minute contact time. Tables 5.3 and 5.4 present the other parameters used in these tests [Publication II].

5.2.3 Impeller-tumbler

The impeller-tumbler impact-abrasive wear tester crushes rock with three rotating impellers, which are also the studied samples, as illustrated in Fig. 5.8. Thus, it is a sort of miniature impact crusher, but in this study, it was used to simulate wear caused by rocks dropping on the dumper truck wear plates [Publication I] and wear in the cutting edges of mining loader buckets [Publication II]. The tumbler rotates at a slow speed in the same direction as the impellers. The sample angle can be varied by changing the sample holder from 15° to 90° [19].

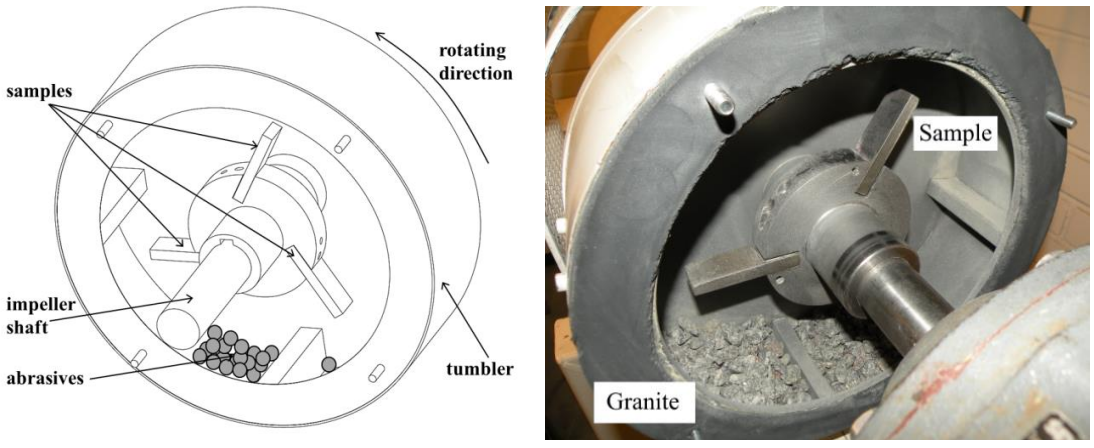

a) *b)*

Figure 5.8. The impeller-tumbler test device a) a schematic [14] *and b) a photo of the test chamber [Publication II].*

In the current tests, the reference sample had a fixed slot, but the two test samples were swapped after every 15 minute test cycle. The abrasive was also changed after every test cycle. Table 5.4 lists the test parameters used in this study.

Table 5.4. Test parameters used in the impeller-tumbler tests.

	Publication I	**Publication II**
Case	Dumper truck wear plate	Cutting edge of mining loader bucket
Test duration [min]	4 x 15	24 x 15
Wear area [mm²]	1200	1200
Impeller speed [rpm]	700	700
Tumbler speed [rpm]	30	30
Speed at sample tip [m/s]	7.7	7.7
Sample angle [°]	60	60
Abrasive	Sorila granite	Sorila granite
Abrasive size [mm]	10-12.5	8-10
Amount of abrasive in one test cycle [g]	900	900
Running-in [min]	15	-

5.2.4 High speed slurry-pot with dry abrasive gravel bed

The high-speed slurry-pot was originally designed to simulate wear in the slurry pumps used in the mines [6], as described in Chapter 3.4. However, it has proven a very versatile testing system that is suitable also for testing samples in a dry abrasive gravel bed [85]. In this study, it was used to simulate high-stress abrasion in mineral handling and haulage in mines, including the wear plates of dumper bodies [Publication I], cutting edges of mining loader buckets [Publication II], and wear plates in a feed hopper [unpublished].

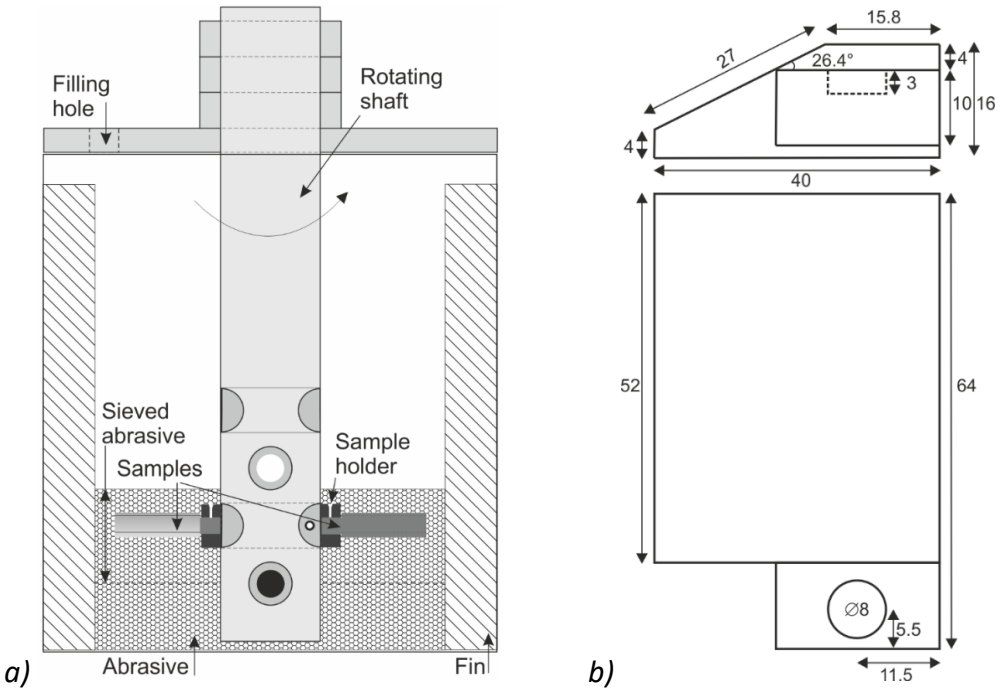

Figure 5.9. The dry-pot test setup for the cutting edge shaped samples: a) a schematic picture of the test chamber and b) a drawing of the sample [Publication III].

Fig. 5.9.a presents a schematic picture of the slurry-pot with dry gravel bed (dry-pot), when the samples are positioned on level 2 at a 0° sample angle. The samples are attached to the sample holders in a rotating shaft with locking screws. Fig. 5.9.b shows the sample dimensions for the cutting edge shaped samples, and Fig 5.10 the appearance of the samples used in the study. In all tests, the bottom of the pot was first covered with 1.35 kg 100-600 µm Nilsiä quartzite to protect the end of the shaft. This bed made also the removal of the packed comminuted rock easier after the test. When the samples were attached to the shaft and the lid was tightly closed, the crushed and sieved gravel was poured to the pot through the filling hole in the lid. Table 5.4 lists the parameter values used in the tests. In the midpoint of the tests, the position of the samples and the gravel were changed. Thus, the small differences in the sample holder positions were largely canceled out with this method.

a) *b)*

Figure 5.10. Photographs of the attached samples after the dry-pot wear tests, a) plate samples at 45° angle [Publication II] and b) cutting edge samples [Publication III].

Table 5.4. Test parameters used in the dry-pot tests.

	Publication II	**Publication III**		**Unpublished**
Case	Cutting edge of mining loader bucket	Cutting edge of mining loader bucket		Feed hopper wear plate
Test duration [min]	2 x 30	2 x 30	2 x 120	2 x 120
Wear area [mm²]	2540	5000	5000	2540
Rotation speed [rpm]	500	500	250	250
Speed at sample tip [m/s]	5	5	2.5	2.5
Travel distance of the tip [m]	18000	18000	36000	36000
Sample angle [°]	45	0		45
Samples in one test	2	2		2
Sample shape	Plate	Cutting edge		Plate
Abrasive	Sorila granite	Sorila granite, Kuru granite, quartzite, chromite		Sorila granite
Abrasive size [mm]	8-10	8-10		8-10
Amount of abrasive in one test cycle [kg]	9000	9000 (chromite: 13800)		9000

5.2.5 Tribometer

To conduct simplified wear tests with controlled loads, a CETR UTM-2 tribometer was used to conduct scratch tests on the R500HB steel. The scratching was performed on polished surfaces circularly at a 0.1 mm/s sliding speed using a standard Rockwell-C indenter with a tip radius of 200±10 µm. Single or multiple cycles (1, 2, 5, or 10) were run in the same scratch groove using 20

N, 40 N, 60 N, and 80 N constant normal loads. These tests were part of a larger test series published earlier by Lindroos et al. [22].

5.2.6 High velocity particle impactor

The High Velocity Particle Impactor (HVPI) was originally developed for oblique single and multiple impact testing and to be used as a verification method for the numerical simulation of impact wear tests [17]. Fig. 5.11 presents a schematic of the HVPI with a cooling system that enables testing at temperatures ranging from room temperature down to -70°C and even lower. The HVPI system enables controlled shooting of single projectiles to a tilted target material using pressurized air. The impact velocity varies typically between 44 m/s and 165 m/s [25,116], depending on the mass of the projectile and the air pressure. Typical projectiles are 9 mm bearing balls made of WC-Co, steel, ZrO_2, or Si_3N_4 with properties determined by SFS-ISO 3290- standards [117,118].

In the present study, the HVPI system was used to study the properties of steels in the Arctic conditions [Publication IV]. Three steels, S355, 400HB, and R500HB, were impacted at room temperature (RT, 22-23°C), -20°C, and -60°C. Table 5.5 lists the parameter values used in these tests. Three individual impacts were made on each of the steels at all test temperatures. In addition to single impact tests, the 500HB samples were impacted five times with overlapping impacts at RT, -20°C, and -60°C. The samples were always re-cooled to the test temperature before the next impact. The 9 mm, grade 10 WC-Co balls contained 6% cobalt (ISO K20) and had an average 1800 HV_{10} hardness.

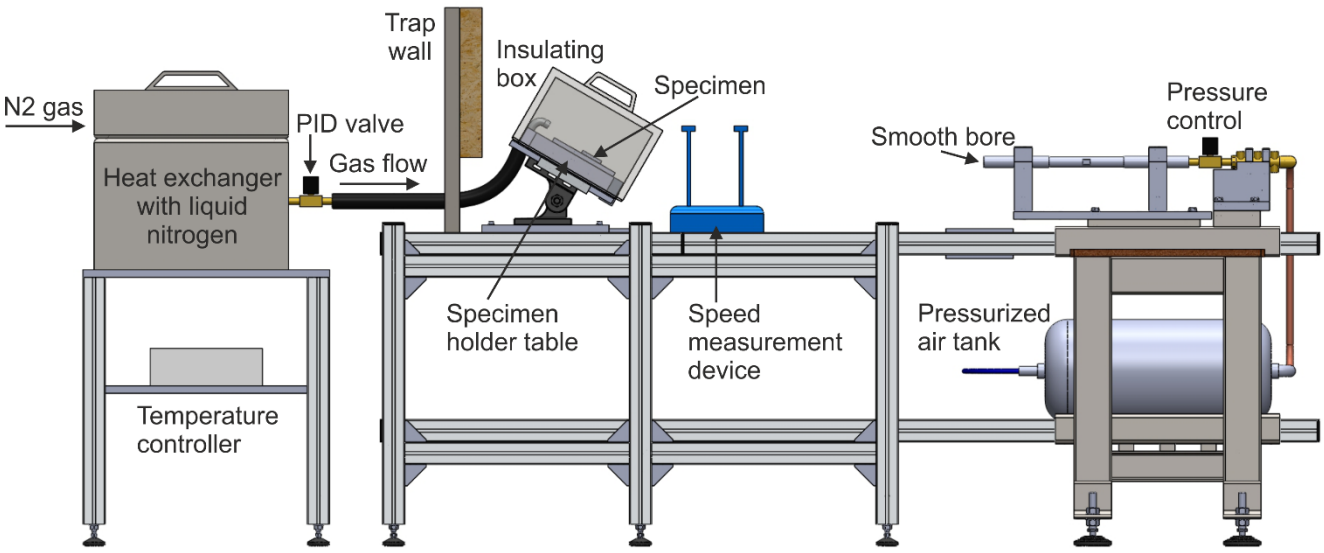

Figure 5.11. Schematic of the high velocity particle impactor with a subzero cooling system [Publication IV].

Fig. 5.12 shows how the polished 40 x 40 x 4 mm samples were attached to the sample holder with steel clamps. The final polishing of the samples was made with 1 µm diamond paste. Two K-type thermocouples were spot-welded on them to measure the temperature of the sample surfaces. The attached samples were cooled inside an insulating box by nitrogen gas flowing through a heat exchanger immersed in liquid nitrogen. Two impacts were made on each specimen, as seen in Fig. 5.12. The samples were cooled a few degrees below the target temperature and kept there for a few minutes to even out the temperature before the actual test. The first cooling cycle from room

temperature down to -60°C took about 30 minutes with this system, but when the sample holder was already cold, the other tests were much faster to execute. The ice formed from the condensed air moisture was wiped off with a cotton cloth just before the impact.

Table 5.5. Test parameters used in the high velocity particle impactor tests.

	Publication IV
Case	Arctic environment
Test temperatures	RT, 1°C, -1°C, -20°C, -60°C
Impact velocity [m/s]	110-114
Impact pressure [bar]	14
Sample angle [°]	60
Sample size [mm]	40 x 40 x 4
Sample shape	Plate
Projectile	WC-Co bearing ball
Projectile size [mm]	9
Projectile weight [g]	5.7

Figure 5.12. Two impact marks on the steel plate sample attached to the sample holder.

Although the ice layer formed during the cooling was wiped off before the tests, there was still enough time for the formation of a new thin ice layer right before the exact moment of impact. The effect of the ice layer on the test results was studied by conducting a pair of tests at +1°C and -1°C using the R500HB steel. At -1°C, a visibly thick frost layer was let to form on the sample surface before the impact. At 1°C, the surface was wiped clean before the test in a similar manner as in the other tests. The result of this experimentation was that there was no essential difference between the results obtained from the tests with or without an ice layer on the sample surface [Publication IV].

5.2.7 Component tests of grooved rollers

The wear of a grooved roller in a hoist system was simulated by a component test that utilized the same rope and similar groove geometry as used in the in-service operation [Publication V]. The tested component samples were received from an industrial partner for wear surface examinations. Fig. 5.13 presents a schematic of the component test system and the position of the characterized invert roller. The wire rope ran over three freely rotating invert rollers and a drive roller that rotated first 0.5 m clockwise and then back counterclockwise so that the total length of one cycle was 1 m. The wire rope was fastened to the drive roller in order to prevent sliding. The fleet angle of the wire

rope was 0°, i.e., the rope left the groove directly without an angle. The tests were run with two different rope forces, 10 kN and 15 kN. The 10 kN test lasted 639198 running cycles, and the 15 kN test 309969 running cycles. The wire rope, which was lubricated with additive-free paraffinic vaseline, was changed five times during each the test. In the 10 kN test, the changing was done on average after every 127000 cycles, and in the 15 kN test after every 62000 cycles.

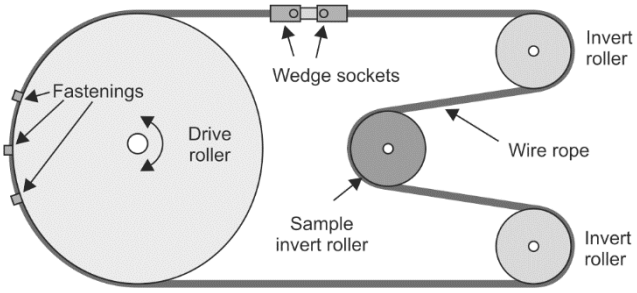

Figure 5.13. Schematic picture of the component test used in Publication V for a grooved roller.

5.2.8 Twin-disc

In order to simulate the contact behavior of the roller materials, a twin-disc tester was used [Publication V]. The counterpart needed in the tests was prepared by rolling a 1.4 mm steel wire in a spiral form on the grooved disc so that it formed initially two contact points with the nodular cast iron sample disc, as visualized in Fig. 5.14. The diameter of both discs was 50 mm, and the surface of the sample disc had a 100 mm radius curvature in the axial direction. In the tests, the two discs were rolling against each other under a 500 N normal force. There was a slip of about 0.2 % between the discs, because the rotation speed of the sample disc was set to 3.0 m/s and to 2.94 m/s for the wire-coated disc. During the test, the speed of the discs changed and the number of contact points increased due to the wear of the disc and the wires. The contact was lubricated with a paraffinic vaselin drop (petrolatum) every 30 min. During the 48 h test, the rolling distance was 518000 m and the sliding distance about 1000 m.

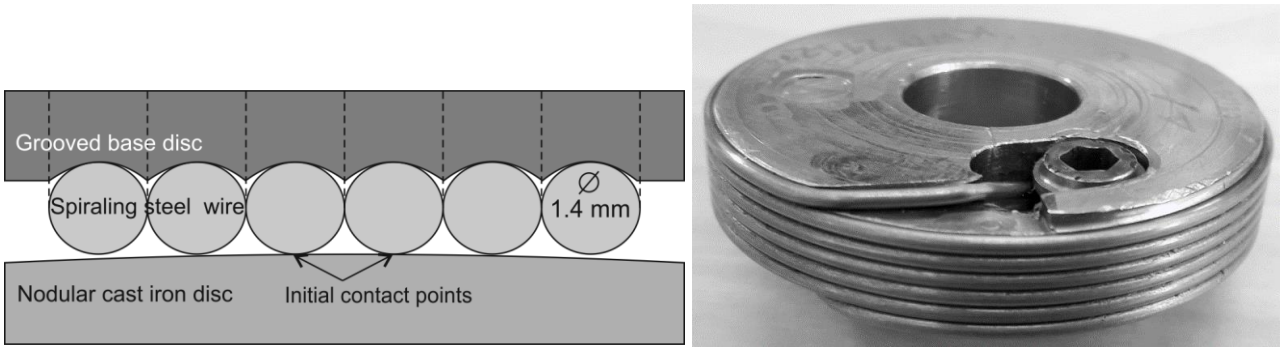

a) *b)*

Figure 5.14. Twin-disc test setup a) a schematic cross-section and b) a photo of the wire-coated disc used in Publication V.

5.3 Field tests

Samples from three field tests in a mine and one from a hoisting machinery were received for characterization and comparison with the laboratory test results.

5.3.1 Cutting edges of mining loader buckets

In the bucket of an underground mining load-haul-dumper (LHD), the cutting edge is exposed to very harsh conditions. In this thesis, two in-service cases were characterized and compared to the results of several different laboratory tests [Publications II & III]. Lapland University of Applied Sciences was responsible for the field testing in the Outokumpu Kemi chromite mine. In both cases, the cutting edge was welded to the bucket of the CAT R2900G LHD loader (Fig. 5.15.). The LHD loaders were used in a normal operation, and the cutting edges were measured with the ATOS 3D scanner when they were replaced. In recent years, the average changing interval of the cutting edges in the Kemi chromite mine has been 1014 hours. The loaders haul quarry gravel, including granite, chromite, barren rock, and slurry paste.

Figure 5.15. CAT R2900G underground mining load-haul-dump loader [119].

In the first in-service case [Publication II], the cutting edge of the mining loader bucket was manufactured from the R500HB steel. It was replaced after 928 hours [120]. In the second case [Publication III], the cutting edge was submerged arc welded (SAW) from two pieces, as shown in Fig. 5.16. The tested steels were R500HB and 550HB. During the 217 hours of operation, the cutting edge was used to load a total of 51514.6 tons of quarry gravel and slurry.

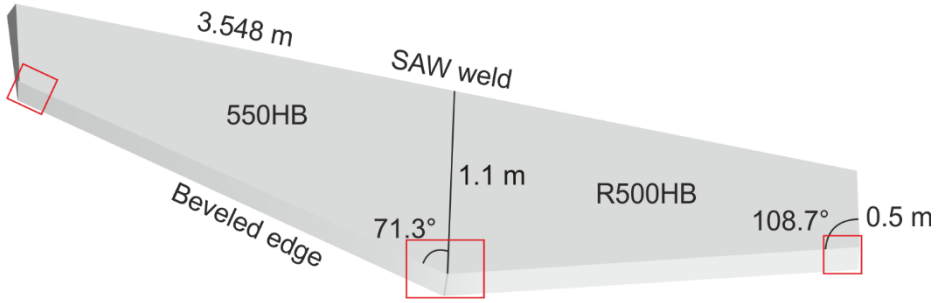

Figure 5.16. Schematic of the in-service cutting edge in the 217h test [Publication III]. The squares illustrate the locations of the characterized parts.

5.3.2 Wear plates of feed hopper

The side wear plates of a feed hopper were tested by Lapland University of Applied Sciences in the Outokumpu Kemi chromite mine [unpublished]. The wear plates were positioned at a 53° angle on the opposite sides of the feed hopper of a conveyer belt, as visualized in Fig. 5.17. The wear plates were made of R500HB and 600 HB steels, and their size was 250 mm x 500 mm x 40 mm. The wear profiles were determined by ATOS 3D-scanning.

During the 13 weeks of in-service operation, 473 596 000 kg of chromite ore with 0-250 mm grain size was fed to the feed hopper. The operational efficiency during the test time was about 71%, because there were several routine maintenance shutdowns.

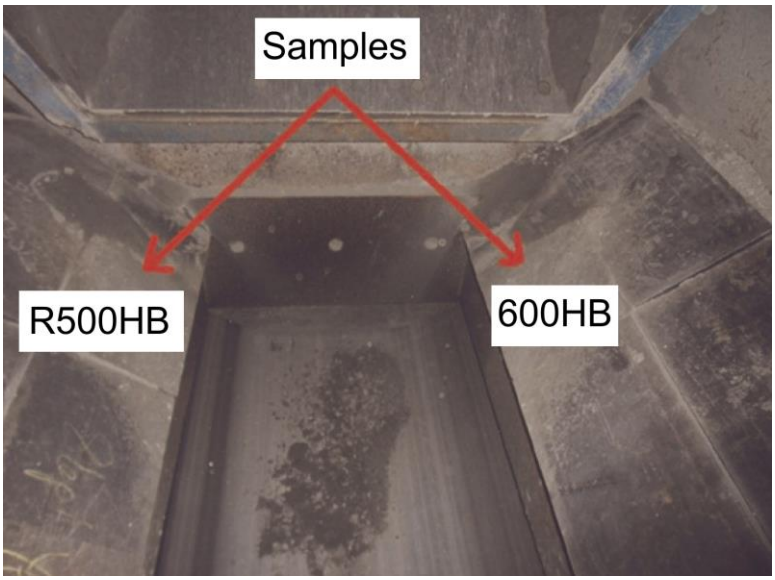

Figure 5.17. Side plates of the feed hopper, photo modified from [121].

5.3.3 Grooved roller

A ductile cast iron roller from a hoist system was studied and compared to the results of various laboratory tests simulating the contact [Publication IV]. The approximate use time of the examined invert roller was 400-500 hours. The fleet angle of the rope varied when the roller changed the running direction during operation. The rope forces were similar on both sides of the roller, and thus there was practically no sliding between the wire rope and the freely rotating invert roller. The wire rope was lubricated with paraffinic vaseline before installation.

5.4 Characterization methods

The in-service samples and samples tested in laboratory were characterized by various methods, including microscopy, surface profiling, hardness testing, and residual stress measurements.

5.4.1 Microscopy

The wear surfaces and the microstructures before and after the wear tests were characterized by scanning electron microscopy and various optical microscopes. Zeiss ULTRAplus field emission gun scanning electron microscope (FEG-SEM) was equipped with INCAx-act Energy Dispersive X-ray Spectrometer (EDS). Philips XL30 scanning electron microscope (SEM) with EDAX EDS system was also used. The optical microscopes used in this work were Nikon Eclipse MA 100 optical microscope, Leica DM 2500 materials microscope system, and Leica MZ 7.5 Zoom stereo microscope.

The wear surfaces of the in-service samples obtained from the mining industry are typically heavily oxidized. The iron oxide layer was removed with 10% USF 175 acidic detergent in an ultrasound cleaner before characterization. The acidic solution caused also slight pitting corrosion on the surface, as well as removal of the embedded rock. All SEM samples were also cleaned with ethanol in an ultrasound cleaner and with K1050XT RF Turbo plasma asher. The polished cross-sectional samples were etched with 4% Nital.

The FEG-SEM images from the wear surfaces were typically taken by combining (50:50) secondary electron (SE) and angle selective backscatter electron (AsB) images. Thus, the elemental contrast between steel and embedded rock was enhanced, but also the topographical contrast provided by the secondary electrons was well visible. The in-lens secondary electron detector was also utilized, when finer details from the microstructure of the steels were characterized. The wear surfaces of the samples were characterized from all sides, but the area and the cross-section cutting line that were mainly used in the published images are marked in Fig. 5.19 together with the residual stress characterization points.

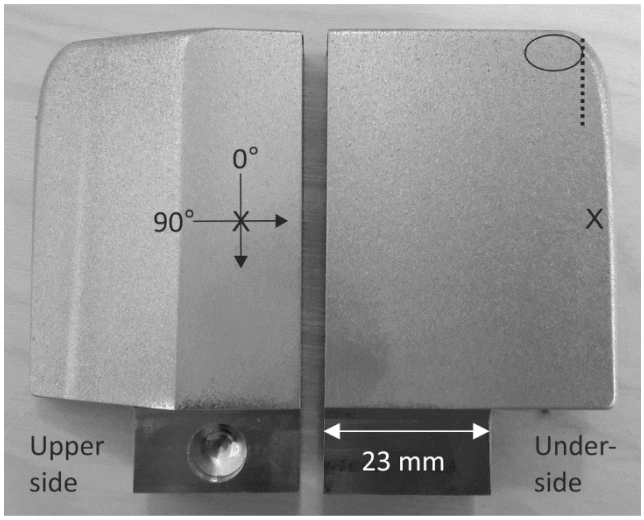

Figure 5.19. Characterization area/location of the wear surface mainly used in this thesis (oval), cross-sectional sample cutting line (dashed line), and residual stress analysis points (X) of the dry-pot samples with the measurement directions.

5.4.2 Profilometry

The topographical features of the wear surfaces were characterized by Alicona InfiniteFocus G5 3D optical profiler. The selected surface texture parameters, the root-mean-square height of the

surface (Sq) and the skewness of the surface (Ssk) within a definition area (A), were determined as [122]:

$$S_q = \sqrt{\frac{1}{A}\iint_A z^2(x,y)\mathrm{d}x\mathrm{d}y} \tag{1}$$

$$S_{sk} = \frac{1}{S_q^3}\left[\frac{1}{A}\iint_A z^3(x,y)\mathrm{d}x\mathrm{d}y\right] \tag{2}$$

Veeco Wyko NT-1100 optical profiler was used to determine the surface roughness [Publication I] and the size and volume of the scratch grooves produced by the pin-on-disc tribometer. The volume loss of the grooves and the cutting-to-plasticity ratio were determined with a Matlab program from the 3D data. The cutting-to-plasticity ratio, φ, was determined as:

$$\varphi = \frac{|V_{neg}| - |V_{pos}|}{|V_{neg}|} \tag{3}$$

where V_{neg} is the negative volume below the original surface of the sample and V_{pos} is the positive volume above the surface.

5.4.3 Hardness testing

Duramin-A300 hardness tester was used for the HV_{10} Vickers hardness determinations. The subsurface micro hardness testing at various load levels was performed with Matsuzawa MMT-X7 micro hardness tester. A mechanical Zwick Vickers hardness tester was equipped with a low temperature system for hardness measurements at temperatures below RT. Fig. 5.20 presents a schematic of the system that enables HV_{10} hardness testing down to -150°C. The indentations were measured afterwards with Leica DM 2500 optical microscope.

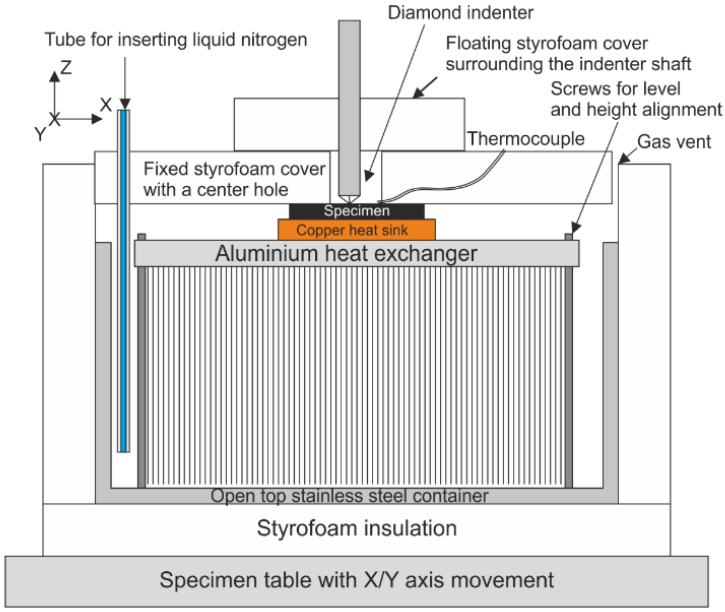

Figure 5.20. Schematic of the low temperature hardness testing system [Publication IV].

5.4.4 Mechanical testing

The mechanical testing of the studied steels was conducted by the steel manufacturer [Publication IV]. The tensile tests were made with a 100 kN MTS servohydraulic testing machine equipped with a low temperature testing chamber. The parallel length of the flat test pieces (L_c) was 70 mm in the low temperature tests and 75 mm in the room temperature tests. The thickness of the test pieces was 5 mm and the width 8 mm. The Charpy v-notch impact tests were made with 300 J nominal energy according to standard SFS-EN ISO 148 [123]. However, the sample size was smaller than specified in the standard, 5 mm x 10 mm x 55 mm, which leads to somewhat lower values. The samples were prepared both longitudinally and transversely to the rolling direction.

5.4.5 Residual stress measurements

The residual stress measurements were done with XStress 3000 x-ray diffractometer using CrKα radiation and the modified χ (chi) method [124]. In steels, the x-ray penetration depth is about 5 µm. The system measures the spacing of the lattice planes that are affected by the residual stresses. The lattice spacing (d) of the sample is measured at different ψ tilts, where ψ is the angle between the normal of the sample and the normal of the diffracting lattice planes. The residual stress is calculated using elastic constants from literature and the slope obtained from a plot of the lattice spacing as a function of $\sin^2\psi$. Table 5.6 lists the measurement parameters.

Table 5.6. Measurement parameters used in the residual stress measurements.

	Unpublished
Case	Cutting edge of mining loader bucket
Measurement directions	0° and 90°
Collimator [mm]	3
ψ tilt angles in one direction (side/side)	6/6
Maximum tilt angle	40°
ψ oscillation	5 °
Radiation	CrKα
Voltage [kV]	30
Current [mA]	6.7
Modulus of elasticity [GPa]	211
Poisson's ratio	0.3

The steel samples were characterized as-machined and between the wear tests with the dry-pot tester. The analysis spots (see Fig. 5.19) were selected so that they were on a flat surface and easy to locate even from a worn-out sample. In addition to surface analysis, depth profiling from the upper sample surface was made using electrolytic polishing with Struers A2 electrolyte for a R500HB and a 500HB dry-pot specimen.

6 Results

This chapter summarizes the main results presented in Publications I-V. In addition, some unpublished results that support and complement the earlier published results will be presented. An unpublished case study of the feed hopper wear plates is also included in the results.

6.1 High-stress abrasion and impact-abrasion in mineral haulage [Publication I]

In this study, the high-stress abrasive and impact-abrasive wear behavior of four steels, S355, 400HB, 450HB, and R500HB were compared using the crushing pin-on-disc, uniaxial crusher, and impeller-tumbler wear test devices. Figure 6.1 presents the wear test results plotted against the nominal ultimate tensile strength R_m and the hardness of the steels. As presented in Fig. 6.1.a, it is possible to compare also quite different test methods, when the wear rate ($WR_{mm/h}$) is determined as the mass loss of the sample (Δm) divided by the wear area (A), contact time (t), and density of the steel (ρ):

$$WR_{mm/h} = \frac{\Delta m}{t \cdot A \cdot \rho} = \frac{\Delta V}{t \cdot A} \quad (4)$$

Another possibility is to normalize the results by the corresponding data obtained for a reference material, as shown in Fig. 6.1b, which reveals the differences between the steels but not between the test methods. This is seen especially in the results of the impeller-tumbler method, i.e., normalizing of the mass loss values leads to bigger differences in the wear rates of the steels. The impeller-tumbler always uses a reference sample in the tests, which largely cancels out the variations between the mineral abrasive loads [16].

Although the highest wear rates were produced by the uniaxial crusher, the crushing pin-on-disc method showed the biggest differences between the wear resistant steels. The impeller-tumbler produced the lowest wear rates and the smallest differences between the steels. While the crushing pin-on-disc and impeller-tumbler test results were quite liner against strength and hardness, the wear rate of the structural steel was in the uniaxial crusher tests relatively much higher. During the uniaxial crusher tests on the wear resistant steels, the wear rates increased quite linearly when plotted against the number of compressions. For the structural steel, however, the wear rate was stabilized only after 500 compressions.

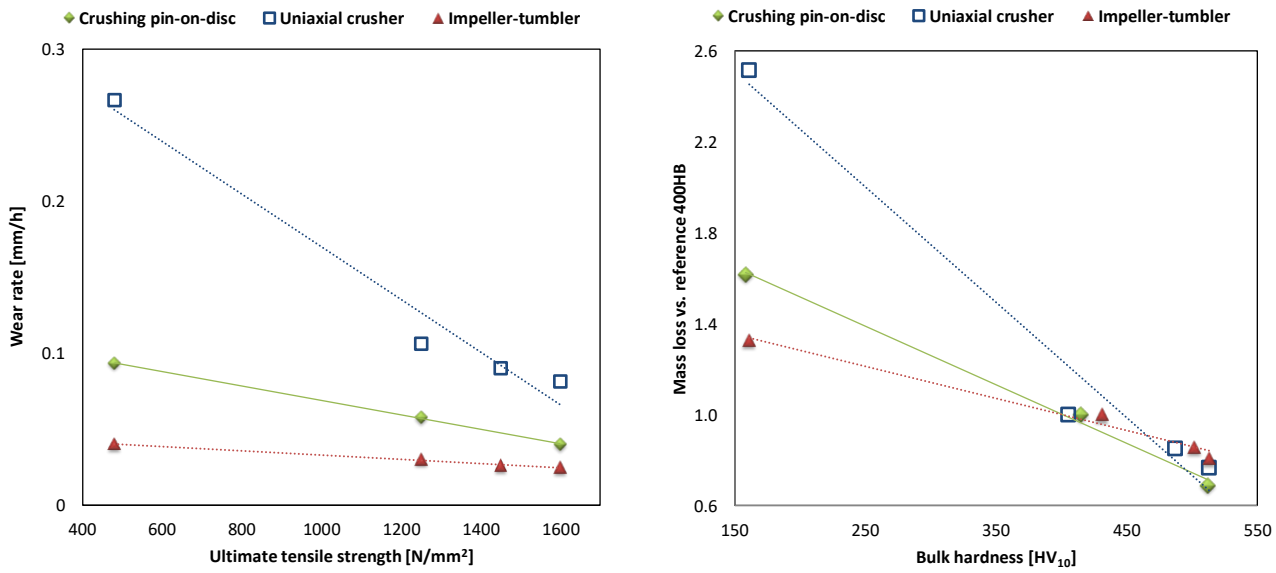

a) *b)*

Figure 6.1. Wear rates of the studied steels in the laboratory tests with Sorila granite a) determined as mm/h and plotted against ultimate tensile strength, and b) mass loss normalized by the 400HB results and plotted against hardness.

In the impeller-tumbler tests, the samples are not in a uniform contact with the abrasive as in the other test methods. However, the true contact area in the impeller-tumbler tests is quite similar to that in the crushing pin-on-disc tests. The impact area in the impeller-tumbler tests was determined from the polished 400HB sample surface, which was tested for two seconds. In that time, about 2.2 % of the sample surface was subjected to impacts. When Fig. 6.2 is compared with Fig. 5.5, which gives a 2.1 % true contact area for a crushing pin-on-disc sample, it can be concluded that the contact conditions are similar enough to justify the comparison of the wear rates as mm/h. However, it should be noted that the impacts are concentrated on the tip of the impeller sample and not on the whole wear area as in the other methods used in this study.

Figure 6.2. Optical profilometer image of a polished 400HB steel sample tested for two seconds with the impeller-tumbler. Scale bar is 5 mm.

6.1.1 Characterization of wear surfaces [Publication I, unpublished]

Clear differences can be observed in the appearance and roughness of the wear surfaces formed in different steels. In general, the surface roughness decreases with increasing initial hardness of the steel. The most distinct scratches were seen on the crushing pin-on-disc tested surfaces, which, on the other hand, exhibited the lowest surface roughness values. Fig. 6.3 shows an example of the wear surfaces brought about by the impeller tumbler tests, which produced the roughest surfaces in the wear resistant steels. The amount of embedded abrasive particles (seen with darker contrast against the lighter steel) was clearly highest on the surfaces of the structural steel S355, and lowest in the hardest steel R500HB. The crushed granite was mechanically mixed with the steel on the wear surfaces through impacts and sliding of the abrasive particles. Marks of cutting and ploughing were most clearly seen on the surfaces of the wear resistant steels. Evidently, the impact angles of the rocks vary, as the sliding marks are not oriented in the direction of the impeller rotation. Overlapping ploughing and impacting cause also surface fatigue, which is seen as cracking of the plastically deformed layers.

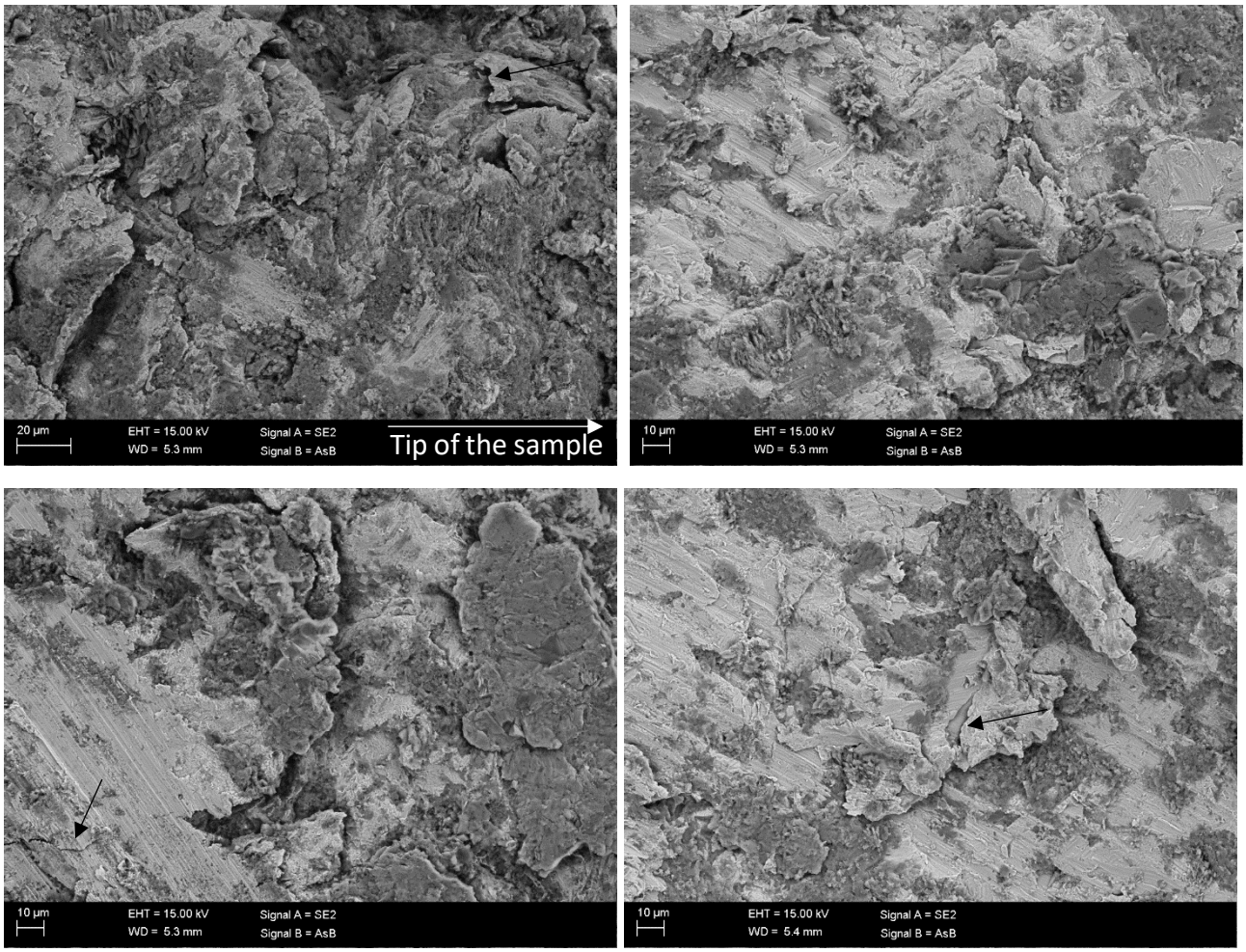

Figure 6.3. SEM images of the 60 minute impeller-tumbler test wear surfaces of a) S355, b) 400HB, c) 450HB, and R500HB. The arrows indicate cracking of the deformed layer.

The case example discussed in Publication I dealt with the wear plates of a dumper truck body and the various operating conditions in loading, haulage, and unloading. However, no actual field tests were done, and just one used piece of a 400HB steel wear plate from a dumper truck body was

received after the publication of the laboratory test results [Publication I]. The operation history of the wear plate is also unknown, and therefore only wear surface and cross-sectional characterization can be used to compare the in-service case with the results of the laboratory tests. The bulk hardness of the wear plate was 423 $\pm$ 3 HV_{10}.

The wear plate was severely deformed by the heavy impacts of the crashing large rocks. The thickness of the plate (when received) was 10 mm, but it was reduced to 8 mm at some points of heavy impacts. Fig. 6.4 shows some of the typical overlapping deep scratches on the surface. Large quantities of embedded rock were also found on the surfaces. The repeated ploughing and cutting of the rocks had also caused surface fatigue, which appears as cracking similar to that found on the impeller-tumbler wear surfaces. However, the scratches were much deeper and longer than produced by any of the used laboratory test methods.

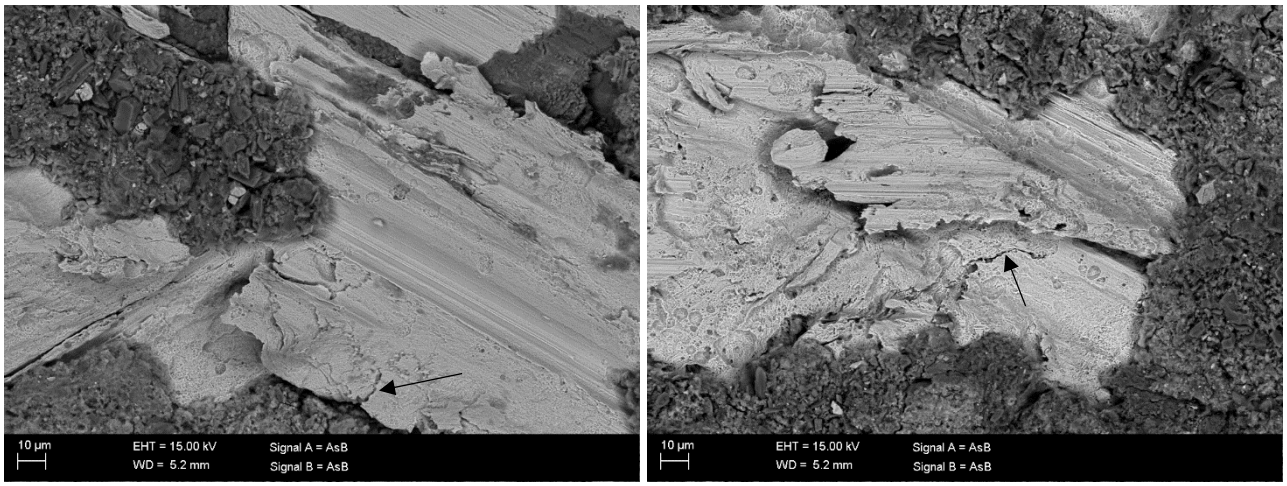

Figure 6.4. SEM images from the wear surface of the tipper body wear plate. The arrows indicate cracking of the deformed layer.

6.1.2 Characterization of the cross-sections of wear surfaces [Publication I, unpublished]

Mechanical mixing of granite abrasives with steel was observed in the surface layers of samples tested with all of the applied methods. Moreover, Fig. 6.5 illustrates the high amount of plastic deformation in the laboratory tested 400HB samples. Occasional sub-surface adiabatic shear bands were observed only in the impeller-tumbler samples. The comparison of the steels revealed that the deformation depth was highest in the S355 samples and lowest in the R500HB steel, as seen for example in Fig. 6.6.

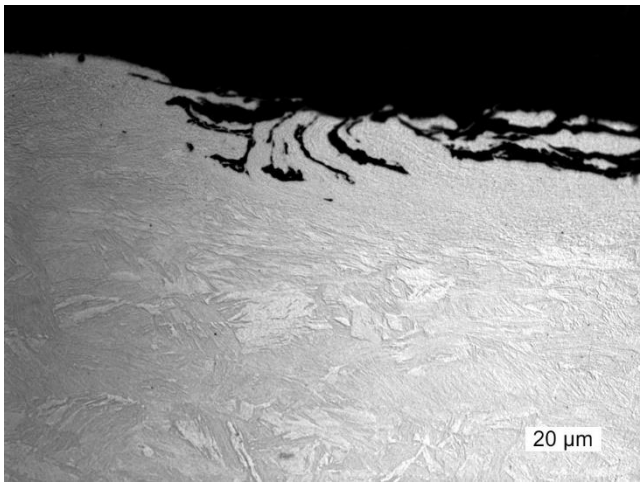

a)

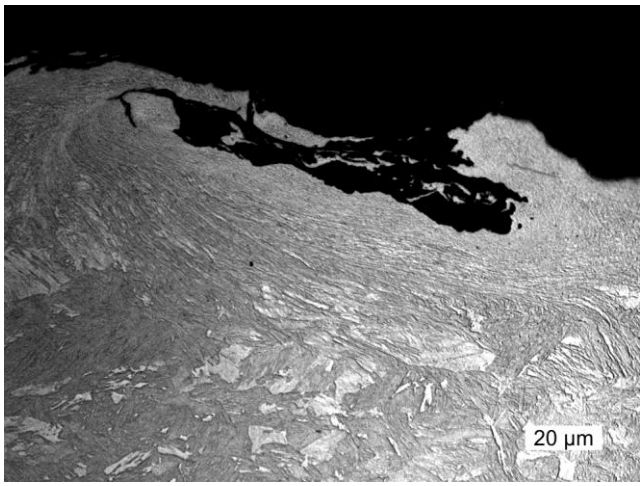

b)

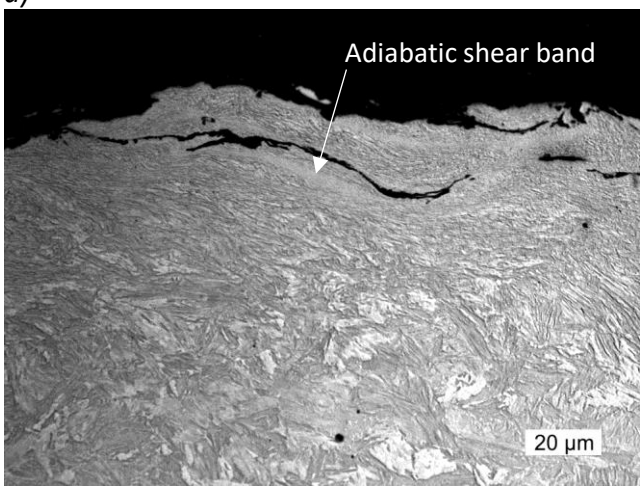

c)

Figure 6.5. Optical micrographs of the wear surface cross-sections of the 400HB steel samples tested with a) crushing pin-on-disc, b) uniaxial crusher, and c) impeller-tumbler.

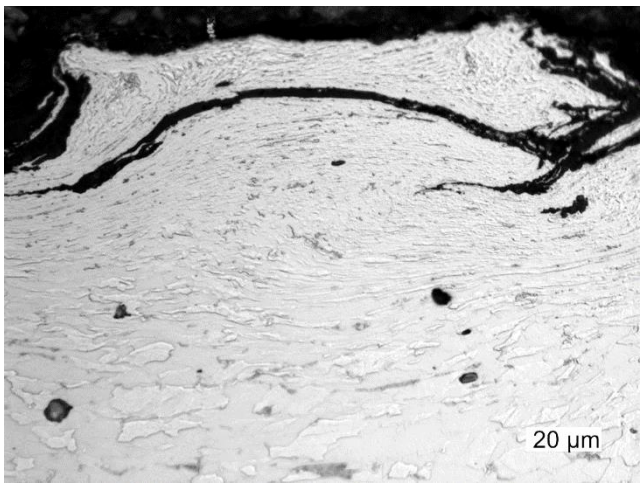

a)

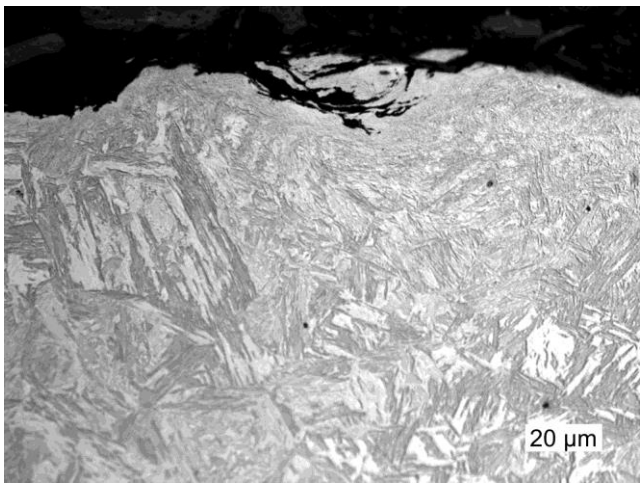

b)

Figure 6.6. Optical micrographs from the cross-sections of the crushing pin-on-disc wear surfaces of a) S355 and b) R500HB.

The cross-sections of the dumper truck wear plate appear to be some kind of a mixture of the cross-sections found in the laboratory test samples. Similar to the impeller-tumbler tests, Fig. 6.7.a shows

the formation of adiabatic shear bands under the wear surface of the wear plate. This kind of sub-surface ASB's indicate very heavy impacts, as presented also by Abbasi et al. [105]. Fig. 6.7.b shows also over 20 µm thick white layers that have been formed on the surface due to high-stress abrasion, in a similar manner as in the cutting edge cases [Publications II & III]. However, this kind of abrasion induced white layers were not observed in the studied laboratory tested samples. In some parts of the dumper truck wear plate, the wear surface was heavily deformed with extensive cracking and delamination (Fig, 6.7.c.), resembling the wear surfaces found after the uniaxial crusher and crushing pin-on-disc tests.

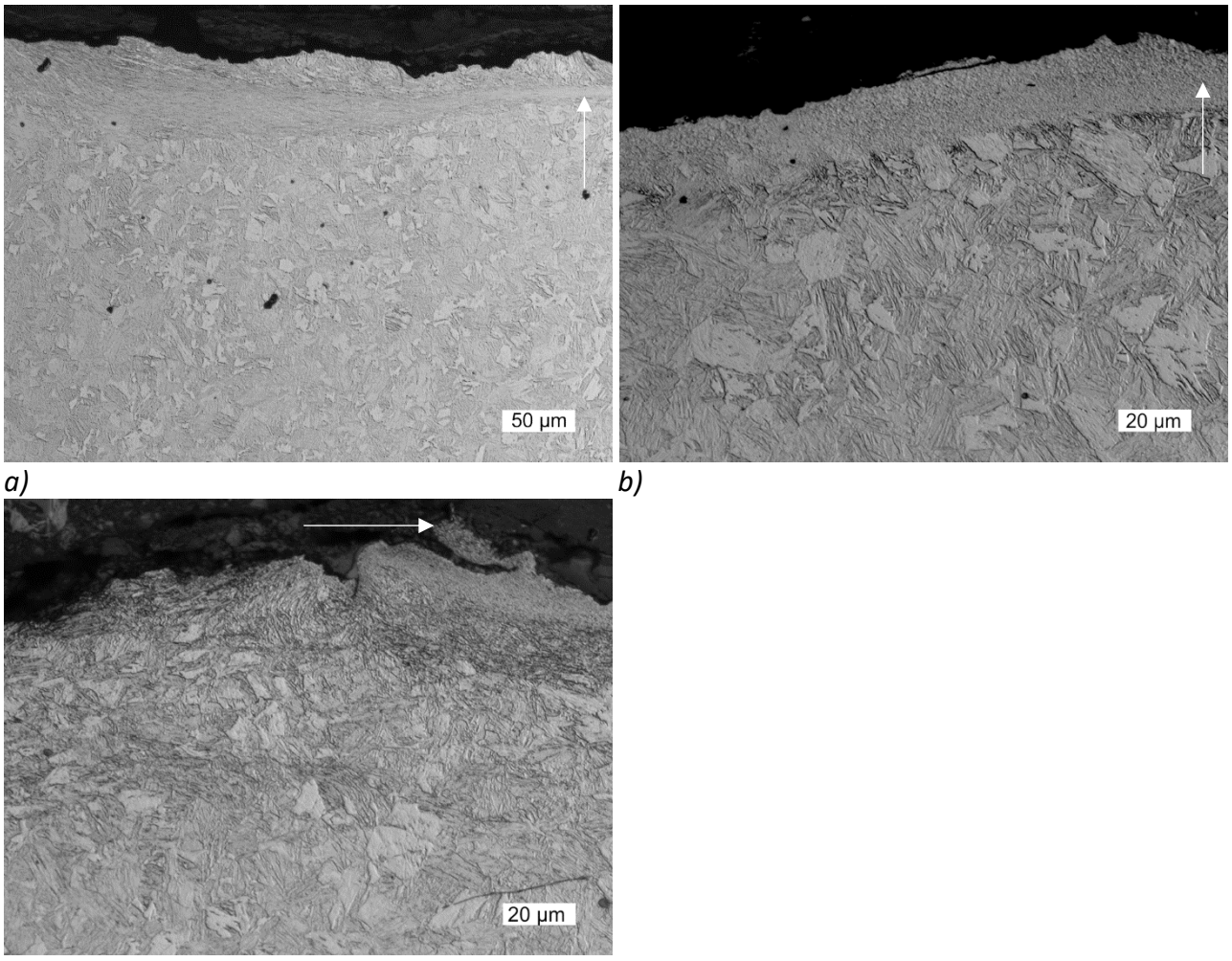

a) *b)*

c)

Figure 6.7. Optical micrographs of the wear surface cross-section of the dumper body wear plate showing a) a subsurface adiabatic shear band, b) a white layer, and c) delamination, as indicated by the arrows in each of the images.

6.2 Cutting edges of mining loader buckets [Publications II & III]

Two different in-service cases of the cutting edges of mining loader buckets were studied and compared with the laboratory wear test results. In the first case [Publication II], the cutting edge was manufactured from the R500HB steel, while in the second case [Publication III] it was welded from two parts made of R500HB and 550HB steels. The first test lasted for 928 hours [120], but the

second one was interrupted after 217 hours because the 550HB steel installation welds were fractured [Publication III]. Fig. 6.8 [120] shows the ATOS 3D scanned images of the R500HB steel cutting edge. The wear was clearly concentrated on the underside of the cutting edge.

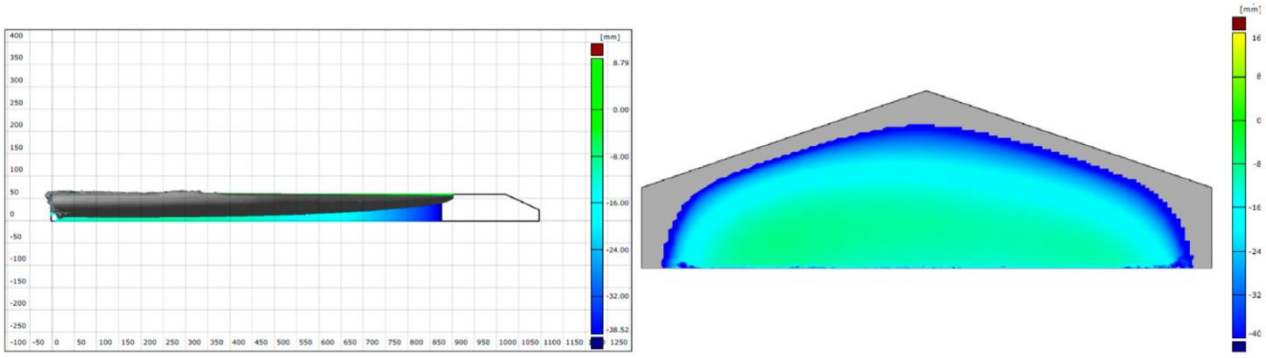

Figure 6.8. ATOS 3D profiles of the cutting edge after 928 h use: a) side view from the middle and b) underside. The original shape is fitted to the images [120].

After the 928 hours of operation, the mass loss of the R500HB steel was about 335 kg [120]. In the 217 h test, the mass loss was 54.95 kg for R500HB and 40.51 kg for 550HB based on ATOS 3D scanning. In the determination of the wear rate, the most challenging part was to evaluate or estimate the actual contact time of the cutting edge with the rock. In the first in-service test, the use of the loader was not followed in detail, thus the contact time was estimated to be 21.5% of the total operation time based on the literature [125]. In the second tests, some videos of the loading stage were taken, and based on them, the contact time (in loading) was estimated to be 25 % of the total haulage process.

There were also challenges in the evaluation of the wear areas, because the wear volumes were very different in the studied in-service cases and in the laboratory tests. Fig. 6.8 shows that most of the wear in the in-service cases was concentrated to the underside of the cutting edge. Moreover, in all three laboratory test methods used in Publication II, there was only one wear surface in contact with the abrasive. Therefore, the contact area was in this case taken as the average worn area on the underside of the cutting edge only. In Publication III, instead, the in-service wear rate was correlated to the wear test results of the dry-pot samples with a profile of a cutting edge, thus experiencing abrasion in both sides of the specimen similar to the in-service sample.

6.2.1 Laboratory wear test results

The study on the relevance of different laboratory test methods for the simulation of the wear of the cutting edges in mining conditions was made by comparing seven test procedures using four different test systems. Fig. 6.9 summarizes the test results for the 400HB, R500HB, and 500HB steels in the laboratory and in the mine. As discussed earlier, the wear rates in the in-service operations are only estimates and therefore not straightforwardly comparable to the laboratory test results. The highest wear rates, which were also closest to the wear rate estimates for the in-service conditions, were produced by the dry-pot tester ran at 500 rpm for 60 min.

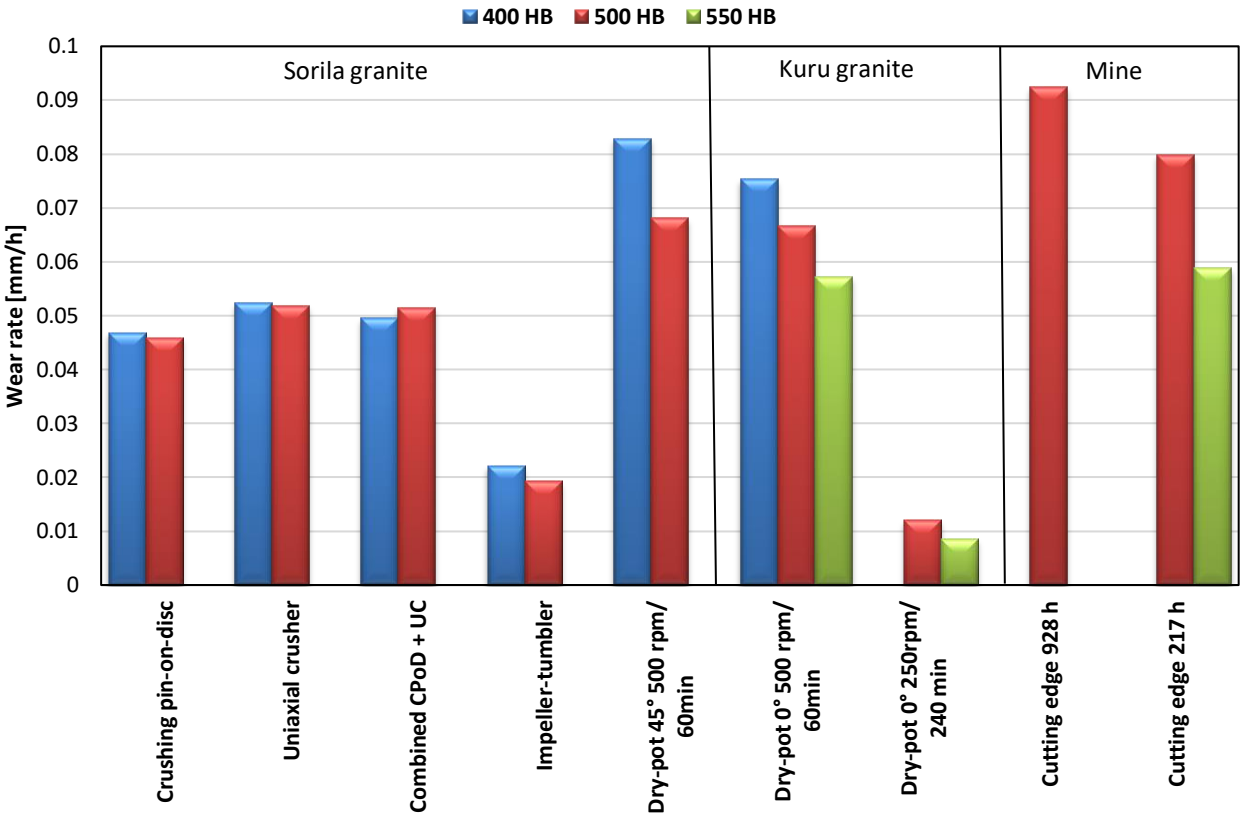

Figure 6.9. Summary of the wear rates of the 400HB, R500HB, and 550HB steels in the in-service operation as cutting edges and in the laboratory tests with Sorila granite [Publication II] or Kuru granite [Publication III].

When the test speed in the dry-pot tests is increased, the differences in the wear rates between the steel grades decrease exponentially. Fig. 6.10.a illustrates the effect of the speed at the tip of the sample with Kuru granite. In the tests at 250 rpm for 240 min, where the tip speed was 2.5 m/s, the differences between the tested steels were quite similar as in the in-service conditions. Fig. 6.10.a shows also the effect of the used abrasive. It indicates that the two granites and chromite give a similar difference (i.e., 23-29 %) with the in-service test for the reduction of the wear rate when R500HB is replaced by 550HB, whereas with quartzite the reduction is only 12-13%.

Fig. 6.10.b shows the mass loss of the R500HB and 500HB samples plotted against the abrasiveness values obtained from the LCPC tests. Quartzite with the highest abrasivity produces the highest wear rates and chromite the lowest. Although the LCPC test is quite similar to the dry-pot test method, the values deviate markedly in the case of Sorila granite, which produced much lower wear rates than could be expected based on the LCPC abrasivity value. In the LCPC tests, the used steel was a low hardness structural steel and the tip speed was higher (11.8 m/s) than in the dry-pot tests (2.5-5 m/s). Thus, the wear mechanism in the LCPC test is more impact-abrasive than abrasive, and in such conditions structural steels behave differently compared to wear resistant steels, as discussed in Chapter 6.1. This should be noted when the LCPC results are utilized in the evaluation of the wear behavior of wear resistant steels.

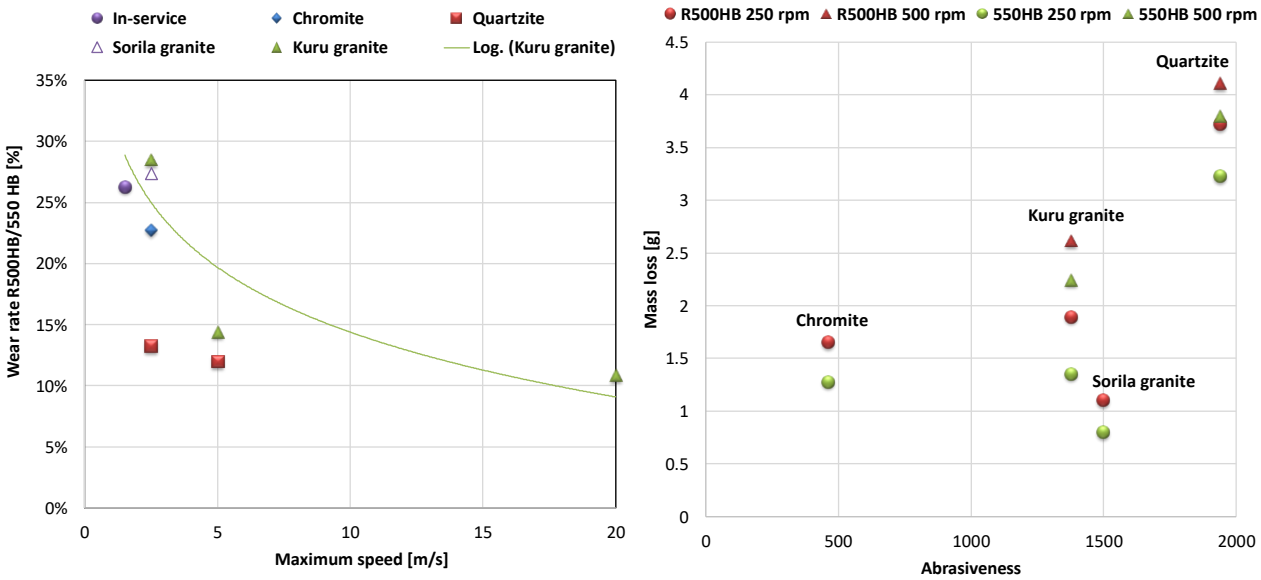

a) *b)*

Fig. 6.10. a) Reduction of the wear rate when R500HB is replaced by 550HB in the in-service conditions and in the dry-pot laboratory tests with different abrasives and test speeds, b) mass loss values of the R500HB and 550HB samples tested with dry-pot at 250 rpm/240 min and at 500 rpm/60 min plotted against the abrasiveness of the test minerals.

6.2.2 Characterization of wear surfaces

The wear surfaces of the cutting edges showed clear marks of high-stress abrasion. Figs. 6.11 and 6.12 show 3D and 2D optical profilometer images of the cutting edge samples after 217 and 928 hours of operation, respectively. The brown area in the 2D images is an oxidation layer including also some embedded rock. The scratches are several millimeters long, and in the laboratory tests only chromite ore produced similar long scratches. Fig. 6.13 shows an example of the R500HB reference steel wear surfaces tested for 240 minutes at 250 rpm, illustrating well the differences in the wear surfaces created by different abrasives. When very small areas, such as in Figs. 6.12 and 6.13.a, are compared, the surface features look surprisingly similar. Although quartzite produced the highest wear rates in the dry-pot tests, the length and width of the scratches were smallest when using this abrasive. High amounts of embedded rock can be seen on the surfaces tested with both granites, but the clusters are larger and thicker in the samples tested with Sorila granite.

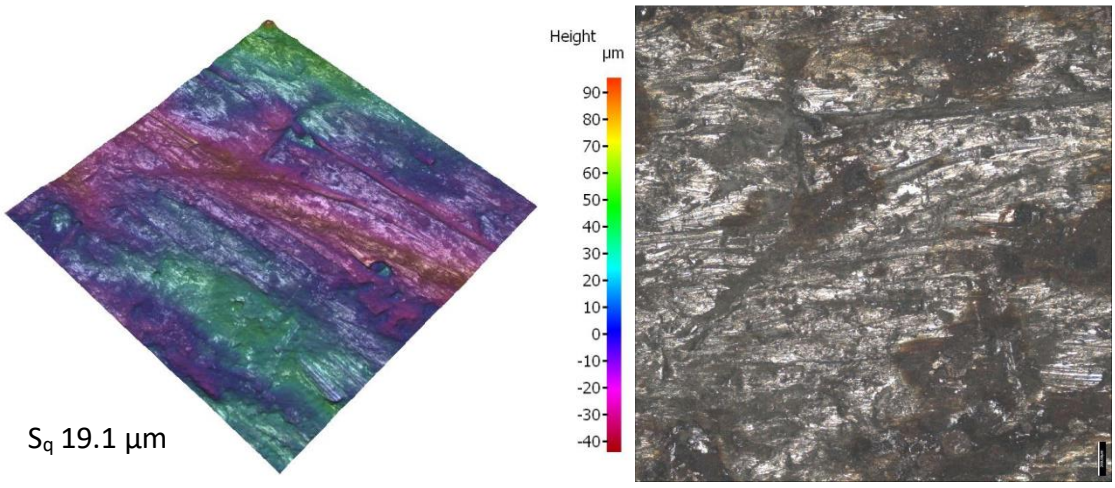

S_q 19.1 µm

a)

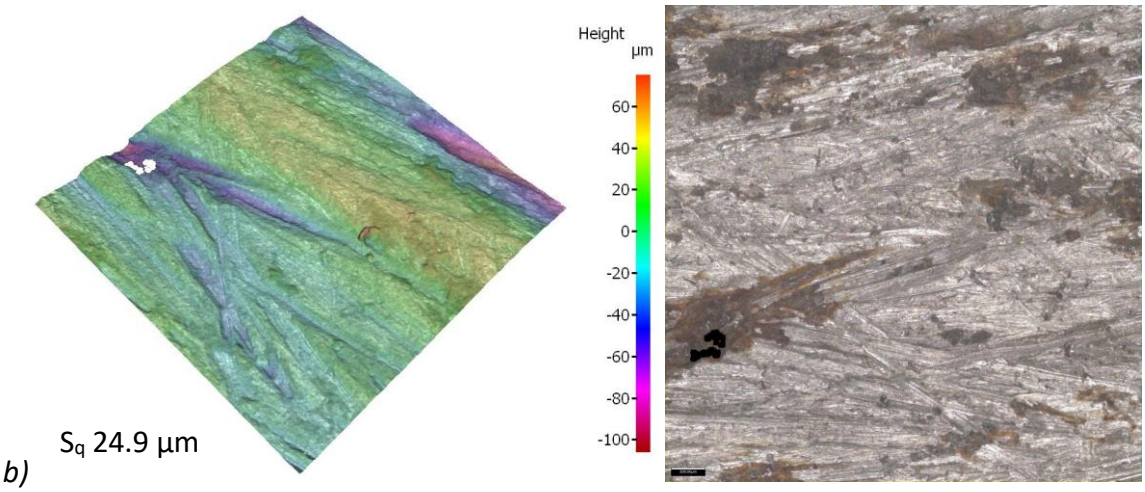

Figure 6.11. Optical profilometer images of the cutting edge samples after 217 h of use, a) R500HB and b) 550HB. Image area 2.8 mm x 2.8 mm, scale bar 200 µm.

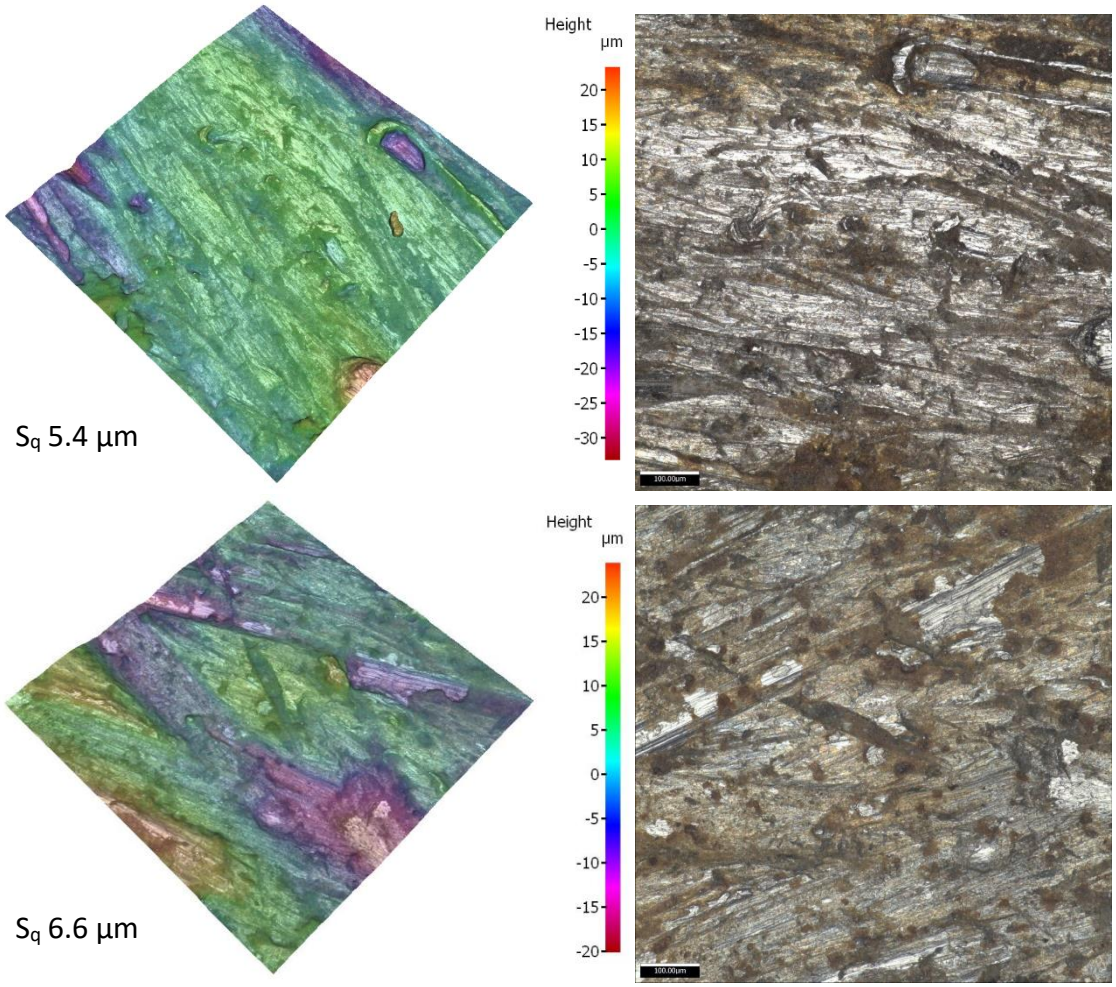

6.12. Optical profilometer images of the underside of the R500HB cutting edge sample after 928 h of use. Image area 0.8 mm x 0.8 mm.

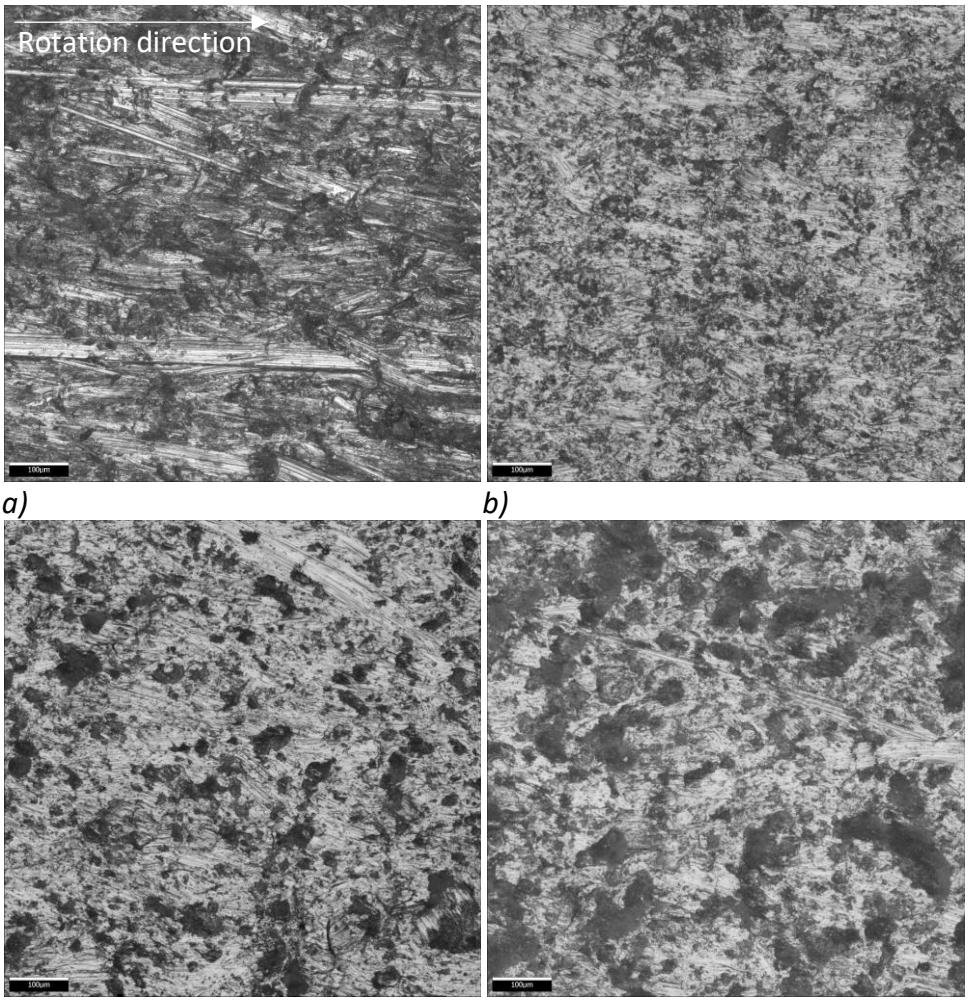

Figure 6.13. Optical profilometer images of the R500HB reference steel sample surfaces tested for 240 minutes at 250 rpm with a) chromite, b) quartzite, c) Kuru granite, and d) Sorila granite. Image area 0.8 mm x 0.8 mm.

In addition to optical imaging, also the surface roughness values were determined from the 3D optical profilometer data. From each sample, an area of 3 mm x 3 mm was scanned with a 20x objective close to the tip of the sample, as shown in Fig. 5.19. Fig. 6.14 presents the root-mean-square height of selected area (S_q) and skewness (S_{sk}) values for the steels tested with dry-pot for 240 minutes at 250 rpm using chromite, quartzite, Kuru granite, and Sorila granite. The wear surface roughness decreased quite clearly with increasing steel hardness. The 600HB sample surfaces had the smoothest surfaces with all abrasives, which is a clear indication of the very limited plastic deformation of this hard and strong steel. Chromite as an abrasive produced the roughest wear surface, while the quartzite tested surfaces were much smoother, as seen also in Fig 6.13. Although chromite is comminuted heavily during the tests, it produced the most well defined scratches. The effect of scratching can also be seen in Fig. 6.10.b as negative skewness values, which means that the surface roughness is more biased to the underneath of the plane level. On the other hand, the positive skewness values in the case of surfaces tested with granite are caused by the embedded rock on the wear surfaces. Especially Sorila granite formed large rock clusters on the wear surfaces, which resulted in the high positive skewness values seen in Fig. 6.14b. The skewness values did not depend on the hardness of the steel.

The roughness values of the wear tested surfaces were much lower compared to the in-service samples. When the measurements were made with similar parameters, the root-mean-square height of a 3 x 3 mm area was on average 15.1 µm after 928 h and 23.8 µm after 217 h for the R500HB steel. Naturally, the scatter in the surface roughness values and in the length of the scratches was much higher in the in-service wear surfaces than in the dry-pot tested samples.

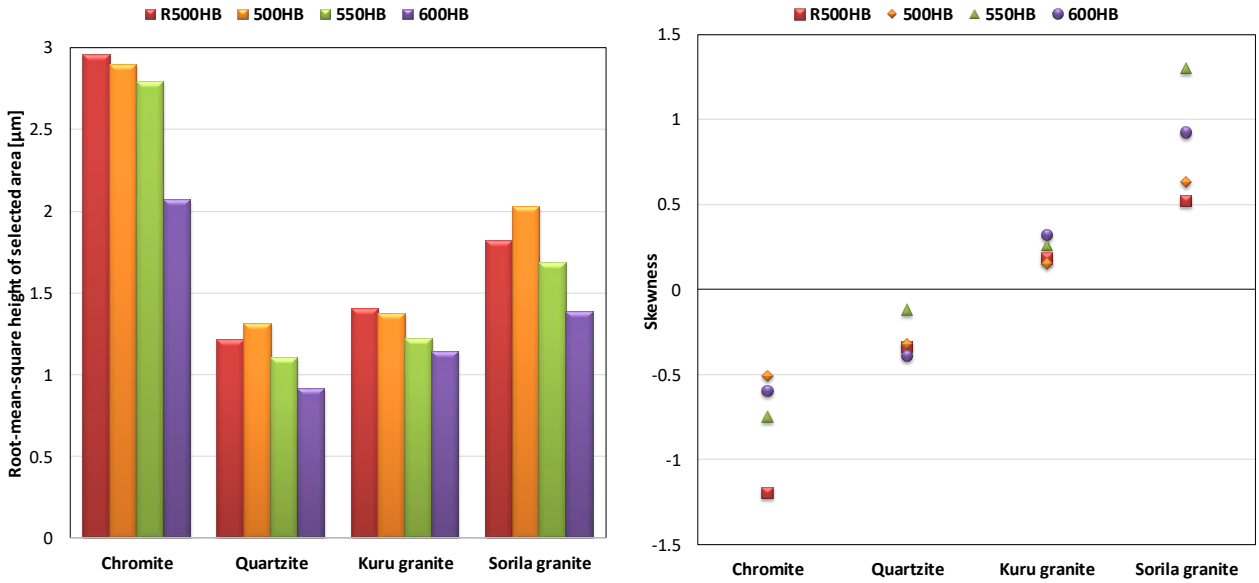

a) *b)*

Figure 6.14. Roughness parameters determined from the 3D profiler data: a) root-mean-square height of selected area and b) skewness.

6.2.3 Characterization of the cross-sections of wear surfaces

In the microscopic studies of the wear surface cross-sections, white layers were frequently found from the in-service cutting edge samples. They were thinner on the upper sides of the plates, up to 50 µm in thickness, but even up to 150 µm thick on the underside. Figures 6.15 and 6.16 show examples of the white layers in a 550HB in-service sample. It was very typical that the white layers were cracked and fractured. The measured hardness of the white layers was up to 790 HV, which means that they had lost much of their ability to deform under high-stress abrasion. However, Fig. 6.16 shows scratches on top of the white layers, which means that their deformation ability was not completely lost. Below the white layer, there was typically another layer sometimes called a 'dark layer' [37], which was softer than the bulk steel. In many occasions, this layer was observed to stop the growth of the cracks initiated in the hard white layer, as shown in Fig. 6.15.b.

Occasional white layers were formed also in the dry-pot tests especially at the outer corners of the samples, as seen in Fig. 6.17. The other applied laboratory test methods did not create as clear white layers as the dry-pot tests. In the dry-pot tests at 500 rpm for 60 minutes, the 5-10 µm thick white layers also started to crack in a similar manner as observed in the in-service samples. However, in the 250 rpm tests with quartzite as abrasive, the formed layers were thicker, up to 25 µm, and thus closer to the observed thicknesses in the in-service cutting edges. However, the hardness of the white layer was the same in both R500HB and 550HB steels and consequently, the formation of a uniform white layer may partly explain the observed small differences between the wear rates of these steel grades in the dry-pot tests with quartzite.

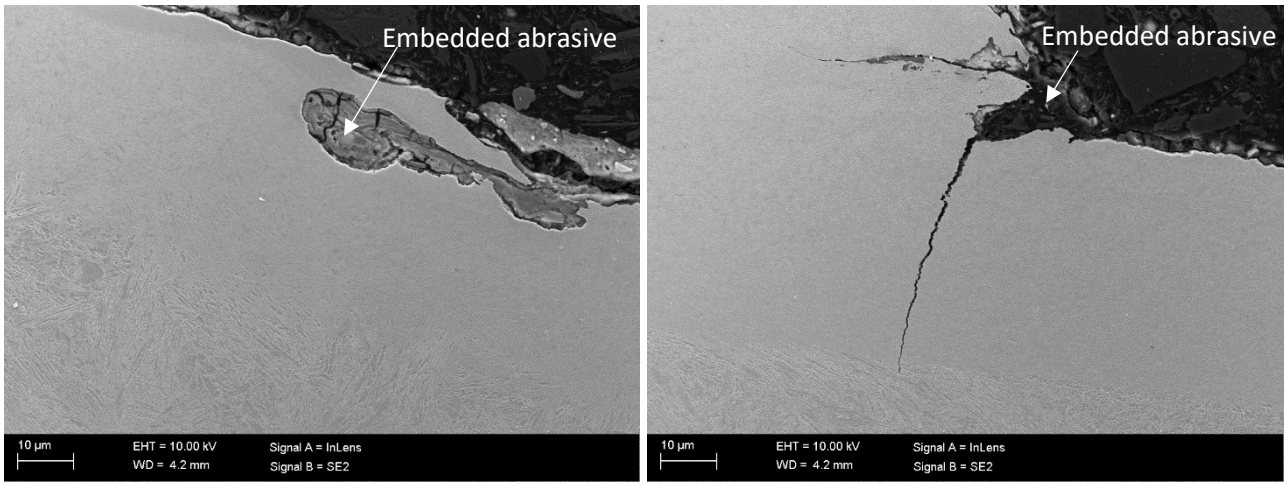

a) *b)*

Figure 6.15. FEG-SEM cross-sectional images of white layers in the 550HB in-service sample.

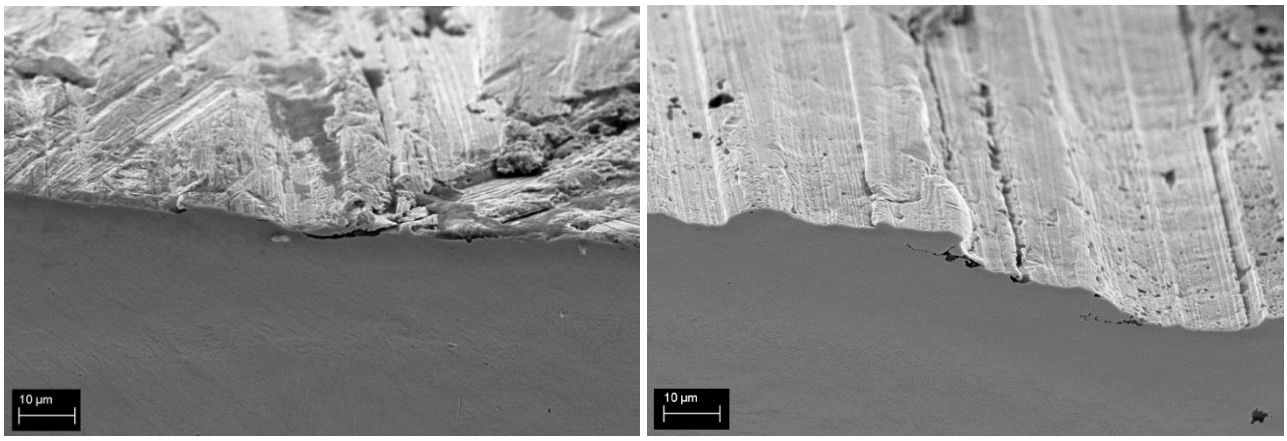

a) *b)*

Figure 6.16. FEG-SEM images of tilted cross-sections of the 550HB in-service sample showing white layers and the wear surface above them.

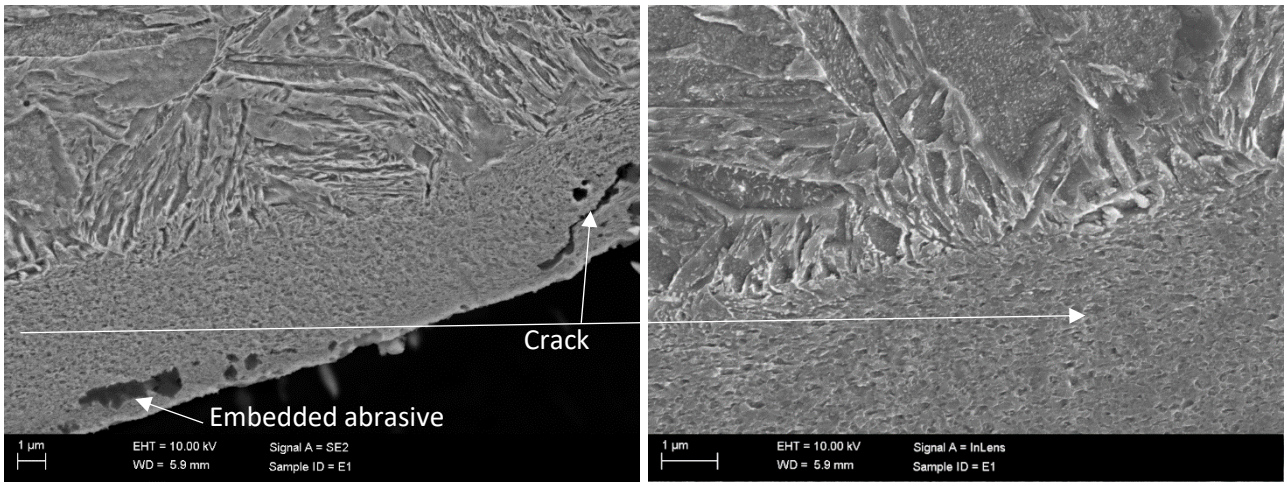

a) *b)*

Figure 6.17. FEG-SEM cross-sectional images of a white layer in the 550HB dry-pot sample tested at 500 rpm for 60 min with quartzite.

6.2.4 Scratch tests [Unpublished]

A scratch test contains and describes the main events that occur in abrasion between a single abrasive asperity and the steel surface. In a well-performed scratch test, the test environment can be controlled very precisely, including the amount of loading and type of contact. In addition, from such a test it is possible to extract many important parameter values, such as the friction coefficient of the contact pair. The scratch testing is widely used for wear testing of steels [126–129]. In this study, the scratch tests were used to study the initial stages of abrasive wear at different loads, and the obtained results were also compared with the in-service condition observations. In this chapter, a detailed study for the R500HB steel is presented, but an overall comparison to other steels has been published already earlier [22].

Fig. 6.18.a presents the results of scratch tests conducted at four different load levels and multiple cycles together with the hardness values of the grooves determined after the tests. As seen, the volume loss normalized by the sliding distance increases notably with increased normal load. The surface hardness at the groove bottoms saturate at 80 N to a little above 700 $HV_{0.2}$, which is close to the hardness values of the white layers in the cutting edges [Publication III]. The cross-sections of the grooves produced at the normal force of 80 N revealed very thin white layers, which also started to delaminate after 10 cycles, as seen in Fig. 6.19.d. The hardening depth in the grooves was over 100 µm.

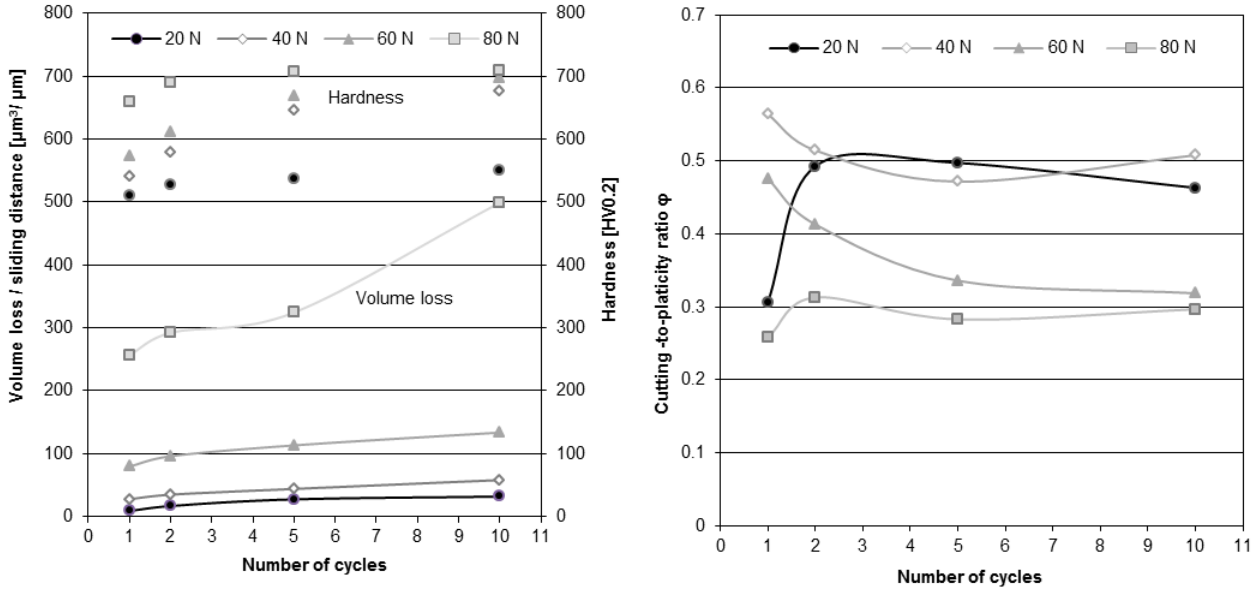

a) *b)*

Fig. 6.18. Results of the scratch tests of R500HB at four normal loads showing a) volume loss per sliding distance and surface hardness at the groove bottom and b) cutting-to-plasticity ratios as a function of overlapping cycles.

The width of the single scratches varied from 43 µm at 20 N to 206 µm at 80 N, which means that the Rockwell indenter produces wider scratches than the rocks in the in-service conditions. Fig. 6.18.b illustrates the abrasion mechanisms in the steel in terms of the cutting-to-plasticity ratio. The closer the φ value is to unity, the higher is the amount of material that has been cut off. At low normal loads, φ value is higher due to the minor formation of ridges. At higher loads, the plastic flow and ploughing of the material into the ridges beside the groove will increase due to the

increasing penetration of the indenter, decreasing the φ value. However, the precise shape of the ridge in the case of cutting is quite difficult to measure accurately with a profilometer, and therefore there may uncertainties in the determination of the φ value [130]. Figs. 6.19.a and b are examples of the large ridges that were formed on the sides of the groove at the 80 N normal load. In a finer scale, similar features are also visible on the wear surfaces of the in-service cutting edges. When this kind of ridges are exposed to further abrasion, they are easily removed during the subsequent loading cycles. This was also seen as an increase in the wear rate when multiple cycles where applied at the same track at 80 N. At 20 N, the tip produced a barely visible and a much narrower scratch compared to that at 80 N, as seen in Fig. 6.19.c.

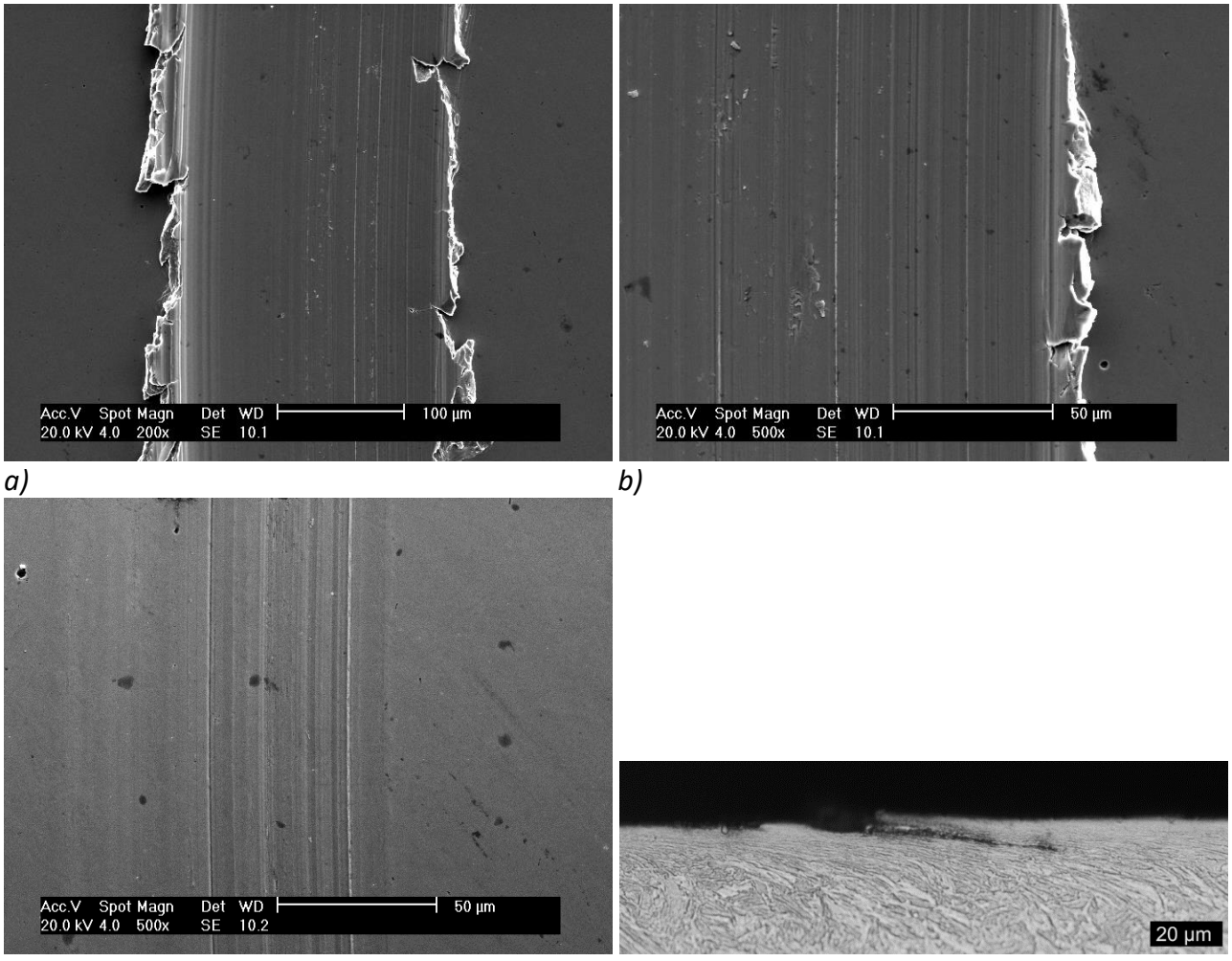

a) *b)*

c) *d)*

Fig. 6.19. SEM images from the wear surface of a single scratch test at a-b) 80 N and c) 20 N normal force, and d) optical micrograph of the cross-section in the sliding direction from the sample tested at 80 N for ten cycles.

6.2.5 Residual stress measurements [Unpublished]

Depth profiling of the residual stresses was made for the upper side of the machined, cutting-edge shaped R500HB and 500HB dry-pot test samples (see Fig. 5.19). The surfaces of the samples were in tension, but below the surface, the stresses were compressive. The compressive region was deeper in the tested 500HB sample compared to the R500HB sample, as seen in Figure 6.20. The full width at half maximum (FWHM) values followed the residual stress curves. For R500HB, all

measured values stabilized between 200…300 µm, but for 500HB with clearly higher surface stresses, similar stabilization took place only after 400 µm. The variation of the residual surface stresses in the machined surfaces of several tested R500HB steel samples was quite large, from -100 MPa to 370 MPa, but mostly the values were clearly positive, i.e., on the tensile side.

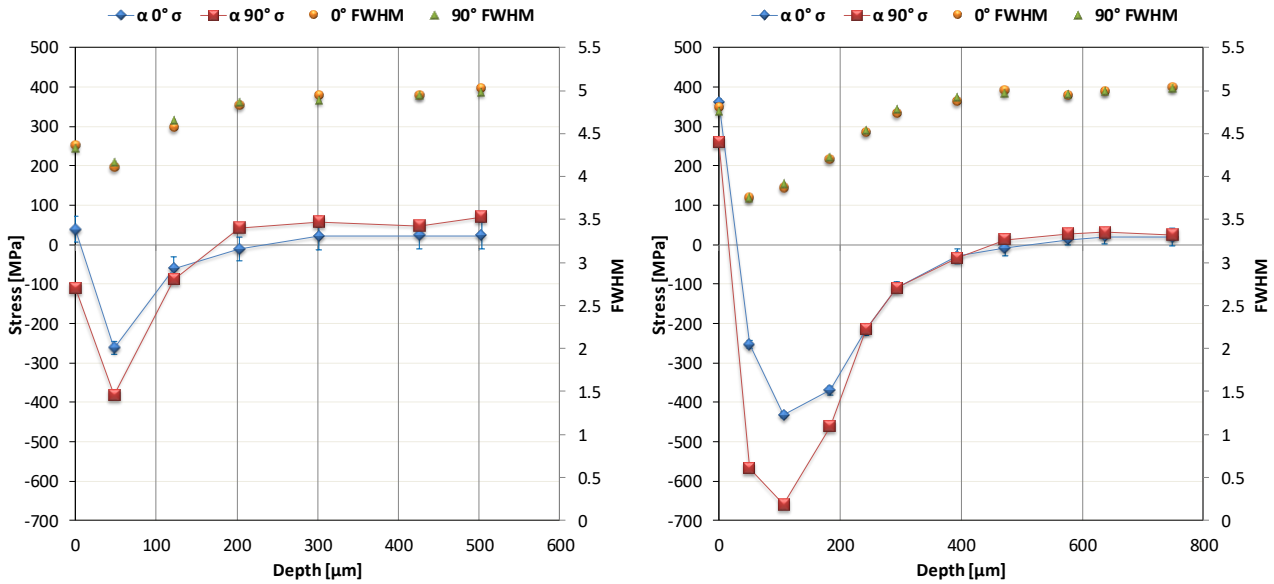

Figure 6.20. Depth profiles of the residual stresses and FWHM values in machined a) R500HB steel and b) 500HB steel samples.

The wear tests with dry abrasives were forming similar compressive stresses on the sample surfaces as shot peening. Fig. 6.21 presents residual stresses on the upper and lower wear surfaces of R500HB and 500HB samples tested with Kuru granite for 60 minutes at 500 rpm. In both samples, the residual stresses stabilized to the compressive (negative) side after 30 minutes of testing. Although the residual stress levels in the steels were different in the machined state, the stress values were quite similar after the dry-pot tests. Although wear was more intensive on the underside of the samples, the compressive residual stress values were quite similar on both sides of the samples.

Fig. 6.22 compares the compressive/tensile residual stress changes on the underside wear surfaces of one 400HB and three R500HB samples tested with quartzite. The good repeatability of the tests is evident. Moreover, the values stabilize at the same levels as in the tests with Kuru granite. It therefore can be concluded that regarding residual stresses, there is no clear difference between the tests using quartzite or Kuru granite as an abrasive. However, the appearance of the wear surfaces is different, as discussed already earlier. Fig. 6.23 shows that quartzite tends to cut the wear surface more, while more embedded and mechanically mixed rock is found on the wear surfaces tested with Kuru granite.

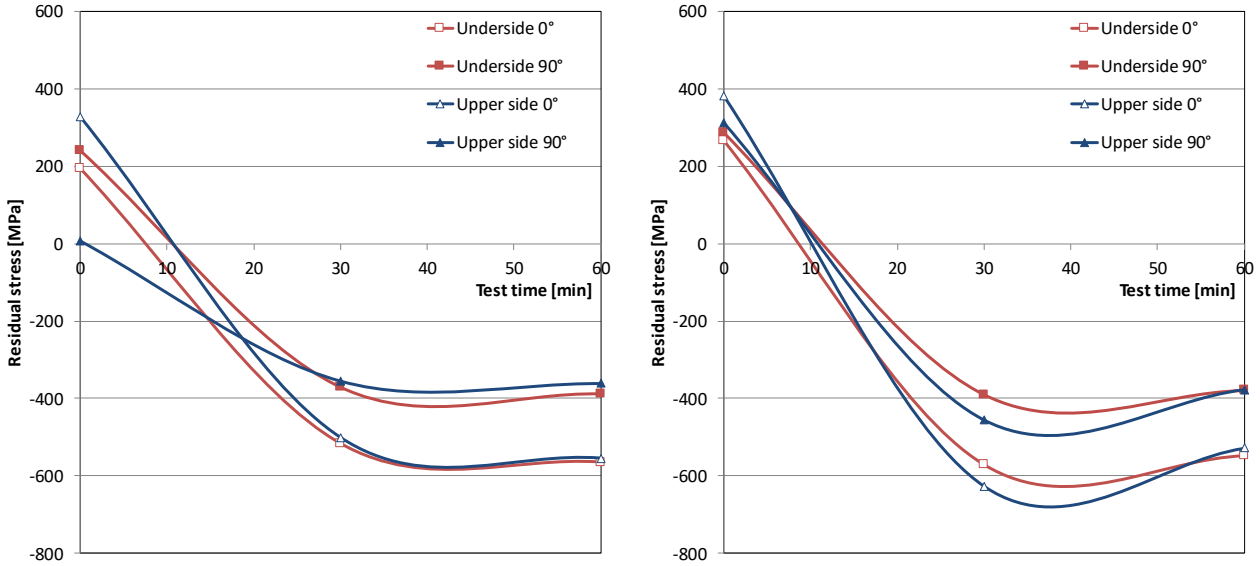

a) b)

Figure 6.21. Residual stresses on the upper and lower surfaces of a) R500HB and b) 500HB samples tested with Kuru granite for 60 minutes at 500 rpm.

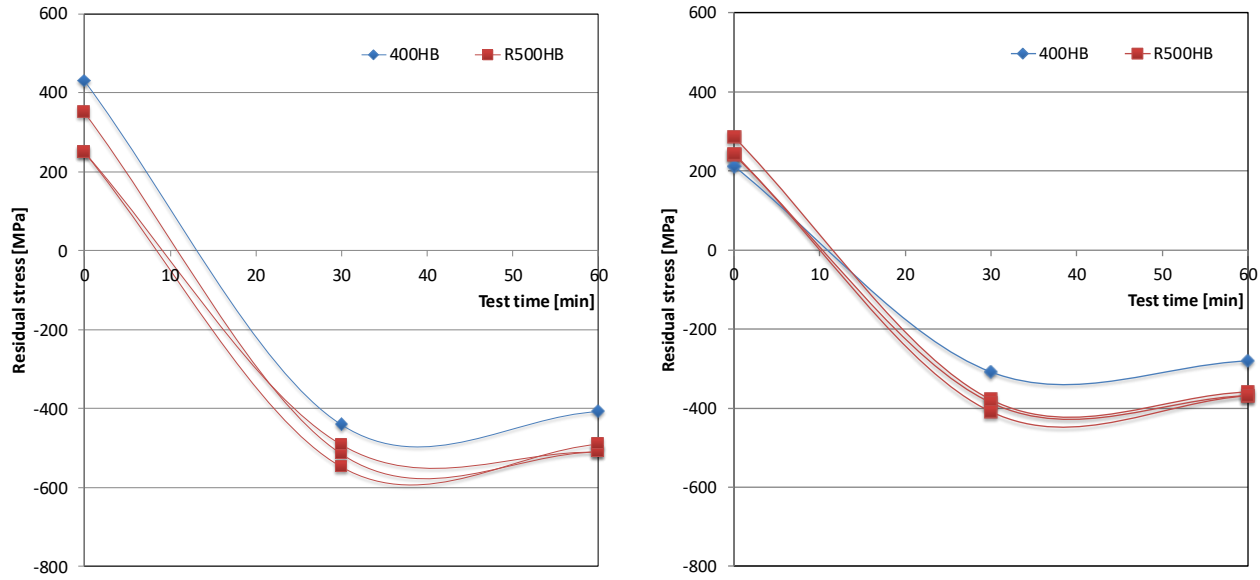

a) b)

Figure 6.22. Residual stresses a) at 0° measurement angle and b) at 90° measurement angle on the undersides of 400HB and R500HB samples tested with quartzite for 60 min at 500 rpm.

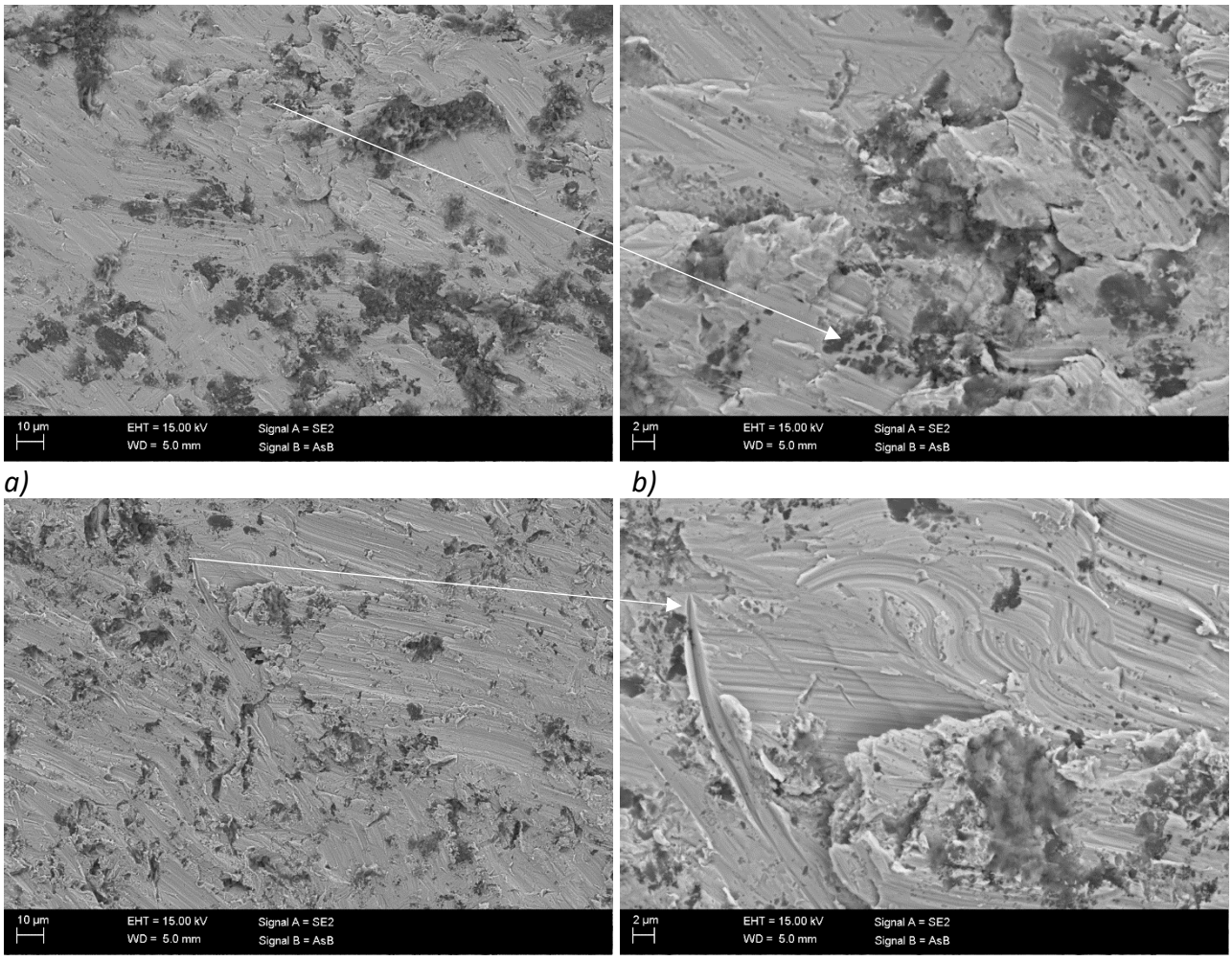

a) *b)*

c) *d)*

Figure 6.23. FEG-SEM images from the residual stress measurement points on the underside of the R500HB samples tested with dry-pot at 500rpm for 60 minutes with a-b) Kuru granite and c-d) quartzite.

6.3 Wear plates of feed hopper [Unpublished]

Wear of the feed hopper side plates was tested in the laboratory and compared to the in-service samples. During 13 weeks in a chromite mine, the mass loss of the wear plates was 4.18 kg for the R500HB plate and 3.65 kg for the 600HB plate. The flow of the chromite ore over the plates formed a deep cavity at the point, where the ore hits the plates when dropped from the feeder. Fig. 6.24 illustrates the gradient wear behavior of the feed hopper wear plates.

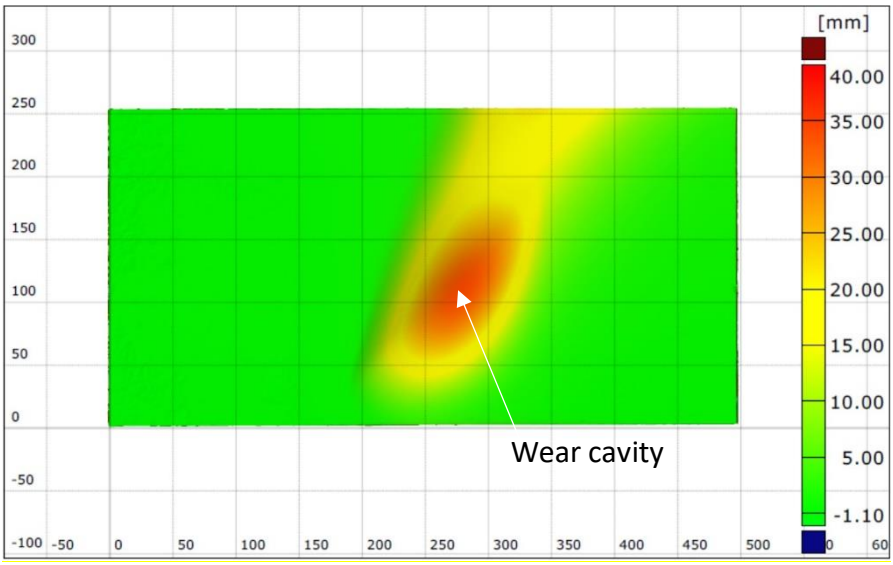

Figure 6.24. ATOS scanned image of the R500HB feed hopper wear plate (by courtesy of Jukka Joutsenvaara and Heidi Kalliosalo, Lapland University of Applied Sciences).

The dry-pot tests were done using a rotational speed of 250 rpm and a 240 min test time similar to the studies of the cutting edges, but now the sample was a plate and tilted to an angle of 45°. In the crushing pin-on-disc tests, the comparison was made using two in-house standards. In the first case, the disc had a similar hardness as the pin sample, while in the second case, the disc was made of a softer S355 steel and the normal force was a little bit higher. The abrasive in the dry-pot tests was Kuru granite and in the crushing pin-on-disc tests Sorila granite, which has been used as an in-house standard abrasive. Fig. 6.25 presents the results of the laboratory wear tests on the 400HB, R500HB, and 600HB steels using two testers and three test procedures. The short test time in the crushing pin-on-disc tests produces quite low mass losses, but when the results are presented as $WR_{mm/h}$, the differences between the test methods are smaller. The highest wear rates are produced by the CPOD with a softer disc material. The wear rates of the wear plates of the feed hopper in the in-service conditions were relatively small, when the whole plate area is used in the calculation. However, the maximum wear depth was 34.05 mm in the R500HB plate and 26.48 mm in 600HB plate. This deepest point of the wear cavity seen in Fig. 6.24 naturally defines the wear life of the wear plates. The wear rates at that point are shown in Fig. 6.25.b as in-service (max) wear rates, and they appear to be very close to the values produced by the 250 rpm/240 min dry-pot tests.

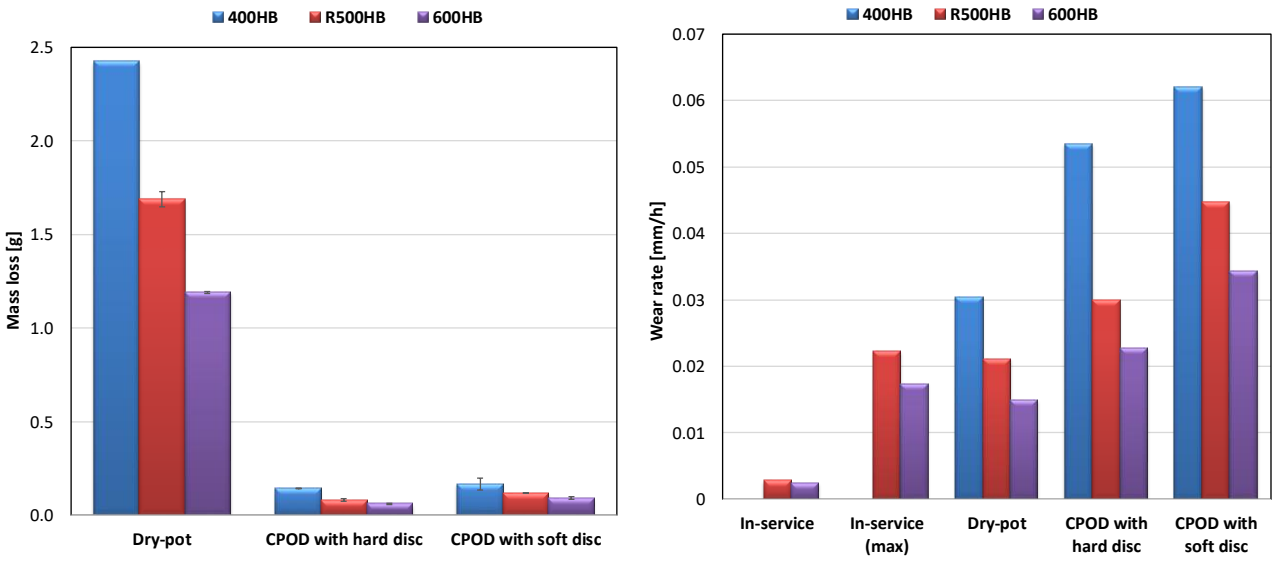

a) *b)*

Figure 6.25. Results of the laboratory wear tests and the in-service wear data, showing a) absolute average mass loss and b) average wear rate ($WR_{mm/h}$). The error bars represent the standard deviation.

A typical way of comparing the wear rates [4,131] is to normalize the measured mass loss (Δm) by the corresponding reference material data, as presented in Fig. 6.26.a and determined as:

$$WR_{ND} = \frac{\Delta m_{600HB}}{\Delta m_{R500HB}} \tag{5}$$

The direct normalization (WR_{ND}) results indicate that the crushing pin-on-disc tests simulated the wear in the feed hopper better than the dry-pot method, which lead to the biggest difference between the steels. Fig. 6.26.b, in turn, shows *how much lower* (in percent) the wear rates of the 600HB steel samples were compared to the R500HB samples, determined as:

$$WR_{N\%} = \frac{\Delta m_{R500HB} - \Delta m_{600HB}}{\Delta m_{R500HB}} \cdot 100\% \tag{6}$$

Although the two presentations in Fig. 6.26 may look quite different (partly due to scaling), it should be noted that they are directly related, as:

$$100\% \cdot WR_{ND} = 100\% - WR_{N\%} \tag{7}$$

Which one of the above presentations is better depends on what aspects one wishes to emphasize: the direct normalization is a more common way to present and compare the wear test results, but the percent normalization ($WR_{N\%}$) shows directly how much longer the 600HB steels would last in the application compared to the R500HB steel. Both of these ways are applicable for comparing the wear rates of steels, but as indicated already in Chapter 6.1, the $WR_{mm/h}$ value (used in Fig. 6.25.b) shows better the differences between the test methods.

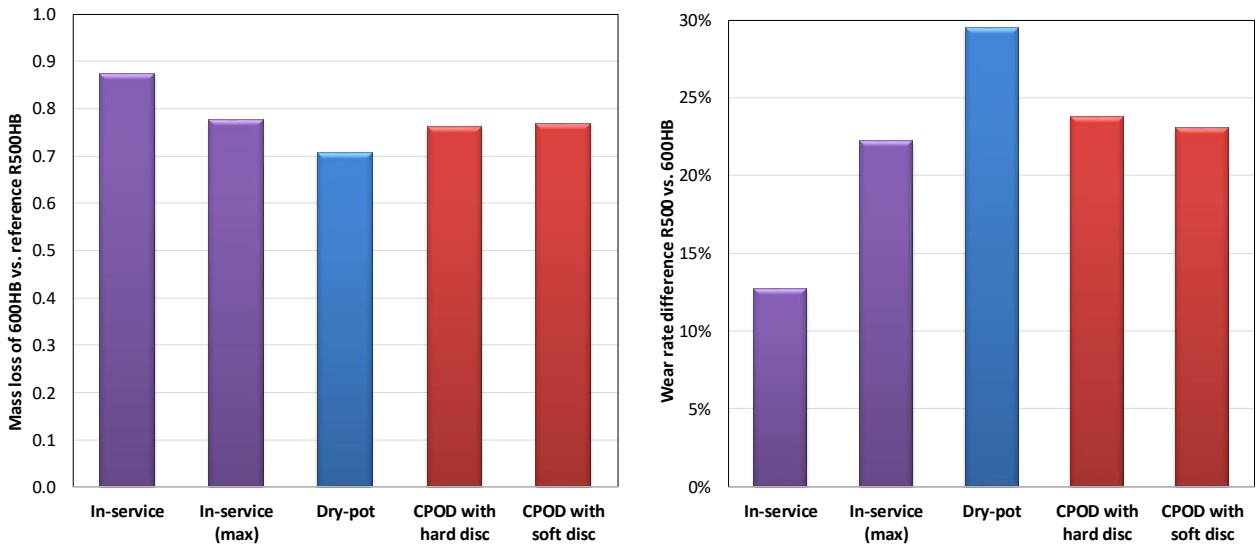

a) *b)*

Figure 6.26. a) Mass loss of the 600HB steel normalized by the mass loss of the reference steel R500HB (WR_{ND}) and b) percentage reduction of the wear rate when R500HB is replaced by 600HB ($WR_{N\%}$) in the in-service conditions and in three different laboratory tests.

6.3.1 Characterization of wear surfaces and cross-sections

The wear surfaces were characterized by FEG-SEM. Fig. 6.27 presents some examples of the wear surfaces of the feed hopper wear plates that were heavily deformed by repeated ploughing and cutting by the chromite ore, including also clear marks of surface fatigue. The ore was embedded deep into the surface, but there was not so much of it. The scratches on the surface were not parallel, which indicates that the direction of the ore flow depends on its momentary amount in the feed hopper. So, the ore may fall directly to the bare wear plate, or to a bed of ore on top of the wear plate.

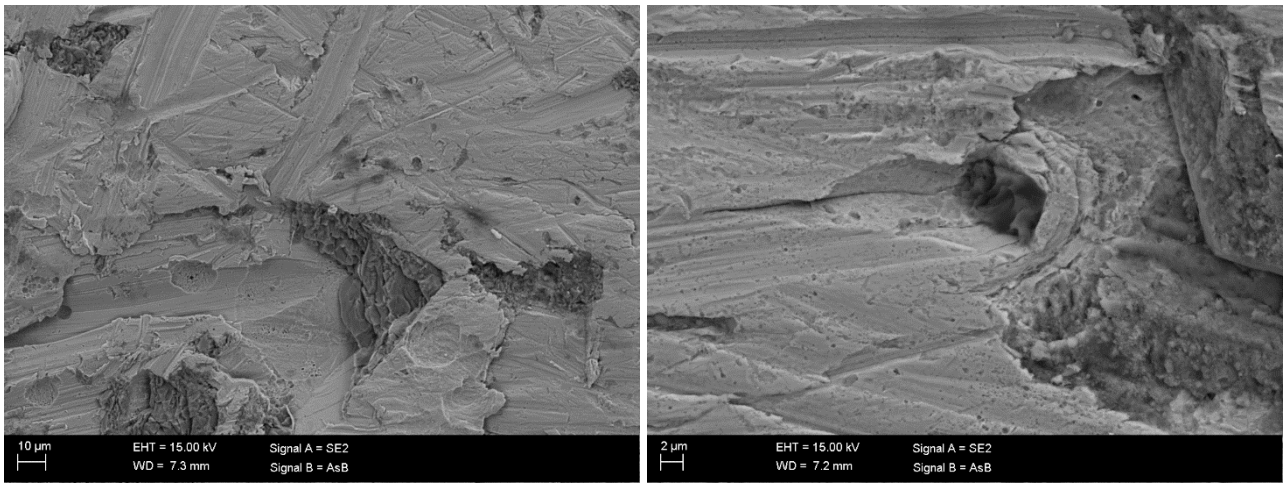

a) *b)*

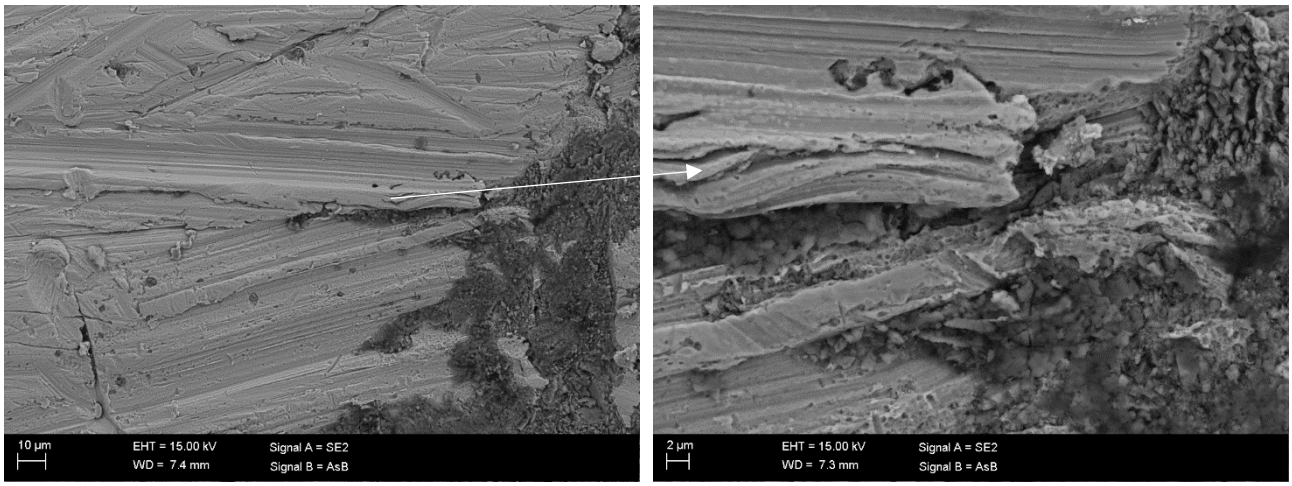

c) *d)*

Figure 6.27. SEM images of the wear surfaces of the in-service feed hopper samples a-b) R500HB and c-d) 600HB.

In the dry-pot tests, Kuru granite produced shallower scratches on the wear surfaces than seen in the in-service case presented in Fig. 6.28. However, the crushing pin-on-disc tests produced much more and better-defined scratches on the test samples (Fig. 6.29). On the other hand, occasional thin white layers were formed on the surfaces of the dry-pot samples just like in the in-service case, while the CPOD tribolayers were more of plastically deformed type, as the comparison of Figs. 6.30 and 6.31 shows.

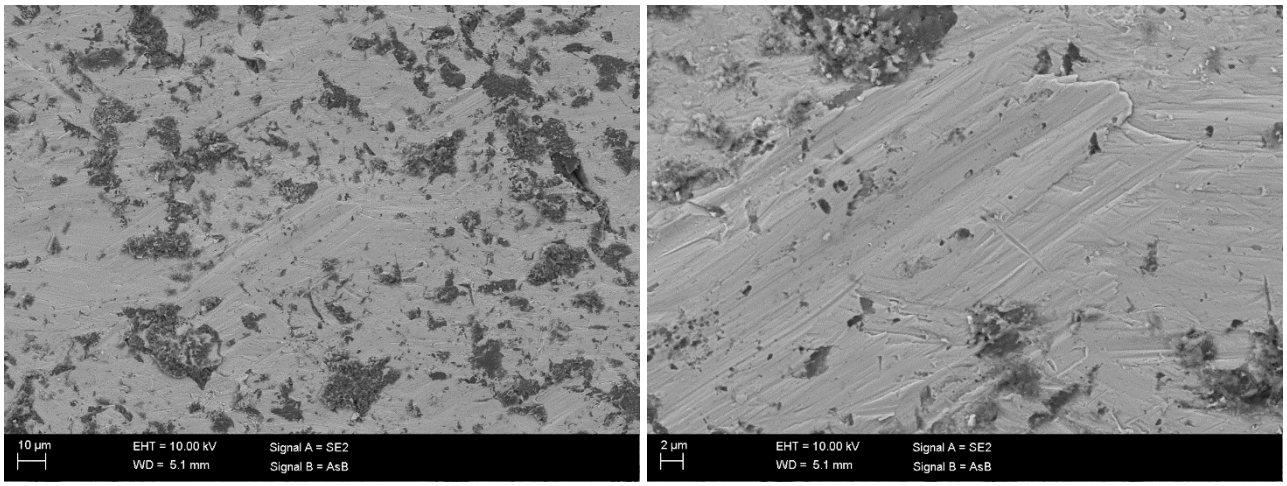

a) *b)*

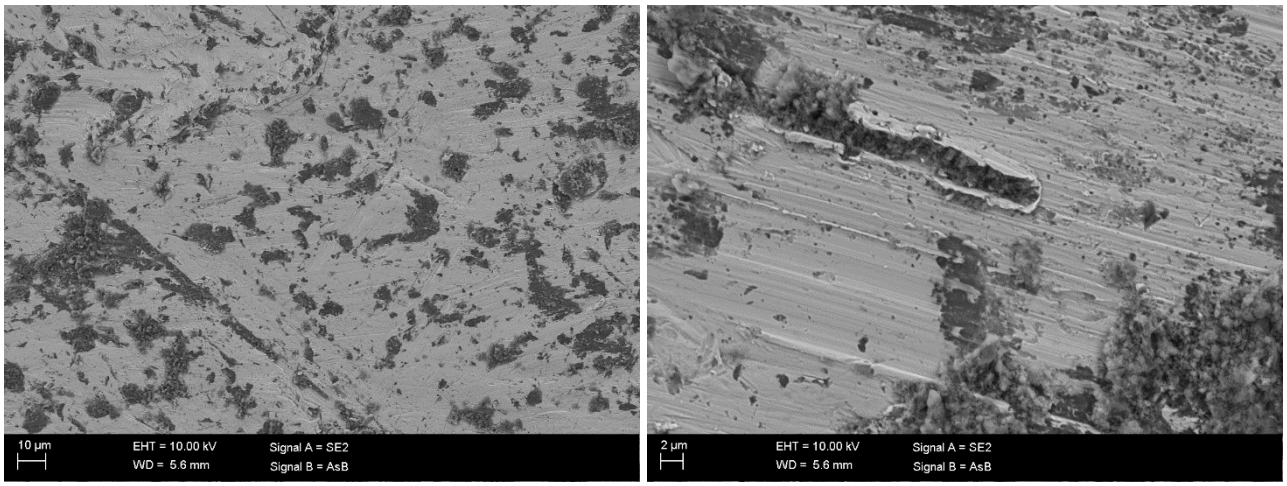

c) *d)*

Figure 6.28. SEM images of the wear surfaces of the dry-pot test samples a-b) R500HB and c-d) 600HB.

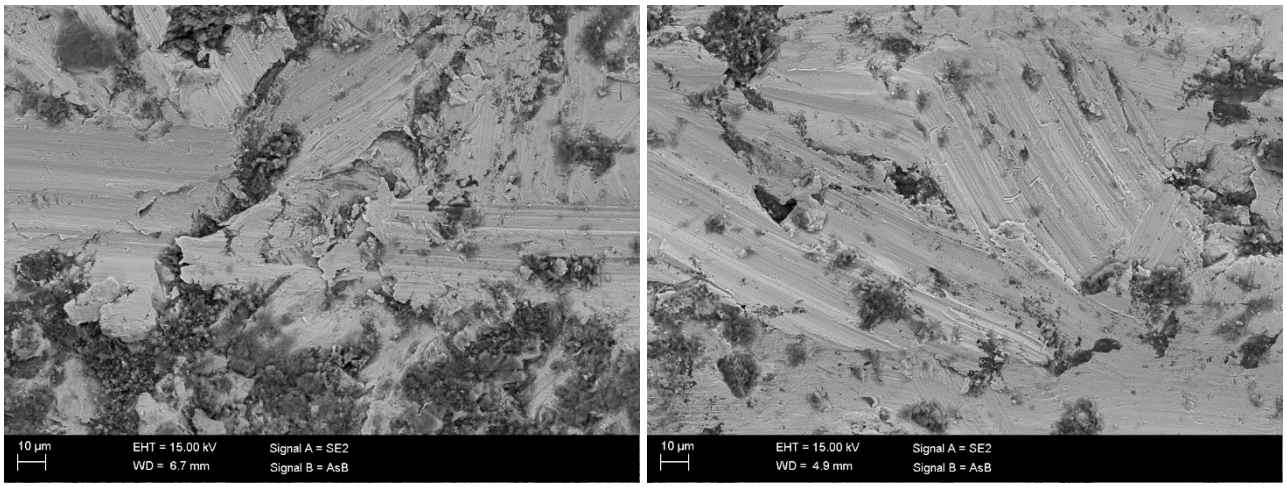

a) *b)*

Figure 6.29. SEM images of the wear surfaces of the crushing pin-on-disc tests with a hard disc counterbody, a) R500HB and b) 600HB.

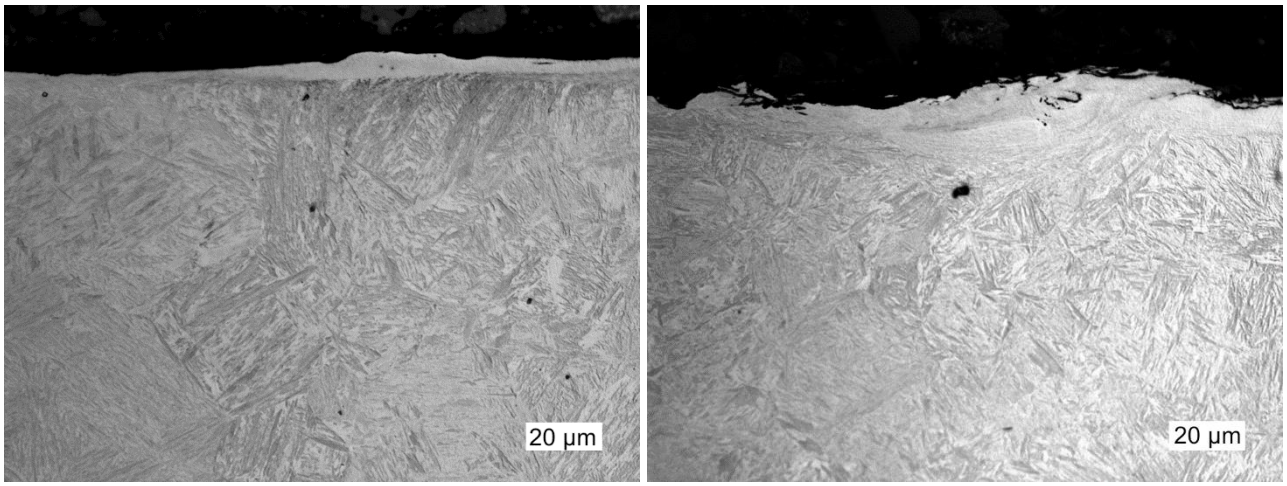

a) *b)*

Figure 6.30. Optical micrographs of the wear surface cross-sections of the 600HB steel samples tested with a) dry-pot and b) crushing pin-on-disc with a hard disc.

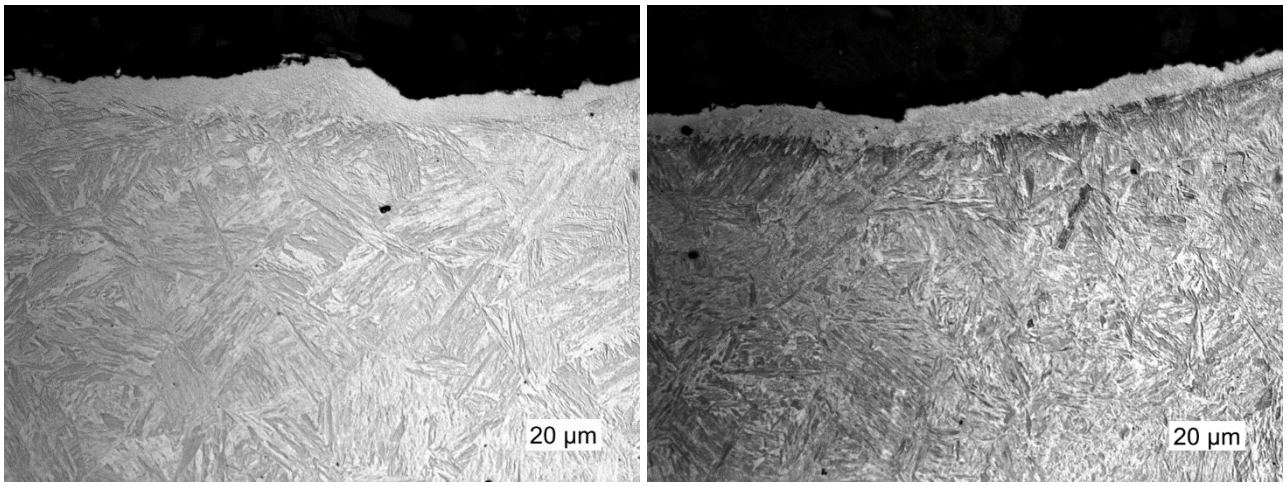

a) *b)*

Figure 6.31. Optical micrographs of the cross-sections of the feed hopper wear plates made from a) R500HB steel and b) 600HB steel.

6.4 Impact wear in Arctic conditions [Publication IV]

The mechanical properties of steels change with temperature. Therefore also the wear behavior changes and must be taken into account for example at the work sites in Arctic conditions. All the studied steels, S355, 400HB, and R500HB with ferritic-pearlitic or martensitic microstructure, are susceptible to ductile-to-brittle transition at subzero temperatures [106]. The impact behavior of the steels was studied at subzero temperatures using the high-velocity particle impactor with a subzero cooling system and compared with their mechanical properties [Publication IV].

As commonly known, the strength of the steels typically increases with decreasing temperature. Thus, the dimensions of the impact marks became smaller when the test temperature was decreased, as illustrated in Fig. 6.32 with quite a linear correlation between the measured impact mark dimensions and strength of the steels at the temperature range from room temperature to -60°C. The decrease of the dimensions at -60°C was in the range of 2-3 % in comparison to the dimensions at RT. For the structural steel S355, the ultimate tensile strength values at -60°C were even 12 % higher than at RT, resulting in 3 % smaller impact marks at -60°C. Fig. 6.33 also shows that in the case of wear resistant steels, there is some correlation between the Charpy impact energy values and ultimate strength, but the temperature dependence of the Charpy results appears to be stronger. For the 400HB steel, the ultimate tensile strength values at -60°C were 6 % higher than at RT, but the Charpy values were 75-83 % higher. However, the Charpy values of the S355 steel did not reduce linearly with temperature [Publication IV], and thus there is no linear correlation between the increasing strength values and decreasing impact toughness values.

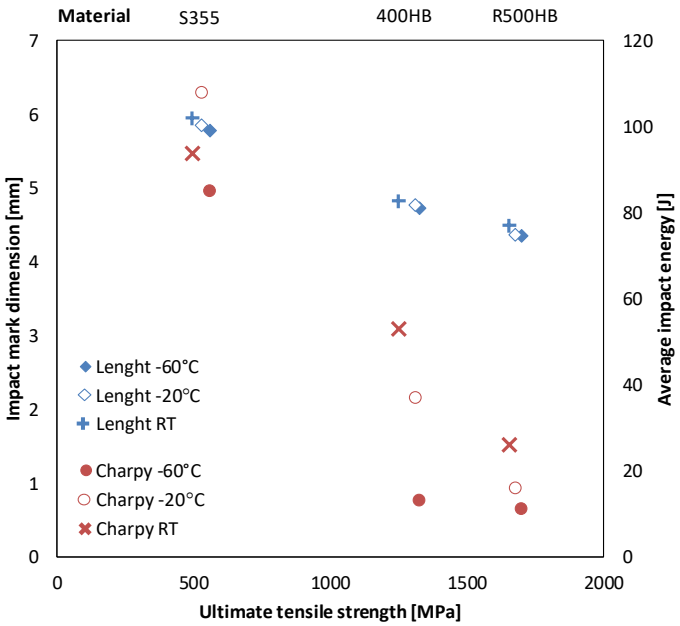

Figure 6.32. Length of the impact marks and Charpy V (longitudinal) impact test results with 5 mm size sample plotted against ultimate tensile strength values at room temperature, -20 ℃, and -60 ℃.

6.4.1 Characterization of impact surfaces

The characterization of the impact surfaces was made using the 3D optical profilometer and the FEG-SEM. However, the profiling of the surfaces was challenging, because the polished surface and the deep impact marks needed different imaging parameters. Fig. 6.33 shows a 3D image of the R500HB sample impacted at -1°C, and Fig 6.34 details of the impact mark. The steel was heavily deformed during the impact, and even wear tongues were formed at the tip of the ridge (Fig. 6.34.b). At subzero temperatures, also plenty of small cracks formed circularly in the region 200-500 µm from the ridge (Fig. 6.34.c). Moreover, at the bottom of the impact mark, the boundaries of martensitic laths and lath packets started to open up, as seen in Fig. 6.34.d.

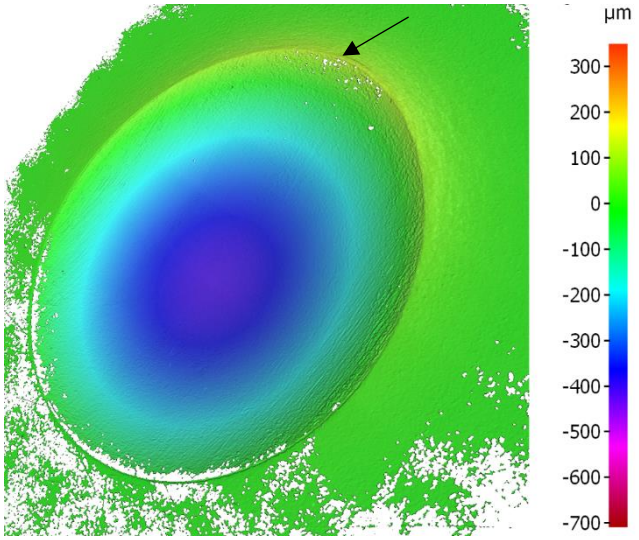

Figure 6.33. Optical profilometer image of a R500HB sample tilted by about 60 ° and tested at -1 ℃ . The length of the impact mark is 4.4 mm. The arrow points to the area characterized in Fig. 6.34.

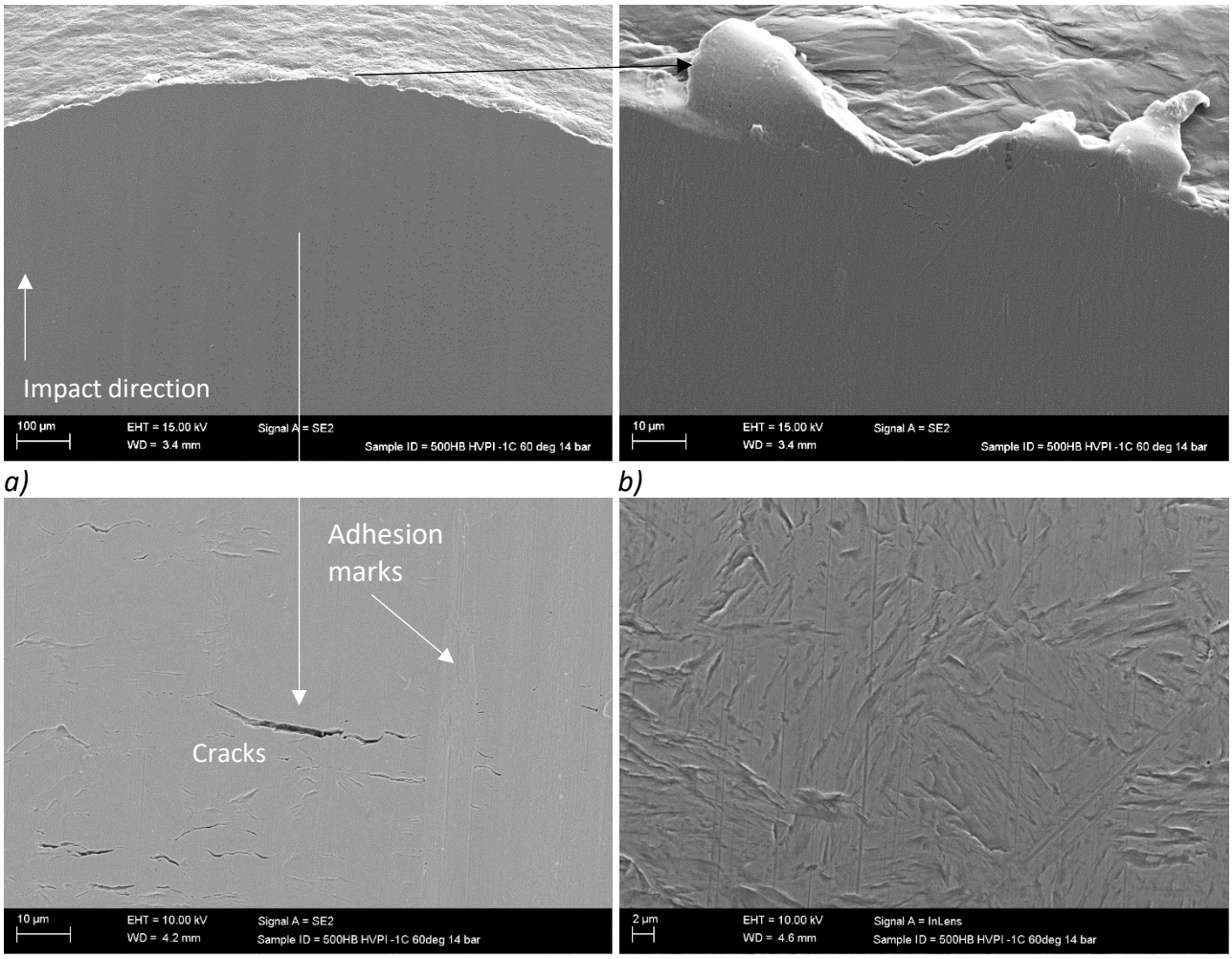

a) *b)*

c) *d)*

Figure 6.34. SEM images of a R500HB steel sample impacted at-1 ℃, a-c) tip of the impact mark and d) bottom of the impact mark.

6.4.2 Characterization of cross-sections

Although the strain rates during the impacts were high and deformations large, so-called white layers or thin shear band layers were formed on the surfaces of the martensitic steels only at -60°C in a region about 100 µm from the tip of the ridge. As an example, Fig. 6.35 shows a 5-10 µm thick white layer in the 400HB steel sample.

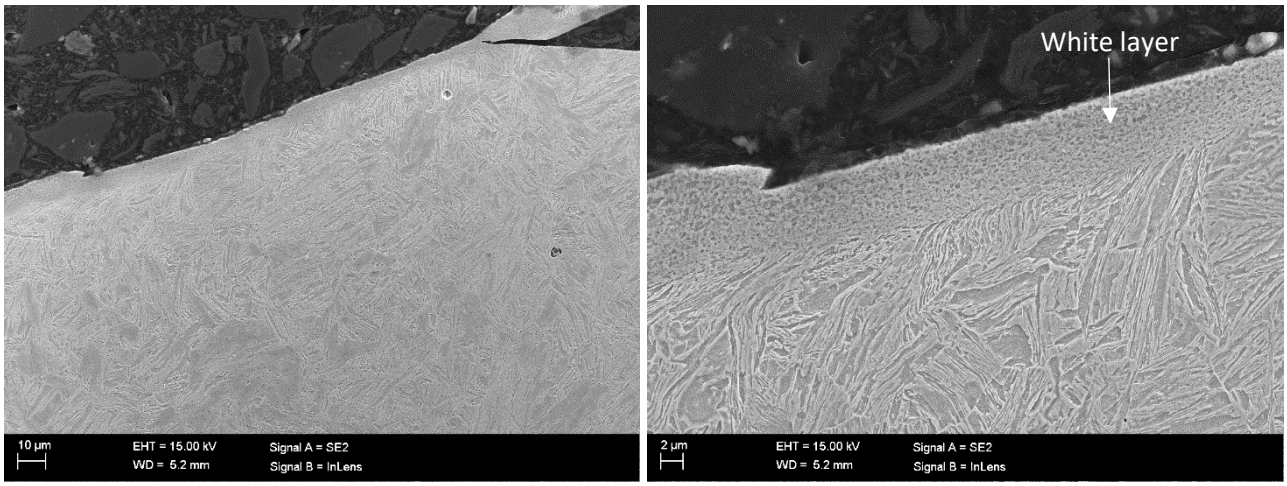

a) *b)*

Figure 6.35. SEM images of the cross-section of the 400HB steel impacted at -60℃.

In single impacts, larger cracks in the cross-sections were found only from the R500HB steel samples over the whole temperature range. They were formed in the area with the highest principal stresses, as also indicated by numerical modeling. The deformation and cracking was more extensive in the multiple impact tests. Fig 6.36 presents an optical micrograph produced by stitching profilometer data from the cross-sectional sample cut from the middle of the R500HB sample impacted five times at -60°C. Marked amount of subsurface adiabatic shear bands (seen as white lines) were formed on the exit side of the impact mark, where the plastic deformation is largest [Publication IV]. Fig. 6.37 shows details of the cracking that was partly induced by the formation of adiabatic shear bands, as can be deduced from the cracks following the subsurface ASB's. The high plastic strain rates created by the fast sliding ball produced also surface ASB's or so-called white layers on the steel surface. Fig. 6.37.b presents an example of the fine nanostructure of that layer.

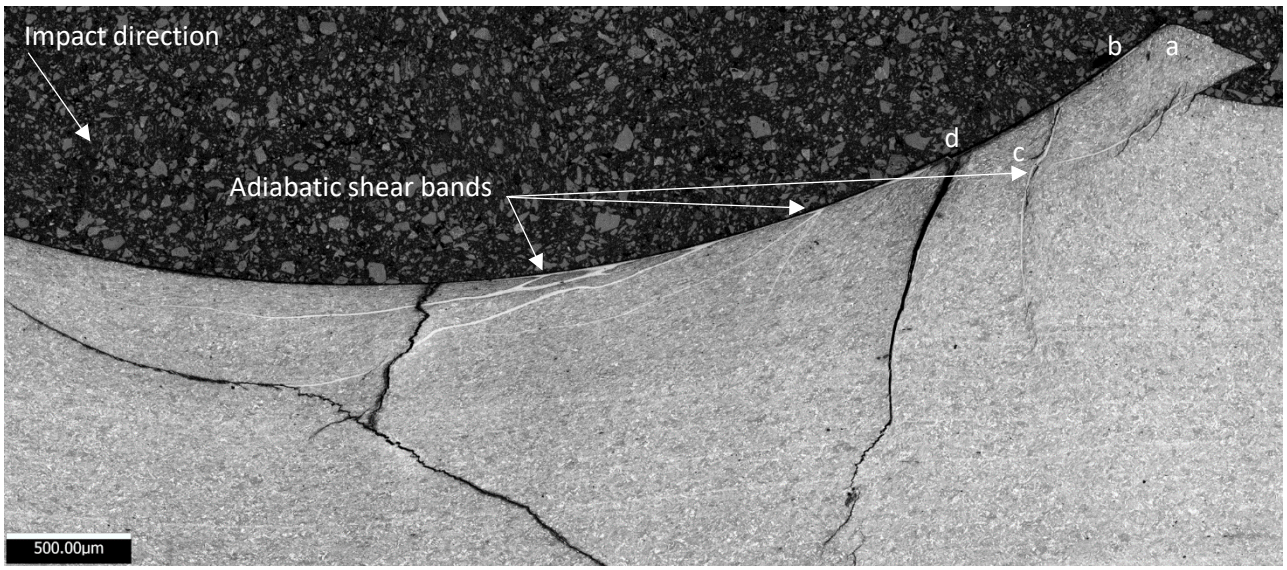

Figure 6.36. Optical micrograph of the cross-section of R500HB steel impacted five times at -60℃. The letters refer to the SEM images in Fig. 6.37.

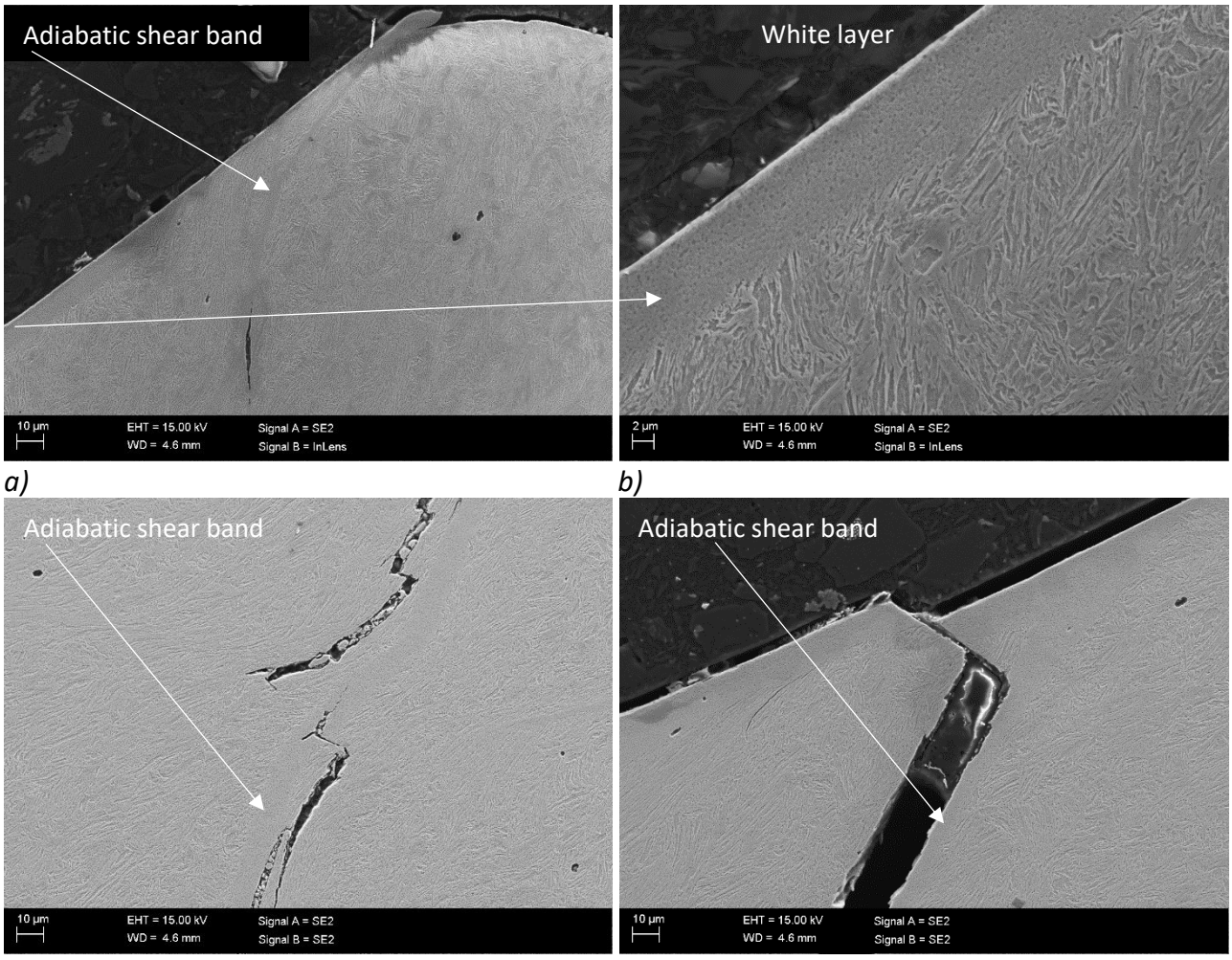

Figure 6.37. SEM images from the cross-section of a R500HB steel sample impacted five times at -60 °C. The locations from where the images are taken are marked in Fig. 6.36.

6.5 Wheels of wire rope drives [Publication V]

In a wire rope drive, a wire rope is bent over rollers that are used to move the wire. In this study, the wear behavior of nodular cast iron rollers was studied using a component testing system and a twin-disc tester, and the results were compared with an in-service case. In the tangential direction of the roller, there is a rolling contact between the grooved roller and the wire rope, but in the parallel direction the contact is sliding, when the rope moves in the groove causing torsional stresses [9]. The comparison of the twin-disc tested and in-service samples was made by characterizing the wear surfaces, amount of deformation, and inter-nodular crack propagation from the cross-sections of the wear surfaces both parallel and perpendicular to the rolling direction, as visualized in Fig. 6.38. The results of these examinations were utilized in the multiscale modeling of the contacts between the wire rope and the rollers [132].

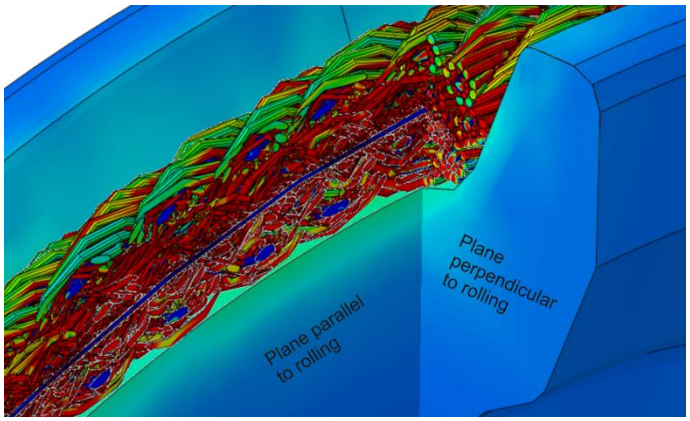

Figure 6.38. Model of the wire rope in contact with a grooved roller, showing the two sample preparation directions in the roller [Publication V].

Fig. 6.39 presents examples of the studied wear surfaces. A typical feature in all of them is the scale-like deformation of the surface. In the grooved roller samples, the scales are oriented parallel to the rolling direction. However, in the twin-disc sample the scales are oriented in the rolling direction, which is also the sliding direction unlike in the roller samples. When the cross-sections of the samples were studied (Fig. 6.40), it was noticed that these scales were formed when the graphite nodules were deformed and cracked in the subsurface region. Occasionally, the cracks between the graphite nodules were connected and the scales were delaminated, leaving a pit on the surface, as shown in Figs. 6.39.a and b. In the FEG-SEM images, graphite is seen as darker gray areas on the wear surface, and excessive amounts of graphite were revealed from under the delaminated scales. In the 15 kN test sample, the surface was visibly more deformed than in the other rollers, and contained also higher amounts of graphite on the wear surface. Moreover, corrugations that were visible by eye had been formed on the wear surface of the 15 kN sample, indicating repeated contact with the wire rope at the same points. Unlike in the other samples, small WC-Co particles from an unknown source were embedded in the in-service roller wear surface. These hard particles, which are seen as white spots in Fig. 6.39.a, had (at some locations) also scratched the wear surface of the in-service roller.

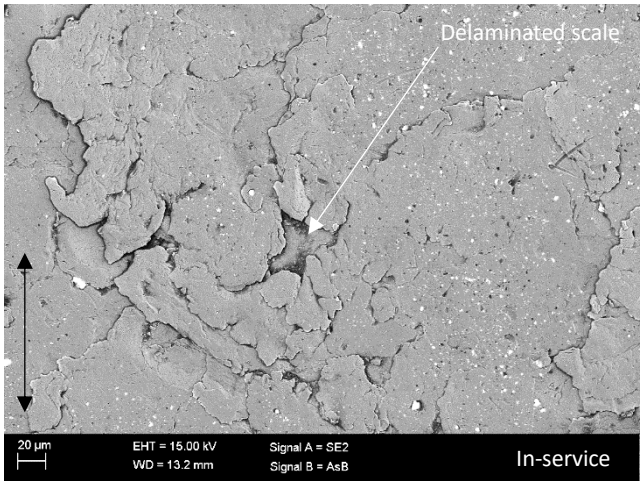

a)

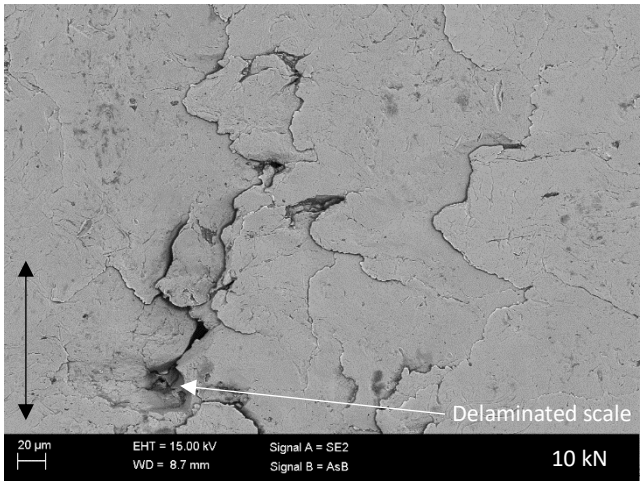

b)

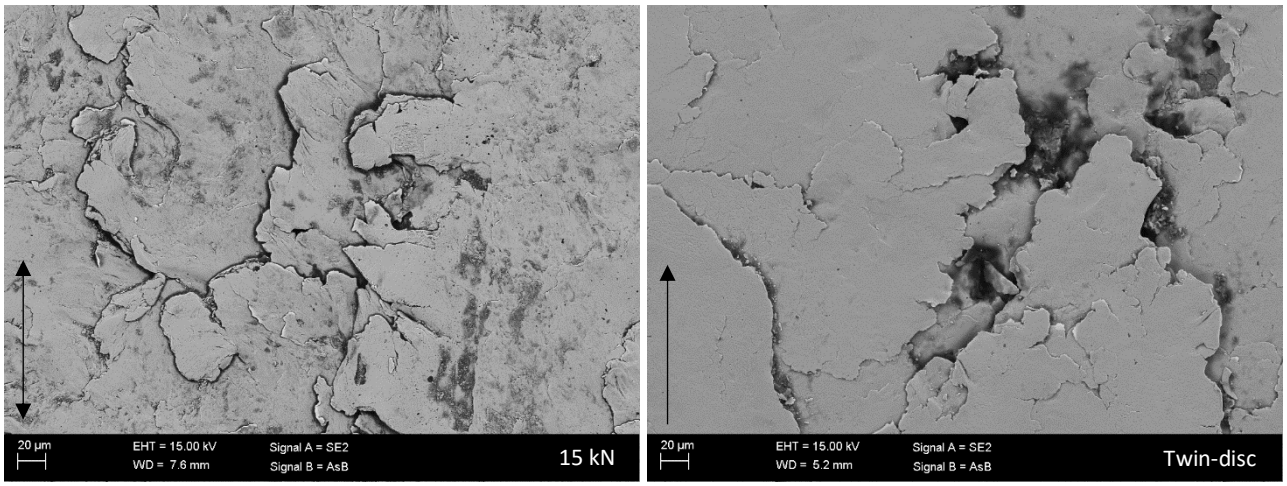

c) *d)*

Fig. 6.39. SEM images from the bottom of the groove of the rollers a) in-service, b) 10 kN test, c) 15 kN test, and d) twin-disc test. The black arrows indicate the rolling direction.

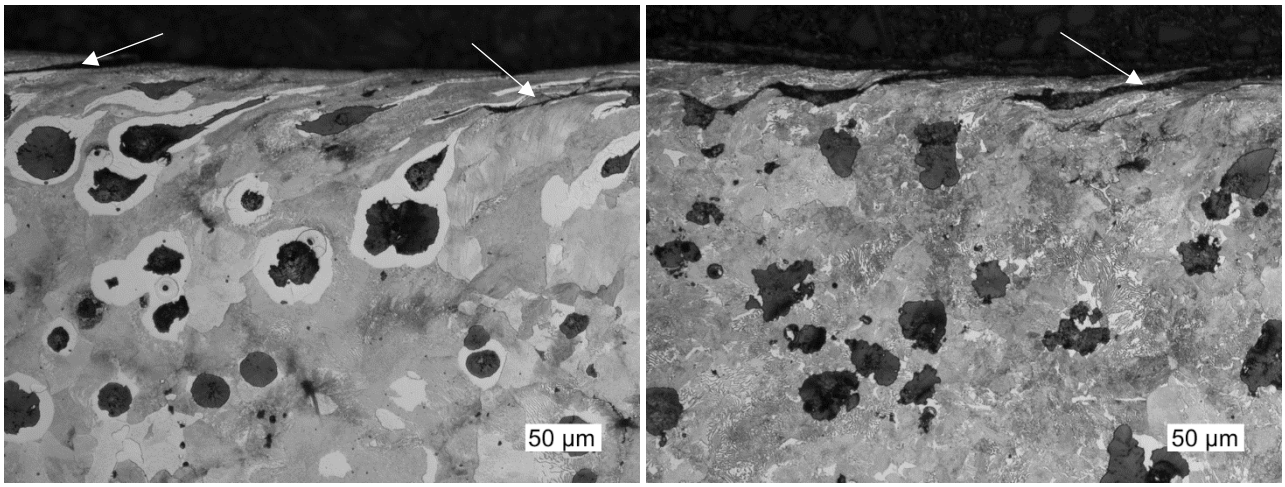

a) *b)*

Fig. 6.40. Optical micrographs of the cross-sections parallel to the rolling direction from the bottom of the groove of a) in-service sample and b) 10 kN test sample. The white arrows indicate cracks.

The cracking of graphite nodules was studied in detail using a statistical analysis. Fig. 6.41 shows the results from the crack depth measurements and illustrates how the crack depths and initiation angles were determined. In the in-service roller and the 10 kN test sample, the majority of the cracks was in the region of 10-30 µm, while in the 15 kN test samples, about 60% of the cracks were concentrated at the depth of 10-20 µm. In the twin-disc test sample, the deformation of the wear surface extended clearly deepest, and some cracks were observed as deep as 75 µm from the surface. Moreover, the cross-sectional studies showed also internodular crack networks at the depth of 10-30 µm. In an unused sample, the cracks caused by machining were found only in the surface layer, and no cracks were observed deeper than 20 µm. The orientation of the cracks in both studied directions was quite similar in all worn roller samples [Publication V]. Also in the twin-disc sample, the crack orientations were otherwise quite similar, but there was a high amount of cracks oriented also at angles in the range of +170°…+180°.

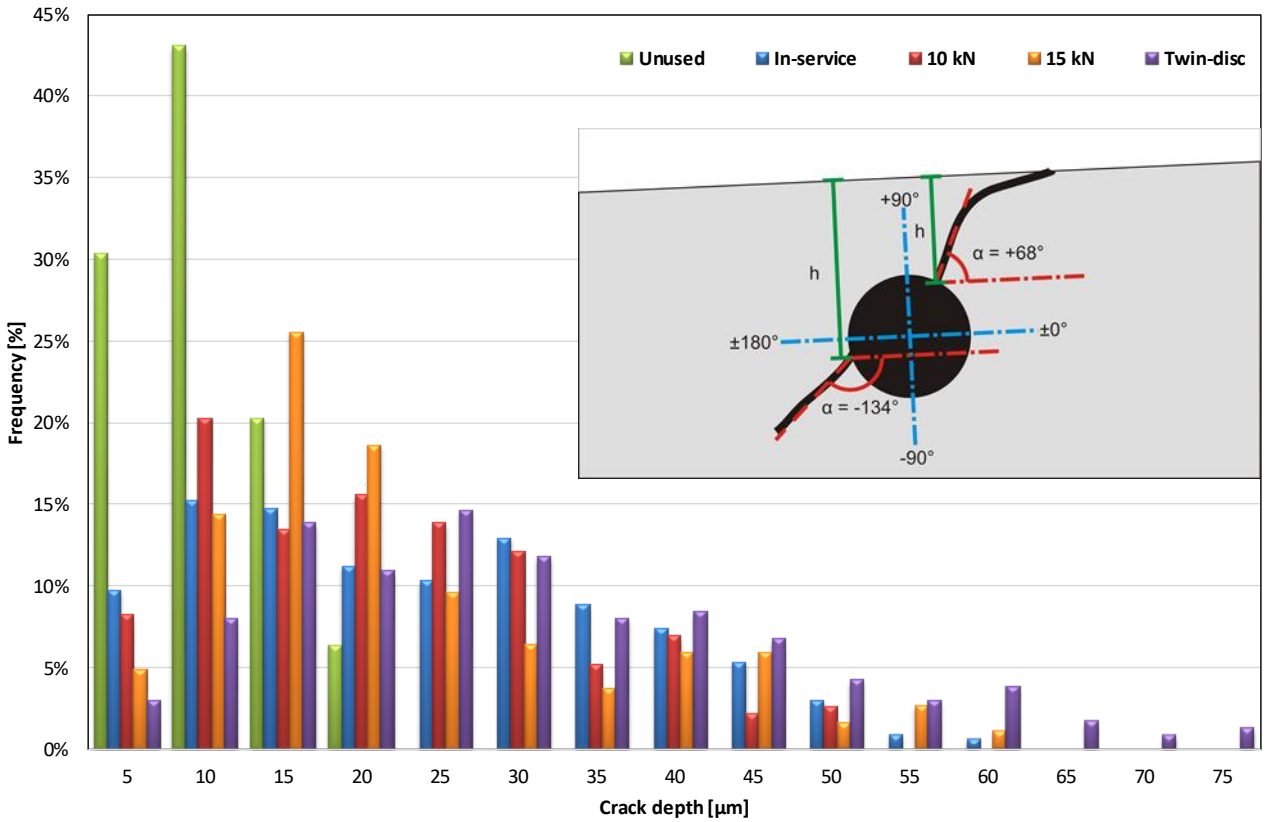

Figure 6.41. Percentage of selected crack depths (frequency) measured from the cross-sections of the studied samples, and a schematic illustration of the determination of the crack depths (h) and the crack initiation angles (α) marked with white dashed lines. The dash-dot lines indicate the vertical and horizontal axes in relation to the general surface line.

7 Discussion

This Chapter discusses the main results and observations of the conducted studies from the point of view of the research questions presented in Chapter 1. The Chapter is divided into three parts, including the wear behavior of steels in high-stress abrasive and impact conditions, planning of application oriented wear tests, and research methodologies for the evaluation of the relevance of laboratory wear experiments.

7.1 Wear behavior of steels in high-stress abrasive and impact wear

The wear behavior of the dumper body wear plates, the cutting edges of the mining loader buckets, and the feed hopper wear plates was simulated using several application oriented testing methods. Moreover, the wear mechanisms of the martensitic wear resistant steels were characterized using various analyzing techniques.

7.1.1 Effect of mechanical properties

In the abrasive, impact-abrasive, and impact tests, the wear behavior of the studied steels, in general, paralleled their hardness and strength. However, when the differences in the hardness values were less than 50 HV, the microstructural properties and the composition of the steels had an increasingly marked effect on the wear resistance. For example, in the dry-pot tests, the R500HB steel with a 2.5 % higher hardness than the 500HB steel showed higher wear rates in all test conditions, and even 10.6 % higher wear rates when the tests were conducted at 250 rpm for 240 minutes with chromite. Although the differences in the results were quite small, they can be readily explained by the more homogenous microstructure of the 500HB steel. After an extensive crushing pin-on-disc study on 400 HB grade steels, Ojala et al. [20] concluded that higher nickel-molybdenum alloying increases the hardenability of the steels and thus also their wear resistance in abrasion. In the present case, the nominal Ni-Mo content of the R500HB steel was 1.5 %, while for the 500HB steel it was 2.1%. Thus, the results obtained in this work are in accordance with the results of Ojala et al. [20].

7.1.2 Characterization of wear surfaces

When the samples tested with the crushing pin-on-disc, the uniaxial crusher, the impeller-tumbler, and the dry-pot were compared, the amounts of sliding abrasion and plastic deformation were found to vary notably. The crushing pin-on-disc produced the most well defined scratches through cutting and ploughing. As the samples in this test method are able to rotate freely around their vertical axis during the tests, most of the scratches are also non-parallel. In the uniaxial crusher tests, the deformation of the wear surface layers was clearly highest, but only a few (short) scratches were observed. Thus, the forces in the uniaxial crushing tests are closer to the studied in-service cases, but the amount of cutting is clearly lower. Therefore, combining of the uniaxial crusher and crushing pin-on-disc methods is recommended, when simulating high-stress wear in a mining environment. In the impeller-tumbler tests, the impact wear dominates and the formed scratches are relatively short. Therefore, the impeller-tumbler is a suitable test method when the aim is to simulate wear contacts by impacts, such as in the dumper truck wear plate. The dry-pot test methods produced wear surfaces that were comparable to the cutting edge of the loader bucket. The wear rates, in turn, depended on the used rotation speed. Moreover, the tests highlighted the role of the used abrasive material. Chromite produced a scratched surface that resembled most closely the studied wear surface of the real cutting edge of a mining loader. In all test methods, the amount of embedded abrasive increased with decreasing hardness of the tested steel.

When the rotational speed in the dry-pot tests was decreased from 500 rpm to 250 rpm, the test was better able to distinguish the differences between the steel grades. Thus, this type of a test is well suited for steel development purposes, when especially high wear resistance in high-stress abrasive conditions is targeted. In addition to wear tests, the dry-pot test method suits well for the abrasivity testing of minerals, when the prevailing conditions in the intended application are abrasive rather than impact-abrasive, for which the LCPC test in turn is better. This is because the dry-pot tests, especially when run at 250 rpm, do not crush the minerals by impacts in the same way as the LCPC test, and thus they may simulate the in-service conditions better in many cases. However, a clear disadvantage is the high amount of abrasives (min. 9 kg) needed in the dry pot tests.

The single scratch tests at 60-80 N loads produced abrasion marks with ridges that had a similar appearance as the scratches found in the in-service samples. However, the scratch width in the scratch tests was up to 200 µm, while the asperities in the rock particles typically form scratches with the width of only a few micrometers. Moreover, about ten overlapping scratches produced at high (40- 80 N) loads were needed to cause similar hardening of the surface as in the in-service case. Therefore, single scratch tests should not be used for the evaluation of abrasive wear behavior of materials with high work hardening ability. In addition, the applicability of the cutting-to-plasticity ratio (or the material removal factor) should be carefully considered, as for example Franco and Sinatora [130] have presented results which show that it does not correlate well with the applied loads.

7.1.3 Formation of adiabatic shear bands

In martensitic steels, adiabatic shear bands were observed to form both by high-stress abrasion and high-speed/high-energy impacts. The subsurface transformed ASBs were formed due to high-

energy oblique angle impacts during the impeller-tumbler tests, and at subzero temperatures also in the samples impact tested with the HVPI system. ASBs were found also in the dumper truck wear plate, which had experienced heavy impacts during loading of the truck. The subsurface ASBs acted often as initiation sites for cracks, which is an observation reported also earlier for example in conjunction of Hopkinson Split Bar tests [40] and steel scrap shear blades [105].

In high-stress abrasion, the adiabatic phase transformation occurred on the wear surfaces, and the ASB's were seen as so-called white layers in the cross-sectional samples. The harder and stronger the steel, the thicker and more common the white layers. In the 500 HB grade and harder steels, the white layers were found to form with all used test methods. However, the thickest white layers were seen in the in-service samples. Although the maximum hardness of the white layers was as high 790 $HV_{0.05}$, their formation did not necessarily increase the wear resistance of the steels, because the layers were prone to cracking and delamination, as observed also earlier by Cho, Lee, and Lee [38]. The cracks in the white layers typically stopped at the softer deformed steel layer under the ASBs, which appeared darker than the base material in the cross-sectional analysis. These so-called dark layers are formed when the steel is heating up during the formation of white layers, leading to overtempering of the underlying martensite [37]. In addition to wear studies, the formation of white and dark layers in martensitic steels is typically observed in conjunction of machining [133–138].

7.2 Planning of application oriented wear tests

Simulation of the in-service wear conditions in a laboratory scale needs a lot of information from various sources. Planning of the selection, or development, of the test methods usually starts from gathering all available information and physical test pieces and samples from industry. All possible factors in the wear environment, such as the applied loads, running speeds and times, contact angles, abrasive materials, and so forth, have an effect on the wear behavior of the materials. In many cases, however, the available data is ambiguous or some factors are totally lacking, and getting representative in-service samples can also be quite challenging. On the other hand, accelerated wear tests are often needed, when the expected life times of the parts are long. Thus, many compromises, simplifications, and estimations have to be made when planning the tests. Nevertheless, as presented in this study, reproduction of the correct wear mechanisms and contacts of the in-service conditions should always be the primary starting point for wear testing that seeks to simulate in-service conditions. Fig. 7.1 summarizes the main planning parameters for application oriented wear testing.

When the test procedure has been selected, there are still many factors that will affect the quality of the obtained results and the repeatability and reproducibility of the wear tests, as presented in Figure 7.2 [139]. It is also good to remember that not only the material and the tribosystem will dictate the outcome of the tests, but also the operator can affect the results significantly. Therefore, the at least three repetitions of each wear test suggested by Blau [139] sounds quite reasonable, when all possible sources of variety and errors in the results are considered.

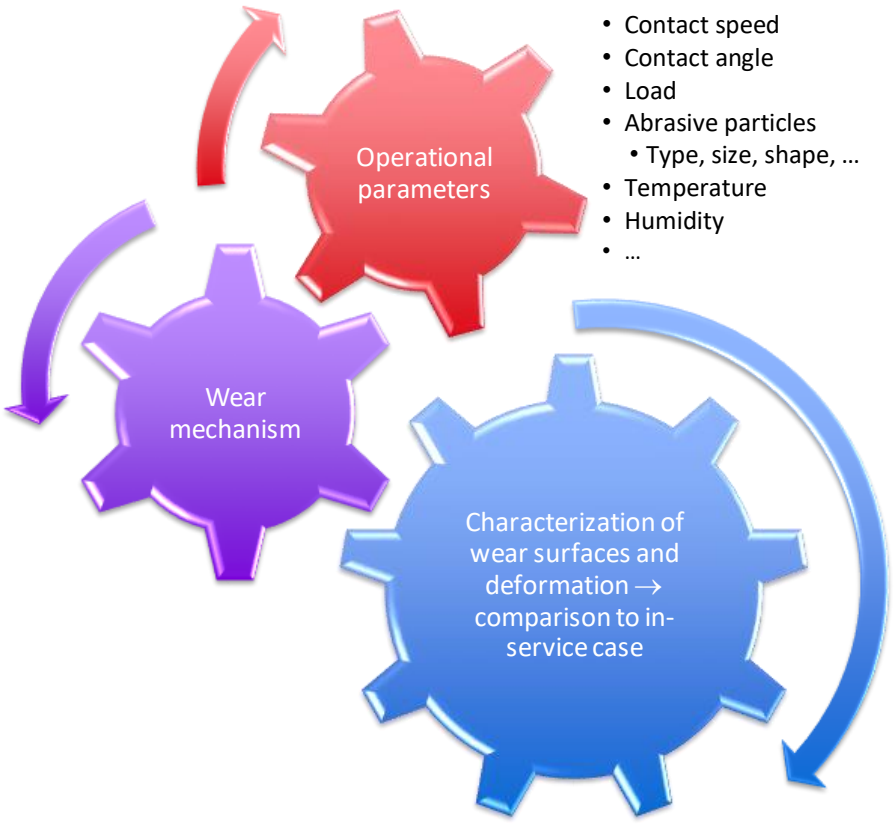

Figure 7.1. Planning of application oriented wear tests.

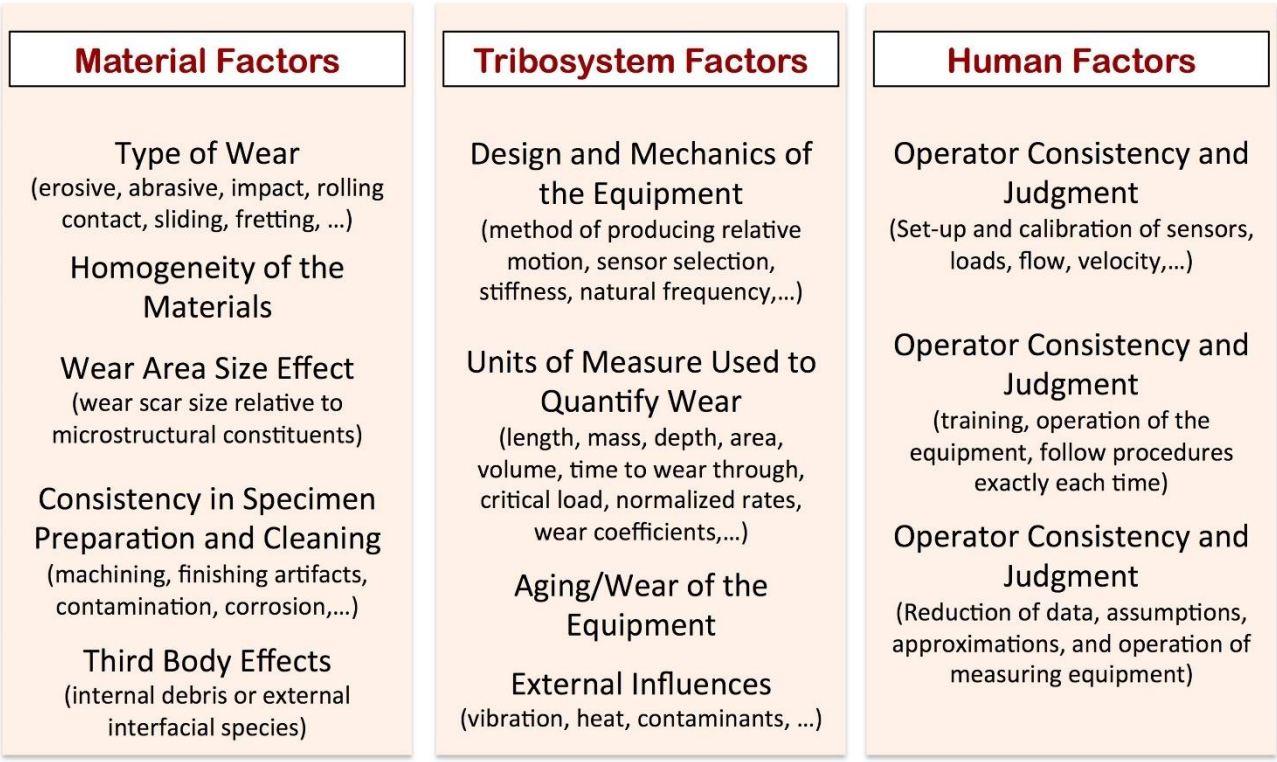

Figure 7.2. Factors affecting the repeatability and reproducibility of wear tests [139].

7.2.1 Reference samples

The use of a reference sample in the wear tests is highly recommended. In an ideal case, the reference sample is tested simultaneously with the actual samples, as happens for example in the impeller-tumbler and dry-pot methods. It is also sensible to produce a high number of reference samples from the same material batch, and if a new batch is needed, to determine the difference between the samples from different batches by cross testing.

In the selection of the reference material, attention should be paid on the homogeneity of the microstructure and properties of the material, as well as on its wear behavior in the test environment. For example, in the uniaxial crusher tests the wear rate of the structural steel relative to its hardness was higher than that of the martensitic wear resistant steels. Moreover, the wear rate of the structural steels was not stable during the tests, evidently due to their unsufficient compression resistance compared to the martensitic steels. In the impeller-tumbler tests, in turn, the structural steel was prone to form visible burrs over the edges of the sample, which was not normally seen with other (harder) steels. So, the lesson learned from those observations is that structural steels should not be used as a reference material in high-stress abrasion wear tests of much harder wear resistant steels.

7.2.2 Running-in period

A running-in should be performed, if the target should exhibit steady state wear during the entire actual test. In this study, the running-in was used in the crushing pin-on-disc tests, in the uniaxial crusher tests, and in the 60 minute impeller-tumbler tests. Previous studies [1] have shown that in the beginning of these tests, the embedment of rock into the surfaces leads to a different wear rate than observed later when the test reaches a steady (wear) state. Because the test times are relatively short, the running-in period may therefore have a marked effect on the total wear rate.

The running-in period also cancels out small differences in the surface quality of the samples, including roughness. In addition, the residual stress measurements of the samples revealed that there are marked differences between the steels and the samples in the initial machined stage. However, the wear tests with natural abrasives worked like sand blasting or shot peening of the steel surfaces. Consequently, the tensile stress state in the surface region changed to a compressive stress state, as observed also in shot peening tests [140]. The differences in the initial residual stresses, especially if they extend deeper into the material, may have an effect on the wear test results. Thus, a running-in stage is recommended before the actual wear test commences, especially if the duration of the test is relatively short.

7.2.3 Abrasives

The selection of the abrasive material for a wear test is very critical. Use of the exactly same mineral as used in the in-service wear environment may not be possible for the simple reason that there is a huge variety of minerals around, as can be seen for example in the study of the Kemi chromite deposit by Huhtelin and Alapieti [141]. Moreover, the properties of the main mineral in the deposit may limit its usability in the wear tests. For example, the crushability of the Kemi chromite is so high that it was difficult to prepare a suitable size fraction of particles for the wear tests. Thus, there was

a limited amount of chromite available for the tests, although two 200 l barrels of ore was originally received from the mine.

The test environment used to aid in the materials selection process seldom targets one particular mine, which means that the selection of the abrasive material must be based on some other criteria. Quartzite is used in some standard methods, such as in the rubber wheel abrasion tests [44], because it is a hard and quite homogenous mineral with high abrasiveness. In the dry-pot tests with freely flowing abrasive, quartzite indeed produced the highest wear rates, for example up to three times higher for the R500HB steel than Sorila granite [Publication III], but the appearance of the wear surfaces was not similar to the ones found in the in-service cutting edges of the mining loader buckets. Furthermore, the differences between the wear rates of steels with different hardness were lowest in the tests with quartzite. Gates et al. [57] reported a similar effect for martensitic steels in quartzite tests, when they compared different abrasives using a ball mill abrasion tester. When using a similar testing system as Gates et al. [57], Albertin and Sinatora [56] concluded that quartzite is not a suitable standard abrasive for laboratory ball mill tests, because it abrades the matrix material too aggressively and the exposed carbides in the high chromium cast irons are easily fractured by impacts. On the other hand, when the wear test is used to simulate crushing, such as the crushing pin-on-disc tests of steels, granite may be more aggressive because it has two times higher uniaxial compressive strength than quartzite [5]. Quartzite has also a tendency to form in-situ composites with steels, when the fine crushed flakes are mechanically mixed with the surface layer of the test material during crushing [21]. In this study, it was also observed that the formed white layers were thickest and most uniform in the quartzite tested dry-pot samples. As the hardness of the white layer does not vary as much as the bulk hardness of the steels, this may partly explain the smaller differences in the quartzite tested steels.

Based on this study, Kuru granite appears to be a good abrasive material for wear tests, especially when the hard rock mining conditions in the Nordic countries are being simulated. Kuru granite has a more homogenous microstructure than many other granites, including Sorila granite, and it also has a relatively high quartzite content. Sorila granite forms much larger rock clusters on the wear surfaces, which tends to lead to lower wear rates than expected based on its abrasiveness value. Kuru granite does not produce as high wear rates as pure quartzite, but it usually produces bigger differences between the steel grades. With Kuru granite, the produced differences between the steel grades were also quite similar as found in the cutting edge of the mining loader bucket [Publication III]. All things considered, Kuru granite appears to be one of the best abrasives when steels are being developed for hard rock mining environments.

7.2.4 Contact simulation in high-stress abrasion

In this study, most of the applied wear testing methods were found to simulate, although to varying degrees, the high-stress abrasion of steels in the mining conditions. However, even though all the test methods were able to deform the steels plastically and produced similar wear surfaces as found in the real mining conditions, it should be noted that none of the methods was able to produce as high normal forces and impact loads as observed in practice. For example, it is really difficult to simulate all the forces acting on the cutting edge of the mining loader bucket in a laboratory test, such as the entire weight of the loader resting on the bucket when it penetrates into the rock pile, or the impact loads that the wear plate of a dumper body experiences, when big boulders of rock

are dropped onto it. Therefore, to guarantee the best possible outcome for the simulations of complex wear environments, it is in many cases advisable to use several different test methods to cover as many aspects of the real conditions as possible.

In the simulation of freely flowing abrasives, such as in the loading stage of a mining loader, the dry-pot test method proved to be an appropriate and relevant method. However, an obvious limitation or drawback of this method is the rounding of the abrasive particles during testing, which is a problem that plagues also all the other wear testing methods, which are based on batch loading of the abrasives. Tests with a larger number of shorter cycles with renewed abrasives would mitigate the problem, but for example in the case of the dry-pot tester, it would require a huge amount of the abrasive material and the total test time would easily become much too long. Overall, the dry-pot method is an extremely versatile wear testing method as regards, for example, the adjustment of the testing parameters and the possibility to use samples with various shapes and sizes.

The crushing pin-on-disc produced very similar scratches on the samples as observed in the wear plates used in the dumper truck body and the feed hopper. However, the normal forces used in these tests are significantly lower than in most of the mining applications, and thus combining these tests with the uniaxial crusher tests is recommended. The hydraulic cylinder of the uniaxial crusher can produce normal forces up to 86 kN, which are usually capable of deforming the steel surfaces quite efficiently. For some materials, such as Hadfield manganese steels with extraordinary work hardening capability, pre-deformation of the surface before other wear tests has a marked effect on the final test results [142].

The impeller-tumbler method combines efficiently high-stress abrasion and impact wear. Due to the rather heavy loading of the sample surfaces, the impeller-tumbler tests were found to produce even subsurface adiabatic shear bands, which is quite unusual for most of the wear test methods in common use. Thus, the impeller-tumbler is a suitable wear testing method for applications where oblique angle impacts by mineral particles are responsible for most of the wear damage, such as impact crushers and the tail plates of dumper trucks.

7.2.5 Component and contact tests

In the case of the rollers of wire rope drives, there was a possibility to characterize the wear surfaces obtained from three different types of tests, including the in-service case, the component tests, and the contact simulating twin-disc tests [Publication IV]. The study yielded also important and detailed information for the multiscale modeling of the wire ropes and their complex contacts with rollers [132]. The characterization results showed that with the component test setup it is possible to simulate the in-service wear environment quite well, when the test parameters are selected correctly. However, the component tests take a very long time to perform, and thus they are not the ideal choice for the early stage material testing. The twin-disc tests enable controlled rolling and sliding between the surfaces, and if the test parameters are properly adjusted, the twin-disc test has a good potential to be used as the first testing step in the material selection for the rollers.

7.3 Research methodologies for the evaluation of the relevance of laboratory wear experiments

One of the main targets of this study was to assess and improve the relevance of laboratory wear experiments in high-stress abrasive and impact-abrasive conditions. For this aim, wear behavior of altogether seven different steels related to three mining case studies was simulated using five test systems and sixteen different test parameters. The comparison even between the test methods was not straightforward, not to mention the comparison to the in-service cases. Therefore, several approaches to present and compare the obtained results were used.

7.3.1 Presentation of the wear test results

There are many different ways to present the wear test results. A good example of this is given by Blau [131], who analyzed the presentations in Wear of Materials Conferences and found over sixty different ways how the wear rates were reported in a single conference. According to Blau, the most common ways were either to report the direct values of mass or volume loss, or to normalize them for example by the sliding distance or the applied load. Blau [131] criticized that the normalization method typically assumes steady-state wear throughout the test, although that is not always the case. In the present work, however, the steady state of wear was achieved using a running-in period in most of the tests, which avoids Blau's criticism and at least for that part justifies normalization of the results. Only in the long dry-pot and impeller tumbler tests the running-in stage was omitted, but in these cases, the steady state was achieved in any case relatively early in the test.

In this work, the wear rates were presented in various ways in order to better compare the different aspects of wear and wear environments. The abrasion test results were presented as mass losses, using normalization by the reference data (WR_{ND} or $WR_{N\%}$) or by the wear area and contact time $WR_{mm/h}$. Different approaches were also obtained by plotting the results against the hardness or strength of the test materials, the contact time, sample speed, or even the abrasiveness of the mineral. As discussed already in the results section (Chapter 6.3), normalization of the test results by the reference data does not reveal the differences in the wear rates between the test methods so well, but it is an easy and commonly used method especially when the contact parameters are not known, which is often the case when comparisons involve also in-service cases [4,86]. Moreover, WR_{ND} or $WR_{N\%}$ show the small differences between the materials, when a reference sample is used simultaneously in the tests and thus even improves the quality of the measurement data. Use of $WR_{mm/h}$ reveals better the differences between the test methods, and gives numerical data also for the comparison with the in-service cases. However, a pitfall of this method is that the wear area and contact time are not always unambiguous and they may change with time, as presented in the study of the cutting edges of the mining loader buckets.

There are also other approaches to the normalization of the test results by reference data. For example, Dommarco et al. [88] used the inverse value of WR_{ND} and called it the relative wear resistance index. Thus, when plotted against service life, the decreasing values of the relative wear resistance index indicate an increased wear rate compared to the reference material. Tylczak, Hawk, and Wilson [4], on the other hand, compared the normalized values produced by two different test

methods by plotting them against each other, and found that the correlation could be described reasonably well by a simple exponential function.

In some earlier studies with the same test methods as used in this thesis [7,14,20], the hardness values used in the reporting of the wear test results were determined from the machined sample surfaces before the tests. In this practice, the wear behavior of the sample during the tests is compared to the initial stage of the sample surface. In quenched and tempered steels, the hardness of the bulk material often varies [20], but this fact is rather difficult to account for in the calculations or in the presentations of the results. On the other hand, due to the machining, the hardness values in the thin surface layer tend to be much higher than deeper in the bulk of the sample, but this layer wears out quite quickly and thus its hardness does not represent the sample too well. For example, in the machined dry pot test samples, the measured surface hardness values were 8-18% higher than the average bulk hardness values. Therefore, in this work the comparison between the studied wear resistant steels was made based on their average bulk hardness values.

When there are big differences between the studied materials, especially in their work hardening behavior, other approaches should also be considered. Saha [143] simulated the wear of digger teeth using the impeller-tumbler method and scratch testing for six steels with large initial hardness and microstructure differences. Saha normalized the results by the wear rate of 198 HV mild steel and plotted them against the surface hardness measured after the wear tests. With this method, for example the wear rate of the Hadfield steel was scaled better compared to the initial hardness value of the steel.

In the scratch tests conducted in the present work, the results were given as volume losses normalized by the sliding distance ($\mu m^3/\mu m$), which is a quite typical way of presenting the scratch test results. This practice can also be applied to normalizing, e.g., dry-pot test results, where the travel length can be precisely determined. However, in this study this method was not used, because the travel length in the in-service conditions was not known. When several materials are compared using different normal loads, the results normalized by the sliding distance value can be further normalized by the normal force, yielding the volume loss in the units of m^3/Nm [144].

7.3.2 Characterization of the wear surfaces and cross-sections

In addition to any type of numerical values that are used for presenting the wear test data, it is essential that also characterization of the wear surfaces and material deformations be conducted in a proper manner. If the prevailing wear mechanisms are not verified, the applicability of the wear test method will remain questionable. By comparing the wear surfaces and cross-sections of the in-service samples with the laboratory wear tested samples, the (possible) similarities and dissimilarities can be observed.

The appearance of the in-service wear surfaces is typically diverse, and even the wear mechanism may change is some areas, such as in the tip of the cutting edge of the mining loader bucket. The surfaces of the wear parts may also be heavily corroded. Thus, finding a representative sample may be a challenge. Consequently, in the characterization of the wear surfaces, it is advisable to use several methods in order to get a reliable and comprehensive view of the important and relevant features of the surfaces. With a stereo microscope and a 3D profilometer, it is possible to study quite large areas, even the entire surface of the wear tested sample. The 3D profilometer provides

also surface roughness data, and it can be used to measure and analyze the wear volumes. The most detailed study of the wear surfaces should always be performed with a scanning electron microscope. Especially the combined information from the secondary electron and backscatter electron detectors reveals both the topographical and compositional differences in the observed surface, including for example the abrasives embedded into the steel sample. The in-lens secondary electron detector revealed very small details from the surface in higher magnifications and worked well in the characterization of etched cross-sections.

However, finding and identifying the representative areas from the samples is the most important and often the most difficult task, irrespective of the characterization method. In this study, the same (or equivalent) area was selected from each sample type for characterization, and all replicate samples of each test type were analyzed from the exactly same area of interest. Naturally, other areas of the samples were also characterized or at least visually examined, but all presented numerical values and images were selected based on this criterion. Moreover, the same selected magnifications were used throughout the project(s) of rather long duration(s), making it possible to compare easily all studied wear surfaces with each other. The imaging of the samples was always started with small magnification overview images, and the representative areas and details were selected from those when systematically changing to higher magnifications.

In addition to the wear surfaces, it is important to analyze the deformation of the materials and the formed tribolayers. In the characterization of steels and cast irons, optical microscopy and scanning electron microscopy complement each other. For example, the transformed adiabatic shear bands are seen clearly as white lines with optical microscopy, but the nanostructural details are visible only in SEM. In addition, with SEM it is also possible to determine the crystallographic orientation of the grains using the electron backscatter diffraction method [10].

In the wear surface characterization of the nodular cast iron rollers, the main feature was the deformation of graphite nodules in the rolling-sliding contact with the wire ropes. That deformation was seen as oriented wear tongues on the wear surfaces, and as cracking of the structure in the cross-sectional studies. The statistical analysis of the length and orientation of the cracks confirmed the visual observations from the wear surfaces, when the component and contact simulating wear testing methods were compared to the in-service case. As a result, it was possible to select the correct testing parameters for the component tests.

8 Concluding remarks

There is no single, unambiguous research methodology for determining the relevance of laboratory wear experiments for the evaluation of in-service performance of materials. However, when using carefully selected application oriented test methods and correct ways to extract the relevant information from the test results, a reliable bridge between the laboratory experiments and real life applications can be built.

It is also important to remember that wear is not the only reason for failures in the mining industry. Especially fatigue plays an important role in the failure of machine parts. Thus, before the introduction of new wear resistant materials, the whole production chain needs attention. For example, the cutting and welding parameters have a marked effect both on wear and fatigue behavior of the parts.

In this thesis, various high-stress abrasive and impact abrasive wear test methods were used to simulate the wear behavior in several different industrial applications. The main results of these studies have been reported in the attached scientific publications and well as in the introductory part of this thesis. The main scientific contributions of this thesis are as follows:

- Increased understanding of high-stress abrasive and impact-abrasive wear of martensitic wear resistant steels by conducting and analyzing a wide range of different application oriented wear tests.
- Based on the scientific analysis, detailed information was gained about the wear behavior of steels and cast irons in industrial applications.
- Research methodologies for the evaluation of the relevance of laboratory wear experiments to describe and predict the in-service performance of materials were developed.

8.1 Research questions revisited

In the following, the three research questions introduced in Chapter 1 are once again revisited and answered based on the results and their analysis presented in this thesis and the related five publications.

What kind of effects the mechanical properties and the microstructure have on the wear behavior of martensitic wear resistant steels in various wear environments?

In the studied martensitic wear resistant steels, the hardness and strength had quite a linear correlation with the high-stress abrasive and impact wear behavior of the steels. The microstructural features had a more marked effect, when the hardness differences were less than 100 HV. The initial microstructure and strain hardenability of the steels affected also the formation of adiabatic shear bands. The adiabatic shear bands were formed by abrasion in the surface layers of the materials, and by impact in the subsurface areas, leading to the initiation of cracking in the tests. The harder the steel and the lower the test temperature, the more prone the steels were to form hard adiabatic shear bands capable of initiating cracks.

What kind of laboratory wear test methods could be used and how the tests should be planned to assist the materials selection for the selected in-service case studies?

In mining and haulage of minerals, the wear parts are subjected to abrasion and impacts produced by rocks and boulders. In this study, several application oriented wear test methods were used to simulate the complex conditions in the cutting edges of mining loaders and the wear plates of feed hoppers and dumper trucks. The philosophy in the planning of the tests was to use relatively large natural rocks and high enough forces to crush them and to deform the surfaces of the samples. Moreover, the effect of abrasives was studied. In the selected test procedures, the main difference was the contact conditions between the rocks and the sample surface. In the dry-pot method, the samples moved inside the freely flowing abrasive bed, and the formed adiabatic shear bands in surface layers were similar as in the in-service cases. In the crushing pin-on-disc tests, the rocks were sliding and rolling between two moving bodies, and the formed scratches were longer and deeper than in the other methods. The impeller-tumbler, in turn, produced impact-abrasive conditions, while the uniaxial crusher deformed the surfaces with high normal forces. All these methods simulate some parts or aspects of the mineral haulage, and therefore it is recommended that at least two of these methods or test procedures be utilized, when the complex high-stress abrasion environments are simulated in the laboratory scale.

The component test was the best approach for the wear study of the rollers of wire rope drives. With a quite simple test set-up, very similar contact conditions as in the in-service case could be produced. However, the test times in the component tests are very long, and thus also the twin-disc tests can be used as part of the material selection procedure.

What kind of research methodologies are best applicable for the evaluation of the relevance of the laboratory wear experiments relative to the in-service behavior and performance of materials?

Normalizing of the mass loss data using a reference material, or determining the wear rate by dividing the measured volume losses by the effective wear time and wear area are both potential methodologies, depending on what kind of comparison and results we are looking for. The use of a reference sample is a good practice especially for the comparison of materials, while the differences between the test methods can be seen only when the correct (absolute) values of various test parameters, such as area and contact time or travel length, are used. Although the numeric values are important, it is essential to verify the suitability of the wear test method also by analyzing the wear mechanism by characterization of the wear surfaces and deformation of materials.

8.2 Future studies

This study showed that quartzite, which is widely used as a standard abrasive material for example in the low-stress rubber wheel abrasion tests, is actually not very suitable for high-stress abrasion testing of steels. As a further task, it would be interesting to study the effects of abrasives in the low-stress abrasion testing of steels and to compare the results with the high-stress tests. A critical study on the applicability of the rubber wheel testers for wear testing of materials used in mining industry applications would also be needed.

Although the utilized wear test methods were quite good for simulating the examined in-service conditions, naturally there is plenty of place for improvement. A marked improvement would be adding a controlled compressive force element to the dry-pot testing, for example by 'drilling' the samples through the gravel bed during the rotating motion. A smaller modification would be redesigning the sample holder used in the crushing pin-on-disc tests to prevent its free rotation, and in the impeller-tumbler tests, a possibility to use higher amount of gravel with larger particle size would increase the wear rates and thus the accuracy of the method notably.

The study of the wear properties of selected steels at Arctic conditions should be continued with abrasion studies, and new application oriented test methods should be developed for that purpose (or the existing equipment modified). For example, the same cooling system that was used in the low temperature high velocity particle impactor could be used in the dual pivoted jaw crusher, and with some modifications, perhaps also in the impeller-tumbler system. A possible problem with crushing systems is that the moisture in the cold air easily agglomerates the small particles and dust, which can have an effect on the wear rates and complicate the comparison of the results with room temperature tests.

In this thesis, a preliminary study was made also on the effects of abrasive wear on the residual stresses on the steel surfaces, and vice versa. The next step could be to use shorter tests to determine how long it takes to neutralize the tensile stresses on the surfaces, and conduct depth profiling of the affected layers after the tests. These studies could clarify the possible role of residual stresses on the wear behavior of steels.

In high-stress abrasion, adiabatic shear band were formed on the surface layers of the studied martensitic wear resistant steels, and during heavy impacts, also subsurface adiabatic shear bands were formed. In both cases, these hard layers initiated the formation of cracks and thus had a marked effect on the progression of wear in the studied steels. Thus, development of martensitic wear resistant steel grades that are not so prone to the formation of adiabatic shear bands might be one of the future avenues for obtaining better materials for the mining and mineral handling industries. Moreover, it would be interesting to evaluate the effect of the subsurface ASBs and white layers on the wear rates. Detailed scratch studies and tribological analysis of the in-service wear surfaces would complete that study.

References

[1] Ratia V. Behavior of Martensitic Wear Resistant Steels in Abrasion and Impact Wear Testing Conditions. Tampere University of Technology, 2015.

[2] Holmberg K, Kivikytö-Reponen P, Härkisaari P, Valtonen K, Erdemir A. Global energy consumption due to friction and wear in the mining industry. Tribol Int 2017;115:116–39. doi:10.1016/j.triboint.2017.05.010.

[3] Sare IR, Constantine AG. Development of methodologies for the evaluation of wear-resistant materials for the mineral industry. Wear 1997;203–204:671–8. doi:10.1016/S0043-1648(96)07398-X.

[4] Tylczak JH, Hawk JA, Wilson RD. A comparison of laboratory abrasion and field wear results. Wear 1999;225–229:1059–69. doi:10.1016/S0043-1648(99)00043-5.

[5] Ratia V, Heino V, Valtonen K, Vippola M, Kemppainen A, Siitonen P, et al. Effect of abrasive properties on the high-stress three-body abrasion of steels and hard metals. Finnish J Tribol 2014;32:3–18.

[6] Ojala N, Valtonen K, Kivikytö-Reponen P, Vuorinen P, Kuokkala V-T. High speed slurry-pot erosion wear testing with large abrasive particles. Finnish J Tribol 2015;33:36–44.

[7] Ojala N, Valtonen K, Antikainen A, Kemppainen A, Minkkinen J, Oja O, et al. Wear performance of quenched wear resistant steels in abrasive slurry erosion. Wear 2016;354–355:21–31. doi:10.1016/j.wear.2016.02.019.

[8] Ojala N, Valtonen K, Minkkinen J, Kuokkala VT. Edge and particle embedment effects in low- and high-stress slurry erosion wear of steels and elastomers. Wear 2017;388–389:126–35. doi:10.1016/j.wear.2017.06.004.

[9] Oksanen V, Andersson P, Valtonen K, Holmberg K, Kuokkala V-T. Characterization of the wear of nodular cast iron rollers in contact with wire ropes. Wear 2013;308:199–205. doi:10.1016/j.wear.2013.06.014.

[10] Ratia V, Rojacz H, Terva J, Valtonen K, Badisch E, Kuokkala V-T. Effect of Multiple Impacts on the Deformation of Wear-Resistant Steels. Tribol Lett 2015;57. doi:10.1007/s11249-014-0460-7.

[11] Terva J, Kuokkala V-T, Valtonen K, Siitonen P. Effects of compression and sliding on the wear and energy consumption in mineral crushing. Wear 2018;398–399:116–26. doi:10.1016/j.wear.2017.12.004.

[12] Terva J, Kuokkala V-T, Valtonen K, Siitonen P. A new jaw crusher design for testing of high stress abrasion. 5th World Tribol Congr WTC 2013 2014;3:2657–60.

[13] Terva J, Kuokkala V-T, Kivikytö-Reponen P. The edge effect of specimens in abrasive wear testing. Finnish J Tribol 2012;31:27–35.

[14] Ratia V, Miettunen I, Kuokkala V-T. Surface deformation of steels in impact-abrasion: The effect of sample angle and test duration. Wear 2013;301:94–101. doi:10.1016/j.wear.2013.01.006.

[15] Ratia V, Lindroos M, Valtonen K, Apostol M, Kuokkala V-T. Impact behavior of martensitic steel at low temperatures. 17th Nord. Symp. Tribol. - Nord. 2016 Conf. Proc., Hämeenlinna: 2016, p. 1–9.

[16] Ratia V, Valtonen K, Kuokkala V-T. Impact-abrasion wear of wear-resistant steels at perpendicular and tilted angles. J Eng Tribol 2013;227:868–77. doi:10.1177/1350650113487831.

[17] Apostol M, Kuokkala V-T, Laukkanen A, Holmberg K. High velocity particle impactor – modeling and experimental verification of impact wear tests. WTC 2013 World Tribol. Congr., Torino: 2013, p. 1–4.

[18] Ojala N, Valtonen K, Kivikytö-Reponen P, Vuorinen P, Siitonen P, Kuokkala V-T. Effect of test parameters on large particle high speed slurry erosion testing. Tribol - Mater Surfaces Interfaces 2014;8:98–104. doi:10.1179/1751584X14Y.0000000066.

[19] Ratia V, Valtonen K, Kemppainen A, Kuokkala V-T. The Role of Edge-Concentrated Wear in Impact-Abrasion Testing. Tribol Online 2016;11:410–6. doi:10.2474/trol.11.410.

[20] Ojala N, Valtonen K, Heino V, Kallio M, Aaltonen J, Siitonen P, et al. Effects of composition and microstructure on the abrasive wear performance of quenched wear resistant steels. Wear 2014;317:225–32. doi:10.1016/j.wear.2014.06.003.

[21] Heino V, Valtonen K, Kivikytö-Reponen P, Siitonen P, Kuokkala V-T. Characterization of the effects of embedded quartz layer on wear rates in abrasive wear. Wear 2013;308:174–9. doi:10.1016/j.wear.2013.06.019.

[22] Lindroos M, Valtonen K, Kemppainen A, Laukkanen A, Holmberg K, Kuokkala V-T. Wear behavior and work hardening of high strength steels in high stress abrasion. Wear 2015;322–323:32–40. doi:10.1016/j.wear.2014.10.018.

[23] Lindroos M, Apostol M, Kuokkala V-T, Laukkanen A, Valtonen K, Holmberg K, et al. Experimental study on the behavior of wear resistant steels under high velocity single particle impacts. Int J Impact Eng 2015;78:114–27. doi:10.1016/j.ijimpeng.2014.12.002.

[24] Lindroos M, Apostol M, Heino V, Valtonen K, Laukkanen A, Holmberg K, et al. The deformation, strain hardening, and wear behavior of chromium-alloyed hadfield steel in abrasive and impact conditions. Tribol Lett 2015;57. doi:10.1007/s11249-015-0477-6.

[25] Lindroos M, Ratia V, Apostol M, Valtonen K, Laukkanen A, Molnar W, et al. The effect of impact conditions on the wear and deformation behavior of wear resistant steels. Wear 2015;328–329:197–205. doi:10.1016/j.wear.2015.02.032.

[26] ASTM G40, Standard Terminology Relating to Wear and Erosion 2017:9. doi:10.1520/G0040-17.

[27] Kato K, Adachi K. Wear Mechanisms. In: Bushnan B, editor. Mod. Tribol. Handb. – Vol. 1, Boca Raton, USA: CRC Press LCC; 2001, p. 273–300.

[28] Budinski KG. Guide to Friction, Wear, and Erosion Testing. ASTM International, West Conshohocken, PA; 2007. doi:10.1520/MNL56-EB.

[29] Hutchings I, Shipway P. Wear by hard particles. Tribology. 2nd ed., Oxford, United Kingdom: Elsevier; 2017, p. 165–236. doi:10.1016/B978-0-08-100910-9.00006-4.

[30] Hutchings I, Shipway P. Sliding wear. Tribology. 2nd ed., Oxford, United Kingdom: Elsevier; 2017, p. 107–64. doi:10.1016/B978-0-08-100910-9.00005-2.

[31] Stachowiak GW, Batchelor AW. Abrasive, Erosive and Cavitation Wear. Eng. Tribol., Elsevier; 2014, p. 525–76. doi:10.1016/B978-0-12-397047-3.00011-4.

[32] Gates JD. Two-body and three-body abrasion : A critical discussion. Wear 1998;214:139–46.

[33] Lewis R, Dwyer-Joyce R. Impact Wear Failures. Fail. Anal. Prev. ASM Handb., vol. 11, ASM International; 2002, p. 965–974.

[34] Gates JDD, Gore GJJ, Hermand M.-PJ, Guerineau M.-PJ, Martin PBB, Saad J. The meaning of high stress abrasion and its application in white cast irons. Wear 2007;263:6–35. doi:10.1016/j.wear.2006.12.033.

[35] van Mourik P, van Dam J, Picken S. Materials Science in Design and Engineering. VSSD; 2012.

[36] Xu Y, Zhang J, Bai Y, Meyers MA. Shear localization in dynamic deformation: Microstructural evolution. Metall Mater Trans A Phys Metall Mater Sci 2008;39 A:811–43. doi:10.1007/s11661-007-9431-z.

[37] Nikas GK. Modeling Dark and White Layer Formation on Elastohydrodynamically Lubricated Steel Surfaces by Thermomechanical Indentation or Abrasion by Metallic Particles. J Tribol 2015;137:031504. doi:10.1115/1.4029944.

[38] Cho DH, Lee SA, Lee YZ. Mechanical properties and wear behavior of the white layer. Tribol. Lett., vol. 45, 2012, p. 123–9. doi:10.1007/s11249-011-9869-4.

[39] Hossain R, Pahlevani F, Witteveen E, Banerjee A, Joe B, Prusty BG, et al. Hybrid structure of white layer in high carbon steel - Formation mechanism and its properties. Sci Rep 2017;7:1–12. doi:10.1038/s41598-017-13749-7.

[40] Boakye-Yiadom S, Bassim MN. Effect of prior heat treatment on the dynamic impact behavior of 4340 steel and formation of adiabatic shear bands. Mater Sci Eng A 2011;528:8700–8. doi:10.1016/j.msea.2011.08.036.

[41] Pursche F, Mayer L. Correlation Between Dynamic Material Behavior and Adiabatic Shear Phenomenon for Quenched and Tempered Steels. Eng Trans 2011;59:67–84.

[42] Lindroos M, Laukkanen A, Kuokkala V-T. A Crystal Plasticity Approach for Shear Banding in Hot Rolled High-Strength Steels. Metall Mater Trans A Phys Metall Mater Sci 2017;48:5608–15. doi:10.1007/s11661-017-4285-5.

[43] ASTM G190, Standard Guide for Developing and Selecting Wear Tests 2015:5. doi:10.1520/G0190-15.

[44] ASTM G65, Standard Test Method for Measuring Abrasion Using the Dry Sand/Rubber Wheel Apparatus 2016:14. doi:10.1520/G0065-16E01.

[45] ASTM G105, Standard Test Method for Conducting Wet Sand/Rubber Wheel Abrasion Tests 1989:9. doi:10.1520/G0105-16.

[46] ASTM B611, Standard Test Method for Determining the High Stress Abrasion Resistance of Hard Materials 2013:6. doi:10.1520/B0611-13.

[47] ASTM G81, Standard Test Method for Jaw Crusher Gouging Abrasion Test 2013:7. doi:10.1520/G0081.

[48] Budinski KG, Budinski ST. On replacing three-body abrasion testing with two-body abrasion testing. Wear 2017;376–377:1859–65. doi:10.1016/j.wear.2017.01.001.

[49] Konyashin I, Ries B. Wear damage of cemented carbides with different combinations of WC mean grain size and Co content. Part II: Laboratory performance tests on rock cutting and drilling. Int J Refract Met Hard Mater 2014;45:230–7. doi:10.1016/j.ijrmhm.2014.04.021.

[50] Hyttel MW, Olsson DD, Reisel G, Bøttiger J. Comparison of a newly developed compression-twist abrasive wear test with the ASTM G65 test method. Wear 2013;307:134–41. doi:10.1016/j.wear.2013.08.023.

[51] Petrica M, Katsich C, Badisch E, Kremsner F. Study of abrasive wear phenomena in dry and slurry 3-body conditions. Tribol Int 2013;64:196–203. doi:10.1016/j.triboint.2013.03.028.

[52] Konyashin I, Ries B. Wear damage of cemented carbides with different combinations of WC mean grain size and Co content. Part I: ASTM wear tests. Int J Refract Met Hard Mater 2014;46:12–9. doi:10.1016/j.ijrmhm.2014.04.021.

[53] Sare IR, Constantine AG. Design and Analysis of Jaw Crusher Gouging Abrasion Tests. J Test Eval 1991;19:115–22. doi:10.1520/JTE12543J.

[54] Gates J, Eaton RA. Real Life Wear Processes. Mater Forum 1993;17:369–81.

[55] Osara K, Tiainen T. Three-body impact wear study on conventional and new PM/ + HIPed wear resistant materials. Wear 2001;250–251:785–94. doi:10.1016/S0043-1648(01)00717-7.

[56] Albertin E, Sinatora A. Effect of carbide fraction and matrix microstructure on the wear of cast iron balls tested in a laboratory ball mill. Wear 2001;250–251:492–501. doi:10.1016/S0043-1648(01)00664-0.

[57] Gates JD, Dargusch MS, Walsh JJ, Field SL, Hermand MJP, Delaup BG, et al. Effect of abrasive mineral on alloy performance in the ball mill abrasion test. Wear 2008;265:865–70. doi:10.1016/j.wear.2008.01.008.

[58] Blickensderfer R, Tylczak JH. A large-scale impact spalling test. Wear 1983;84:361–73. doi:10.1016/0043-1648(83)90276-4.

[59] Laird G, Collins WK, Blickensderfer R. Crack propagation and spalling of white cast iron balls subjected to repeated impacts. Wear 1988;124:217–35. doi:10.1016/0043-1648(88)90245-1.

[60] Akhondizadeh M, Mahani M, Mansouri SH, Rezaeizadeh M. A New Procedure of Impact Wear evaluation of Mill Liner. Int J Eng 2015;28:593–8.

[61] Blickensderfer R, Forkner BL. A Ball-on-Block Impact-Spalling Wear Test and Results on Several Iron Alloys. 1983.

[62] Franek F, Badisch E, Kirchgaßner M. Advanced Methods for Characterisation of Abrasion/Erosion Resistance of Wear Protection Materials. FME Trans 2009;37:61–70.

[63] Winkelmann H, Badisch E, Varga M, Danninger H. Wear mechanisms at high temperatures. part 3: Changes of the wear mechanism in the continuous impact abrasion test with increasing testing temperature. Tribol Lett 2010;37:419–29. doi:10.1007/s11249-009-9534-

3.

[64] Chen H, Zhao D, Wang Q, Qiang Y, Qi J. Effects of impact energy on the wear resistance and work hardening mechanism of medium manganese austenitic steel. Friction 2017;5:447–54. doi:10.1007/s40544-017-0158-6.

[65] Ge S, Wang Q, Wang J. The impact wear-resistance enhancement mechanism of medium manganese steel and its applications in mining machines. Wear 2017;376–377:1097–104. doi:10.1016/J.WEAR.2017.01.015.

[66] Xie Y, Jiang J, Tufa KY, Yick S. Wear resistance of materials used for slurry transport. Wear 2015;332–333:1104–10. doi:10.1016/j.wear.2015.01.005.

[67] Bootle M. Wear in Rotodynamic (Centrifugal) Slurry Pumps Modes of Wear in Slurry Pumps. Calgary Pump Symp., 2009.

[68] Pintaude G, Bartalini NM. Revisiting gouging abrasion test for jaw crushers. REM - Int Eng J 2018;71:111–5. doi:10.1590/0370-44672017710060.

[69] Thuro K, Käsling H. Classification of the abrasiveness of soil and rock. Geomech Und Tunnelbau 2009;2:179–88. doi:10.1002/geot.200900012.

[70] Abrasimeter. Paris, France: Matériales des Laboratoires des Ponts et Chaussées; 1985.

[71] Jarry C, Gall D Le. NFP 18 579 Granulats - Essai d'abrasivité et de broyabilité 1990.

[72] Drucker P. Validity of the LCPC abrasivity coefficient through the example of a recent Danube gravel. Geomech Tunn 2011;4:681–91. doi:10.1002/geot.201100051.

[73] Küpferle J, Röttger A, Alber M, Theisen W. Assessment of the LCPC abrasiveness test from the view of material science. Geomech Tunn 2015;8:211–20. doi:10.1002/geot.201500002.

[74] ASTM D7625, Standard Test Method for Laboratory Determination of Abrasiveness of Rock Using the CERCHAR Method 2010. doi:10.1520/D7625-10.

[75] Majeed Y, Abu Bakar MZ. Statistical evaluation of CERCHAR Abrasivity Index (CAI) measurement methods and dependence on petrographic and mechanical properties of selected rocks of Pakistan. Bull Eng Geol Environ 2016;75:1341–60. doi:10.1007/s10064-015-0799-5.

[76] Rostami J, Ghasemi A, Alavi Gharahbagh E, Dogruoz C, Dahl F. Study of dominant factors affecting cerchar abrasivity index. Rock Mech Rock Eng 2014;47:1905–19. doi:10.1007/s00603-013-0487-3.

[77] Hamzaban MT, Memarian H, Rostami J. Continuous monitoring of pin tip wear and penetration into rock surface using a new cerchar abrasivity testing device. Rock Mech Rock Eng 2014;47:689–701. doi:10.1007/s00603-013-0397-4.

[78] Abu Bakar MZ, Majeed Y, Rostami J. Effects of rock water content on CERCHAR Abrasivity Index. Wear 2016;368–369:132–45. doi:10.1016/j.wear.2016.09.007.

[79] Thuro K. Prediction of drillability in hard rock tunnelling by drilling and blasting. In: Golser, Hinkel, Schubert, editors. Tunnels for People, Balkema, Rotterdam; 1997, p. 103–8.

[80] Rosiwal A. Neue Untersuchungsergebnisseüber die Härte von Mineralien und Gesteine.

Verhandlungen Der Kais Geol Reichsanstalt 1896:475–491.

[81] Plinninger RJ. Hardrock abrasivity investigation using the Rock Abrasivity Index (RAI). 11th IAEG Congr., Taylor & Francis, London; 2010, p. 3445–52.

[82] Plinninger RJ, Düllmann J. On the Influence of Rock Mass Scale Effects on Tool Wear Prediction in Hardrock Tunnelling. EURO-TUN 2017 - Comput. Methods Tunn. Subsurf. Eng., Innsbruck, Austria: 2017.

[83] Jost HP. Tribology — Origin and future. Wear 1990;136:1–17. doi:10.1016/0043-1648(90)90068-L.

[84] Blickensderfer R. Design criteria and correction factors for field wear testing. Wear, vol. 122, 1988, p. 165–82. doi:10.1016/0043-1648(88)90076-2.

[85] Vuorinen E, Ojala N, Heino V, Rau C, Gahm C. Erosive and abrasive wear performance of carbide free bainitic steels - Comparison of field and laboratory experiments. Tribol Int 2016;98:108–15. doi:10.1016/j.triboint.2016.02.015.

[86] Fernández J. E, Vijande R, Tucho R, Rodríguez J, Martín A. Materials selection to excavator teeth in mining industry. Wear, vol. 250, 2001, p. 11–8. doi:10.1016/S0043-1648(01)00624-X.

[87] Walker CII, Robbie P. Comparison of some laboratory wear tests and field wear in slurry pumps. Wear, vol. 302, Elsevier; 2013, p. 1026–34. doi:10.1016/j.wear.2012.11.053.

[88] Dommarco R, Galarreta I, Ortíz H, David P, Maglieri G. The use of ductile iron for wheel loader bucket tips. Wear 2001;249:100–7. doi:10.1016/S0043-1648(01)00531-2.

[89] Sarkar M, Ghosh SK, Mukherjee PS. Analysis of wear generation in mine excavator bucket. Ind. Lubr. Tribol., vol. 67, 2015, p. 52–8. doi:10.1108/ILT-09-2013-0102.

[90] Lundy JS. The Abrasive Wear of Agricultural Ground Tools. The University of South Australia, 1998.

[91] Bialobrzeska B, Kostencki P. Abrasive wear characteristics of selected low-alloy boron steels as measured in both field experiments and laboratory tests. Wear, vol. 328–329, 2015, p. 149–59. doi:10.1016/j.wear.2015.02.003.

[92] Jakobsen PD, Langmaack L, Dahl F, Breivik T. Development of the Soft Ground Abrasion Tester (SGAT) to predict TBM tool wear, torque and thrust. Tunn Undergr Sp Technol 2013;38. doi:10.1016/j.tust.2013.07.021.

[93] Jakobsen PD, Lohne J. Challenges of methods and approaches for estimating soil abrasivity in soft ground TBM tunnelling. Wear 2013;308:166–73. doi:10.1016/j.wear.2013.06.022.

[94] Alavi Gharahbagh E, Rostami J, Talebi K. Experimental study of the effect of conditioning on abrasive wear and torque requirement of full face tunneling machines. Tunn Undergr Sp Technol 2014;41:127–36. doi:10.1016/j.tust.2013.12.003.

[95] Küpferle J, Röttger A, Theisen W, Alber M. The RUB Tunneling Device - A newly developed test method to analyze and determine the wear of excavation tools in soils. Tunn Undergr Sp Technol 2016;59:1–6. doi:10.1016/j.tust.2016.06.006.

[96] Oñate Salazar CG, Todaro C, Bosio F, Bassini E, Daniele U, Peila D. A new test device for the

study of metal wear in conditioned granular soil used in EPB shield tunneling. Tunn Undergr Sp Technol 2017;73:1–24. doi:https://doi.org/10.1016/j.tust.2017.12.014.

[97] Majeed Y, Abu Bakar MZ. Effects of variation in the particle size of the rock abrasion powder and standard rotational speed on the NTNU/SINTEF abrasion value steel test. Bull Eng Geol Environ 2017:1–18. doi:10.1007/s10064-017-1211-4.

[98] Barzegari G, Uromeihy A, Zhao J. Parametric study of soil abrasivity for predicting wear issue in TBM tunneling projects. Tunn Undergr Sp Technol 2015;48:43–57. doi:10.1016/j.tust.2014.10.010.

[99] Zare S, Bruland A. Applications of NTNU/SINTEF drillability indices in hard rock tunneling. Rock Mech Rock Eng 2013;46:179–87. doi:10.1007/s00603-012-0253-y.

[100] Abu Bakar MZ, Gertsch LS, Rostami J. Evaluation of fragments from disc cutting of dry and saturated sandstone. Rock Mech Rock Eng 2014;47:1891–903. doi:10.1007/s00603-013-0482-8.

[101] Kallel M, Zouch F, Antar Z, Bahri A, Elleuch K. Hammer premature wear in mineral crushing process. Tribol Int 2017. doi:10.1016/j.triboint.2017.06.025.

[102] Pereira JI, Machado PC, Penagos JJ, Sinatora A. Wear characterization from field and laboratory tests of pearlitic steels used for SAG mill liners. Wear 2017;376–377:37–45. doi:10.1016/j.wear.2017.01.094.

[103] Beste U, Jacobson S. A new view of the deterioration and wear of WC/Co cemented carbide rock drill buttons. Wear 2008;264:1129–41. doi:10.1016/j.wear.2007.01.030.

[104] Tkalich D, Li CC, Kane A, Saai A, Yastrebov VA, Hokka M, et al. Wear of cemented tungsten carbide percussive drill–bit inserts: Laboratory and field study. Wear 2017;386–387:106–17. doi:10.1016/j.wear.2017.05.010.

[105] Abbasi E, Luo Q, Owens D. Case study: Wear mechanisms of NiCrVMo-steel and CrB-steel scrap shear blades. Wear 2018;398–399:29–40. doi:10.1016/j.wear.2017.11.014.

[106] Wessel ET. Abrupt yielding and the ductile-to-brittle transition in bcc metals. J Met 1957;9:930–5.

[107] Ma L, Shi LB, Guo J, Liu QY, Wang WJ. On the wear and damage characteristics of rail material under low temperature environment condition. Wear 2018;394–395:149–58. doi:10.1016/J.WEAR.2017.10.011.

[108] Lyu Y, Bergseth E, Olofsson U. Open system tribology and influence of weather condition. Sci Rep 2016;6. doi:10.1038/srep32455.

[109] Haiko O, Somani M, Porter D, Kantanen P, Kömi J, Ojala N, et al. Comparison of impact-abrasive wear characteristics and performance of direct quenched (DQ) and direct quenched and partitioned (DQ&P) steels. Wear 2018;400–401:21–30. doi:10.1016/j.wear.2017.12.016.

[110] Yang SH, Hanski E, Li C, Maier WD, Huhma H, Mokrushin A V., et al. Mantle source of the 2.44–2.50-Ga mantle plume-related magmatism in the Fennoscandian Shield: evidence from Os, Nd, and Sr isotope compositions of the Monchepluton and Kemi intrusions. Miner Depos 2016;51:1055–73. doi:10.1007/s00126-016-0673-9.

[111] Fourmeau M, Gomon D, Vacher R, Hokka M, Kane A, Kuokkala V-T. Application of DIC Technique for Studies of Kuru Granite Rock under Static and Dynamic Loading. Procedia Mater Sci 2014;3:691–7. doi:10.1016/j.mspro.2014.06.114.

[112] SFS-EN 1563 Founding. Spheroidal graphite cast irons 2012:48.

[113] Terva J, Teeri T, Kuokkala V-T, Siitonen P, Liimatainen J. Abrasive wear of steel against gravel with different rock-steel combinations. Wear 2009;267. doi:10.1016/j.wear.2009.02.019.

[114] Lindroos M. Experimental and Numerical Studies on the Abrasive and Impact Behavior of Wear Resistant Steels. Tampere University of Technology, 2016.

[115] Heino V, Kaipiainen M, Siitonen P, Ratia V, Valtonen K, Lepisto T, et al. Compressive Crushing of Granite with Wear- Resistant Materials. Finnish J Tribol 2011;30:21–8.

[116] Sarlin E, Apostol M, Lindroos M, Kuokkala V-T, Vuorinen J, Lepistö T, et al. Impact properties of novel corrosion resistant hybrid structures. Compos Struct 2014;108:886–93. doi:10.1016/j.compstruct.2013.10.023.

[117] SFS-ISO 3290-1:en Rolling bearings. Balls. Part 1: Steel balls 2008:11.

[118] SFS-ISO 3290-2 Rolling bearings. Balls. Part 2: Ceramic balls 2008:12.

[119] Caterpillar. R2900G Underground Mining Load-Haul-Dump (LHD) Loader 2018. https://www.cat.com/en_ID/products/new/equipment/underground-hard-rock/underground-mining-load-haul-dump-lhd-loaders/18234906.html (accessed February 15, 2018).

[120] Keltamäki K, Ylitolva M. Kaivoskoneen kauhan huulilevyn kulumistutkimus. Lapland University of Applied Sciences; 2014.

[121] Rissanen T. Kaivosteollisuuden teräkset. Lapland University of Applied Sciences; 2014.

[122] ISO 25178-2: Geometrical product specifications (GPS) - Surface texture: Areal Part 2: Terms, definitions and surface texture parameters 2007:51.

[123] SFS-EN ISO 148-1: 2009 Metallic materials. Charpy pendulum impact test. Part 1 : Test method 2009:30.

[124] SFS-EN 15305 Non-destructive Testing. Test Method for Residual Stress analysis by X-ray Diffraction 2008:87.

[125] Jaakonmäki A, Johansson B, Mäkinen I, Räsänen H, Ulvelin K, Vennelä T. Kiven käsittely ja kalusto. In: Hakapää A, Lappalainen P, editors. Kaivos- ja louhintatekniikka, Opetushallitus; 2009, p. 183–213.

[126] Rojacz H, Premauer M, Varga M. Alloying and strain hardening effects in abrasive contacts on iron based alloys. Wear 2018;410–411:173–80. doi:10.1016/J.WEAR.2018.05.022.

[127] Xu X, van der Zwaag S, Xu W. The effect of martensite volume fraction on the scratch and abrasion resistance of a ferrite-martensite dual phase steel. Wear 2016;348–349. doi:10.1016/j.wear.2015.11.017.

[128] Machado PC, Pereira JI, Penagos JJ, Yonamine T, Sinatora A. The effect of in-service work hardening and crystallographic orientation on the micro-scratch wear of Hadfield steel. Wear

2017;376–377:1064–73. doi:10.1016/J.WEAR.2016.12.057.

[129] Hokkirigawa K, Kato K, Li ZZ. The effect of hardness on the transition of the abrasive wear mechanism of steels. Wear 1988;123:241–51. doi:10.1016/0043-1648(88)90102-0.

[130] Franco LA, Sinatora A. Material removal factor (fab): A critical assessment of its role in theoretical and practical approaches to abrasive wear of ductile materials. Wear 2017;382–383:51–61. doi:10.1016/j.wear.2017.04.006.

[131] Blau PJ. How common is the steady-state? The implications of wear transitions for materials selection and design. Wear 2014;332–333:1120–8. doi:10.1016/j.wear.2014.11.018.

[132] Demanding Applications – DEMAPP. Fimecc Publication series 3/2014. FIMECC Oy; 2014.

[133] Manco GL, Caruso S, Rotella G. FE modeling of microstructural changes in hard turning of AISI 52100 steel. Int J Mater Form 2010;3:447–50. doi:10.1007/s12289-010-0803-3.

[134] Mao C, Zhou Z, Zhang J, Huang X, Gu D. An experimental investigation of affected layers formed in grinding of AISI 52100 steel. Int J Adv Manuf Technol 2011;54:515–23. doi:10.1007/s00170-010-2965-z.

[135] Ji W, Shi J, Liu X, Wang L, Liang SY. A Novel Approach of Tool Wear Evaluation. J Manuf Sci Eng 2017;139:1–8. doi:10.1115/1.4037231.

[136] Attanasio A, Umbrello D, Cappellini C, Rotella G, M'Saoubi R. Tool wear effects on white and dark layer formation in hard turning of AISI 52100 steel. Wear 2012;286–287:98–107. doi:10.1016/j.wear.2011.07.001.

[137] Hosseini SB, Klement U, Yao Y, Ryttberg K. Formation mechanisms of white layers induced by hard turning of AISI 52100 steel. Acta Mater 2015;89. doi:10.1016/j.actamat.2015.01.075.

[138] Chen T, Qiu C, Liu X, Qian X, Liu G. Study on test method of white layer microhardness in hard cutting based on chord tangent method. Int J Adv Manuf Technol 2017:1–9. doi:10.1007/s00170-017-0197-1.

[139] Blau PJ. Lessons learned from the test-to-test variability of different types of wear data. Wear 2017;376–377:1830–40. doi:10.1016/J.WEAR.2016.11.012.

[140] Sorsa A, Santa-aho S, Wartiainen J, Suominen L, Vippola M, Leiviskä K. Effect of Shot Peening Parameters to Residual Stress Profiles and Barkhausen Noise. J Nondestruct Eval 2018;37:1–11. doi:10.1007/s10921-018-0463-7.

[141] Alapieti T, Huhtelin T. The Kemi intrusion and accosiated chromite deposit. In: Alapieti T, Kärki A, editors. Geol. Surv. Finland, Guid. 51a, 1989, p. 13–31.

[142] Lindroos M, Kuokkala V-T, Lehtovaara A, Kivikyto-Reponen P. Effects of strain and strain rate on the abrasive wear behavior of high manganese austenitic steel. Eng Mater Tribol 2013;527:211–6. doi:10.4028/www.scientific.net/KEM.527.211.

[143] Saha G. Abrasive wear of alloys for ground engaging tools. Deakin University, 2017.

[144] Kabir MS, Munroe P, Zhou Z, Xie Z. Scratch adhesion and tribological behaviour of graded Cr/CrN/CrTiN coatings synthesized by closed-field unbalanced magnetron sputtering. Wear 2017;380–381:163–75. doi:10.1016/J.WEAR.2017.03.020.

Original publications

Publication I

Vilma Ratia, Kati Valtonen, Anu Kemppainen, Minnamari Vippola, and Veli-Tapani Kuokkala

High-stress abrasion and impact-abrasion testing of wear resistant steels

Tribology Online 8 (2013) pp. 152-161

Tribology Online
Japanese Society of Tribologists

Tribology Online, 8, 2 (2013) 152-161.
ISSN 1881-2198
DOI 10.2474/trol.8.152

Article

High-Stress Abrasion and Impact-Abrasion Testing of Wear Resistant Steels

Vilma Ratia[1)*], Kati Valtonen[1)], Anu Kemppainen[2)] and Veli-Tapani Kuokkala[1)]

[1)]Tampere University of Technology, Department of Materials Science, Tampere Wear Center
P.O.Box 589, 33101 Tampere, Finland
[2)]Ruukki Metals Inc.
P.O.Box 93, 92101 Raahe, Finland
*Corresponding author: vilma.ratia@tut.fi

(Manuscript received 10 March 2012; accepted 15 January 2013; published 15 February 2013)
(Presented at Technical Session in the International Tribology Conference Hiroshima 2011)

Energy can be saved by enhancing the service life of machinery and by designing lighter units. These design changes enable, for example, lower fuel consumption and larger payloads. The implementation of this kind of solutions, however, requires development of better wear resistant materials. In this study, the wear resistance of a structural steel and three grades of wear resistant steel was evaluated with granite abrasive in tests simulating the conditions in heavy machinery in mining and transportation. Two high-stress abrasion and one impact-abrasion wear testing methods were used. In all tests, higher hardness led to decreased mass loss, but in impact-abrasion the hardness dependence was smaller than in the heavy abrasion tests. This may, however, at least partly result from deformation of softer materials over the sample edges, which is not shown as mass loss. Wear surfaces of structural steel samples exhibited the highest degree of plastic deformation due to their lower hardness and higher ductility compared to the wear resistant steels. On the other hand, in harder materials the scratches were more visible, indicating a change in wear mechanism. Both differences and similarities in the behavior and wear mechanisms of the selected steels were observed in the applied conditions.

Keywords: abrasion, hardness, impact, steel, wear

1. Introduction

Severe conditions in earthmoving and mining cause heavy wear in equipment used in the field. For example, it has been estimated that 6350 kg of steel is used for replacements per excavation bucket in just six months [1]. In the development towards less energy consumption, besides reducing the use of materials, energy can be saved by enhancing the service life of machinery and by designing lighter units. Lighter units enable less fuel consumption and larger payloads. However, the implementation of these solutions requires the use of more durable materials.

The suitability of materials for a certain application can be assessed by field and laboratory testing. Laboratory testing enables controlled conditions and lower costs. In laboratory tests, however, the testing conditions need to be simplified in order to create a well controlled system. Wear testing is often conducted by using industrial abrasives of a narrow size distribution for better control of the abrasive properties. On the other hand, to simulate the real conditions properly, also testing with natural abrasives is important.

In applications such as earthmoving and mining machinery, the gravel and minerals generate heavy abrasion and impact wear. Moreover, the material can be subjected to several different kinds of conditions during its service. Loading, unloading and transportation all cause slightly different conditions to the tipper body, as the movement of the abrasive relative to the material surface and the applied load vary. Thus, more than one type of testing with various conditions and parameters is needed to assess the wear properties of the materials. In this work, the wear of selected steel grades was studied using natural granite as an abrasive in three different test procedures to simulate the severe conditions in these kinds of applications. Two high-stress abrasion and one high-stress impact-abrasion methods were used.

One of the classifications of abrasive wear is the division into high-stress abrasion and low-stress abrasion. In high-stress abrasion, the stress in the wear area is sufficient to cause crushing of the abrasive. In low-stress

abrasion, the abrasives remain intact. [2] In all testing methods used in this study, crushing of the abrasives occurs. Thus, based on this classification, they all are high-stress abrasion testing methods.

In earlier studies [3-5], similar impact-abrasion wear testing equipment has been used in addition to, for example, dry sand rubber wheel or pin-on-disc testing. However, the particle size used in the latter mentioned abrasive testing methods has been typically much smaller than the one used in impact-abrasion testing, i.e., 40-300 μm compared to 1.6-25 mm.

Rendón and Olsson [3] compared the results of impeller-tumbler and pin-on-disc with abrasive paper. 12-20 mm quartzite gravel was used in the impeller-tumbler tests and SiC paper of mesh 320 in the pin-on-disc tests. The authors observed clear differences in the resulting wear surfaces and formed tribolayers under the surface: the impeller-tumbler produced a thicker tribolayer with embedded abrasives whereas the samples tested with the pin-on-disc did not have any embedded abrasives. However, in those tests, the abrasive for testing the impact-abrasive and the abrasive wear was not similar and the difference in the grain size was substantial. Moreover, the abrasives in the abrasive wear method were fixed to a paper, causing mainly two-body abrasive wear. Considering mining and transportation applications, the abrasive material is usually loose.

The low and high impact loading impeller-tumbler tests of four hardfacing alloys were compared to standard ASTM G65 rubber wheel test and single impact test results by Badisch et al. [4]. They used 212-300 μm Ottawa silica sand for the ASTM G65 tests and 1.6-2.2 mm silica sand or 5-10 mm corundum for the low and high impact loading tests in impeller-tumbler, respectively. It was found that the performance of the materials in those tests strongly depended on the microstructure. However, although impact, impact-abrasive and abrasive conditions were covered in the testing, the abrasive was different in all methods and thus the significant difference in abrasive properties also had an effect on the results.

Tylczak et al. [5] tested several steel types in the field and in multiple laboratory tests. They used pin-on-drum testing with approximately 100 μm garnet as the abrasive, ASTM G65 rubber wheel testing with 200-300 μm rounded silica, jaw crusher test with 25.4 mm quartzite, and impeller-tumbler with 19-25 mm quartzite. Increased hardness reduced the wear of the materials with a linear correlation in the abrasive pin-on-drum and ASTM G65 tests. However, the gouging abrasion in jaw crusher and impact-abrasion in impeller-tumbler caused different wear behavior and the correlation between hardness and wear resistance was negligible. This extensive study with several testing methods produced variable wear environments, but there was a notable difference between the used abrasive sizes.

In real-life applications, the used abrasive media causes both impacts and abrasion. Thus, it is important to use comparable abrasives when testing several wear modes with different tests. In the present study, the abrasive was natural stone granite in all testing methods. The particle sizes in the abrasive and impact-abrasive tests were on average 5-6 mm and 11 mm, respectively, so they were close to each other. To correlate to the real life applications, the testing methods were selected to simulate the steps of a transportation process: loading, transportation and unloading. The impact-abrasive impeller-tumbler method simulates loading, where the gravel falls onto the tipper body with abrasion resistant steel plates. Crushing abrasion by the uniaxial crusher method simulates the compaction and transportation of the heavy loads. The unloading, where the load slides on the floor plates of the tipper body, is simulated by the crushing pin-on-disc, in which the samples are subjected to heavy abrasive conditions between a pin and a rotating disc. The study aims to present differences and similarities in the behavior and wear mechanisms of the selected steel grades in versatile heavy abrasion conditions, which are typical for earth moving and mining processes. The results assist the material selection in these applications.

2. Experimental methods

This Chapter presents the tested steels and the abrasive. In addition, the used wear testing methods are introduced together with the analyzing equipment used to determine the mass losses and to characterize the wear surfaces after the tests.

Table 1 Surface hardness and typical mechanical properties of the test materials

	Hardness [HB]				
Material	**Crushing pin-on-disc**	**Uniaxial crusher**	**Impeller-tumbler**	**Tensile strength R_m [N/mm^2]**	**Elongation A5 [%]**
S355	162	162	154	430-530	24
Raex 400	368	368	403	1250	10
Raex 450	-	445	456	1450	8
Raex 500	492	469	492	1600	8

Table 2 Parameters of the applied testing methods

Method	Wear type	Motion	Force	Abrasive size
Crushing pin-on-disc	High-stress abrasion	crushing sliding	200 N	2-10 mm
Uniaxial crusher	High-stress abrasion	crushing	53 kN	4-6.3 mm
Impeller-tumbler	High-stress impact-abrasion	impact sliding	N/A	10-12.5 mm

2.1. Materials

The materials studied in this work were a structural steel (S355) and three martensitic wear resistant steels (Raex) manufactured by Ruukki Metals, Inc. Table 1 presents the Brinell hardness values and typical tensile strengths and elongation values of the test materials. The hardness of the same steel grades used in different tests varied, because they were from different batches.

Granite was the abrasive used in all tests, but its size distribution varied slightly with the test method. To minimize the effect of natural variation in the properties of the rock material, the abrasives were all from a single batch from Sorila quarry in Finland. Table 2 presents the size distributions used for different testing methods. The abrasive size distributions were chosen to cause the most severe wear conditions within the limits of the testing devices. The abrasive was crushed and angular in shape.

2.2. Methods

The materials were tested using two high-stress abrasive and one high-stress impact-abrasive wear testing method. The equipment was designed and constructed at the Tampere Wear Center. The differences between the methods are the motion of the sample surface and the applied force. In the crushing pin-on-disc method, the sample is subjected to both crushing and sliding, whereas in the uniaxial crushing method the motion is uniaxial and there is no sliding movement between the sample and the counterpart. In the current tests, the applied force was substantially higher in the uniaxial crusher, approximately 265 times that in the crushing pin-on-disc. In the impeller-tumbler method, the sample is subjected to both impacts and sliding of loose abrasives. Table 2 presents the characteristic parameters of each testing method. All tests were conducted at room temperature.

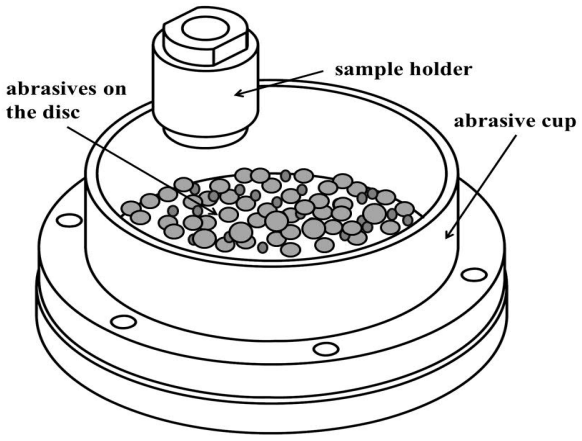

Fig. 1 Crushing pin-on-disc wear test device

2.2.1 Crushing pin-on-disc

The crushing pin-on-disc test method [6], which is based on the common pin-on-disc principle, was used to determine the abrasion wear resistance of the test materials. In the crushing pin-on-disc method, loose abrasive is placed between the rotating disc and the pin, which is cyclically pressed against the abrasive. Figure 1 illustrates the crushing pin-on-disc device. The pin and the disc are not in direct contact at any point of the test.

In the current tests, the pin sample was a solid cylinder with a diameter of 36 mm, creating a wear area of 1000 mm^2. The orientation of the sample pin was not fixed and thus it could rotate around its own axis to cause even wear throughout the sample surface. The diameter of the disc was 160 mm. The used discs were structural steel for the S355 and wear resistant steel for Raex samples. Table 3 presents the hardness of the used discs. The rotating speed of the disc was 28 rpm and the sliding distance of the pin center point during the test

Table 3 Hardness of the discs used in crushing pin-on-disc

Disc	Hardness [HB]
S355	205
Raex 400	461
Raex 500	520

Table 4 The abrasive size distribution used in the crushing pin-on-disc testing method

Size distribution [mm]	Mass [g]
2-4	50
4-6.3	250
6.3-8	150
8-10	50
Σ	500

approximately 120 m. The force used in the current tests was 200 N.

Table 4 presents the size distribution of the abrasive mixture used in the tests. This distribution causes efficient wear in the samples in this testing method. The total amount of gravel in one test was 500 g. The abrasive in the cup was not changed during the test, which led to changing testing conditions due to comminution of the abrasive by crushing. However, the abrasive in the pin-rock interface was replenished between each crush by cyclically lifting the pin above the gravel bed. The pin was cyclically pressed down for 5 s and then lifted up for 2.5 s for the abrasive to change in the pin-rock interface due to the rotation of the disc. The duration of the test was 30 minutes, which equals approximately 240 compressions and 20 minutes of contact time. To reach the steady-state wear, the samples were subjected to a 20 minute running-in stage before the actual test. The standard deviation of the results obtained with the crushing pin-on-disc method is on average 7%.

2.2.2 Uniaxial crusher

The uniaxial crusher method [7] was used to evaluate the durability of the test materials under plain compression by the abrasive media. Figure 2 presents the crushing section of the uniaxial crusher device. In the present study, the gravel was crushed between the sample and the tool steel counterpart with hardness of 690 HV in a rubber cup. The movement of the sample is vertical, so the sample and the counterpart do not move in relation to each other. For every compression, the gravel is replaced using an automatic supply tube that fills the cup. A rotary actuator tilts the cup to empty it from the crushed abrasive at the end of each cycle. The used abrasive was granite of the size distribution 4-6.3 mm. This size enabled steady removal and replacement of the abrasive.

The samples were similar to those used in the crushing pin-on-disc tests, having a wear surface of 1000 mm^2. The used force was 53 kN. The running-in stage included 100 compressions, and the duration of the actual test was 900 compressions. The standard deviation of the results with this method is approximately 15%.

2.2.3 Impeller-tumbler

The impeller-tumbler wear tester was used to measure the impact-abrasion wear resistance of the test

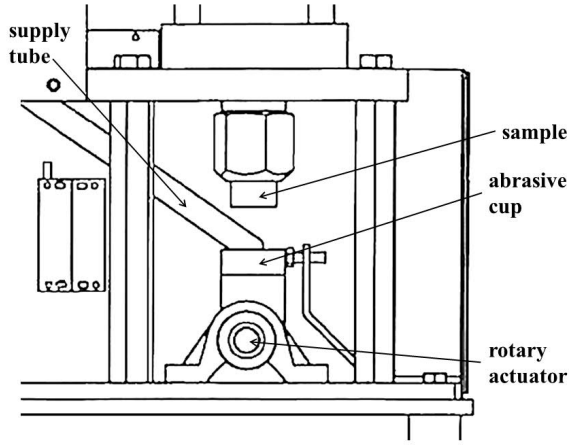

Fig. 2 Crushing section of the uniaxial crusher device

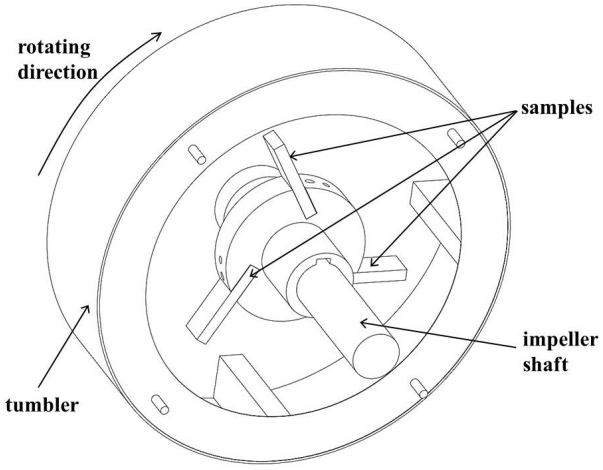

Fig. 3 Impeller-tumbler wear test device

materials. Figure 3 presents a schematic picture of the impeller-tumbler device. The samples act as impeller blades attached to the sample holder, and the tumbler contains the gravel. Both the impeller and the tumbler rotate in the same direction at rotation speeds of 700 rpm and 30 rpm, respectively. During the test, the samples are impacted and scratched by the moving abrasives, which are kept in motion with the tumbler. The diameter of the tumbler is 350 mm.

In the present tests, the sample size was 75 × 25 ×5 mm, of which 1200 mm^2 constituted the wear surface. The distance from the outer edge of the sample to the center of the sample holder was approximately 105 mm. The samples were attached at a 60° angle to the sample holder perimeter. It must, however, be emphasized that the sample angle in this method is not equal to the abrasive incidence angle, as the abrasive particles are loose and move freely inside the tumbler and thus impact the samples at arbitrary angles.

The duration of each test was 60 minutes. The

samples were weighted and the abrasive was renewed every 15 minutes. The running-in stage was 15 minutes. Three samples were tested simultaneously, one of which was always a Raex 400 reference sample. This enabled accounting for the effects of property variance of the natural abrasives. The samples were circulated in the sample holder slots to exclude the possible effects of the sample positions. The reference sample was kept in the same slot for the whole test to provide steady conditions for it. The mass losses were calculated as an average of the result from three samples in relation to the mass loss of the reference sample. The standard deviation of the results was less than 3%.

The used abrasive was granite of 10-12.5 mm in size. Larger particle size correlates with higher wear rates, which is why a larger abrasive size was used with the impeller-tumbler than with the other methods. The amount of gravel in the tumbler was 900 g. As the abrasive was renewed every 15 minutes, the total amount of abrasive in a 60 minute test was 3600 g. The particle count was approximately 410 in each 900 g gravel batch.

2.2.4 Analyzing methods

The wear rate was determined by measuring the mass loss during the test. The samples were cleaned with pressurized air or ethanol before weighting. The accuracy of the used balance was 0.001 g.

Veeco Wyko NT1100 optical profilometer was used for surface roughness measurements. The measurements were conducted with 5x objective and 0.5 field of view lens. The results were filtered using the median 3 filter.

The Vickers hardness HV0.1 of the worn samples was measured with Matsuzawa MMT-X7 microhardness tester from the cross sections as close to the surface as possible to reveal the possible work hardening of the material. The penetration depth in the wear scars was determined from the cross-sections with Leica DM 2500 M optical microscope. The cross sections from the length of 5 mm were studied and the maximum depth of each distinguishable scar inside the 5 mm region was measured.

The wear surfaces were characterized with Leica MZ 7.5 zoom stereomicroscope and Philips XL30 scanning electron microscope (SEM). The samples were cleaned in ultrasonic bath and sputtered with a thin layer of gold to avoid charging of the abrasive remnants on the surface.

3. Results

In this Chapter, the wear test results and their correlation to the mechanical properties are presented. Moreover, the characterization of wear surfaces by surface roughness, penetration depth and hardness measurements are presented along with observations made by optical and electron microscopy.

3.1. Wear tests

The wear rate of the samples was determined by mass loss measurements. The effect of the abrasive remnants on the mass loss measurements was minimized by doing a running-in phase to all samples. In this way, the steady state of wear was reached before starting the actual test.

3.1.1 Crushing pin-on-disc

Figure 4 presents the mass loss results for the pins in the crushing pin-on-disc tests. The mass loss of S355 was much higher than that of the wear resistant steels. The difference between the wear resistant steels was evident as well, the mass loss of Raex 500 being approximately 30% lower than the mass loss of Raex 400.

3.1.2 Uniaxial crusher

Figure 5 presents the mass loss results from the uniaxial crusher tests. The mass loss of S355 was more than double compared to the wear resistant steels. On the other hand, the wear resistant steels showed smaller differences between each other than in the crushing pin-on-disc test.

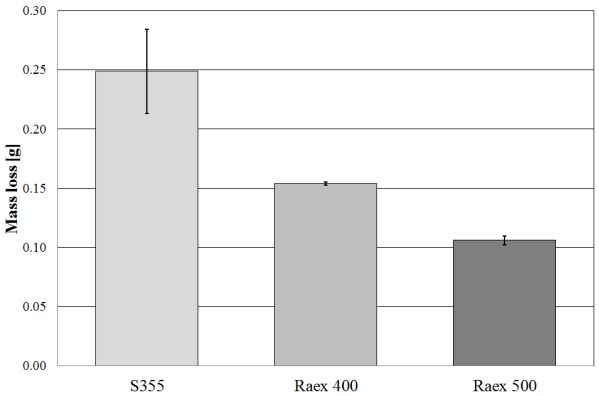

Fig. 4 Crushing pin-on-disc wear test results. The error bars indicate standard deviation

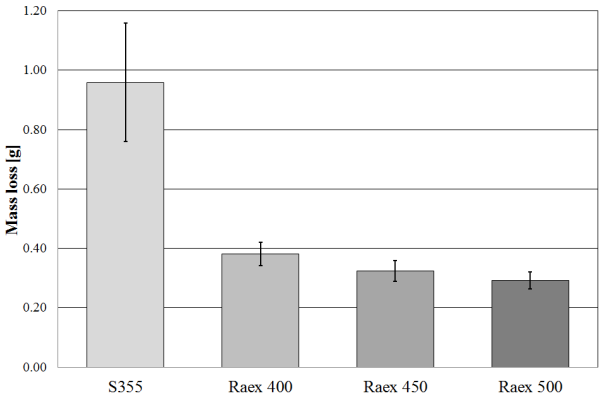

Fig. 5 Uniaxial crusher wear test results. The error bars indicate standard deviation

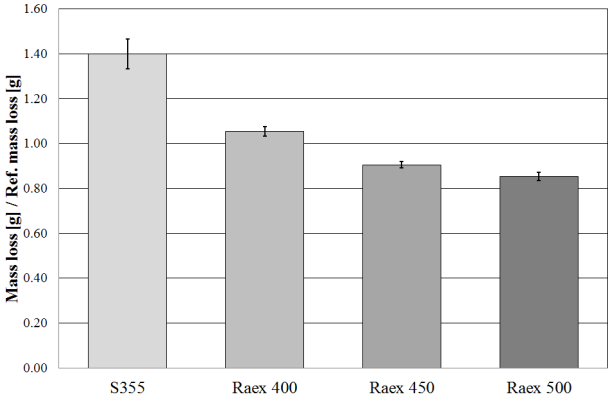

Fig. 6 Impeller-tumbler wear test results. The error bars indicate standard deviation

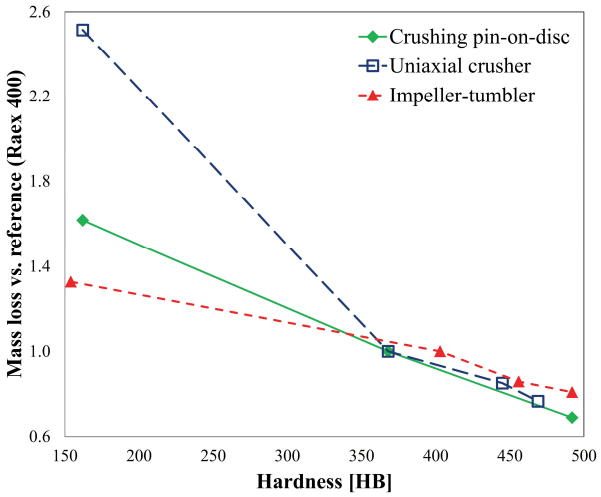

Fig. 7 Results of the wear tests as mass loss vs. material hardness. The mass losses have been normalized by the mass loss of the reference material

3.1.3 Impeller-tumbler

The results of the impeller-tumbler wear tests are presented in Figure 6. The results reveal that the difference between the wear resistant steels and the structural steel is substantially smaller than with other methods used in this study. The difference within the wear resistant steels is similar to that in the uniaxial crusher results.

3.2. Role of mechanical properties

A summary of the wear test results for all test methods in correlation with hardness is presented in Figure 7. To be able to compare the results obtained by different methods and conditions, the results were scaled by the wear rate of the reference material. The used reference material was Raex 400, as it gave reasonably constant results and was thus well suited for a reference material.

In all tests, higher hardness led to lower wear rate, but the strength of this relationship varied. The crushing pin-on-disc and impeller-tumbler tests produced quite linear curves. For impeller-tumbler results, the correlation of the higher hardness with the reduction of wear was lower than for the other methods. In the uniaxial crusher tests, the difference in the wear rates between the structural steel and wear resistant steels was large. However, in this method the dependence of wear on hardness for the wear resistant steels was much weaker.

The correlation between the wear test results and the ultimate tensile strength was very similar to the correlation between the hardness and wear, which was expected as the tensile strength and hardness usually show a quite linear correspondence. In all methods, higher ultimate tensile strength decreased wear. In impact-abrasion with impeller-tumbler, the dependence was weaker than in the abrasive methods.

Considering the typical elongation or ductility values, higher ductility correlated with higher mass loss results. Again, the strength of the dependence varied with test conditions, abrasive methods producing a stronger correlation than the impact-abrasion method.

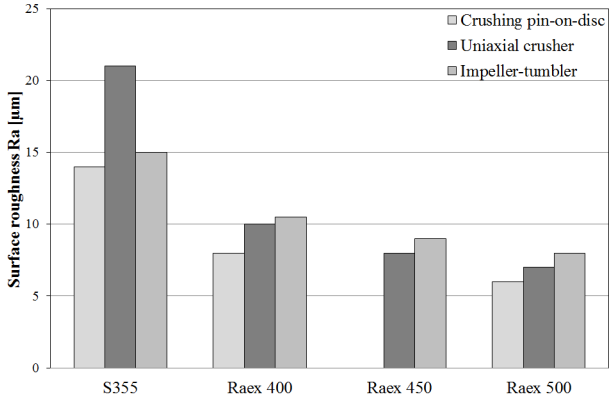

Fig. 8 Ra values for wear tested samples [µm]

3.3. Hardness of the worn surface

The results indicated that work hardening takes place to some extent in all studied steels, but the effect is much smaller in harder steels. In the structural steel, the hardness increased substantially in samples tested with all methods. The increase of hardness in the region down to 50 µm from the surface was 100-160 HV. In wear resistant steels the hardening could not be observed as clearly. In Raex 400, the hardness increased approximately 30-50 HV in the corresponding region. In harder Raex 500, the increase was even smaller. There was no distinct difference observed between the methods.

3.4. Surface roughness measurements

The surface roughness was determined with an optical profilometer. The initial surface roughness of the samples was approximately 0.5 µm. Figure 8 presents the results as an average of five measurements for each

sample. Materials with lower hardness showed in general higher surface roughness values after the tests. In the abrasion tests, the difference between the structural and wear resistant steels was significantly larger than in the impact-abrasion tests. In the high-stress abrasion tests, the surface roughness of the S355 samples was at least 70% higher than that of the wear resistant steels.

3.5. Penetration depths

The deepest individual scars were observed in uniaxial crusher samples, where the deepest scars found in the studied regions were 133 μm for S355 and 71 μm for Raex 500. The uniaxial crusher produced the deepest scars also on average, whereas the crushing pin-on-disc produced the shallowest scars on average. However, the scatter of the measurements was large, as every wear scar is different and therefore the average penetration depth value can be heavily influenced by a few deeper wear scars. When comparing materials, the harder materials had smaller penetration depths both on average and defined by the deepest individual scars within the studied regions.

3.6. Wear surface studies

The wear surfaces of tested samples were characterized using a stereomicroscope and a scanning electron microscope. The stereomicroscope enabled the observation of larger surface formations, while with SEM it was possible to study the wear surfaces in detail. The abrasive remnants were easily distinguished from the steel with a backscatter electron detector (BSE). To provide quantitative information about the amount of abrasive remnants, energy dispersive X-ray spectrometry (EDS) was used.

3.6.1 Crushing pin-on-disc

Both two-body and three-body abrasive wear occurred in all steel samples, and scratches and rolling marks were present on all surfaces. Figure 9 presents a SEM image of a S355 sample with a clear scratch mark on an otherwise evenly deformed wear surface. In the BSE image, the lighter areas are metal and abrasive remnants are shown as dark.

Signs of both ploughing and cutting were detected on all studied surfaces. The degree of plastic deformation was much higher in the structural steel than in the wear resistant steels, and also the amount of embedded abrasives was much larger. The structural steel had some large burrs on the surface, whereas in the wear resistant steels the formations were more chip-like, smaller and edgier, obviously due to the lower ductility of the material. Signs of severed chips were more visible in harder steels.

The surfaces of wear resistant steels were clearly flatter, as indicated also by the surface roughness measurements. Figure 10 presents shallow scratches on the wear surface of Raex 500. The scratches were more visible in steels with higher hardness. When determining the number of scratches from stereo optical images, the number of detectable scratches was approximately twice as high in Raex 500 as in S355.

3.6.2 Uniaxial crusher

The wear surfaces of the samples tested with the uniaxial crusher revealed indentations, plastic

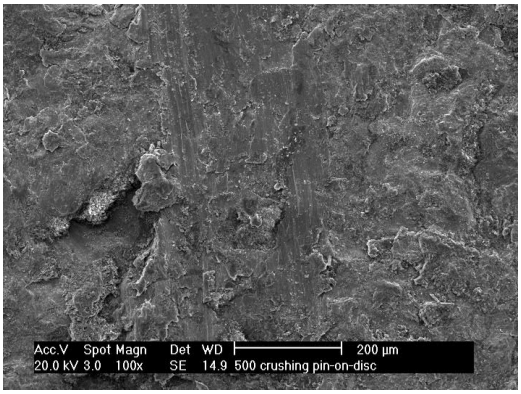

Fig. 10 SEM image of a wear surface of Raex 500 tested with the crushing pin-on-disc

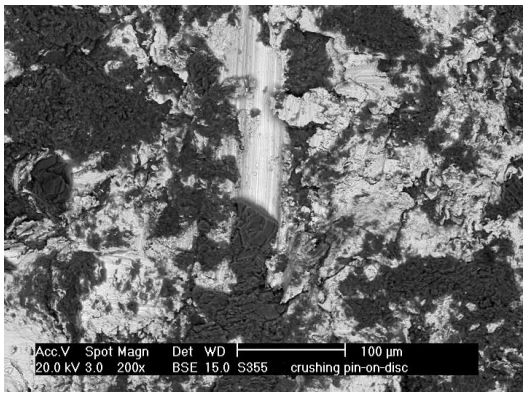

Fig. 9 SEM image of a wear surface of S355 tested with the crushing pin-on-disc (BSE mode)

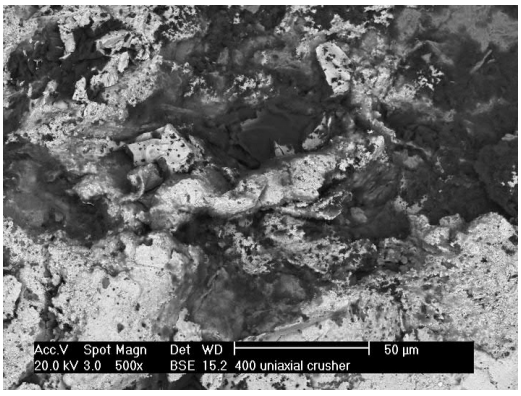

Fig. 11 SEM image of a wear surface of Raex 400 tested with the uniaxial crusher (BSE mode)

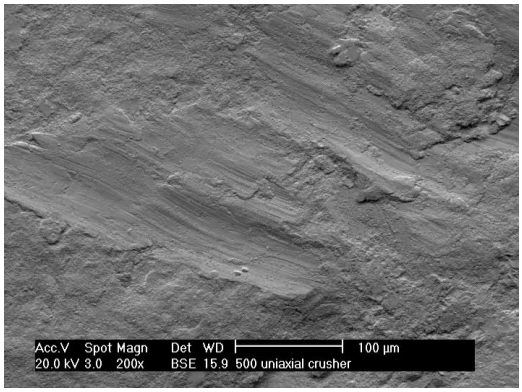

Fig. 12 SEM image of a wear surface of Raex 500 tested with the uniaxial crusher (topographic BSE mode)

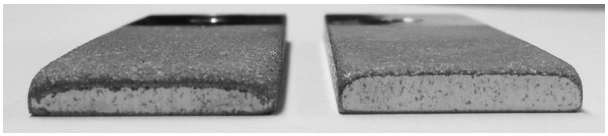

Fig. 13 Impeller-tumbler sample edges of S355 (on the left) and Raex 400 (on the right)

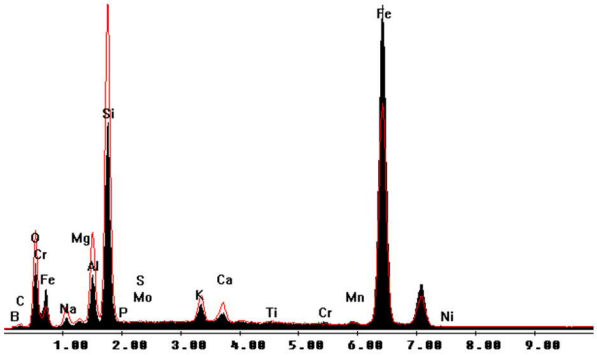

Fig. 14 Comparative EDS spectra from worn surfaces of S355 (red line) and Raex 500 (black graph)

deformation and microscratches. As the rocks in the abrasive bed were crushed, they moved relative to each other and could slide for short distances on the surface of the sample. The structural steel contained more abrasive remnants than the wear resistant steels, but embedded abrasive could be found in all samples. Figure 11 shows dark abrasive remnants on the lighter metal surface of worn Raex 400.

Similarly to the crushing pin-on-disc tests, the structural steel was severely deformed while the harder materials exhibited flatter and smoother surfaces. On the other hand, there were more well-defined short scratches in the harder materials. Figure 12 presents a SEM image of scratches on the surface of Raex 500.

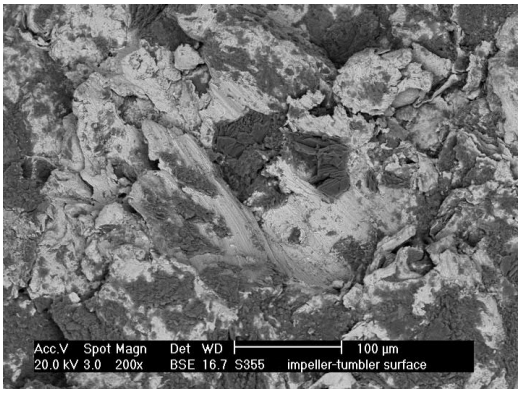

Fig. 15 SEM image of a wear surface of S355 tested with the impeller-tumbler (BSE mode)

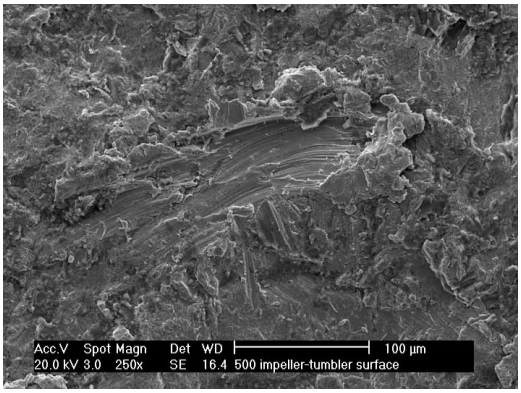

Fig. 16 SEM image of a wear surface of Raex 500 tested with the impeller-tumbler

3.6.3 Impeller-tumbler

In the samples tested with the impeller-tumbler, wear was most severe in the sample edges. Figure 13 shows the edges of the structural steel and Raex 400 samples. In both samples the edges are clearly rounded, but in the structural steel the rounding is much heavier and the material has been displaced over the sample's edge as a burr. In the wear resistant steel only slight burring was observed.

When studying the wear surfaces in the center areas of the samples, the structural steel contained more abrasive remnants compared to the wear resistant steels. Figure 14 presents EDS spectra from both S355 and Raex 500 impeller-tumbler wear surfaces. Compared to Raex 500, the analysis from the S355 surface contains considerably more silicon, aluminum and potassium, which are the major elements in granite [8]. This also indicates a larger amount of embedded rock on the S355 surface.

Figure 15 presents a heavily deformed wear surface of S355 with extensive ploughing, wedges and chips. In the wear resistant steels, the chips and wedges were smaller and the degree of deformation was lower. It

seemed that besides scratching, wear has occurred largely by the removal of the formerly deformed areas through the following impacts.

Figure 16 presents a scratch on the wear surface of Raex 500. In general the scratches were more well-defined and the surfaces smoother in the harder materials. When determining the number of scratches from the stereo optical images, the number of detectable scratches was approximately twice as high in Raex 500 as in S355.

4. Discussion

In agreement with the common observation, also in the current tests higher hardness correlated with better wear resistance, but the degree of this relation varied with the applied wear conditions. In general, a harder material resists the penetration of the abrasive through its higher surface hardness and strength, decreasing the wear rate. For samples tested in the impact-abrasion conditions (i.e., the impeller-tumbler tests), the positive effect of hardness was substantially smaller than for the high-stress abrasion methods. Also Rendón et al. [3] and Hawk et al. [9] have reported that in the impeller-tumbler tests the change in the wear rate can be notably small even for relatively large changes in the alloy hardness.

The results of this study, however, could at least partly be connected to edge-concentrated wear. The sample edges were not shielded in any of the applied test types, but in the impeller-tumbler samples the wear of the edges was clearly most severe. One explanation for the relatively low wear rate (as quantified by the mass loss) of the structural steel in the impeller-tumbler tests is the higher ductility that enables the material to deform around the edges by forming a burr without actual removal of the material. In the wear resistant steels only very small burrs could be observed, which suggests that the removal of the material in the edges occurs mostly by cutting and cracking of the deformed edges.

In order to enable the comparison of the abrasion wear resistance of materials in the center areas of the sample, i.e., to exclude the edge effects, the tests should be conducted with shielded edges. Especially in the impeller-tumbler tests, wear at the sample edges possibly dominates the measured mass losses. However, the wear of the edges correlates well with the real wear conditions in the tipper body, where the edge part of the tail plate is subjected to most severe wear.

There were some similarities in the wear surfaces produced by all testing methods. All the studied wear surfaces were plastically deformed and contained abrasive remnants on the surface. The structural steel was always the most heavily deformed and contained most abrasive remnants. On the other hand, the most distinct scratches were found in the harder steels in all methods.

However, the differences in the wear conditions and their effects on the steels' behavior could be easily detected also on the wear surfaces. In the structural steel samples, wear was most severe in samples tested with the uniaxial crusher, where the relative mass loss, surface roughness and penetration depth values were clearly the highest of all samples. This is a direct result of the much higher forces applied in this test method.

In the impeller-tumbler test, the nature of the contact between the abrasive and the sample is more of an impact than in the other test methods. Sundström et al. [10] have determined the ratio of impact and abrasion to be 100/1 in a similar type test equipment. In the structural steel the material can be more easily deformed and displaced than removed due to its higher ductility compared to wear resistant steels, in which the material seems to be more easily cut away from the surface by impacts. This decreases the effect of hardness on the wear rate.

The crushing pin-on-disc is a three-body abrasion test method, and thus the effect of the counterpart cannot be excluded. Axén et al. [11] stated that the amount of rolling increases as the hardness of the counterpart material increases. In their study, self-mated steel surfaces in three-body abrasion showed about equal amounts of rolling and sliding. In the tests of the present study, the counterpart was slightly harder than the sample, possibly promoting rolling of abrasives on the pin sample. Differences in the behavior of the pin materials could be observed. Based on wear surface examination, the amount of scratching increased as the material hardness increased. Both the surface roughness and penetration depth were the smallest for Raex 500 in this method, suggesting that even when the amount of scratches was higher, they were only shallow and thus did not cause substantial material removal. The similarity of the hardness of the Raex 500 pin and the disc, and thus the higher pin/disc hardness ratio compared to the other tested materials, may have promoted sliding on the Raex 500 pin surface in this method. However, higher amount of scratches was observed also in the Raex 400 pin.

For all methods, harder materials contained more scratches. This was basically for two reasons: in these materials less deformation occurs to cover the previous scratches, and the proportion of sliding is higher than in softer materials. The increased sliding results from the ability of the harder material to resist the penetration of the abrasives. For an angular abrasive to roll, some deformation, either elastic or plastic, must occur in the surface. The harder surface resists this more, thus increasing the propensity to sliding instead of rolling. Gore and Gates [12] reported that increased specimen hardness led to a transition from rolling to sliding of the abrasive particles in three-body abrasive wear, which agrees with the wear scars found in this study. Also Fang et al. [13] observed more scratches in harder materials in their study concentrating on abrasive wear in materials with a wide range of hardness. For impeller-tumbler, a same kind of observation about the scratches, although less defined, was done by Sundström et al. [10].

5. Conlusions

For all materials and test methods used in this study, higher hardness led to decreased mass loss. The strength of this dependence, however, varied depending on the test method and other properties of the materials. Impact-abrasion showed the weakest dependence on hardness, possibly due to the concentration of wear by cutting on the specimen edges. In this case, the higher ductility of the structural steel enabled the material to deform and create burrs over the sample edges without actual loss of material.

In all testing methods, the degree of plastic deformation was the highest in the structural steel, which was the softest material. On the other hand, in harder materials the scratches were more well-defined and visible, indicating a change in the wear mechanism. For an angular abrasive to roll, some kind of deformation must occur in the surface. The harder surface resists this more, increasing the possibility of sliding. The lower degree of plastic deformation was also not sufficient to cover the formed scratches as effectively as in the softer materials.

This study shows that the performance of different steels depends on the conditions of abrasive wear. The used test methods complement each other and provide useful laboratory scale simulations of the wear conditions typical in earth moving and mining.

Acknowledgements

The work has been done within FIMECC Ltd and its DEMAPP program. We gratefully acknowledge the financial support from Tekes and the participating companies.

References

[1] Hawk, J. A. and Wilson, R. D., “Tribology of Earthmoving, Mining, and Minerals Processing,” in Modern Tribology Handbook, Vol. 2, Bhushan, B. (ed.), CRC Press, Boca Raton, 2000.

[2] Zum Gahr, K.-H. (ed.), “Grooving Wear,” in Tribology Series, Vol. 10, Elsevier, Amsterdam, 1987, p. 132.

[3] Rendón, J. and Olsson, M., “Abrasive Wear Resistance of Some Commercial Abrasion Resistant Steels Evaluated by Laboratory Test Methods,” Wear, 267, 11, 2009, 2055-2061.

[4] Badisch, E., Kirchgaβner, M., Polak, R. and Franek, F., “The Comparison of Wear Properties of Different Fe-Based Hardfacing Alloys in Four Kinds of Testing Methods,” Tribotest, 14, 4, 2008, 225-233.

[5] Tylczak, J. H., Hawk, J. A. and Wilson, R. D., “A Comparison of Laboratory Abrasion and Field Wear Results,” Wear, 225-229, 2, 1999, 1059-1069.

[6] Terva, J., Teeri, T., Kuokkala, V.-T., Siitonen, P. and Liimatainen, J., “Abrasive Wear of Steel against Gravel with Different Rock-Steel Combinations,” Wear, 267, 11, 2009, 1821-1831.

[7] Heino, V., Kaipiainen, M., Siitonen, P., Ratia, V., Valtonen, K., Lepistö, T and Kuokkala, V-T., “Compressive Crushing of Granite with Wear-Resistant Materials,” Finnish Journal of Tribology, 30, 1-2, 2011, 21-28.

[8] Silva, B. and Aira, N., Martínez-Cortizas, A., Prieto, B., “Chemical Composition and Origion of Black Patinas on Granite,” Science of the Total Environment, 408, 1, 2009, 130-137.

[9] Hawk, J. A., Wilson, R. D., Tylczak, J. H. and Doğan, Ö. N., “Laboratory Abrasive Wear Tests: Investigation of Test Methods and Alloy Correlation,” Wear, 225-229, 2, 1999, 1031-1042.

[10] Sundström, A., Rendón, J. and Olsson, M., “Wear Behaviour of Some Low Alloyed Steels under Combined Impact/Abrasion Contact Conditions,” Wear, 250, 1-12, 2001, 744-754.

[11] Axén, N., Jacobson, S. and Hogmark, S., “Influence of Hardness of the Counterbody in Three-Body Abrasive Wear – An Overlooked Hardness Effect,” Tribology International, 27, 4, 1994, 233-241.

[12] Gore, G. J. and Gates, J. D., “Effect of Hardness on Three Very Different Forms of Wear,” Wear, 203-204, 1997, 544-563.

[13] Fang, L., Zhou, Q. D. and Li, Y. J., “An Explanation of the Relation between Wear and Material Hardness in Three-Body Abrasion,” Wear, 151, 2, 1991, 313-321.

Publication II

Kati Valtonen, Vilma Ratia, Niko Ojala, and Veli-Tapani Kuokkala

Comparison of laboratory wear test results with the in-service performance of cutting edges of loader buckets

Wear 388–389 (2017) pp. 93-100

Wear 388–389 (2017) 93–100

Contents lists available at ScienceDirect

Wear

journal homepage: www.elsevier.com/locate/wear

Comparison of laboratory wear test results with the in-service performance of cutting edges of loader buckets

K. Valtonen*, V. Ratia, N. Ojala, V.-T. Kuokkala

Tampere University of Technology, Faculty of Engineering Sciences, Laboratory of Materials Science, Tampere Wear Center, P.O. Box 589, FI-33101 Tampere, Finland

ARTICLE INFO

Keywords:
Wear testing
Abrasion
Impact wear
Steel
Mining

ABSTRACT

The in-service cutting edge of a mining loader bucket was investigated and its wear behavior compared with samples tested in the laboratory to assess how well the wear testing methods correlate with the in-service conditions. The examined in-service cutting edge of a bucket made of a wear resistant steel had been run in an underground mine with quarry gravel. The wear behavior of the cutting edge was simulated in the laboratory scale with several application oriented abrasive and impact-abrasive wear testing methods. In addition to the contact mode, high loads, large abrasive size, abrasive type, and the comminution of the abrasive formed the basis for the design of the laboratory experiments. The wear surfaces and cross-sections of the original cutting edge and the test samples were characterized, and the wear behaviors were compared with each other. Work hardening of the steels occurred in all cases, but the amount of plastic deformation and the depth of the wear scars varied.

1. Introduction

The simulation of in-service wear environments in the laboratory-scale is challenging. In the planning of the test procedures, the effect of many variables, such as the contact mode, loading energy, abrasive properties, and the environment on the active wear mechanism and the resulting wear rate must be carefully taken into consideration. The interpretation of the laboratory test results is normally easier and the repeatability of the tests is better than in the complex and expensive in-service tests [1]. On larger wear parts and complex applications, the comparison of materials using field tests is very difficult, laborious, and expensive. On the other hand, the utilization of the field test results is usually quite straightforward and the tests easily reveal the possible problems in the design or selection of materials. Thus, to select the best possible testing approach for each case, it is important to have a good understanding of the relevance of the laboratory wear tests compared to the in-service performance of the materials in high stress wear conditions.

The wear conditions are very demanding in hoisting and hauling of rocks in mining, excavation, and construction. One example of the used wear parts is the cutting edge of a mining loader bucket. The cutting edges are welded or mechanically attached to the front of the bucket and replaced when the worn-out edge restricts the loading procedure. With proper material selection, it is possible to markedly improve the lifetime of the wear part that affects directly the operating costs. The part must naturally resist high stress abrasive wear. Moreover, the selected material should have high strength and sufficient ductility to withstand also various dynamic loading events.

A large number of laboratory studies have been conducted for the material selection of bucket tips, teeth, and cutting edges of earth moving machines [2–6]. Some studies even compare the field tests of these kinds of wear parts with laboratory tests. However, the laboratory tests have usually been conducted as standardized rubber wheel abrasive tests with low contact pressure and fine abrasives. In these tests, it was often noted that the wear environment produced by the rubber wheel tests was not similar to the real conditions and that the laboratory tests did not correlate well with the field tests results [2].

The properties of the selected abrasive have a marked effect on the abrasive wear testing. For example, the very hard but also highly crushable quartz may produce an embedded quartzite powder layer on steel surfaces during testing thus affecting the wear test results [7]. On the other hand, the measured abrasiveness and crushability values of the natural minerals may be a basis for incorrect assumptions about the wear rates due to the different contact conditions [8].

The material selection based on laboratory tests needs test methods, which simulate as well as possible the in-service conditions, such as the contact conditions and real abrasives. Consequently, careful analysis of the relevance of the laboratory test methods is essential. In this study, the wear behavior of a cutting edge was simulated in the laboratory scale using several application oriented wear testing methods. The

* Corresponding author.
E-mail address: kati.valtonen@tut.fi (K. Valtonen).

http://dx.doi.org/10.1016/j.wear.2017.06.005
Received 30 September 2016; Received in revised form 9 June 2017; Accepted 10 June 2017
Available online 13 June 2017

Table 1
Nominal properties of the studied steels.

	400 HB	500 HB
Microstructure	Martensitic	Martensitic
Rp0.2 [N/mm^2]	1000	1250
Rm [N/mm^2]	1250	1600
A [%]	10	8
Hardness HBW [kg/mm^2]	360 – 440	450 – 540
Impact toughness −40 °C [J]	30	30
C [wt%] max.	0.23	0.30
Si [wt%] max.	0.80	0.80
Mn [wt%] max.	1.70	1.7
Cr [wt%] max.	1.5	1.5
Ni [wt%] max.	1.0	1.0
Mo [wt%] max.	0.5	0.5
B [wt%] max.	0.005	0.005
CEV	0.57	0.66
Density [g/cm^3]	7.85	7.85

crushing pin-on-disc, the uniaxial crusher, the impeller-tumbler, and the high-speed slurry-pot with dry abrasive bed systems produce high stress abrasive or impact-abrasive conditions with large natural rock abrasives. Thus, they simulate the harsh conditions during loading and unloading of the loader bucket. The wear behavior of the in-service cutting edge was compared with the wear tested samples by analyzing the wear rates and by characterizing the wear surfaces and microstructures.

2. Materials and methods

The material used in the wear testing and the in-service application was an ultra-high-strength 500 HB grade wear resistant steel. In addition, a 400 HB grade steel was used as a reference material in the wear tests. The microstructure of both steels was martensitic with some retained austenite and untempered martensite. Table 1 lists the mechanical properties and the maximum nominal compositions of the steels given by the manufacturer. The typical carbon equivalent values are determined using CEV = C + Mn/6 + (Cr + Mo + V)/5 + (Ni + Cu)/15.

2.1. In-service history

The cutting edge of a CAT R 2900 G underground mining loader bucket had been run for 928 h in an underground mine with quarry gravel, including granite, chromite, and barren rock [9]. The loader was used in normal operation in various tasks. The dimensions of the cutting edge had been determined before and after the test by ATOS 3D scanner at Lapland University of Applied Sciences. Fig. 1 presents a schematic of the cutting edge. The thickness of the steel plate was originally 60 mm, the width 3.354 m, and the depth 1.1 m in the middle and 0.5 m on the sides [9]. The front of the cutting edge was beveled to a 25° angle. A test piece 3.9 mm wide and 17.5 mm long was cut from the middle area of the tip of the cutting edge for failure analysis. The heavily oxidized surfaces were cleaned with USF 175 acidic detergent in an ultrasound cleaner in order to remove the corrosion products from the wear surfaces.

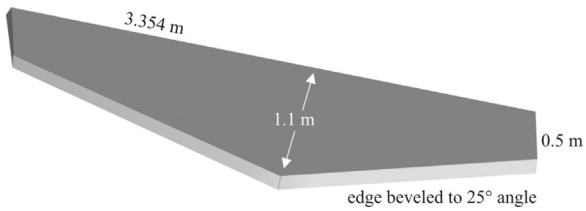

Fig. 1. Schematic of the cutting edge.

2.2. Application oriented laboratory wear tests

Four wear testing devices built at Tampere Wear Center were used in the study: a crushing pin-on-disc, a uniaxial crusher, an impeller-tumbler, and a high-speed slurry-pot with a dry abrasive bed (dry-pot). Fig. 2 presents pictures of the devices designed to simulate the wear conditions in mining, mineral processing, and crushing with different wear mechanisms. A detailed description of the test methods has been published by Ratia et al. [10] and by Vuorinen et al. [11]. In this study, the test parameters were selected to simulate the varying conditions in a mining loader bucket. The abrasive was highly abrasive granite rock from Sorila quarry in Finland.

In the crushing pin-on-disc tests, a cylindrical 35 mm long sample pin with a 1017 mm^2 wear area (∅ 36 mm) was pressed against the rotating granite gravel bed with a 240 N force. The loading was cyclic; after 5 s of compression, the gravel bed rotated freely for 2.5 s. Thus, in a 90 min test the actual contact time was 60 min. The sliding distance of the center of the sample in contact with the gravel was approximately 370 m. The rotating speed of 28 rpm of the 160 mm diameter disc was adjusted so that the freely rotating pin landed always on the highest pile of the abrasive. The gravel batch contained 50 g 2–4 mm, 250 g 4–6.3 mm, 150 g 6.3–8 mm, and 50 g 8–10 mm crushed granite. The initial granite particle size was severely comminuted during the tests. For this reason, it was changed every 30 min while samples were weighted every 7.5 min. This procedure is an in-house standard, which has been shown to produce high and stable wear rates [12]. The standard deviation of the weight loss of the three measurements was below 5%. S355 structural steel with initial hardness of 216 HV was selected for the disc material. With such a softer disc material, granite adheres to the disc and produces more sliding wear compared with harder disc materials [12]. Before the actual test cycle, a 15 min run-in was completed to produce steady state wear in the test.

The uniaxial crusher utilized similar pin samples as the crushing pin-on-disc device, as seen in Fig. 2b. The pin crushed the 4–6.3 mm granite gravel against a tool steel counterpart in a rubber cup with a 53 kN uniaxial force produced by a hydraulic cylinder. After each compression, the cup was emptied and then refilled with fresh gravel using an automated purging and refilling system. In total, 500 compression cycles were made. The samples were weighted after every 100 compressions. The compression time in each cycle was on average 1.8 s. Thus, the total contact time in 500 compressions was about 15 min. The standard deviation on the weight measurements varied between 2 and 7 percent.

In addition to separate tests with the crushing pin-on-disc and the uniaxial crusher, a combination test procedure was used. In these tests, the samples were first compressed 500 times with the uniaxial crusher and then tested with the crushing pin-on-disc for 30 min. The test parameters were otherwise similar to the individual tests with these two devices.

In the impeller-tumbler device, three 75x25 × 10 mm size samples were attached to 60 degree angle as impellers and then rotated at 700 rpm in the gravel-filled tumbler rotating in the same direction but at a lower speed of 30 rpm (Fig. 2c). The gravel flowed in the tumbler freely, and thus the impacting angle of the abrasive particles varied during the test. The actual wear area of the samples was 1200 mm^2. The granite was initially sieved to a size distribution of 8–10 mm, but the test comminuted the granite gravel and rounded the particles efficiently. For that reason, the abrasive batch of 900*g* of granite was replaced every 15 min. The total test time was 360 min and therefore only one test for both materials was made, while three tests were made with the other methods. In the shorter impeller-tumbler tests, the standard deviation of the weight measurements is typically less than 3% [10].

The high-speed slurry-pot was modified for an abrasive wear tester (dry-pot) by filling the pot with 9 kg of dry 8–10 mm gravel. To simulate the filling of the loader bucket, two 60x40 × 6 mm samples were positioned at a 45° angle to the rotating axle, as seen in Fig. 2d. The

Fig. 2. Test chambers of the used wear testing devices with samples: a) crushing pin-on-disc, b) uniaxial crusher, c) impeller-tumbler, and d) dry-pot.

actual wear area of the samples was 2540 mm^2. The rotation speed was 500 rpm, which corresponds to the tangential speed of 5 m/s in the outer edge of the samples. The gravel and the sample position were changed after 30 min in the tests with a total duration of 60 min. The sliding distance of the tip of the sample was about 18000 m and the standard deviation of the weight measurements was about 5%.

2.3. Characterization

The wear surfaces were characterized using Philips XL30 scanning electron microscope (SEM), Alicona InfiniteFocus G5 optical 3D measurement system, and Leica MZ 7.5 zoom stereo microscope. The microstructures of the sample cross-sections were studied with Nikon Eclipse MA100 optical microscope. The Vickers hardness values of the wear test samples were measured with Struers Duramin-A300. For microhardness measurements, Matsuzawa microhardness tester was used.

3. Results

3.1. In-service cutting edge of an underground mining loader bucket

The underground mining loader was used in normal operation in the Kemi mine. During 928 h of operation, the cutting edge had lost 27.1 percent of its weight equivalent to 335 kg [9]. In the demanding conditions, the material loss had been high both in the front and on both sides of the cutting edge. The original thickness of the steel plate had been 60 mm, but in the remaining part the material thickness varied and was thickest, 49 mm, in the middle [9]. The wear rate had been highest on the underside of the bucket. The size of the handled particles in mining conditions can be anything from slurry or sand to one meter wide blocks. Moreover, the loader can be used to clean or plow the bedrock in the mining tunnels.

The wear surfaces of the cutting edge were characterized by both optical and scanning electron microscopy. Fig. 3 presents scanning electron micrographs of the wear surfaces taken from different parts of the sample. All surfaces showed marks of high-stress abrasion, but the top surface exhibited most clear signs of micro cutting. Both micro cutting and micro ploughing were identified on all surfaces as mechanisms of abrasive wear, with micro cutting being dominant. The tip and the underside surface were particularly heavily deformed. Fig. 3c shows some surface cracks formed by surface fatigue, which may also act as starting points for delamination. Moreover, a lot of rock had embedded into the tip, completely covering the surface in some areas.

The wear surfaces were strongly work hardened, the depth of the work hardened layer varying from 150 to 300 μm on the underside. Fig. 4 presents a white layer in the underside surface cross-section. Also an average hardness profile in one location is shown. These white layers were from a few micrometers up to 130 μm thick and in some cases over four millimeters wide. The microhardness of the white layers was up to 700 HV0.05. On the top surface, the depth of the hardened layer was up to 200 μm with microhardness generally below 600 HV0.05. Below the hard white layer there was in some cases a layer with lower hardness, as seen for example in Fig. 4b.

3.2. Application oriented wear tests

The crushing pin-on-disc (CPoD), the uniaxial crusher (UC), their combination (UC + CPoD), the impeller-tumbler, and the high-speed slurry-pot with dry abrasive bed test systems were utilized to simulate the field conditions. Fig. 5 presents the wear test results as mass loss in proportion to the initial wear area for the 500 HB steel samples. The wear rates were highest in the dry-pot and crushing pin-on-disc tests. However, during the tests the rock comminutes and the wear rate starts

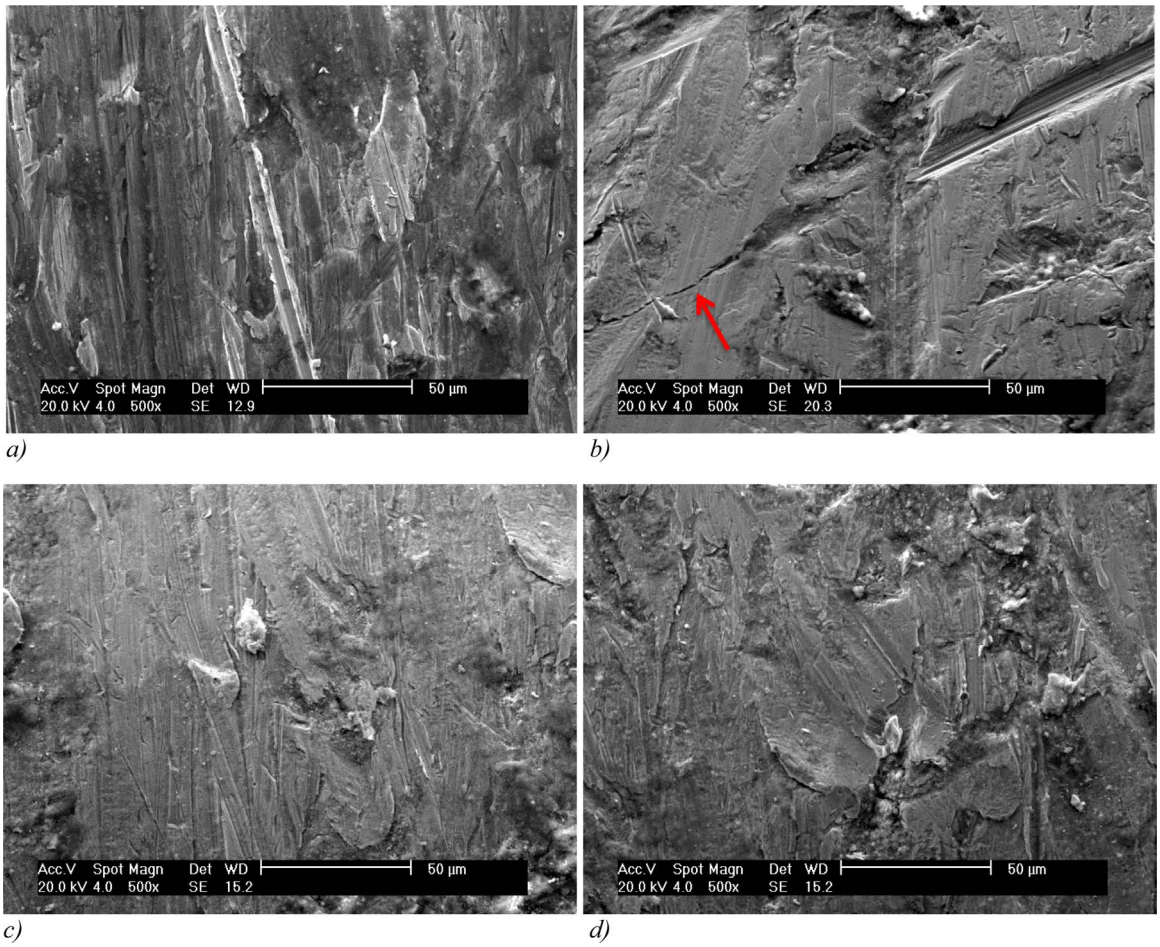

Fig. 3. Scanning electron microscope images of the cutting edge wear surfaces a) top part, b) tip on the underside, and c), d) underside. The arrow indicates a crack.

to decrease in the end of the test cycle before the gravel is renewed. This effect is seen as slight cyclic variations in the crushing pin-on-disc test results. As a general trend, the wear rate also decreased during the CPoD tests, as shown by the increasing deviation of the data points from the straight line formed by the dry-pot results in Fig. 5. The wear rate in the impeller-tumbler tests was clearly the lowest in this comparison. However, compared to the other methods, the contact mechanism in the impeller-tumbler is more impacting than abrasive, which at least partly explains the different results.

In the combined UC + CPoD tests, the mass loss in the crushing pin-on-disc test was 70% higher during the first 10 min compared to end of the test. This effect can be explained by the removal of the embedded rock layers and the white layers seen in the optical micrograph in Fig. 6b. Fig. 6c shows one of the several initial delamination points that were observed in the cross-sections of the combined UC + CPoD test samples. White layers were also formed in the tips of the dry-pot samples of both steels, but they were not as thick as in the in-service sample, as seen when comparing the micrographs in Fig. 6. In the impeller-tumbler sample cross-sections, such as in Fig. 6d, adiabatic shear bands similar to the case of single impacts were observed [13].

All wear surfaces were plastically deformed, work-hardened, and contained embedded rock. Fig. 7, however, illustrates that also distinct differences exist between the wear surfaces produced by the different test methods. The crushing pin-on-disc wear surface resembles quite well the wear surfaces of the cutting edge. The surface is deformed with long scratches and contains occasional embedded crushed granite and marks of delamination. However, the direction of the scratches on the CPoD surfaces is random, because the pin can rotate freely during the test. Cutting was more prevalent in the 500 HB steel compared to the 400 HB steel (Fig. 8a).

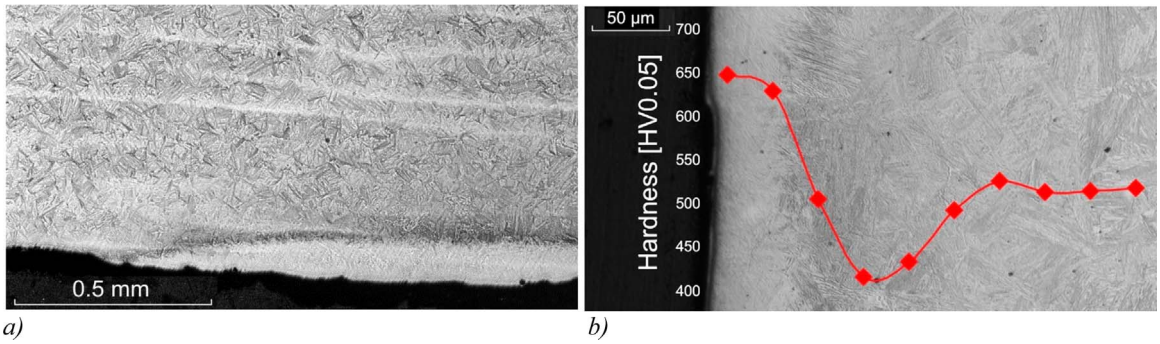

Fig. 4. Optical micrograph of the underside cross-section of the cutting edge showing a) a white layer and b) a typical hardness profile over a white layer.

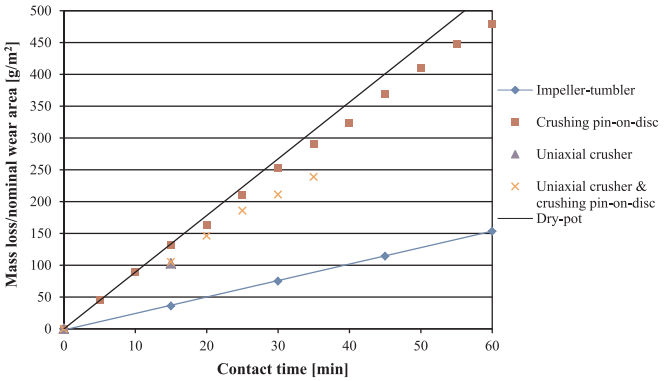

Fig. 5. Cumulative wear rates of the 500 HB steel in laboratory wear tests as a function of contact time.

In the uniaxial crusher, the gravel is always fresh with sharp edges. The used high compression forces deform the surface intensely and produce large dents and embed granite into the surface. When the surfaces were studied with a stereo microscope, they were found quite similar in appearance as the tip of the cutting edge. The wear scars were up to 70 μm deep, and the crushing of rock also caused occasional micro cutting of the wear surface.

One limitation of the crushing pin-on-disc method is that the applicable forces are quite low. The highest force that the system can produce is 500 N, but already then the rocks tend to ricochet under the pin sample. The uniaxial crusher can produce a significantly higher normal force of 53kN, which deforms the surface of the steel samples much more, but the amount of cutting is very low. Combining these two methods, however, is easy as the same samples fit to both systems. Thus, cyclic operation, high compressive forces, and sliding abrasive conditions were combined by testing the samples first with the uniaxial crusher followed by a crushing pin-on-disc test. Fig. 7c shows an example of the increased propensity of the wear surface to delamination compared to the normal crushing pin-on-disc test.

In the impact-abrasive conditions created by the impeller-tumbler, the wear surfaces were highly deformed, as seen for example in Fig. 7d. In these tests, the amount of sliding was much lower than in the crushing pin-on-disc tests or in the in-service conditions. The edges of the samples were rounded, because the gravel rotates freely in the tumbler and tends to cause chipping of the initially sharp edges. Moreover, the wear rate in the tip area was visibly higher than in the areas closer to the sample holder, because the higher radial speed of the sample tip causes a gradient in the contact conditions. The cross-sections of the impeller-tumbler wear surfaces showed only very thin occasional white layers. The impact dents were up to 45 μm deep, but the variation in the depth of individual dents was high.

The dry-pot tests produced highly deformed wear surfaces with shorter scratches than the crushing pin-on-disc method (Figs. 7e and 8b). The rocks are able to rotate freely in the test pot, and therefore both rolling and sliding abrasion are included similar to the in-service conditions. Of the studied wear surfaces, the one in Fig. 7e resembles quite much the wear surface of the underside of the cutting edge shown in Fig. 3c and d.

3.3. Comparison of the in-service sample with laboratory test samples

The underside of the cutting edge is in contact with gravel for a

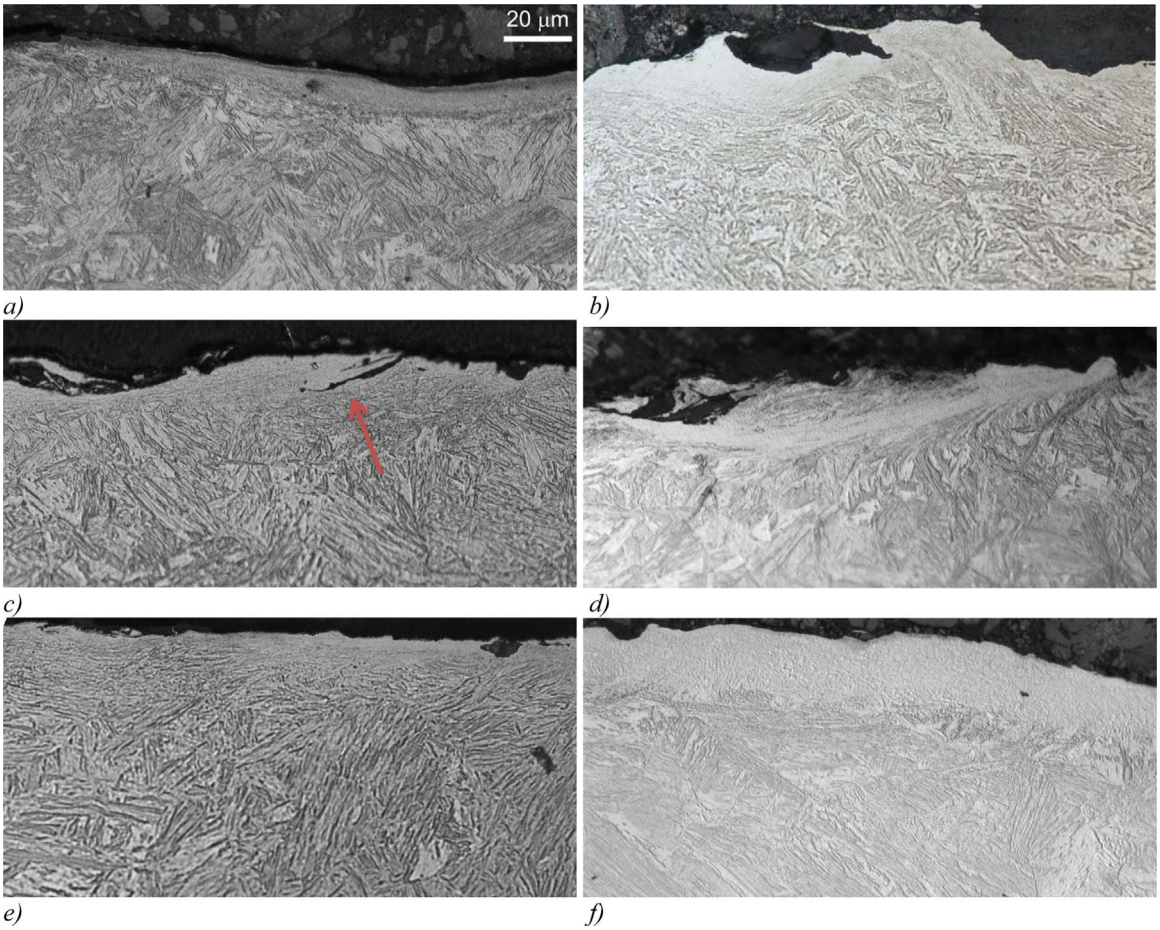

Fig. 6. Optical micrographs of the wear surface cross-sections of the 500 HB grade steel samples tested with a) crushing pin-on-disc, b) uniaxial crusher, c) combined uniaxial crusher and crushing pin-on-disc, d) impeller-tumbler, e) dry-pot, and f) in-service cutting edge. The arrow indicates delamination.

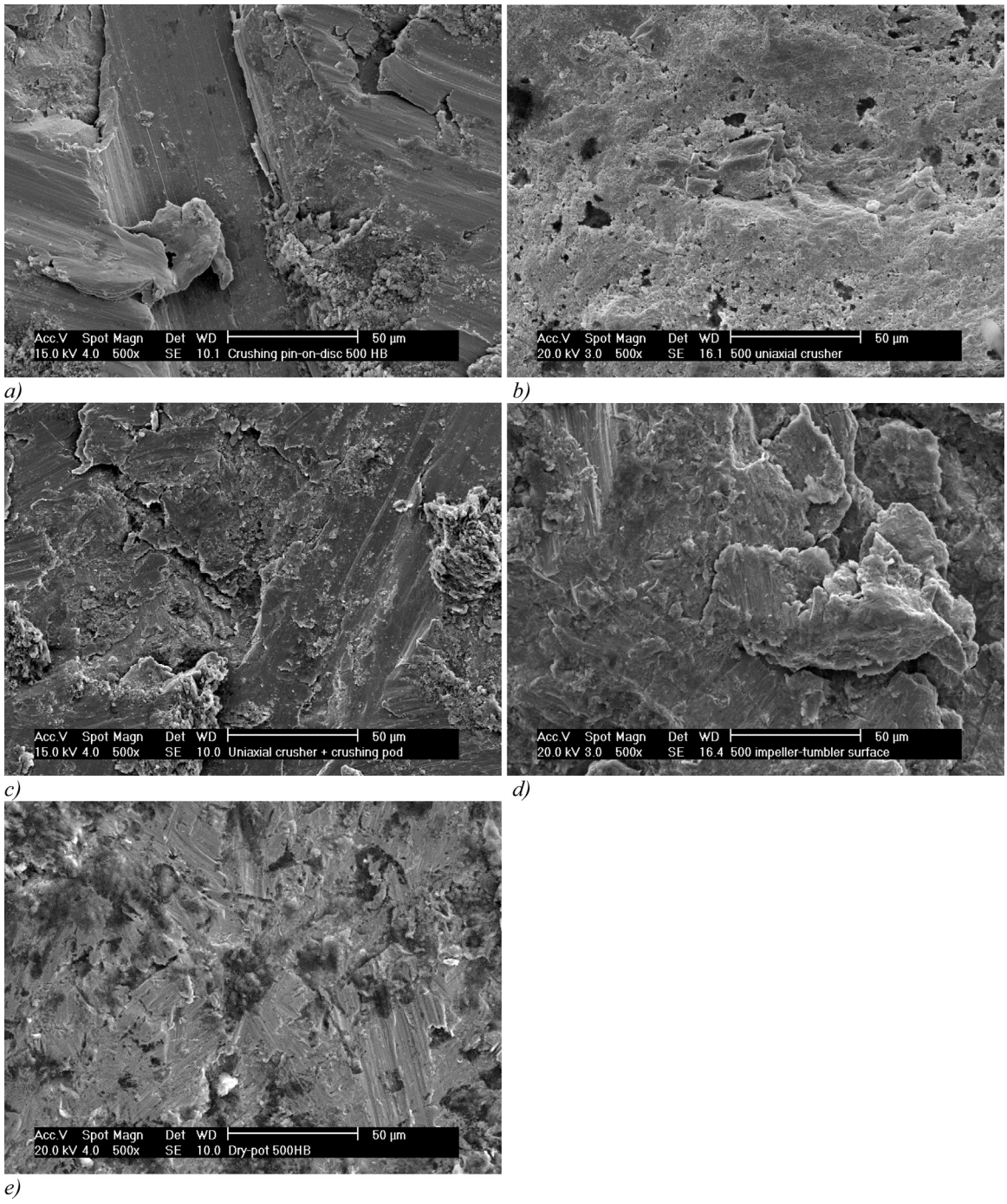

Fig. 7. Scanning electron microscope images of the wear surfaces of the 500 HB grade steel samples tested with a) crushing pin-on-disc, b) uniaxial crusher, c) combined uniaxial crusher and crushing pin-on-disc, d) impeller-tumbler, and e) dry-pot.

relatively short period of time during loading and unloading of the bucket. However, it is challenging to estimate the actual contact time of the cutting edge during operation, as it depends for example on the operator and the distances between the loader and the dumper. In order to obtain at least a rough estimate for the wear rate of the cutting edge for comparison with the laboratory test results, the total mass loss was spread over the average area of the cutting edge underside, because most of the material loss had concentrated there [9]. The contact time was selected as 21.5% of the total operation time, which is a typical loading time when the loader is close to the loading chute [14]. The shorter the real contact time, the higher is the wear rate. Fig. 9, which displays the wear rates (mm/h) for all tests and conditions, shows that the estimated wear rate during the in-service operation is higher than in the laboratory tests. Of these tests, the dry-pot system produced the highest wear rates, which are also quite close to the estimated wear rate of the studied edge of the loading bucket.

4. Discussion

The five different laboratory wear tests were selected with assumptions that the crushing pin-on-disc and dry-pot tests simulate the loading of a bucket, the uniaxial crusher portrays the heavy loads at the tip of the bucket, and the impeller-tumbler reproduces best the impacts during loading and unloading. All these methods produce high stress abrasive or impact abrasive conditions with relatively large abrasive size. The used normal forces and the amount of sliding and rolling

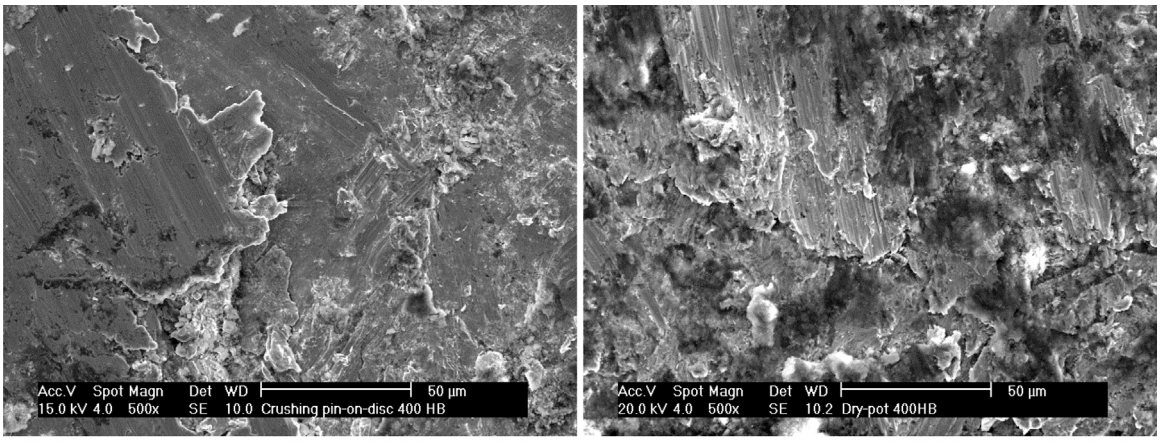

Fig. 8. Scanning electron microscope images of the wear surfaces of the 400 HB grade steel samples tested with a) crushing pin-on-disc, and b) dry-pot.

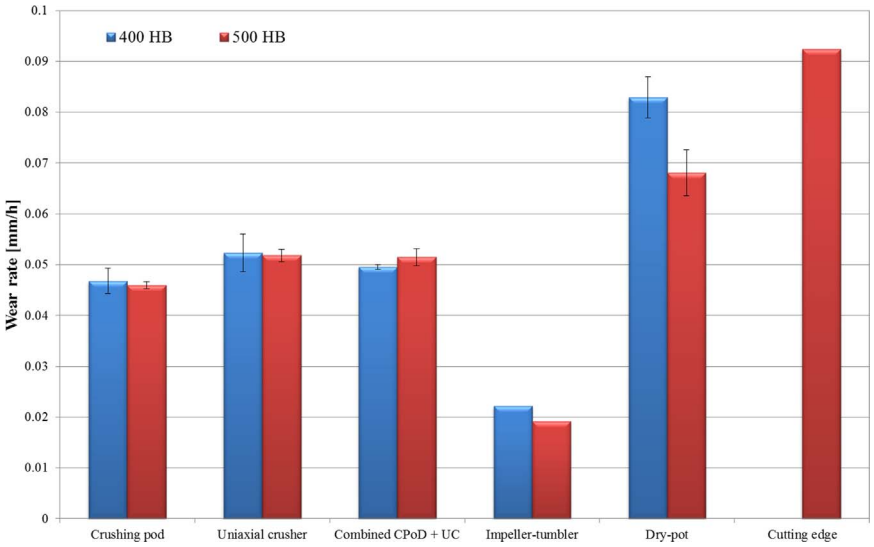

Fig. 9. Wear rates (mm/h) in the in-service operation of the cutting edge underside and in the laboratory tests with error bars presenting the standard deviation.

abrasion vary in each method, and thus they complement each other. However, it is quite challenging to assess the real relevance of these laboratory tests for the evaluation of the in-service performance of the cutting edges of mining loader buckets.

Work hardening of the steel occurred both in the field conditions and in the laboratory tests, but the amount of sliding abrasion and plastic deformation varied in each case. In the impeller-tumbler test impact wear dominates, and therefore it is not a very suitable method for simulating wear in this kind of application. The crushing pin-on-disc produced quite high relative wear rates and wear surfaces that were comparable to the cutting edge of the loader bucket. The forces that are used in the uniaxial crushing tests are closer to real applications, but the amount of cutting is clearly lower. Consequently, the hard white layers were thickest in the uniaxial crusher samples, which may momentarily improve the abrasion wear resistance of the steel against rocks. However, when a certain critical load is reached, the layers may start to delaminate [15]. This was the case especially when the UC and CPoD tests were combined. The white layers formed during the uniaxial crushing started to delaminate during the crushing pin-on-disc test. The wear rate of the 500 HB steel during the crushing pin-on-disc test cycle was slightly higher than that of the 400 HB steel. Hence, the harder white layers in the 500 HB steel laminated easier than the white layers in the 400 HB steel.

The white layers in the subsurface region of the in-service sample were much thicker than those observed in the laboratory tests. Xu et al. [6] concluded that the effect of white layers in the wear performance of digger teeth is negligible. They produced the white layers artificially before laboratory wear tests and noticed that they only slightly reduced the wear rates. However, the effects of surface hardening and the formation of tribological layers on the wear performance of steels should not be disregarded. The loading conditions have a marked effect on the material properties and also on the behavior of the surface in wear environments [16,17].

The abrasive particle shape has a significant effect on the abrasive wear of steels. For example, Stachowiak & Stachowiak [18] showed that angular particles produced more cutting and sharp notches compared to round particles. Moreover, they stated that particle toughness and possible embedment in the steel affect the wear rates. In the mine, the loaded gravel is always sharp and the abrasive type and size vary markedly, from millimeter scale to meters. In this study, the selected abrasive was very close to real conditions. The hard granite gravel was always sharp in the uniaxial crushing, because the gravel was changed after every crushing cycle. In the crushing pin-on-disc method, the abrasive particles comminute but still stay quite sharp in the process. Blunting of the abrasives is highest with the impeller-tumbler and the dry-pot methods, where the freely moving abrasives tend to become rounded. For this reason, in these tests the abrasive was changed regularly.

In the mining conditions, the rock always contains some amount of water, which may even be acidic. The water tends to lower the strength of the rock. On the other hand, the acidic conditions may increase the wear rates of the steel [19]. The rock material used in this study was

granite, which is the most common rock type in the Finnish bedrock. The rock was dried at ambient room temperature to stabilize the test conditions. Consequently, possible tribocorrosion mechanisms were not included in this study, but with this kind of high wear rates it can be assumed that abrasion is too dominant for corrosion to have a marked effect on the results.

Dommarco et al. [2] stated that the relative wear rates of field tested bucket tips made from austempered ductile iron were at least four times higher than in the standard laboratory rubber-wheel tests. Moreover, they did not take into account the contact time during the bucket operation that still increases the difference. Thus, the wear conditions in that case were much more severe in the field compared with the laboratory tests, which was also visible in the comparison of the wear surfaces [2]. In the present study, the high stress dry-pot laboratory wear tests with large quarried granite particles produced 75% of the wear rate of the estimated wear rate (mm/h) in the operating conditions, which is a quite reasonable result. All things considered, the test systems used in this study, especially the dry-pot, are much closer to the in-service application than the rubber-wheel test considering both the contact mechanisms and in the type and size of the abrasives.

It is estimated that in the mining industry 210,000 M€ is spent annually for wear and friction [20]. The potential savings achievable by better materials selection are therefore significant both economically and in terms of CO_2 reductions. This of course requires that the methods used in the materials selection processes are relevant to the application in question. It is also always possible to improve non-standardized in-house built laboratory test equipment and associated test practices to better correspond to the in-service conditions. In this study, for example, adjustments for this aim were made by selecting granite as the abrasive, a long testing time for the impeller-tumbler tests, and the structural steel disc to be used as the counterpart in the crushing pin-on-disc tests. Moreover, the dry-pot testing enabled selecting the speed and angle of the contact between the abrasives and the specimens. With proper adjustment, the dry-pot system was found to simulate quite well the loading of the bucket, where the steel blade slides into the pile of rock.

5. Conclusions

Several application oriented abrasive and impact-abrasive wear testing methods were used to simulate the wear behavior of the cutting edge of an underground mining loader bucket. Moreover, the relevance of laboratory testing in the evaluation of the in-service performance of cutting edges was assessed.

The work hardening behavior of the studied steels could be simulated with all testing methods used in this work. The hardened layers, however, appear to be thinner than in the in-service conditions due to the lower applied forces. The dry-pot wear testing method with an abrasive gravel bed produced similar wear rates and wear surfaces as the in-service operation. The abrasive type and size and the contact mechanisms were also quite similar when compared to the in-service conditions. In the crushing pin-on-disc tests the wear type was also similar but the forces much lower than in the in-service conditions. In the uniaxial crushing tests, the rock embedded in the sample in a similar manner as in the tip of the cutting edge due to the high compression forces. In the impeller-tumbler tests, the impact effect is dominant and wear concentrates on the tip and the edges of the sample. The results of this work indicate that proper simulation of the in-service conditions demands constant development of the test methods and careful evaluation of the obtained results.

Acknowledgements

This work was done within the DIMECC BSA (Breakthrough Steels and Applications) Programme as part of the DIMECC Breakthrough Materials Doctoral School. We gratefully acknowledge the financial support from the Finnish Funding Agency for Innovation (Tekes) and the participating companies. The authors also gratefully acknowledge Specialist Anu Kemppainen from SSAB Europe Oy for her help and advices, Specialist Kimmo Keltamäki from Lapland University of Applied Sciences, Industry and Natural Resources RDI, for his help with the in-service sample details, and B.Sc. Atte Antikainen for his assistance with the wear tests and sample preparation.

References

[1] K. Holmberg, Tribological accelerated testing, Finn. J. Tribology 9 (1990) 13–35.
[2] R. Dommarco, I. Galarreta, H. Ortíz, P. David, G. Maglieri, The use of ductile iron for wheel loader bucket tips, Wear 249 (2001) 101–108.
[3] S. Laino, J. Sikora, R.C. Dommarco, Wear Behavior of CADI Operating Under Different Tribosystems, ISIJ Int. 50 (2010) 418–424.
[4] G. Francucci, J. Sikora, R. Dommarco, Abrasion resistance of ductile iron austempered by the two-step process, Mater. Sci. Eng. A 485 (2008) 46–54.
[5] J.E. Fernández, R. Vijande, R. Tucho, J. Rodríguez, A. Martín, Materials selection to excavator teeth in mining industry, Wear 250 (2001) 11–18.
[6] L. Xu, S. Clough, P. Howard, D. StJohn, Laboratory assessment of the effect of white layers on wear resistance for digger teeth, Wear 181–183 (1995) 112–117.
[7] V. Heino, K. Valtonen, P. Kivikytö-Reponen, P. Siitonen, V.-T. Kuokkala, Characterization of the effects of embedded quartz layer on wear rates in abrasive wear, Wear 308 (2013) 174–179.
[8] V. Ratia, V. Heino, K. Valtonen, M. Vippola, A. Kemppainen, P. Siitonen, V.-T. Kuokkala, Effect of abrasive properties on the high-stress three-body abrasion of steels and hard metals, Finn. J. Tribology 32 (2014) 3–18 ⟨https://journal.fi/tribologia/issue/view/3255/13⟩.
[9] K. Keltamäki, M. Ylitolva, Kaivoskoneen kauhan huulilevyn kulumistutkimus: tekninen raportti, Lapin ammattikorkeakoulu, Rovaniemi, 2014, p. 37 ⟨http://urn.fi/URN:ISBN:978-952-316-039-2⟩.
[10] V. Ratia, K. Valtonen, A. Kemppainen, M. Vippola, V.-T. Kuokkala, High-stress abrasion and impact-abrasion testing of wear resistant steels, Tribology Online 8 (2013) 152–161, http://dx.doi.org/10.2474/trol.8.152.
[11] E. Vuorinen, N. Ojala, V. Heino, C. Rau, C. Gahm, Erosive and abrasive wear performance of carbide free bainitic steels – comparison of field and laboratory experiments, Tribology Int. 98 (2016) 108–115.
[12] J. Terva, T. Teeri, V.-T. Kuokkala, P. Siitonen, J. Liimatainen, Abrasive wear of steel against gravel with different rock–steel combinations, Wear 267 (2009) 1821–1831.
[13] M. Lindroos, M. Apostol, V.-T. Kuokkala, A. Laukkanen, K. Valtonen, K. Holmberg, O. Oja, Experimental study on the behavior of wear resistant steels under high velocity single particle impacts, Int. J. Impact Eng. 78 (2015) 114–127.
[14] A. Jaakonmäki, B. Johansson, I. Mäkinen, H. Räsänen, K. Ulvelin, T. Vennelä, Kiven käsittely ja kalusto, in: A. Hakapää, P. Lappalainen (Eds.), Kaivos- ja louhintatekniikka, Opetushallitus, Vammalan Kirjapaino Oy, Sastamala, Finland, 2009.
[15] D.-H. Cho, S.-A. Lee, Y.-Z. Lee, Mechanical properties and wear behavior of the white layer, Tribology Lett. 45 (2012) 123–129.
[16] K.H. Zum-Gahr, Microstructure and wear of materials, Tribology Series 10, Elsevier Science Publishers B.V., Amsterdam, The Netherlands, 1987.
[17] B. Bartha, J. Zawadzki, S. Chandrasekar, T.N. Farris, Wear of hard-turned AISI 52100 steel, Metall. Mater. Trans. A 36 (2005) 1417–1425.
[18] G.B. Stachowiak, G.W. Stachowiak, The effects of particle characteristics on three-body abrasive wear, Wear 249 (2001) 201–207.
[19] M. İphar, R.M. Göktan, The effect of liquids on mechanical strength and abrasiveness of rocks XVII Eng. & Arch. Fac. Osmangazi University, 2003.
[20] K. Holmberg, P. Kivikytö-Reponen, P. Härkisaari, K. Valtonen, A. Erdemir, Global energy consumption due to friction and wear in the mining industry, Tribology Int. (2017), http://dx.doi.org/10.1016/j.triboint.2017.05.010.

Publication III

Kati Valtonen, Kimmo Keltamäki, and Veli-Tapani Kuokkala

High-stress abrasion of wear resistant steels in the cutting edges of loader buckets

Tribology International 119 (2018) pp. 707-720

Tribology International 119 (2018) 707–720

Contents lists available at ScienceDirect

Tribology International

journal homepage: www.elsevier.com/locate/triboint

High-stress abrasion of wear resistant steels in the cutting edges of loader buckets

K. Valtonen [a,*], K. Keltamäki [b], V.-T. Kuokkala [a]

[a] Tampere University of Technology, Faculty of Engineering Sciences, Laboratory of Materials Science, Tampere Wear Center, P.O. Box 589, FI-33101 Tampere, Finland
[b] Lapland University of Applied Sciences, Industry and Natural Resources RDI, Tietokatu 1, FI-94600 Kemi, Finland

ARTICLE INFO

Keywords:
Wear testing
Abrasion
Steel
Mining
Mineral processing

ABSTRACT

To simulate the wear behavior of the cutting edge of the mining load-haul-dumper bucket, high-stress abrasion laboratory wear tests were conducted and compared to the in-service tests. The effects of test parameters and different abrasives on the wear rates and wear mechanisms of wear resistant steels were studied using the high-speed slurry-pot with a dry abrasive bed (dry-pot) and in the actual in-service use as a cutting edge. The laboratory wear tests produced results that are well comparable with the in-service case observations. Especially at the higher sample rotation speed with granite as an abrasive, the wear rates were quite similar as determined from the cutting edge of a loader bucket that had been used in a mine.

1. Introduction

In the mining conditions, it is practically impossible to perform two or more identical wear tests for the cutting edges of the mining loader buckets. Good examples of the variables affecting the results are the different types of rock being loaded, and even the different driving styles of the drivers. During a workday, the loader can be used to load slurry, gravel or large rocks, or simply to scrape the roads clean. The weight of the entire loader concentrates on the cutting edge when the bucket is being filled, especially when the rear tires lift up. Consequently, the cutting edge of the bucket may bend down as much as 50-60 mm [1]. Furthermore, the wear environment and also the mechanical properties of the cutting edge material and the welds affect the lifetime of the cutting edge, which may need to be replaced only once or several times a year.

There are several standardized tests for evaluating the abrasiveness of the rock. The most used ones are the LCPC test (Laboratoires des Ponts et Chaussées, Paris [2]), the Cerchar Abrasivity Index (CAI) test, and the determination of the equivalent quartz content (EQu) from a thin section or using an X-ray diffractometer [3]. In the LCPC test, two steel impellers are rotating 5 min at 4500 rpm in a pot with 500 g of 4–6.3 mm gravel [2]. The limitations of the LCPC test procedure are the quite small amount of abrasives of rather small size, the high rotation speed, and the use of structural steel with low hardness (60-75 HR B [4]) as impellers. In the LCPC tests, quite small differences in the steel properties may have a marked effect on the wear rates that naturally affects directly the obtained abrasiveness values [4,5]. On the other hand, the used steel grade is also quite different from the wear resistant materials used in the mining operations.

The Cerchar Abrasivity Index test is a more controlled test, where the rock samples are scratched with five 55 HRC steel styluses using a 70 kN force [6,7]. Five 10 mm scratches are made on then rock surfaces in two perpendicular directions at the speed of 1 mm/s. The CAI index is determined by measuring the flat area formed in the steel styluses. It has been stated that the CAI index correlates well with the strength [7] and the equivalent quartz content of the rocks [3]. Moreover, its correlation with the LCPC abrasivity index is surprisingly good, when the difference between the test methods is taken into consideration. However, the technique is not suitable for testing of the abrasivity of small particles [3].

In high-stress abrasive wear, so-called white layers can form by a thermomechanical process where the surface temperature during the wear contact first exceeds the austenite formation temperature, followed by a rapid cooling by the underlying bulk metal that leads to the formation of untempered martensite [8–10]. The simultaneous severe plastic deformation can cause the formation of a very fine nanostructure with higher strength and hardness than those of the original surface [14]. In addition, below the white layer the temperature may exceed about 200 °C, leading to overtempering of the martensite. The hardness of this so-called dark layer can therefore be markedly lower than the initial

* Corresponding author.
E-mail address: kati.valtonen@tut.fi (K. Valtonen).

https://doi.org/10.1016/j.triboint.2017.12.013
Received 20 October 2017; Received in revised form 8 December 2017; Accepted 10 December 2017
Available online 11 December 2017

Table 1
Typical mechanical properties and nominal compositions of the tested steels.

	400HB	450HB	R500HB	500HB	550HB	600HB
Hardness [HV10]	401 ± 23	435 ± 6	493 ± 18	481 ± 18	554 ± 8	609 ± 16
Rp0.2 [N/mm^2]	1000	1200	1250	1300	1400	1650
Rm [N/mm^2]	1250	1450	1600	1550	1700	2000
A [%]	10	8	8	8	7	7
Impact toughness −40 °C [J]	30	30	30	37	30	20
C [wt%] max.	0.26	0.26	0.30	0.30	0.37	0.47
Si [wt%] max.	0.80	0.80	0.80	0.70	0.50	0.70
Mn [wt%] max.	1.70	1.70	1.7	1.60	1.30	1.4
Cr [wt%] max.	1.5	1.5	1.5	1.5	1.14	1.20
Ni [wt%] max.	1.0	1.0	1.0	1.5	1.4	2.50
Mo [wt%] max.	0.5	0.5	0.5	0.6	0.6	0.70
B [wt%] max.	0.005	0.005	0.005	0.005	0.004	0.005
CEV typical	0.57	0.57	0.66	0.45	0.72	0.61

Table 2
Properties and nominal composition of the abrasives.

	Quartzite	Chromite	Kuru granite	Sorila granite
Quarry	Baskarp Svedudden, Sweden	Outokumpu Tornio Works Kemi Mine, Finland	Kuru, Finland	Sorila, Finland
Solid density [t/m^3]	2.65	3.46	2.64	2.72
Crushability [%]	35	79	38	38
Abrasiveness	1940	460	1380	1500
Median hardness [HV1]	992 ± 162	1059 ± 97	977 ± 134	955 ± 159
Nominal mineral contents [%]	Quartz 99	Chromite 99	Quartz 35 Plagioclase 30 Orthoclase 28 Biotite 3 [20]	Plagioclase 45 Quartz 25 Orthoclase 13 Biotite 10 Amphibole 5 [21]

hardness of the steel [8]. The formation of both of these layers is frequently observed and studied for example in conjunction of machining experiments [11–16].

The high-speed slurry-pot with a dry abrasive bed (dry-pot) has been successfully used to simulate the wear performance of carbide free bainitic steels in an iron ore sorting machine [17,18]. Moreover, in the comparison of four abrasive and impact abrasive test methods with the in-service mining loader bucket wear behavior, the dry-pot method showed the highest wear rates in heavy abrasive wear conditions [19]. In this article, the dry-pot is also used to study the abrasivity of crushed rock.

This research deals with the effects of test parameters and abrasives on the wear rates and wear mechanisms of steels. High-stress abrasion wear tests were conducted to simulate the wear behavior of the in-service cutting edge of a mining loader in a chromite mine. Six martensitic wear resistant steels of varying hardness were tested using the high-speed slurry-pot equipment with a dry abrasive bed and compared to the in-service cutting-edge steels tested in a chromite mine. The steel samples used in the tests had profiles similar to the actual cutting edges used in the bucket loaders. The abrasives were 8–10 mm crushed and sieved particles of quartzite, chromite, and two granites.

2. Materials and methods

2.1. Materials

Six wear resistant steels in the hardness range of 400 HB to 600 HB were wear tested in the laboratory with four abrasives. Table 1 lists the steels and their nominal compositions and typical mechanical properties, including Vickers hardness, yield strength (Rp0.2), ultimate tensile strength (Rm), elongation (A), and impact toughness at -40 °C. The typical carbon equivalent values (CEV) were determined using CEV = C + Mn/6 + (Cr + Mo + V)/5 + (Ni + Cu)/15. The microstructure of the studied steels was martensitic with some retained austenite and untempered martensite.

Swedish quartzite, Finnish chromite, and two granites from Finland were used as abrasives. The initial sieved particle size used in the tests was 8–10 mm. Table 2 lists some properties of the abrasives and Fig. 1 shows their microstructures. The two studied granites have quite similar abrasiveness and crushability, but Kuru granite has a much finer and heterogeneous structure compared to Sorila granite. Moreover, there is a marked difference in their composition; the main constituent in Kuru granite is quartz, while in Sorila granite it is plagioglase (sodium calcium feldspar).

2.2. Methods

Two of the studied steels, R500HB and 550HB were tested also in the in-service mining conditions in Kemi chromite mine. Fig. 2 shows a schematic image of the cutting edge used in an underground mining loader bucket constructed from the above mentioned steels by submerged arc welding (SAW). A CAT R2900G load-haul-dump (LHD) loader was used in normal mine operations for 217 h, including loading of 51514.6 tons of chromite ore, granite, slurry, and barren rock. The mass loss of the cutting edge of the bucket was determined by ATOS 3D-scanning, which gives three-dimensional measurements of the product for further analysis with Atos software. The wear pattern analysis was made by comparing the 3D scan of an unused cutting edge to the worn cutting edge after the test period.

A high-speed slurry-pot with a dry abrasive bed (dry-pot) was used in the tests to simulate the in-service wear behavior of the cutting edge of the mining loader in a laboratory scale. The test system has been described in details elsewhere [17,22]. The cutting edge profiled samples were attached to the second sample holder level in the rotating shaft, as shown in Fig. 3. The total wear area was about 5000 mm^2. Two samples were rotated inside the gravel bed simultaneously. The tests were done in two parts so that the abrasive and the position of the samples were changed in the middle of the tests.

All steels were tested with quartzite and Kuru granite for 60 min at 500 rpm. In these tests, R500HB was the reference sample material. In addition, a comparison of the four abrasives was made using 240 min tests at 250 rpm for two types of steel pairs: i) R500HB and 550HB as used in the in-service cutting edge and ii) 500HB and 600HB. The rotation speeds of 250 rpm and 500 rpm correspond to 2.5 m/s and 5 m/s in the edge of the sample, respectively. The travel distance of the sample edge during the test was doubled from about 18000 m to 36000 m, when

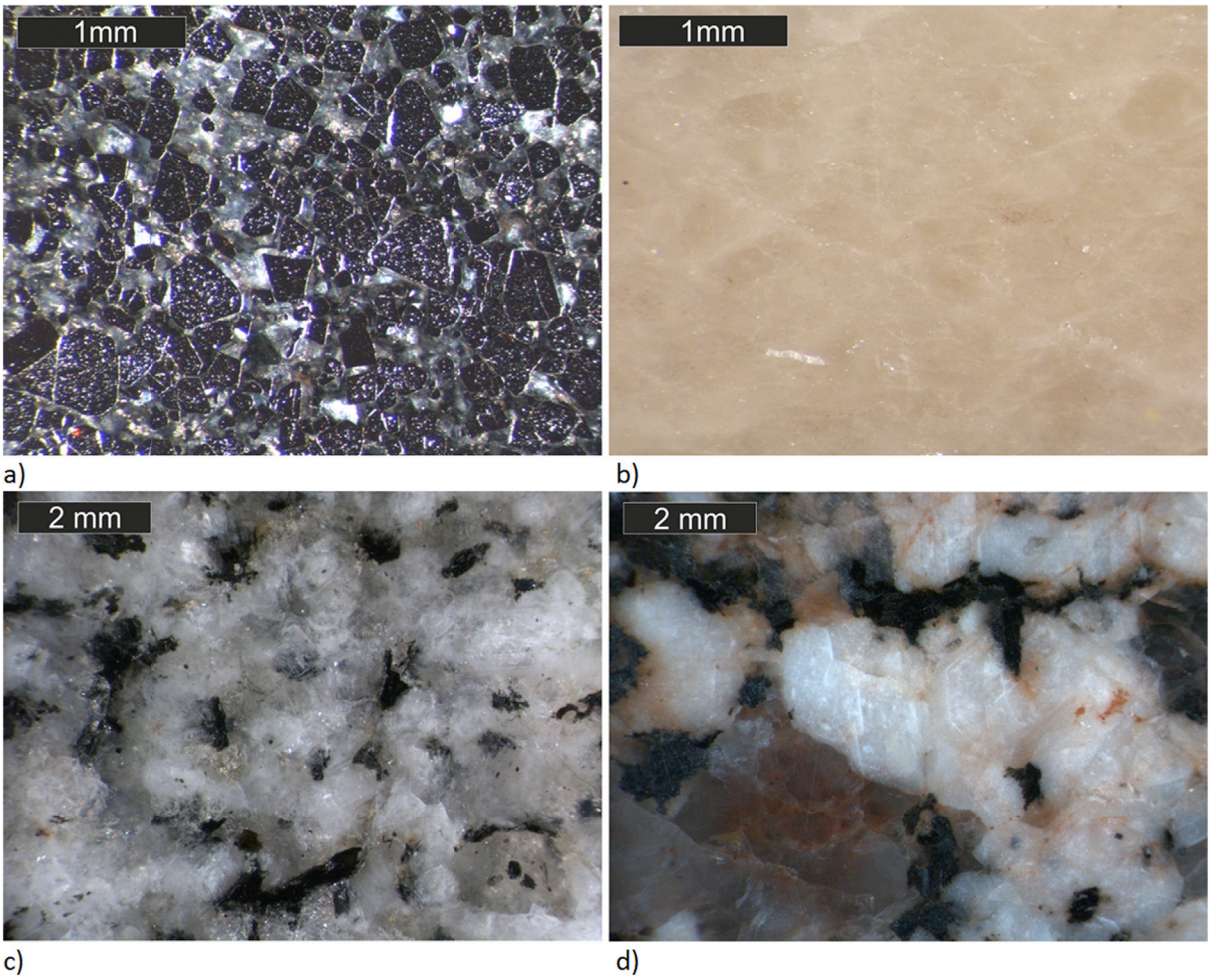

Fig. 1. Stereomicroscope images of the cross-sections of the abrasives: a) chromite, b) quartzite, c) Kuru granite, and d) Sorila granite.

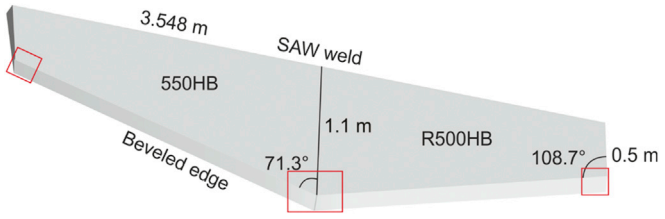

Fig. 2. Schematic of the studied in-service cutting edge. The red squares show the locations of characterized areas. (For interpretation of the references to color in this figure legend, the reader is referred to the Web version of this article.)

the test time was increased from 60 min to 240 min and the test speed was decreased from 500 rpm to 250 rpm.

The amount of 8–10 mm size gravel in one test cycle was 9 kg for quartzite and granites. The amount of chromite, however, was 13.8 kg because the density of chromite is higher than that of the other used abrasives. Thus, the volume of rock was similar in each test, covering the samples as illustrated in Fig. 3a.

Both the laboratory test samples and the in-service cutting edge of the loader bucket were thoroughly characterized. The wear surfaces were studied using Zeiss ULTRAplus field emission gun scanning electron microscope (FEG-SEM) and Alicona InfiniteFocus G5 3D measurement system. The cross-sections were characterized with FEG-SEM and an optical microscope, and the subsurface microhardness testing was performed with Matsuzawa MMT-X7 using a 50 g load (490.3 mN). The composition of the rocks was analyzed by Panalytical Empyrean Multipurpose Diffractometer (XRD). The abrasiveness and crushability of the abrasives were measured using a LCPC abrasimeter [2] at Metso Minerals. The bulk hardness values were determined from the cross-sections with Struers Duramin-A300 Vickers hardness tester using a 10 kg load.

3. Results

3.1. In-service case results

For the in-service testing, the cutting edge was constructed from R500HB and 550HB steels by submerged arc welding. The cutting edge was tested in CAT R2900G Underground Mining Load-Haul-Dumper (LHD), which is seen in operation in Fig. 4. For this dumper, the typical change interval of the cutting edge was about 1000 h.

After 150 h of operation, several cracks appeared near the installation welds on the side of the 550HB steel, next to the bucket-side shroud weld and the weld between the cutting edge and the bucket. The cracks were visible only in the 550HB steel and not in the weld nor in the R500HB steel. The welder repaired the first cracks in the side shrouds, but new cracks appeared in the 550HB plate at the corner. These cracks were so deep that repairing of them was not reasonable. Consequently, the in-service test was terminated after 217 h of operation.

Figs. 5–7 show the wear profiles of the cutting edge measured by ATOS 3D-scanning, illustrating the effect of wear. The dark color in Figs. 6–7 shows the original size of the cutting edge, which was later cut smaller from the sides due to a change to a smaller bucket finally used in the mine. The wear rate was highest on the underside of the cutting edge. Thus, the rocks under the cutting edge combined with the force of the machine

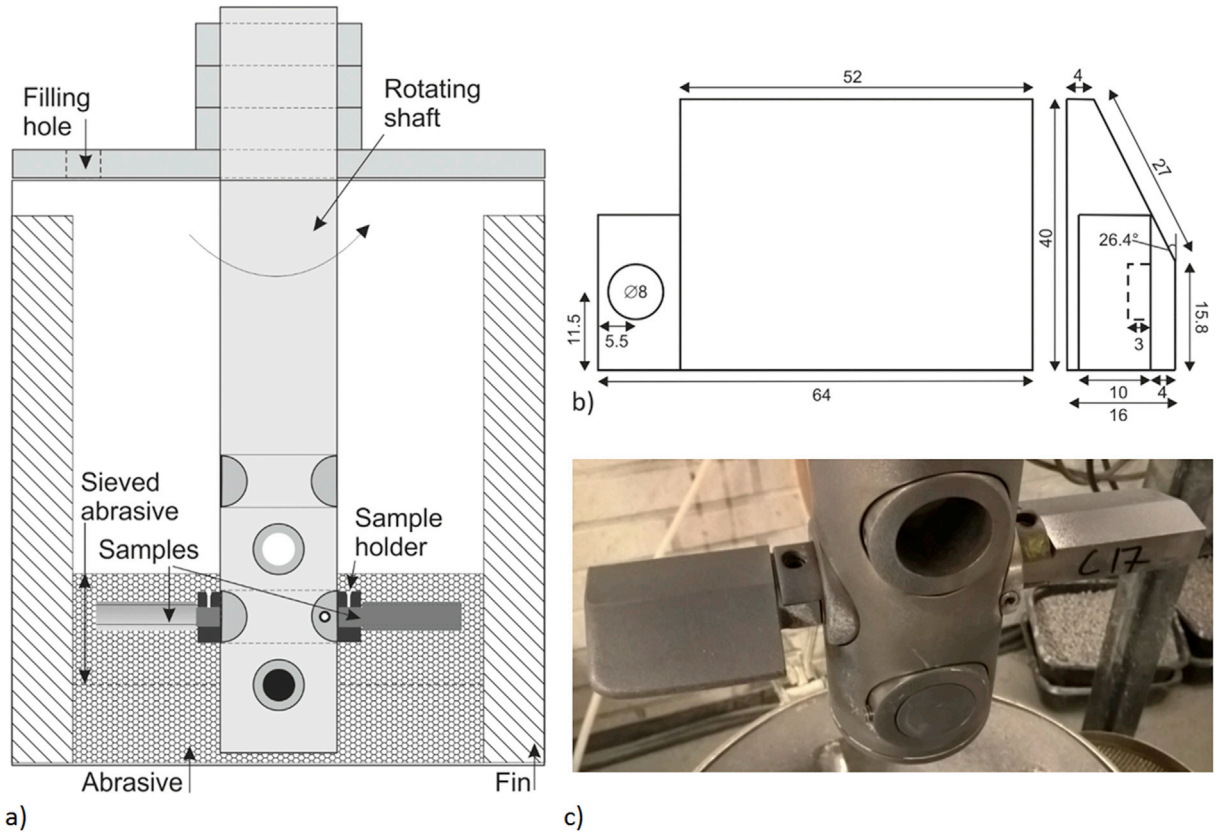

Fig. 3. The test setup: a) schematic image of the test chamber, b) drawing of the sample, and c) photograph of the attached samples after the dry-pot wear test.

Fig. 4. CAT R2900G LHD working on typical size of rocks. For reference, the diameter of the LHD tires is about 2 m.

pressing the cutting edge to the ground are much more abrasive than the rocks flowing inside the bucket. The centerline of the cutting edge is abraded more than the base steels because of the weld. The mass loss of R500HB was 54.95 kg and that of 550HB 40.51 kg, when determined by ATOS 3D-scanning. Thus, the harder 550HB was in these high-stress abrasive conditions significantly more wear resistant than R500HB.

3.2. Laboratory wear test results

The first laboratory wear test series compared the high-stress abrasion of the wear resistant steels with quartzite and Kuru granite at 500 rpm test speed. Fig. 8a presents the mass loss results of the 60 min tests. In these tests, quartzite was clearly more abrasive than Kuru granite, producing 33%-43% higher wear rates. However, the wear rates of the studied steels were not completely arranged by their hardness. For example, although the R500HB steel is harder than the 450HB and 500HB steels, it shows similar or higher mass loss. On the other hand, Fig. 8b shows that when the results are normalized using the reference sample, the R500HB steel exhibits a lower wear rate than the 450HB steel. Moreover, the 500HB steel performed better that its bulk hardness value gives reason to expect. Fig. 8b also indicates that the differences between the steels are more evident when granite is used as an abrasive, even though quartzite is more abrasive of these two.

The effect of abrasives on the wear of steels was further studied with four abrasives using samples made of the four hardest steels included in this study. The test speed was 250 rpm and the test time 240 min. Fig. 9 presents the results of the 240 min tests for one sample per material without a reference sample. The R500HB samples were tested with the 550HB samples and the 500HB samples with the 600HB samples. Once again, quartzite produced the highest mass losses, but chromite and both granites produced larger differences between the steel grades compared to quartzite. Even though the travel distance of the sample edge during the tests was doubled from 18 km to 36 km m, the wear rates were lower in the 250 rpm/240 min tests than in the 500 rpm/60 min tests.

During the tests, the gravel comminutes and the smaller rocks flow down and consolidate as a dense layer in the bottom of the chamber. Thus, the samples rotate inside the largest available freely flowing rock bed. The effect of the comminution of abrasives on the wear test results was studied by sieving the loose abrasives after the test cycles. Thus, Fig. 10 presents the effective rock size distribution causing wear in the samples until the end of the test. The downside of this sampling method, however, is that the finest fractions become underrepresented in the shown size distributions. In the 500 rpm/60 min tests, the abrasives were

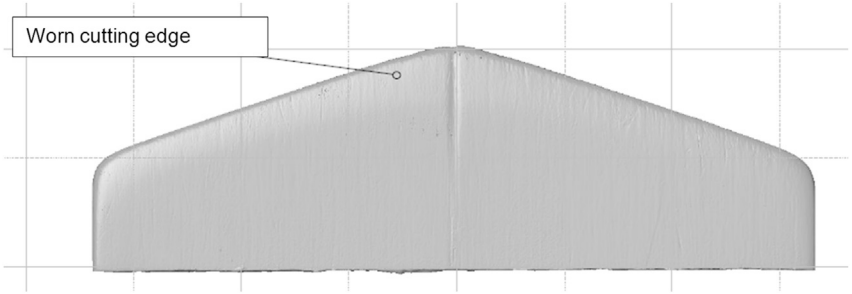

Fig. 5. Underside of the cutting edge after 217 h of operation (550HB on the left).

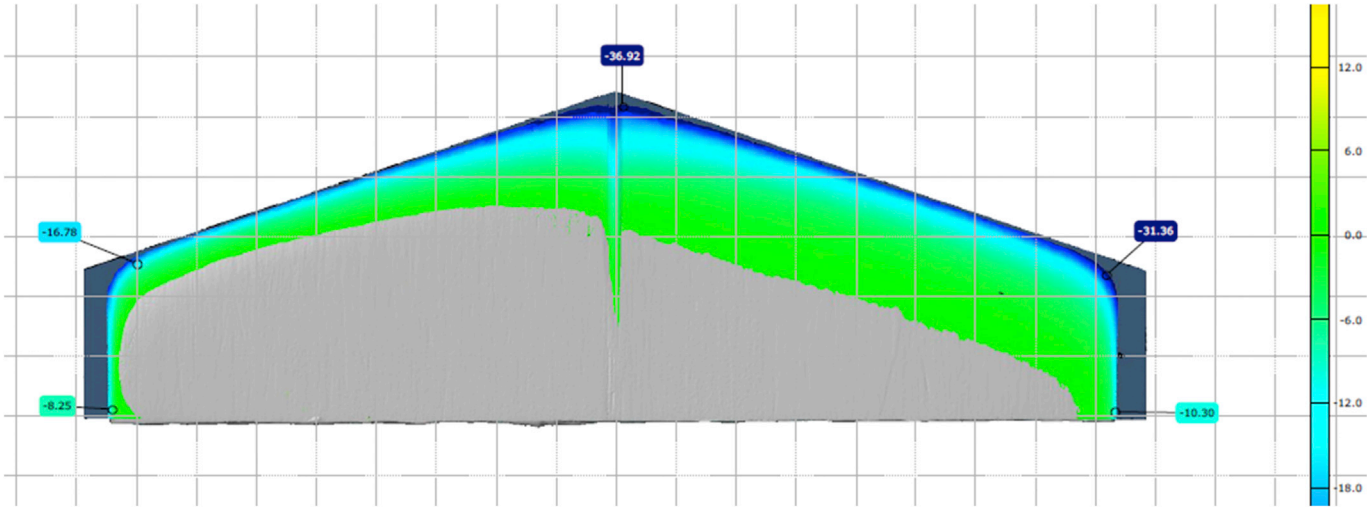

Fig. 6. Wear profile of the underside of the cutting edge (550HB on the left).

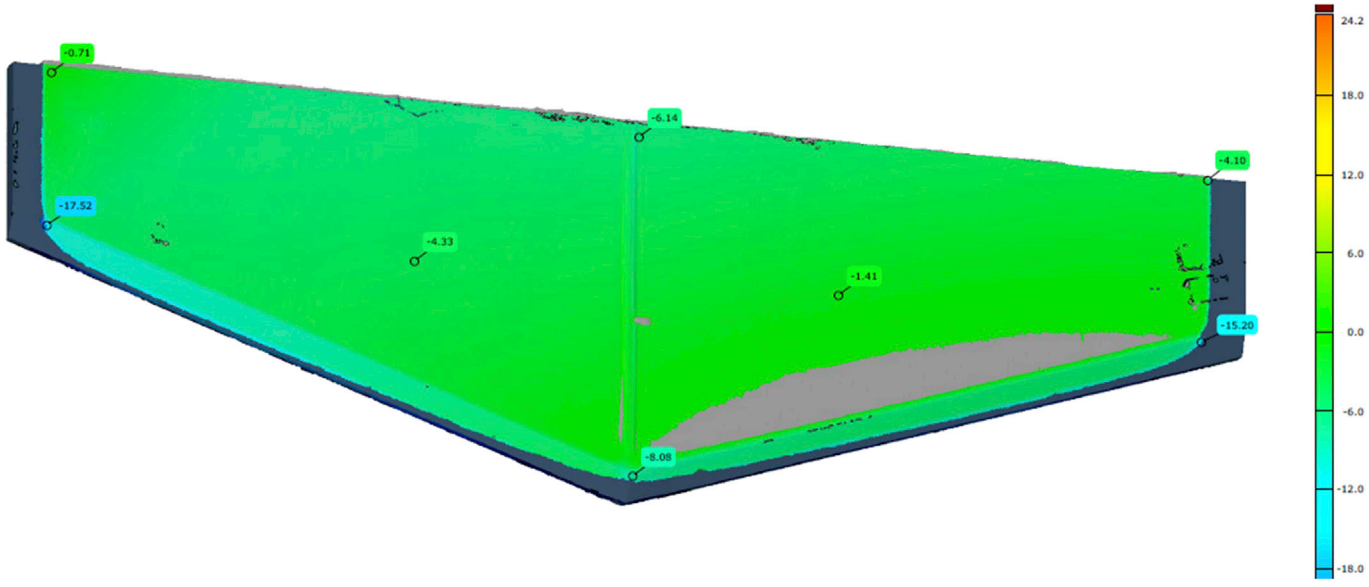

Fig. 7. Wear profile of the upper side of the cutting edge (550HB on the left).

crushed clearly more than in the 250 rpm/240 min tests; less than 50% of the abrasives were in the initial 8-10 mm size range. The chromite comminuted radically more than the other studied abrasives, containing more than 40% of fine particles under 2 mm in size after the tests.

3.3. Surface characterization

The wear surfaces were characterized to study the effect of the steel hardness and the abrasives on the wear mechanisms. In all following

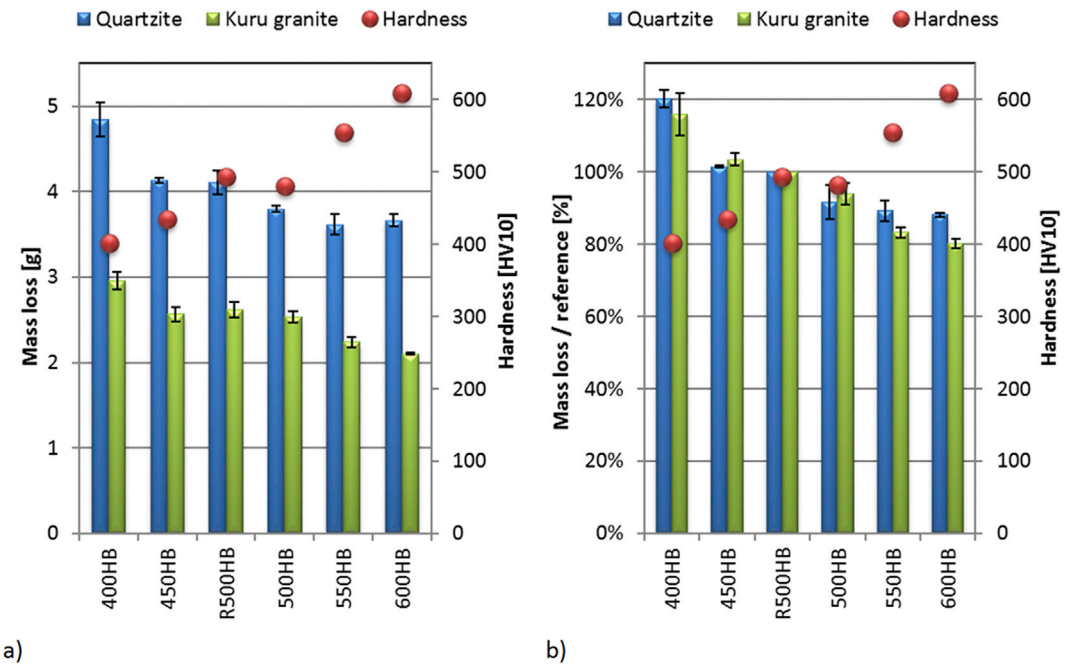

Fig. 8. Test results with quartzite and Kuru granite for 60 min at 500 rpm showing a) absolute average mass loss and b) mass loss relative to the wear of the R500HB reference sample. The error bars represent the standard deviation.

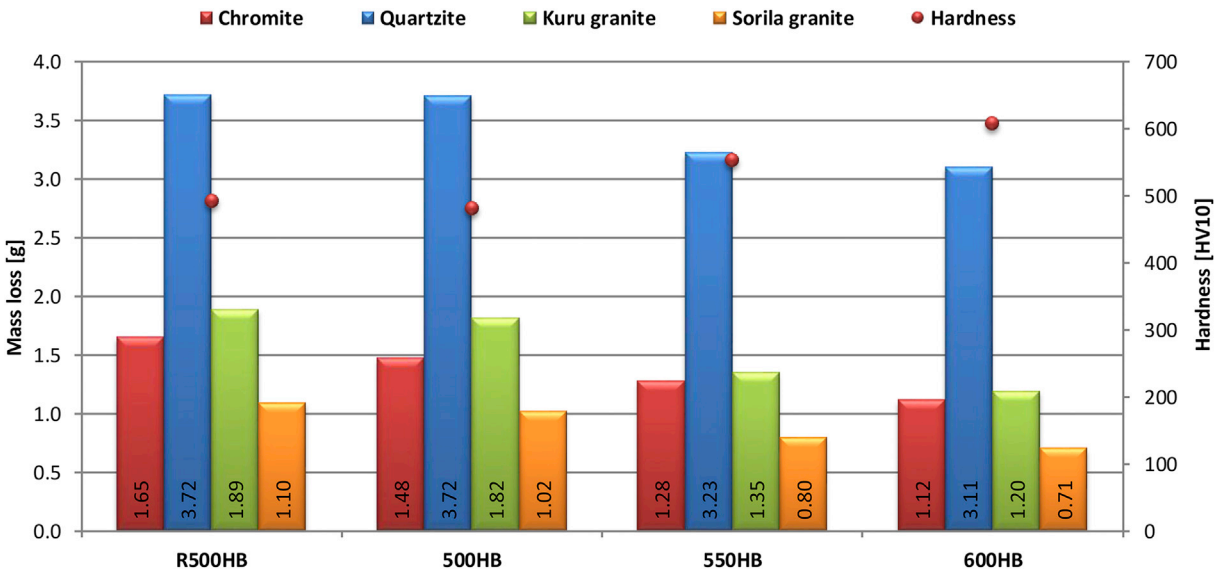

Fig. 9. Mass loss of the samples tested with four minerals for 240 min at 250 rpm.

wear surface images, the sample tip is on the right, i.e. the movement of the rock has been from the right to the left. The images are combined secondary electron and backscattered electron images (50:50) taken with a secondary electron detector SE2 and an angle selective backscattered electron detector AsB, respectively. The embedded rock shows dark grey on the lighter grey steel surface.

The pieces for the characterization of the in-service samples were cut from the middle and both ends of the tip of the cutting edge as marked in Fig. 2. Fig. 11 presents some examples of the characterized wear surfaces of the in-service cutting edge steels R500HB and 550HB. The surfaces show marks of cutting and surface fatigue by repeated ploughing. The scratches are long and deep and visibly deeper on the underside of the cutting edge. Quite high amount of rock was embedded in the steel surfaces, especially on the underside of the cutting edge. The reason for this difference in the embedment is that during loading the underside of the bucket ploughs heavily the ground and the rock pile, while on the upper side of the bucket the rocks have more possibilities to roll and thus cause less wear.

The increase in steel hardness can be seen as decreased surface deformation of the wear surfaces. The scratches were visibly deepest in the softer 400HB steel. Moreover, the embedment of the rock on the surface was lowest in the 600HB steel. Fig. 12 shows SEM images of the wear surfaces tested for 60 min at 500 rpm with Kuru granite. All wear surfaces showed marks of heavy plastic deformation produced by ploughing of the rocks under the test samples. The sharp corners of the crushed minerals formed also micro cutting marks on the surfaces. However, in the present tests the micro fatigue appears to be the most destructive wear mechanism typical to high-stress abrasive wear with natural minerals [23]. In this wear mode, the rocks are ploughing the deformed steel surfaces repeatedly causing eventually material removal.

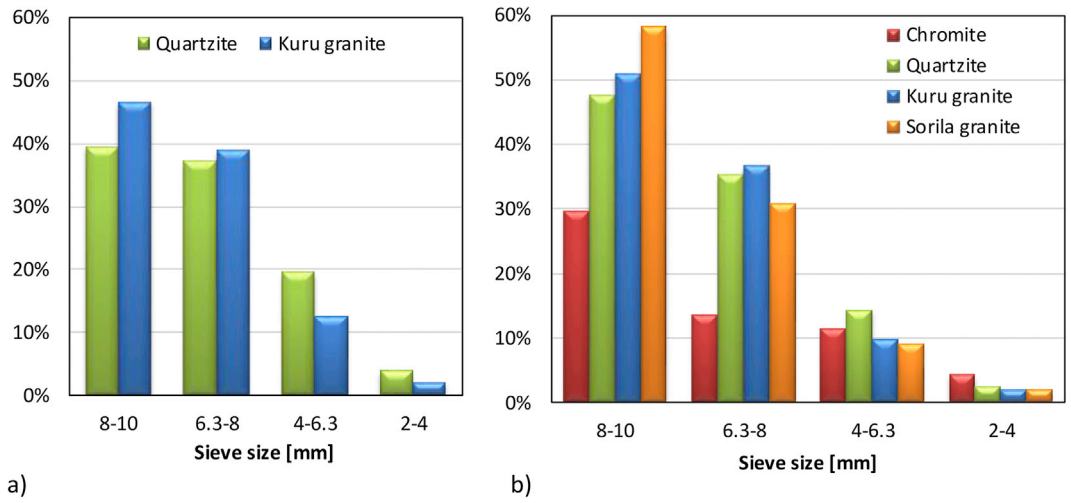

Fig. 10. The sieved fractions of the abrasives taken from the area indicated in Fig. 3a after the test: a) 60 min at 500 rpm and b) 240 min at 250 rpm.

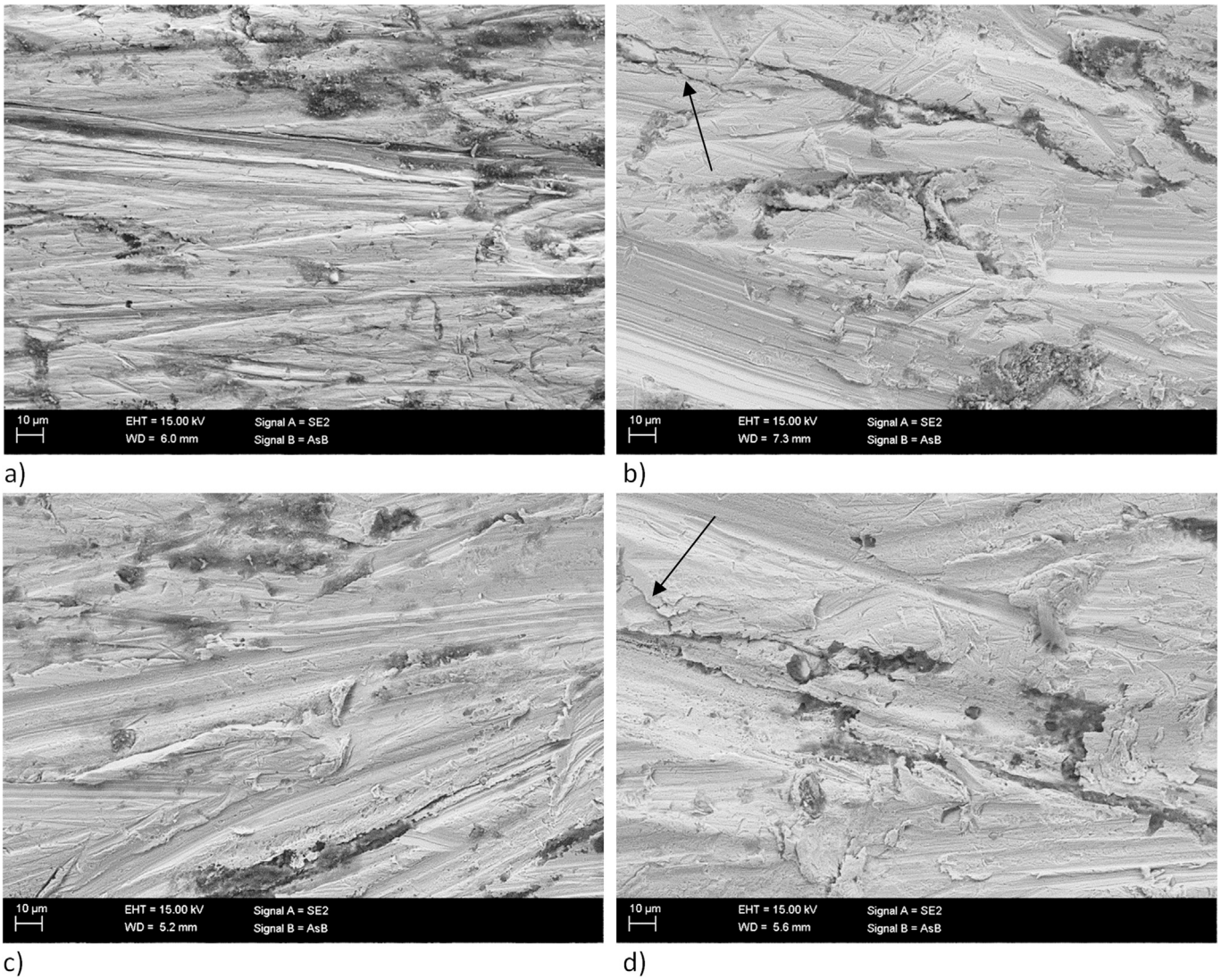

Fig. 11. FEG-SEM images of the wear surfaces of R500HB (a and b) and 550HB cutting edges (c and d): a and c are from the underside and b and d from the upper side of the cutting edge. The arrows indicate cracks on the surface.

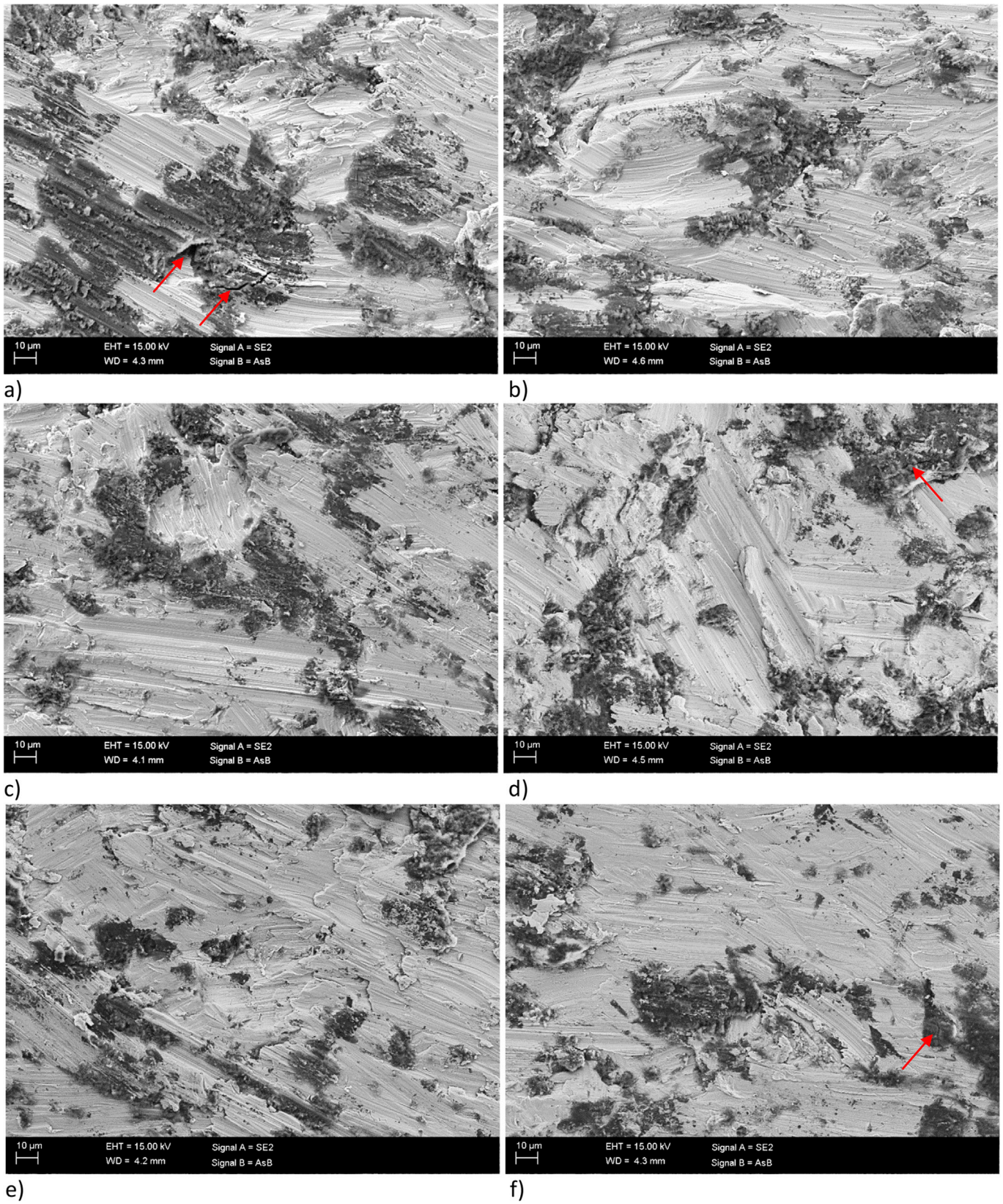

Fig. 12. FEG-SEM images of the underside wear surfaces tested for 60 min at 500 rpm with Kuru granite a) 400HB, b) 450HB, c) R500HB, d) 500HB, e) 550HB, and f) 600HB. The arrows indicate cracks in the mixed rock and steel layer.

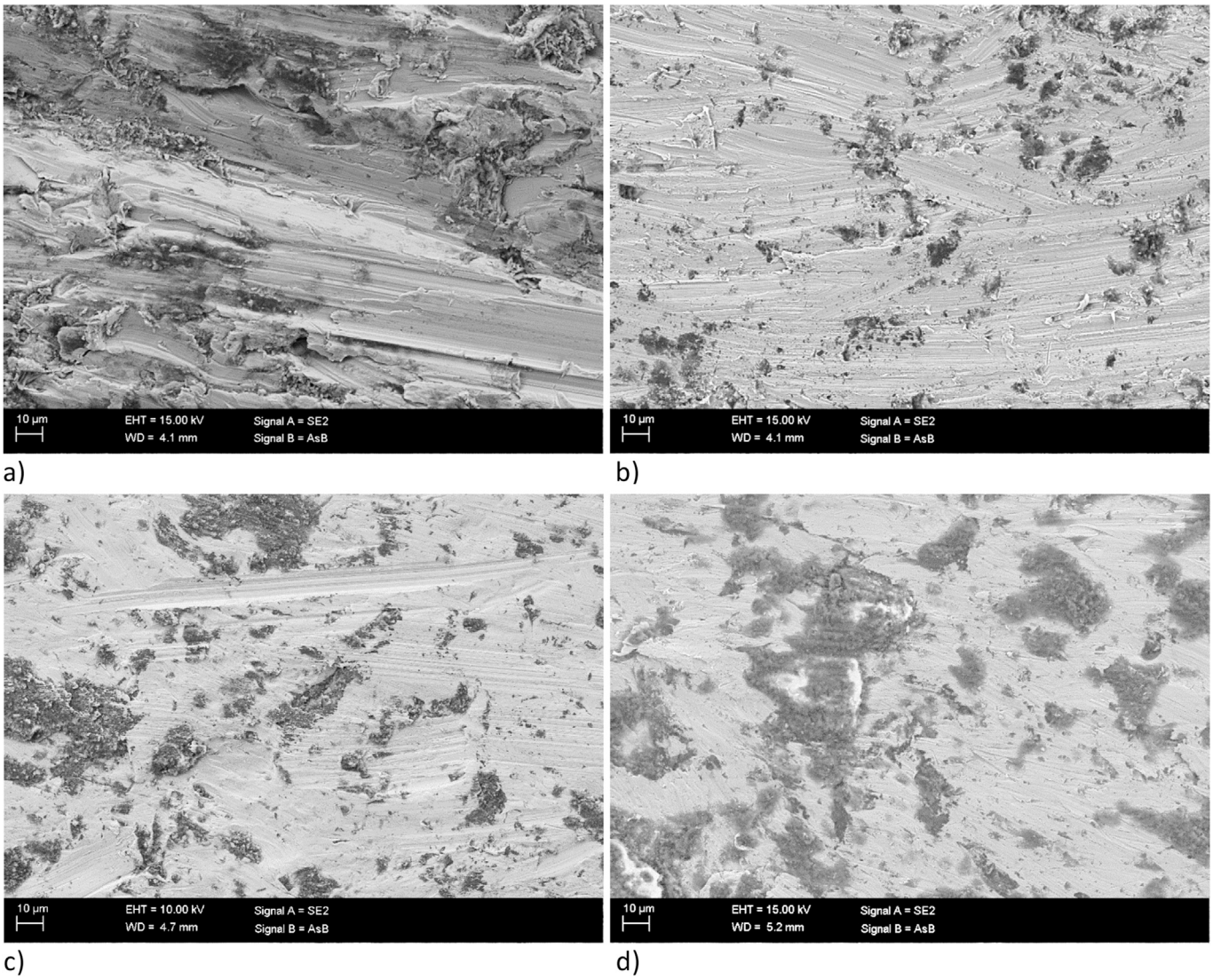

Fig. 13. FEG-SEM images of the underside wear surfaces of the R500HB samples tested for 240 min at 250 rpm with a) chromite, b) quartzite, c) Kuru granite, and d) Sorila granite.

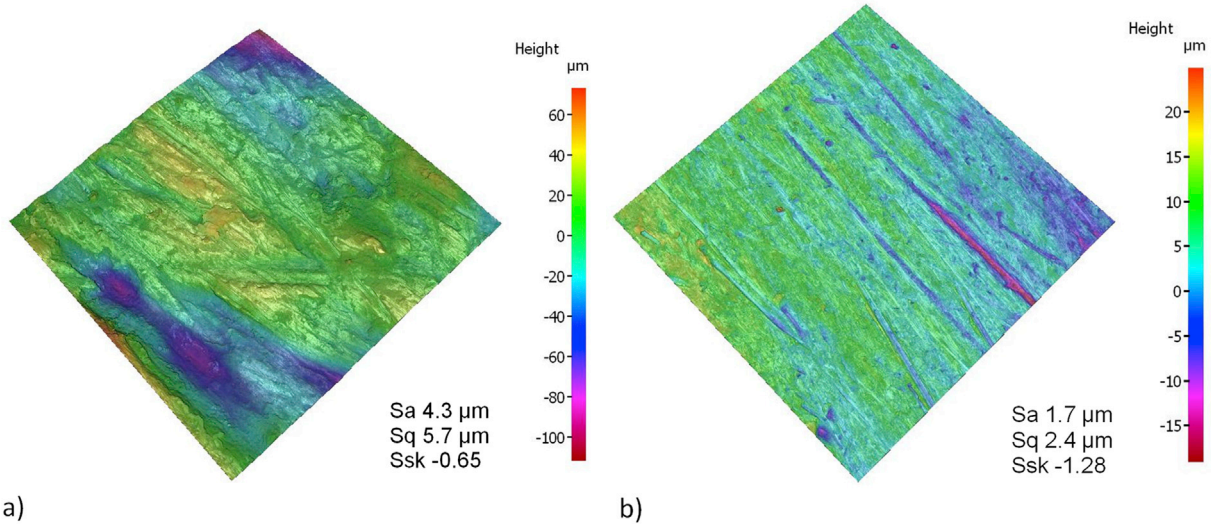

Fig. 14. 3D profilometer images of the R500HB steel surfaces tested a) in the in-service conditions and b) in a laboratory for 240 min at 250 rpm in chromite. Image area is 3 mm × 3 mm.

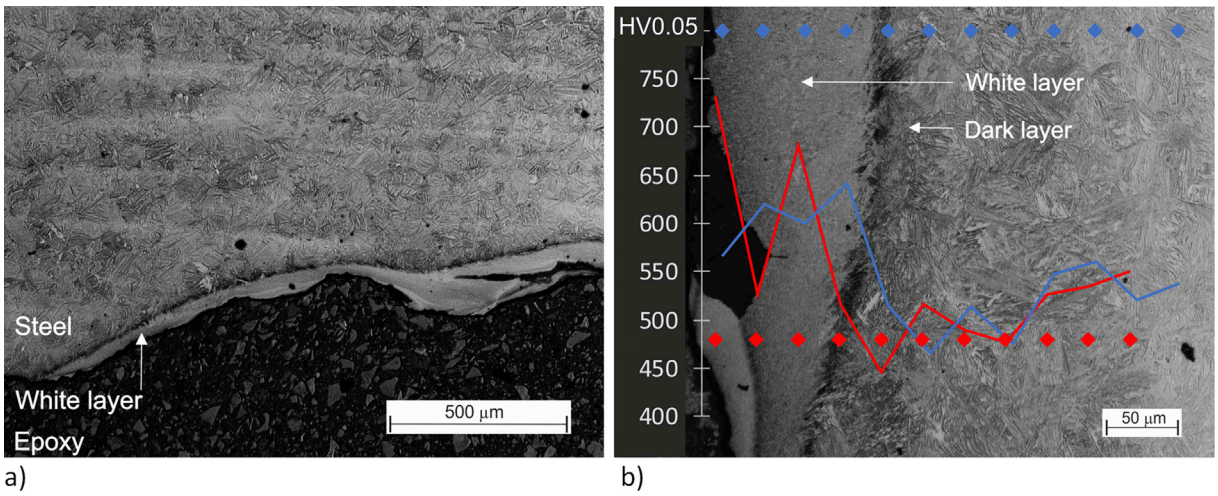

Fig. 15. Optical micrographs from the cross-section of the underside of the in-service R500HB sample showing thick white layers. The hardness profiles (b) were measured from the diamond marker locations.

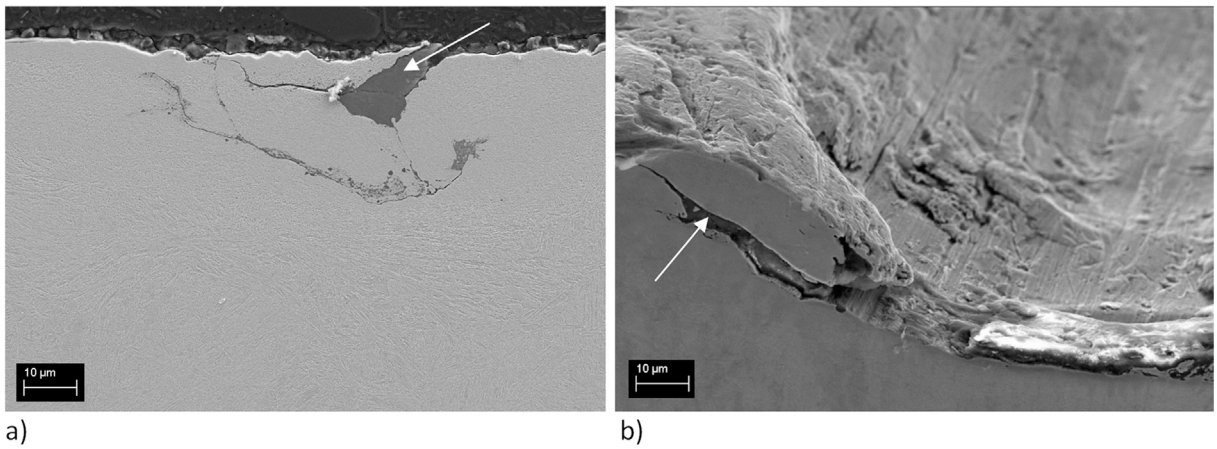

Fig. 16. Cross-section FEG-SEM images of white layers in the 550HB in-service sample. The arrows mark embedded rock particles.

Fig. 12a shows a good example of the cracked and partly detached deformed layer of mixed rock and steel.

The effect of abrasive type on the wear mechanism was greater than the effect of the steel grade. Fig. 13 presents the wear surfaces of R500HB tested for 240 min at 250 rpm using chromite, quartzite, Kuru granite, and Sorila granite. The chromite tested surfaces show the deepest and longest cutting marks and also well defined ridges from ploughing. The scratches are much finer in the quartzite tested surfaces. Moreover, the embedded rock is very fine and scattered as thin particles on the wear surface. The embedded granite formed thick blocks on the wear surfaces, which are clearly thickest when using Sorila granite. The granite particles also tend to round during the long test cycle, and as a consequence, rolling marks were observed on the wear surfaces.

Although the appearance of the in-service and laboratory tested wear surfaces were similar in the micro scale, in a larger scale the effect of much larger rocks causing wear in the mining conditions was clearly visible. Fig. 14 presents 3D profilometer images of R500HB tested in laboratory with chromite and in the in-service conditions. Even in a few square millimeter area, the surface roughness values of the in-service wear surface are clearly higher.

3.4. Cross-section analysis

The cross-section analysis was made to study the deformation and work hardening of the subsurface layers of the steels by microscopy and micro hardness testing. Tens of micrometers thick and partially cracked white layers were observed in the cross-sections of the in-service samples. The white layers were thickest, up to 150 μm on the underside of the cutting edge, where the hardness of the layers was on average 740 ± 25 HV0.05 for both steels. However, even values up to 790 HV0.05 were measured in some locations, where two or more white layers were overlapping. On the upper side of the cutting edges, the thickness of the white layers was typically below 50 μm. Fig. 15 presents examples of the thickness and hardness profiles of the white layers. The high hardness of the white layers explains the brittle nature of the fractures. Fig. 16 shows an example of cracking along the white layers. The cracks stop at the deformed layer below the white layer, i.e. so-called dark layer. In the R500HB steel, the hardness values in this layer were as low as 390 HV0.05. The tilted view in Fig. 16b shows also the appearance of the wear surface above the white layer, where abrasive particles have been trapped under the heavily deformed and cracked lip.

Fig. 17 shows the thin, less than 10 μm thick white layers that were occasionally formed in all laboratory samples. They were found especially in the bottom of deep scratches. The white layers were typically thickest at the highly rounded outer corners of the samples. Moreover, continuous white layers were formed in the outer edge of the samples, where the sample velocities were the highest. Fig. 17d shows delamination of the white layer from the outer edge of the 500HB sample. In the 550HB sample (Fig. 17e), it looks like the white layer has already delaminated and the deformed layer is going to crack. Although the

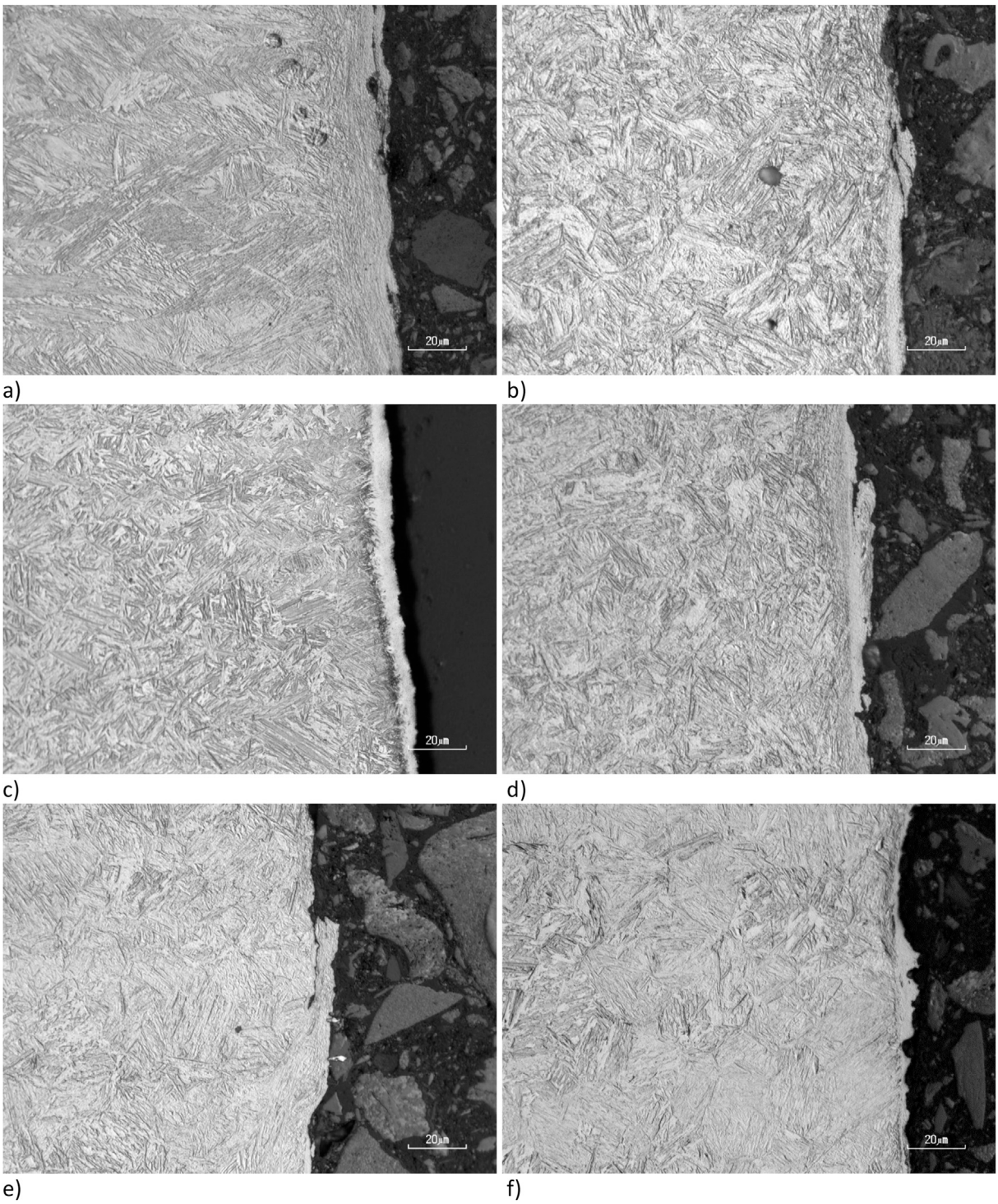

Fig. 17. Optical micrographs of the cross-sections of the outer edges of the samples tested for 60 min at 500 rpm with quartzite a) 400HB, b) 450HB, c) R500HB, d) 500HB, e) 550HB, and f) 600HB.

deformed layers were deepest in the 400HB steel, only a couple of micrometers thick white layers were observed in this material.

In the 250 rpm/240 min tests, the formed white layers were thicker, up to 25 μm and less cracked when compared to the 500 rpm/60 min tests. The hardness of the white layers was up to 800 HV; similar to the in-service cases. It should be noted that the hardness of the white layers in the 600HB steel was at the same level with the 500-550 grade steels. The white layers were thinnest, less than 5 μm, in the chromite tested samples and thickest, even as thick as 25 μm, in the quartzite tested samples. Fig. 18 shows a couple of examples of the white layers formed in the 250 rpm/240 min tests. In general, the harder the steel, the thicker the formed white layers are.

4. Discussion

Although the size of the loaded rocks in a mine can be really big, the true local contact areas between the rocks and the steel surfaces are similar as in the laboratory tests. Accordingly, the width of the scratches

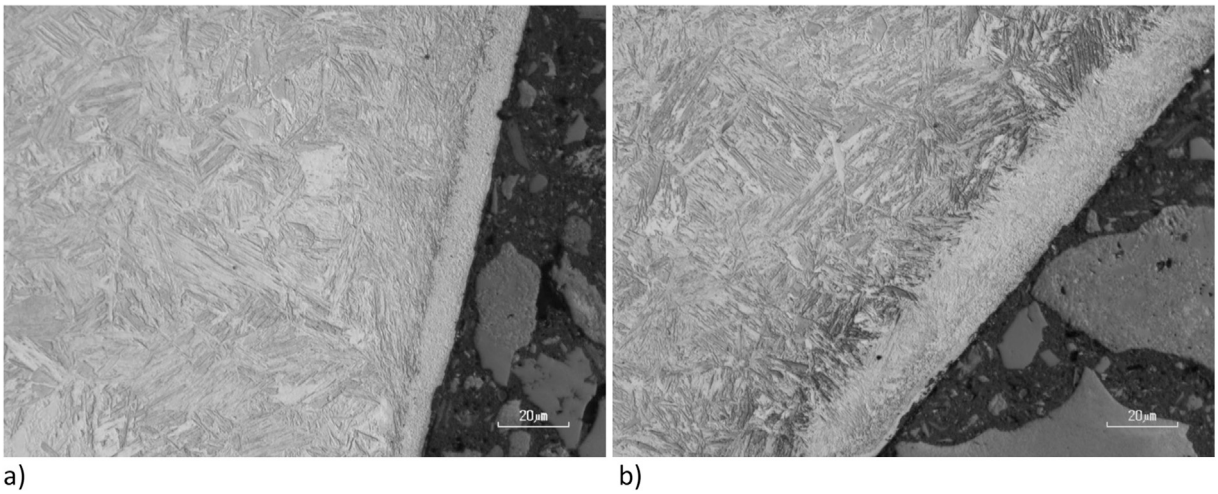

Fig. 18. Optical micrographs of the cross-sections of a) 500HB and b) 600HB samples tested for 240 min with quartzite at 250 rpm.

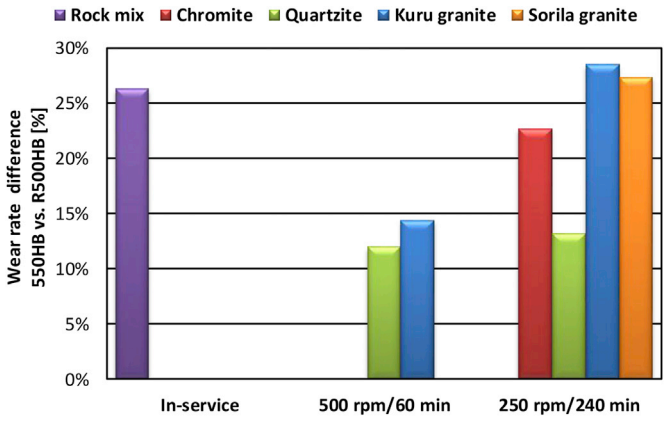

Fig. 19. Reduction of the wear rate when R500HB is replaced by 550HB in the in-service conditions and in the laboratory tests with different abrasives and test conditions.

on the sample surfaces were quite similar in both cases. However, only the small and hard particles in the chromite ore produced similar long and well-defined scratches in the laboratory tests as found in the in-service samples. Granite and quartzite particles, on the other hand, rounded during the tests and thus partially rolled over the sample surface.

In the laboratory wear tests, quartzite produced the highest wear rates at both test speeds and tests times. In the 500 rpm tests, quartzite produced up to 74% higher mass losses than granite in 60 min, and in the 250 rpm tests up to 178% higher mass losses than chromite in 240 min. Despite the high wear rates produced by quartzite, the tests with Kuru granite showed the biggest differences between the wear rates of the studied steels. Fig. 19 shows how much lower the wear rates of the 550HB steel samples were when compared to the R500HB samples. In the 250 rpm/240 min tests, the difference between the steels was quite similar as in the in-service case, when the abrasive was granite or chromite. The difference was much smaller when the abrasive was quartzite or the speed was higher. In abrasive wear, quartzite forms a thin in-situ composite layer with steel, which has been observed to have an effect on the wear behavior of the steels [24].

Fig. 20 presents the wear rates of the R500HB and 550HB steels in mm/h obtained by dividing the determined mass loss by the test time, the initial contact area, and the density. For the in-service samples, the actual contact time with gravel was estimated to be about 25% of the total operation time based on the loading videos taken during the operation in the mine. However, it is only a rough estimate because the loading types changed during the operation of the loader. In the 500 rpm/60 min tests with Kuru granite, the wear rate is in the same level as in the mining conditions with various rock types. Although the travel distance of the sample tip was doubled in the 250 rpm/240 min tests compared to the 500 rpm/60 min tests, the wear rate was much higher in the 500 rpm tests. For example, the wear rates of the 550HB steel were 350% higher with quartzite and as much as 560% higher with Kuru granite than in the

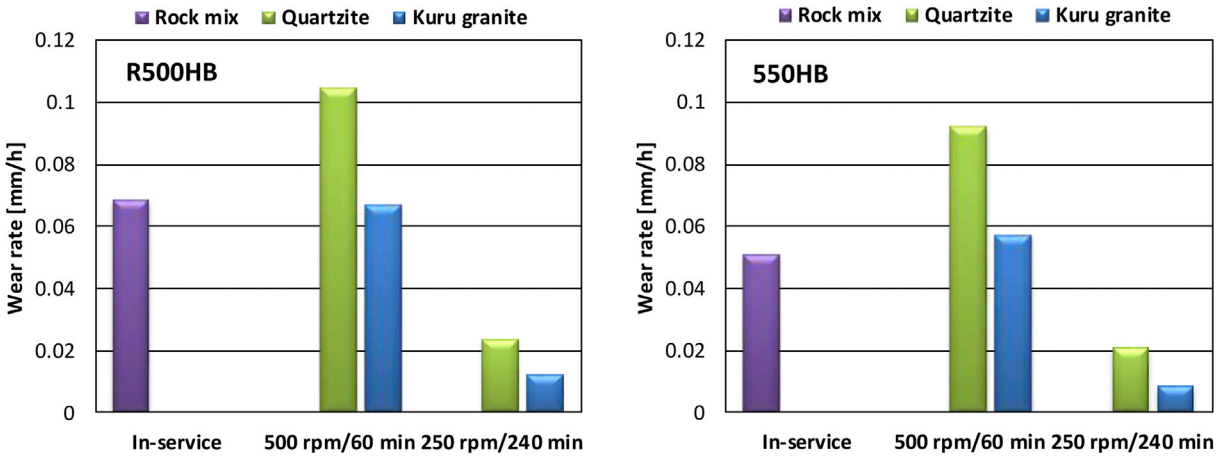

Fig. 20. Wear rates of the R500HB and 550HB steels in the used test environment.

250 rpm/240 min tests. This clearly indicates changes in the wear mechanism: for example, the higher rotation speed of the sample produces higher energy impacts, which will remove material more effectively by means of micro fatigue.

In all laboratory tests, the white layers were formed in the bottom of the scratches and especially on the outer edge and tip of the samples. In the in-service samples, the white layers were thicker (up to 150 μm) than in the laboratory samples (up to 25 μm), but similar failure mechanisms were observed. When the deformability of the hard white layers was exceeded, they cracked and failed. Especially in the 500 rpm/60 min tests, the white layers were cracked and failed in a similar manner as in the in-service case. In the 250 rpm/240 min tests, the formed white layers were 10–20 μm thicker and more intact than in the tests with the higher speed. This indicates that the formation of white layers may protect the steels in milder wear conditions, but at higher speeds and loads they tend to fail, which may even accelerate wear in certain conditions. This is in agreement with the studies of Yang et al. [25,26], who also stated that depending on the direction of the crack propagation, the white layers fail either by delamination or spalling.

The laboratory tests were found to produce white layers and wear surfaces that remind more the upper side of the cutting edge than its more heavily worn underside. Thus, the dry-pot laboratory tests model better the penetration of the cutting edge into the rock pile and sliding of the rock against the upper side of the cutting edge. However, an obvious limitation of the current test system is that there is no vertical compressive force acting on the cutting edge, i.e. the mass of the rock pile and the weight of the loader, as explained in the Introduction.

When there are only small differences observed in the test results, such as in the cases of 450HB and R500HB or 550HB and 600HB, the use of a reference sample is very important, as it reduces the effect of differences between the batches of natural abrasives. On the other hand, the standard deviations in the wear rates of the reference samples were only 3.4% with quartzite and 3.7% with granite, which are reasonably good values for this type of wear test.

The dry-pot test procedure is quite similar to the LCPC abrasiveness tests; two steel impellers are rotating in a pot filled with gravel. The LCPC test gives 40% higher abrasiveness values for quartzite than for Kuru granite, while the dry-pot test produced 50-75% higher mass losses with quartzite. Moreover, the dry-pot test gives Sorila granite higher abrasiveness than for Kuru granite and chromite. The difference is marked with chromite, the abrasiveness of which is only one third of that of Sorila granite. However, in the dry-pot test both Kuru granite and chromite produced higher wear rates compared to Sorila granite. This indicates a marked difference in the wear processes between the LCPC and dry-pot tests. The high energy impacts during the LCPC test break the rock more efficiently. Moreover, the test is much shorter (5 min) and practically covers only the running-in phase of the steel impeller. These results indicate that in the estimation of the abrasivity of the rock in a certain application, the entire wear environment should be taken into consideration and that the simplified abrasivity tests may give incorrect estimations, since they are practically based on measuring the strength of the rock materials. Moreover, the steel grades used in the abrasivity tests have typically very different mechanical properties compared to the ones used in the actual conditions in the field. Moreover, the contact conditions and tests speeds do not match with the in-service conditions either. Based on the presented results and observations, it can be concluded that the dry-pot test method could be suitable also for abrasivity testing for selected mining applications, such as loader buckets, feed hoppers, and screens.

A great advantage of this study was the possibility to characterize two materials that had been used in a chromite mine, and to compare them with laboratory wear tested samples. During two years of recording, the replacement frequency of the cutting edges of the selected LHD loader varied from 447 h to 1588 h. Thus, the 217 h in-service test was much shorter than the average 1041 h between the replacements. The SAW weld connecting the two test steels was of high-quality, but the MIG/MAG installation weld of the 550HB steel failed due to hydrogen embrittlement. Apparently the preheating of the hard steel was made at a too low temperature and the installation welding wire was not good enough for this kind of a hard steel. This is an example of the challenges that are often encountered when new materials are introduced to the in-service use, or when material testing is made in the in-service conditions. However, the wear rates were high enough to produce a clear difference between the two steels used in the test cutting edge. Moreover, the laboratory wear test results support the in-service case results. When the welding parameters are optimized, it is quite realistic to expect an over 25% increase in the lifetime of the cutting edges, if the material is changed from the current R500HB steel to 550HB steel.

5. Conclusions

In this study, the laboratory wear tests with six steel grades, four abrasives, and two testing procedures were conducted. Two of the steels were tested also as cutting edges of the loader bucket in real mining conditions. Based on the analysis of the laboratory and the in-service wear test results and the characterization of the wear surfaces and microstructures, the following conclusions can be drawn:

- The laboratory wear test results are in accordance with the in-service case results; an over 25% increase in the lifetime can be expected, when the current R500HB steel is changed to a harder 550HB steel.
- A low sample rotation speed with a long testing time and granite or chromite as an abrasive produce the highest wear rate differences between the steel grades, which is in accordance with the in-service results.
- When tested at the higher sample rotation speed with granite, the wear rates in the dry-pot tests were similar as in the in-service conditions.
- Although chromite produced similar wear surfaces as found in the in-service samples taken from a chromite mine, the formed white layers were not as thick, because the chromite ore comminuted heavily in the laboratory tests. Thus, granite seems to be the most suitable abrasive for wear testing in this kind of application in the Finnish bedrock.
- The dry-pot tests produce repeatable results with a quite small standard deviation in the mass loss values.
- The dry-pot wear tester is also suitable for determining the abrasivity of rocks in certain mining applications.
- The formation of white layers increased the wear rate in the harder steel grades, when the wear mechanism was more of the impact-abrasive type.

Acknowledgements

This work was done within the DIMECC BSA (Breakthrough Steels and Applications) Programme as part of the DIMECC Breakthrough Materials Doctoral School. We gratefully acknowledge the financial support from the Finnish Funding Agency for Innovation (Tekes) and the participating companies. Pasi Lassuri and Jarmo Räsänen from Outokumpu Kemi Mine are thanked for enabling the testing in the mine. The authors also gratefully acknowledge Specialist Anu Kemppainen from SSAB Europe for her help and advices, and B.Sc. Verner Nurmi for his assistance with the wear tests and sample preparation.

References

[1] Tanttari M. Facing wear challenges in underground loaders. TWC Int. Wear Semin 2009:1–12.
[2] Abrasimeter Paris. France: matériales des Laboratoires des Ponts et Chaussées. 1985.
[3] Thuro K, Käsling H. Classification of the abrasiveness of soil and rock. Geomech Und Tunnelbau 2009;2:179–88. https://doi.org/10.1002/geot.200900012.

[4] Drucker P. In: Validity of the LCPC abrasivity coefficient through the example of a recent Danube gravel Aussagekraft des LCPC-Abrasivitätskoeffizienten am Beispiel eines rezenten Donauschotters, vol. 4; 2011. p. 681–91. https://doi.org/10.1002/geot.201100051.
[5] Küpferle J, Röttger A, Alber M, Theisen W. Assessment of the LCPC abrasiveness test from the view of material science/Bewertung des LCPC-Abrasivitätstests aus werkstofftechnischer Sicht. Geochem Trans 2015;8:211–20. https://doi.org/10.1002/geot.201500002.
[6] Ko TY, Kim TK, Son Y, Jeon S. Effect of geomechanical properties on Cerchar Abrasivity Index (CAI) and its application to TBM tunnelling. Tunn Undergr Space Technol 2016;57:99–111. https://doi.org/10.1016/j.tust.2016.02.006.
[7] Deliormanlı AH. Cerchar abrasivity index (CAI) and its relation to strength and abrasion test methods for marble stones. Construct Build Mater 2012;30:16–21. https://doi.org/10.1016/j.conbuildmat.2011.11.023.
[8] Nikas GK. Modeling dark and white layer formation on elastohydrodynamically lubricated steel surfaces by thermomechanical indentation or abrasion by metallic particles. J Tribol 2015;137:31504. https://doi.org/10.1115/1.4029944.
[9] Cho DH, Lee SA, Lee YZ. Mechanical properties and wear behavior of the white layer. Tribol Lett 2012;45:123–9. https://doi.org/10.1007/s11249-011-9869-4.
[10] Hossain R, Pahlevani F, Witteveen E, Banerjee A, Joe B, Prusty BG, et al. Hybrid structure of white layer in high carbon steel - formation mechanism and its properties. Sci Rep 2017;7:1–12. https://doi.org/10.1038/s41598-017-13749-7.
[11] Manco GL, Caruso S, Rotella G. FE modeling of microstructural changes in hard turning of AISI 52100 steel. Int J Material Form 2010;3:447–50. https://doi.org/10.1007/s12289-010-0803-3.
[12] Mao C, Zhou Z, Zhang J, Huang X, Gu D. An experimental investigation of affected layers formed in grinding of AISI 52100 steel. Int J Adv Manuf Technol 2011;54:515–23. https://doi.org/10.1007/s00170-010-2965-z.
[13] Ji W, Shi J, Liu X, Wang L, Liang SY. A novel approach of tool wear evaluation. J Manuf Sci Eng 2017;139:1–8. https://doi.org/10.1115/1.4037231.
[14] Attanasio A, Umbrello D, Cappellini C, Rotella G, M'Saoubi R. Tool wear effects on white and dark layer formation in hard turning of AISI 52100 steel. Wear 2012:98–107. https://doi.org/10.1016/j.wear.2011.07.001. 286–287.
[15] Hosseini SB, Klement U, Yao Y, Ryttberg K. Formation mechanisms of white layers induced by hard turning of AISI 52100 steel. Acta Mater 2015;89. https://doi.org/10.1016/j.actamat.2015.01.075.
[16] Chen T, Qiu C, Liu X, Qian X, Liu G. Study on test method of white layer microhardness in hard cutting based on chord tangent method. Int J Adv Manuf Technol 2017:1–9. https://doi.org/10.1007/s00170-017-0197-1.
[17] Vuorinen E, Ojala N, Heino V, Rau C, Gahm C. Erosive and abrasive wear performance of carbide free bainitic steels - comparison of field and laboratory experiments. Tribol Int 2016;98:108–15. https://doi.org/10.1016/j.triboint.2016.02.015.
[18] Vuorinen E, Heino V, Ojala N, Haiko O, Hedayati A. Erosive-abrasive wear behavior of carbide-free bainitic and boron steels compared in simulated field conditions. Proc IME J J Eng Tribol 2017. https://doi.org/10.1177/1350650117739125.
[19] Valtonen K, Ratia V, Ojala N, Kuokkala V-T. Comparison of laboratory wear test results with the in-service performance of cutting edges of loader buckets. Wear 2017:93–100. https://doi.org/10.1016/j.wear.2017.06.005. 388–389.
[20] Fourmeau M, Gomon D, Vacher R, Hokka M, Kane A, Kuokkala V-T. Application of DIC technique for studies of Kuru granite rock under static and dynamic loading. Proc Mar Sci 2014;3:691–7. https://doi.org/10.1016/j.mspro.2014.06.114.
[21] Ratia V, Heino V, Valtonen K, Vippola M, Kemppainen A, Siitonen P, et al. Effect of abrasive properties on the high-stress three-body abrasion of steels and hard metals. Finnish J Tribol 2014;32:3–18. https://journal.fi/tribologia/issue/view/3255.
[22] Ojala N, Valtonen K, Kivikytö-Reponen P, Vuorinen P, Kuokkala V-T. High speed slurry-pot erosion wear testing with large abrasive particles. Finnish J Tribol 2015;33:36–44. https://journal.fi/tribologia/issue/view/4140.
[23] Peng SG, Song RB, Sun T, Yang FQ, Deng P, Wu CJ. Surface failure behavior of 70Mn martensite steel under abrasive impact wear. Wear 2016;362–363:129–34. https://doi.org/10.1016/j.wear.2016.05.019.
[24] Heino V, Valtonen K, Kivikytö-Reponen P, Siitonen P, Kuokkala VT. Characterization of the effects of embedded quartz layer on wear rates in abrasive wear. Wear 2013;308:174–9. https://doi.org/10.1016/j.wear.2013.06.019.
[25] Yang YY, Fang HS, Huang WG. A study on wear resistance of the white layer. Tribol Int 1996;29:425–8. https://doi.org/10.1016/0301-679X(95)00099-P.
[26] Yang Y-Y, Fang H-S, Zheng Y-K, Yang Z-G, Jiang Z-L. The failure models induced by white layers during impact wear. Wear 1995;185:17–22. https://doi.org/10.1016/0043-1648(94)06586-1.

Publication IV

Kati Valtonen, Vilma Ratia, Karthik Ram Ramakrishnan, Marian Apostol,
Juuso Terva, and Veli-Tapani Kuokkala

Impact wear and mechanical behavior of steels in subzero conditions

Tribology International 129 (2019) pp. 476-493

Tribology International 129 (2019) 476–493

Contents lists available at ScienceDirect

Tribology International

journal homepage: www.elsevier.com/locate/triboint

Impact wear and mechanical behavior of steels at subzero temperatures

Kati Valtonen*, Vilma Ratia[1], Karthik Ram Ramakrishnan, Marian Apostol, Juuso Terva, Veli-Tapani Kuokkala

Tampere University of Technology, Laboratory of Materials Science, Tampere Wear Center, P.O. Box 589, FI-33101, Tampere, Finland

ARTICLE INFO

Keywords:
Impact
Wear
Low temperature
Steel

ABSTRACT

In this study, the deformation behavior of three steels was studied at Arctic temperatures by controlled single and multiple oblique angle impacts. The results were compared with the mechanical properties of the steels determined at the corresponding temperatures. At subzero temperatures, the hardness and strength of the studied steels increased and their ability to deform plastically steadily decreased. In the martensitic steels, adiabatic shear bands were observed to form during the impacts at subzero temperatures, indicating that the deformation ability of the steels was critically impaired. At −60 °C, the adiabatic shear bands commonly acted as initiation sites for subsurface cracks. Moreover, the surface characterization of the test samples revealed formation of cracks and wear particles, which was connected to the opening of grain boundaries and martensite laths at low temperatures. Finite Element Modeling was also used to obtain more information about the impact event.

1. Introduction

When the temperature of the operating environment is lowered, unforeseen behavior of materials may lead to serious problems for example in Arctic mining, where the challenges created by wear and subzero temperatures easily combine and amplify [1]. According to a report describing the behavior of mining tools during winter in Yakutia, Siberia, “steel tools became so brittle that they broke like match sticks” [2].

Ferritic structural steels and martensitic high-strength steels are widely used materials for construction and machinery, but their body-centered cubic microstructure makes them susceptible to ductile-to-brittle transition (DBT) at low temperatures, where an otherwise relatively ductile material begins to behave in a brittle manner. In practice, this means that operating the machinery at a too low temperature may be a cause for an unexpected failure.

The DBT problems are well recognized in the ship building industry, which now has strict policies and standards for material testing, welding, and design to avoid catastrophic failures such as those of the Liberty ships during World War II [3]. With the widening interest of utilizing the resources in the Arctic, combined with the concern on its environmental impact, also the Arctic offshore structures and building materials have been studied and the critical material characteristics and welding requirements have been considered [4–7].

While the design and welding parameters of steel structures are important, the effect of wear on the materials should not be neglected, since it also affects the long-term endurance and stability of the structures, and in a shorter term, the endurance of different types of machinery with a direct effect on the reliability and productivity of the industry. Testing of the low temperature impact properties of steels is typically done using the standardized tests, such as the Charpy pendulum impact tests [8] and the drop-weight tests [9]. For the testing of steels under high strain rates, the Hopkinson Split Bar method with a cooling system has been successfully utilized [10–12]. Some tribological testing related to cryogenic and space applications have been conducted under sliding conditions [13,14]. Recently also some studies of the effects of low outdoor temperatures on the wear behavior of materials in the wheel-rail contacts have been published [15,16]. Moreover, Ratia et al. [17] studied single impacts on a martensitic steel at temperatures down to −60 °C using the High Velocity Particle Impactor (HVPI) method, which enables studying in particular the early stages of impact wear at Arctic conditions [17].

Adiabatic shear bands (ASB) can form in martensitic steels when they are subjected to high velocity impacts or plastic deformation at high strain rates [18–21]. The ASBs are formed by a process where localized plastic deformation leads to an increase of temperature and austenization of the steel followed by rapid cooling and formation of untempered martensite [19,22]. The transformed ASBs are seen as white etching bands in optical micrographs with a very fine microstructure and a higher hardness than the original bulk material [21]. In

* Corresponding author.
E-mail address: kati.valtonen@tut.fi (K. Valtonen).
[1] Current location: Faculty of Engineering, University of Nottingham, University Park, Nottingham NG7 2RD, UK.

https://doi.org/10.1016/j.triboint.2018.08.016
Received 12 April 2018; Received in revised form 27 June 2018; Accepted 14 August 2018
Available online 17 August 2018

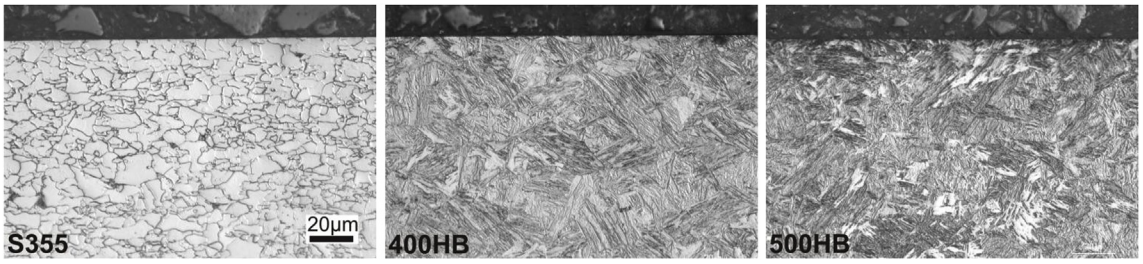

Fig. 1. Initial microstructures of the tested steels.

Table 1
Nominal compositions of the studied steels.

Steel	S355	400HB	500HB
Microstructure	Ferritic-pearlitic	Martensitic	Martensitic
C [wt%] max.	0.12	0.23	0.30
Si [wt%] max.	0.03	0.80	0.80
Mn [wt%] max.	1.5	1.70	1.7
Cr [wt%] max.	–	1.5	1.5
Ni [wt%] max.	–	1.0	1.0
Mo [wt%] max.	–	0.5	0.5
B [wt%] max.	–	0.005	0.005

high stress impacts, the transformed ASBs may also act as initiation sites of cracks [21,23,24]. However, the deformed ASBs, which appear as dark lines when the etched surface is studied with an optical microscope, have not been reported to show cracking [21].

With the improvements in computational capabilities, numerical simulations can now be more efficiently utilized to study also the complex mechanical and thermal interactions encountered in various wear processes [25]. Consequently, modeling is becoming an indispensable tool in the rapid implementation of novel sustainable tribology to practical engineering problems [26]. In addition to providing a cost effective and fast tool for iterating and optimizing the material wear properties, the numerical models enhance the exploitation of the results of experimental wear testing. There are several published articles about the simulation of impacting steel targets, including for example the papers by Arias et al. [27] and Iqbal et al. [28]. However, the focus of these models was on ballistic impacts and penetration and not on the impact wear phenomena at subzero temperatures. Cho et al. [29] simulated the low temperature impacting of steels, but the study concentrated on low velocity impact testing with a drop tower.

In order to understand better the effects of subzero temperatures on the impact wear behavior and microstructural changes of steels due to deformation at relatively high impact energies, two wear resistant steels and a construction steel were tested and characterized. The results were compared with the mechanical properties of the studied steels. Moreover, the response of the steels to impacts was studied using numerical simulations.

2. Materials and methods

2.1. Materials

The materials selected for the tests include two martensitic wear resistant steels, denoted as 400HB and 500HB based on their hardness grades and a ferritic-pearlitic structural steel S355 used as a reference material. Fig. 1 presents the initial microstructures of the tested materials, and Table 1 lists their typical compositions.

2.2. Methods

The High Velocity Particle Impactor is a test device developed for single and multiple impact wear testing at Tampere Wear Center [30]. The HVPI system enables controlled shooting of single 9 mm projectiles to a tilted target material with a temperature ranging from room temperature down to ca. −100 °C. The impact velocity can be as high as 165 m/s, depending on the mass of the projectile that is shot through a smooth bore using pressurized air [31]. The samples are cooled by nitrogen gas flowing through a heat exchanger immersed in liquid nitrogen. Fig. 2 presents a schematic of the HVPI with the cooling system,

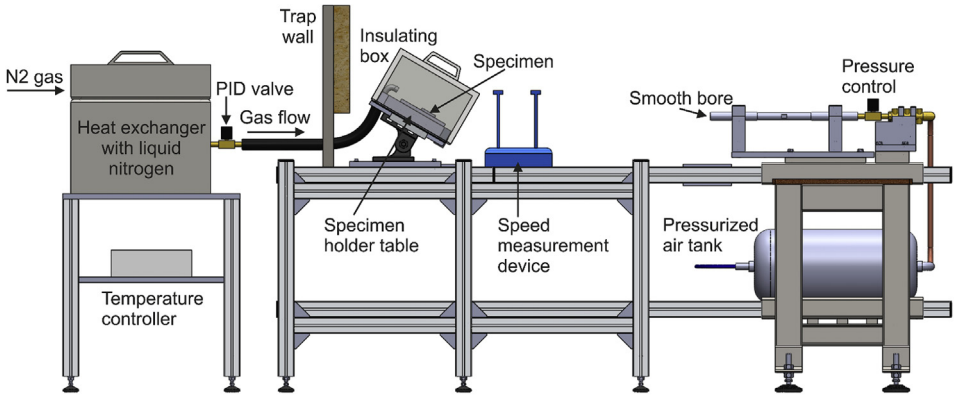

Fig. 2. Schematic of the high velocity particle impactor (HVPI) with a cooling system.

Table 2
Test parameters used in the high velocity particle impactor tests and the mechanical tests.

	HVPI	Charpy	Tensile	Hardness
Test temperatures (*only for 500HB steel)	RT, −20 °C, −60 °C (1 °C, −1 °C)*	40 °C, RT, −20 °C, −40 °C, −60 °C, −70 °C, −80 °C	RT, −20 °C, −40 °C, −60 °C	RT, −60 °C, −100 °C, (-150 °C)*
Test type	Projectile impact test	V-notch	Servohydraulic materials testing machine	Vickers HV10
Impact velocity [m/s]	110–114			
Sample angle [°]	60			
Sample size [mm]	40 × 40 x 4	5 × 10 x 55	5 × 8 x 70 (5 × 8 x 75 at RT)	40 × 40 x 4
Projectile	WC-Co bearing ball			
Projectile diameter [mm]	9			
Projectile weight [g]	5.7			
Nominal energy of projectile/pendulum [J]	35–37	300		

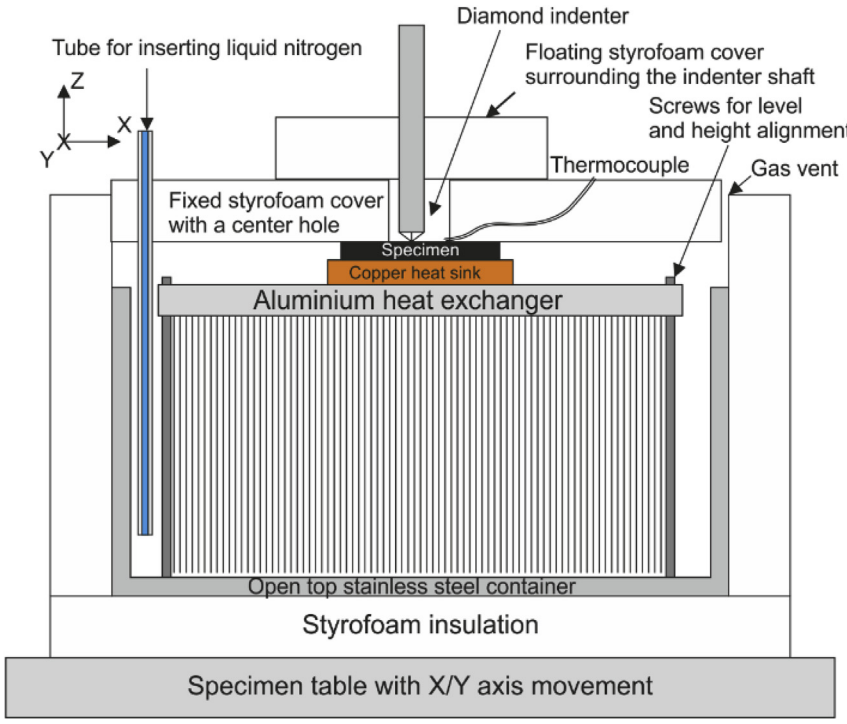

Fig. 3. Schematic of the low temperature hardness testing system.

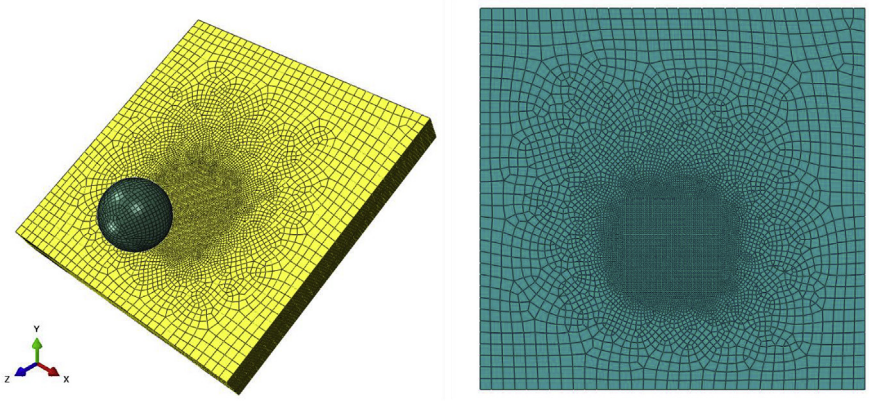

Fig. 4. Finite element model for the simulation of the HVPI steel target.

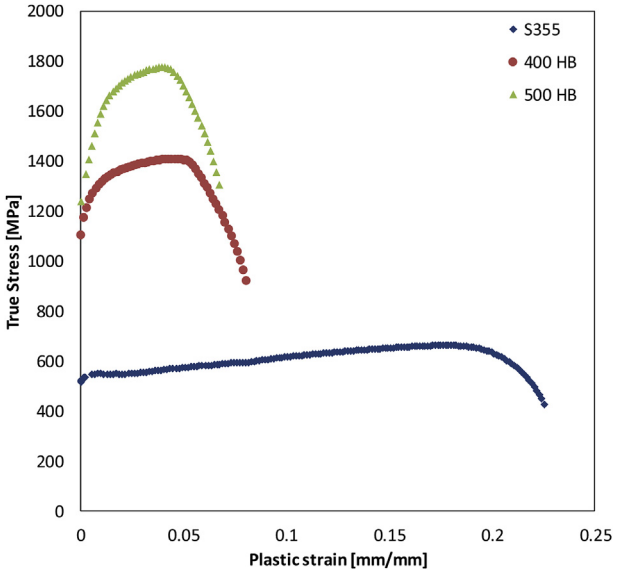

Fig. 5. Post-yield behavior of the 400HB, 500HB and S355 steels at −60 °C used for the FE material models.

which is described in more details by Ratia et al. in Ref. [17]. A similar cooling system has been used earlier for the low temperature Hopkinson Split Bar tests [10]. Before the test, the insulating box is removed and the temperature is let to stabilize for a few minutes to reach the desired test temperature.

In this study, the temperatures of the impacted test materials were room temperature (RT, 22–23 °C), −20 °C, and −60 °C, and the impact velocity of 110–114 m/s and an impact angle of 60° were applied. The selected impact velocity provides the highest possible impact energy, 35–37 J, with WC-Co projectiles [18]. Three separate impacts were made with 9 mm spherical WC-Co (ISO K20 with 6% Co) projectiles under each condition. The projectiles were at room temperature. Before the tests, the surfaces of the 40 × 40 × 4 mm samples were polished with 1 μm diamond paste and two K-type thermocouples were spot-welded on them to measure the temperature of the sample surfaces. The samples were cooled a few degrees below the target temperature and kept there for a few minutes to even out the temperature before the actual test. The ice formed from the condensed air moisture was wiped off with a cotton cloth just before the impact. Table 2 lists the testing parameters of the used test methods.

To study the effect of multiple impacts, the 500HB steel was impacted five times at RT, −20 °C, and −60 °C. The samples were always re-cooled between the impacts. The 500HB steel was tested also at +1 °C and −1 °C to study the effect of the ice layer formation on the impact test outcome. The −1 °C samples were first cooled down to −20 °C and kept there for about 5 min. After that, the cooling was turned off, the insulating box was lifted off, and the sample was let to warm up to the impact temperature. The visibly thick frost layer was not wiped off prior to testing as in the other tests. For the tests at +1 °C, the sample surfaces were wiped dry with a cotton cloth and impacted right after the temperature had raised above the zero temperature. However, water condensation on the cold surfaces was quite rapid, and it was likely that at least a thin film of water was present on the surfaces already at the time of the impact.

The surfaces of the tested samples were characterized using Zeiss UltraPlus field emission scanning electron microscope (SEM), Leica MZ 7.5 zoom stereo microscope, and Alicona G5 InfiniteFocus 3D profiler. Furthermore, the microstructural changes and the deformed layers were studied from the longitudinal cross-sections of the impact marks with Nikon Eclipse MA 100 optical microscope. The cross sections were prepared from the longitudinal middle sections of the impact scars using standard metallographic methods, including etching with 4% Nital.

The mechanical tests, including Charpy V-notch pendulum impact tests and tensile tests at low temperatures, were conducted by the steel manufacturer in controlled temperature chambers cooled with liquid nitrogen. The temperature was measured with a thermocouple attached to the sample. Charpy V-notch pendulum impact tests [8] were made at 40 °C, 20 °C, −20 °C, −40 °C, −60 °C, −70 °C, and −80 °C in the parallel and transverse directions relative to the rolling direction. The sample size was 5 mm × 10 mm x 55 mm. The tensile tests were made at RT, −20 °C, −40 °C, and −60 °C using the sample size of 5 mm × 8 mm x 70 mm produced in the rolling direction. In the room temperature tests, however, the parallel sample length (L_c) was 75 mm.

For the low temperature hardness testing, an insulated heat exchanger was designed and built on a mechanical Zwick Vickers hardness system, as illustrated in Fig. 3. The HV10 indentations were made in the polished sample surfaces in the chamber but the dimensions were measured at room temperature with an optical microscope. The effect of thermal expansion on the measured values was determined to be less than 1 HV at −60 °C. The microhardness testing of the deformed layers was performed as $HV_{0.025}$ (254.2 mN) using Matsuzawa MMT-X7 micro Vickers hardness tester at RT.

2.3. Finite element analysis

The response of steel plates to high velocity particle impacts was

Table 3
Measured mechanical properties of the studied steels at the HVPI test temperatures.

Material (temperature)	Rp0.2 [MPa]	Rm [MPa]	A_5 [%]	Charpy V [J] longitudinal	Charpy V [J] transverse	Hardness [HV_{10}]
S355 (RT)	421 ± 3	492 ± 1	33.5 ± 0.5	94 ± 3	77 ± 2	164 ± 1.5
S355 (−20 °C)	456 ± 3	527 ± 1	35.5 ± 0.4	108 ± 2	80 ± 1	
S355 (−60 °C)	526 ± 2	560 ± 2	36.5 ± 0.2	85 ± 8	58 ± 3	182 ± 1.8
400HB (RT)	1099 ± 17	1247 ± 8	12.9 ± 0.2	53 ± 1	42 ± 0	401 ± 1.5
400HB (−20 °C)	1117 ± 3	1309 ± 11	14.6 ± 0.3	37 ± 9	29 ± 3	
400HB (−60 °C)	1153 ± 11	1328 ± 23	14.4 ± 0.6	13 ± 6	7 ± 4	415 ± 2.8
500HB (RT)	1329 ± 19	1653 ± 15	10.5 ± 0.3	26 ± 2	18 ± 2	506.5 ± 6.5
500HB (−20 °C)	1299 ± 90	1678 ± 3	11.6 ± 0.3	16 ± 2	15 ± 2	
500HB (−60 °C)	1303 ± 39	1700 ± 5	12.2 ± 0.4	11 ± 1	10 ± 1	535 ± 12.1

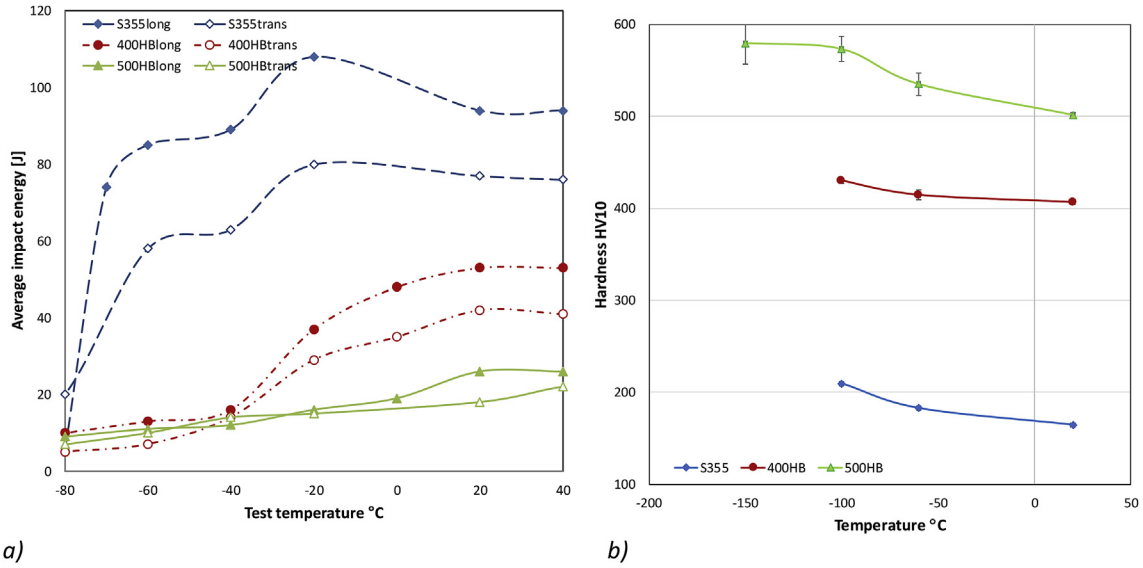

Fig. 6. A) Charpy V impact energy values at different temperatures in the longitudinal (long, sample prepared in the rolling direction) and transverse (trans) directions with a 5 mm × 10 mm x 55 mm sample size, and b) Vickers hardness values of the studied steels as a function of temperature (error bars present the standard deviation).

also examined using Finite Element (FE) analysis with Abaqus/Explicit. The experimental setup, including the target plate and the projectile, was replicated in the FE model. The square plates of 40 mm × 40 mm and 4 mm in thickness were modeled using 8-node linear brick C3D8R elements with reduced integration and hourglass control. The finite element mesh presented in Fig. 4 comprises a densely meshed impact zone and a coarse mesh in the other regions. Fixed boundary conditions were defined to the bottom surface of the target similar to the experiment. The projectile was modeled as a rigid body, and a general contact was defined between the projectile and the target with a coefficient of friction set to 0.3. The impact was modeled for an approach angle of 60° and an initial velocity of 110 m/s similar to the experiment. In order to reduce the runtime of the simulation, the spherical projectile was defined just before it comes to contact with the target plate. In order to choose the most appropriate mesh size, a mesh sensitivity analysis was conducted by varying the number of elements from coarse mesh with 1600 elements to fine mesh with approximately 110000 elements and by comparing the maximum displacements given by the models. Based on this analysis, an element size of 0.2 mm was chosen for the finely meshed impact region and an element size of 1.2 mm for the coarse region.

Numerical models that make use of the known elastic–plastic stress–strain behavior of target materials have been shown to be capable of simulating the abrasive wear of materials with sufficient accuracy [32]. In this work, an isotropic plasticity material model based on the stress-strain data obtained from the uniaxial tensile tests conducted at different temperatures was used to represent the steel targets. The elastic Young's modulus was used to describe the stress-strain relation up to the yield stress, while the post-yield behavior was described with the true stress - true plastic strain data shown in Fig. 5 for the different steels at −60 °C.

3. Results

3.1. Mechanical testing

Table 3 lists the mechanical properties of the test materials, including the yield strength (Rp0.2), ultimate tensile strength (Rm), elongation at fracture (A_5), Charpy impact toughness, and Vickers hardness at the HVPI test temperatures. The ultimate tensile strength (Rm) of all tested materials increased as the temperature decreased. The relative strength increase was the highest for the structural steel S355, which had the lowest strength of the tested materials. At −60 °C its Rm was approximately 25% higher compared to the room temperature value. For the martensitic 400HB and 500HB steels, the increase of strength between room temperature and −60 °C was only 3–5%.

The impact energy values of all test materials determined by Charpy tests [8] are presented also in Fig. 6a. The S355 steel shows a dramatic decrease in the impact toughness between −60 °C and −80 °C, whereas the wear resistant steels, which also at higher temperatures show much lower impact energy values than the structural steel, do not experience such a sudden drop in toughness. The impact toughness values of the 400 H B steel are down to −40 °C clearly higher than those of the 500HB steel. The DBT temperature is between −20 °C and −40 °C. The impact toughness values of the 500HB steel are quite low throughout the entire measurement range. However, it should be noted that the Charpy sample size was only 5 mm × 10 mm x 55 mm, and small sample size generally leads to smaller impact toughness values. There was quite a lot of scatter in the Charpy test results at low temperatures, which especially shows as a winding shape of the S355 impact energy

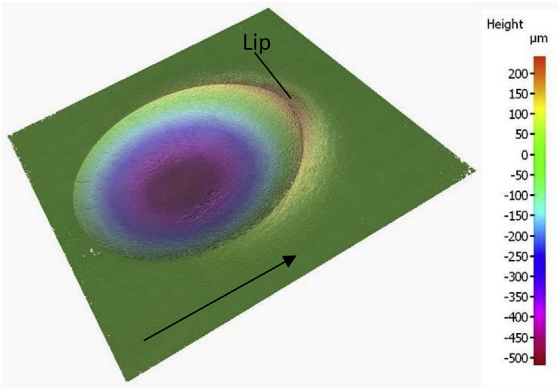

a)

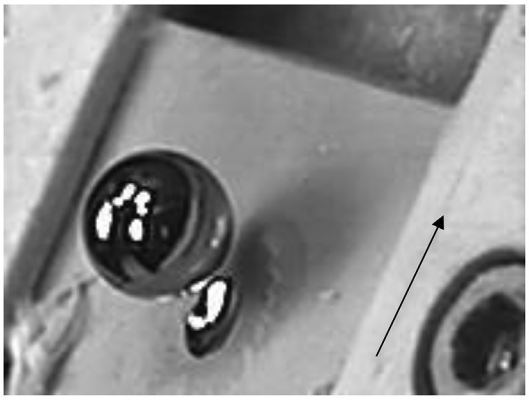

b)

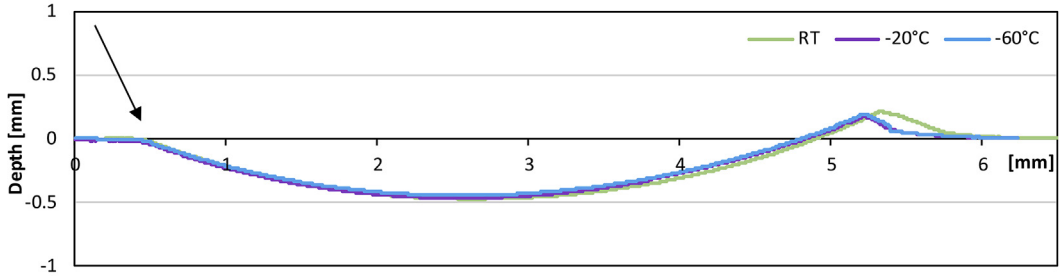

c)

Fig. 7. A) 3D profile of an impact mark in the 400HB steel tested at room temperature, b) snapshot of the impact event at −60 °C, and c) impact crater profiles in the 400HB steel at different test temperatures. The arrows indicate the impact direction.

'curve' between RT and −60 °C.

Fig. 6b shows the low temperature Vickers hardness results for all test materials. Similar to the ultimate strength values, the hardness of all steels increases with decreasing temperature, the increase being over 70 HV10 for the 500HB steel when the temperature decreases from RT to −100 °C.

3.2. Characterization of single impacts

During an impact, the projectile deforms the steel surface markedly. A distinctive lip is formed in the pile-up region, and a sharp ridge appears at the final contact point with the projectile. As an example, Fig. 7a shows the 3D profile of one of the impact marks, and Fig. 7b is a snapshot from a high-speed video recording of the impact event taken immediately after the impact. The amount of plastic deformation decreases with decreasing temperature, which can be seen as a change in

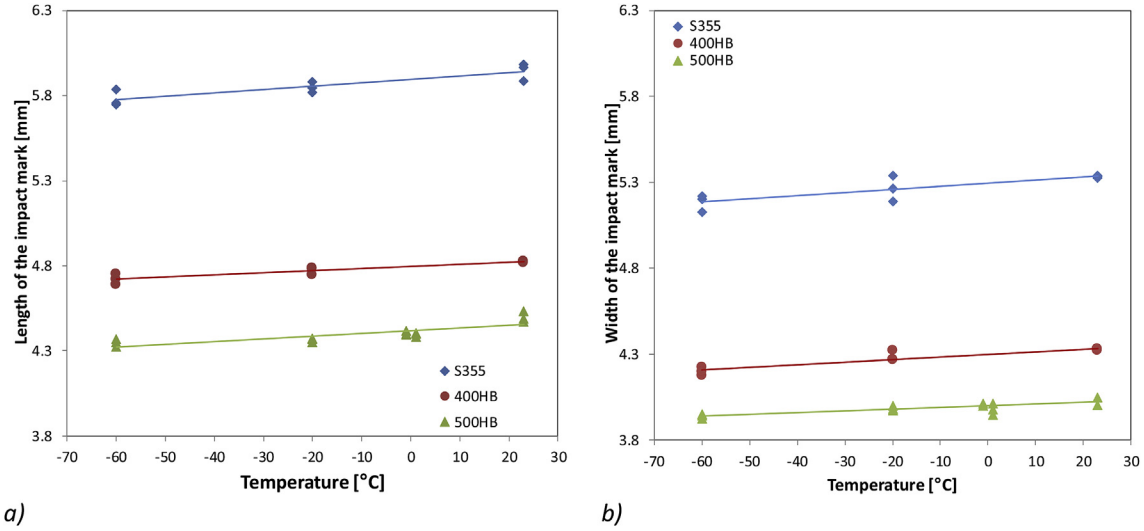

Fig. 8. Measured a) length and b) width of the impact marks of the tested steels at different temperatures.

the form of the lip, as depicted in Fig. 7c.

Supplementary video related to this article can be found at https://doi.org/10.1016/j.triboint.2018.08.016.

The impacts were so severe that they caused the sample sheets to bend slightly. As the determination of the volume loss with a 3D profiler is very sensitive to the flatness of the sample, fracturing of the ridge affected in some cases markedly the obtained volume loss values. Therefore, the dimensional measurements (length and width of the impact mark) with a stereo microscope were found to be a more reliable way of assessing the extent of the surface damage of the samples.

The impact mark length indicates quite well the amount of damage induced in the sample by the impacts of constant impact energy, i.e., by the kinetic energy that the projectile has at the moment of impact. Fig. 8 presents the lengths and widths of the impact marks at the impact test temperatures. There is a distinct but expected difference between the materials, and both dimensions are more or less linearly decreasing with decreasing temperature.

The samples tested at +1 °C and −1 °C were also profiled with the Alicona 3D profiling software to see if there are any differences in the mechanisms of material removal from the surface due to the presence of the frost layer. In addition to profiling, the measurements of the length, width and depth of the impact marks were conducted to assess the amount of material ploughed to the sides of the craters. The measurements showed that all the impact mark dimensions were slightly larger at −1 °C, but the difference was smaller than the scatter and thus not statistically significant.

3.2.1. Surface study

In order to better understand the behavior of the studied steels under subzero conditions, the impact marks were characterized by SEM. The martensitic steels 400HB and 500HB behaved quite similarly. Fig. 9 clearly shows that there are significant differences in the surface features found for example in the 400 HB steel samples impacted at different temperatures. The presented in-lens secondary electron images were taken either about 300 μm from the tip of the impact mark along the centerline of the crater (Fig. 9a, c, and e), or from the center of the impact marks (Fig. 9b, d, and f). In the sample impacted at room temperature, definite marks of abrasion and adhesion can be observed. Even a few tungsten carbide (WC) particles from the projectile, seen as white spots in the image, were attached to the steel surface. At lower temperatures, the grain boundaries and martensite laths of the martensitic steel start to open up, as seen in the center of the impact marks. All these features became clearer with decreasing test temperature. Closer to the exit point of the projectile, i.e., at the tip of the impact mark, also crack formation could be observed at −20 °C and −60 °C. The cracks were circularly distributed to the whole width of the tip. Up to 50 μm long cracks could be identified in the samples (not shown in Fig. 9). At −60 °C, the cracking also initiated the formation of wear particles in the martensitic steels, as seen in Fig. 9e, where micrometer sized particles have been detached from the surface.

The surface microstructures of selected impact marks were etched using Nital to study the position of the cracks and the deformation of surface layer. Although the surface layers were highly deformed, the original microstructural features were still visible in the SEM images seen in Figs. 10 and 11. Fig. 10 shows an example of the opening microstructural features in the 500HB steel and Fig. 11 in the S355 steel after etching of the surface impacted at −60 °C. The etching revealed better the opened lath structures in the martensitic steels and the opened grain boundaries in the ferritic-pearlitic steel. At the center of the impact marks, the microstructure of the steels was visible also in the SEM images (Figs. 9 and 10).

The S355 steel with a ferritic-pearlitic microstructure behaved in the impacts quite similarly to the martensitic steels, but the microstructure was visible already from the polished surface with SEM. However, at the bottom of the impact mark, the differences in the appearance between the ferritic and pearlitic areas were evident as seen in

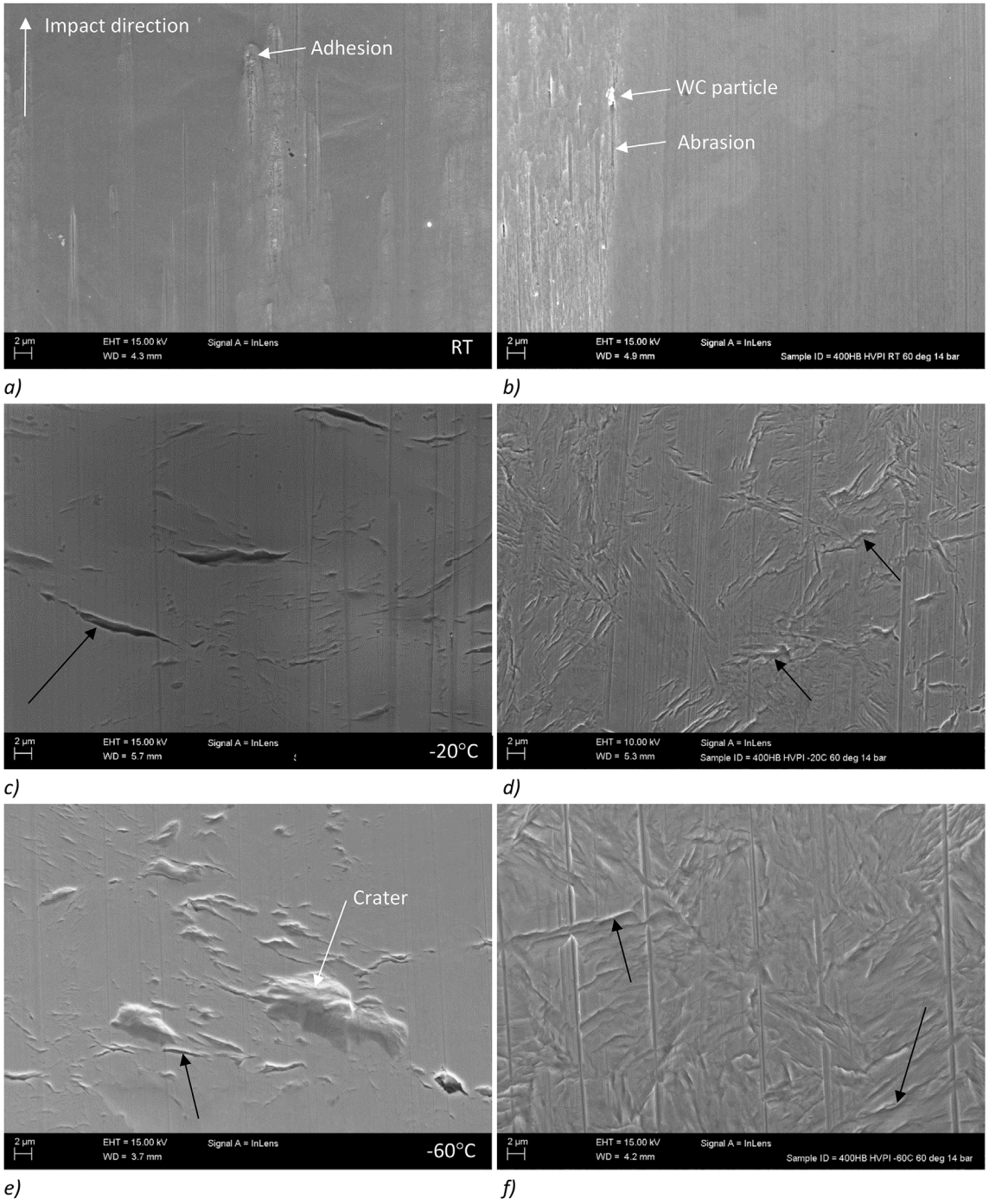

Fig. 9. SEM images from the impact surface of the 400HB steel tested at a-b) RT, c-d) −20 °C, and e-f) −60 °C. Images a, c, and e are taken close to the top of the impact mark, and images b, d, and f from the center of the impact mark. The black arrows indicate opening of the microstructural features. The impact direction is the same in all images.

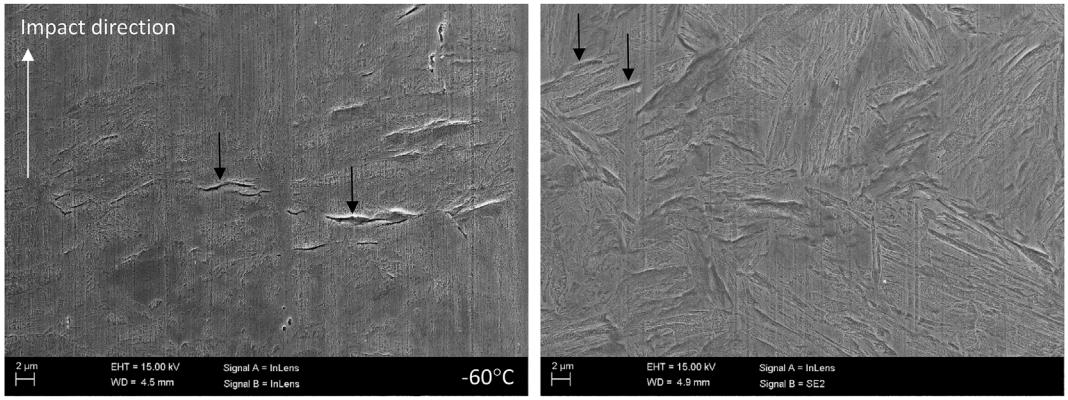

a) b)

Fig. 10. SEM images from the 500HB steel tested at −60 °C and etched with Nital a) close to the tip of the impact mark and b) at center of the impact mark. The arrows indicate some of the opened microstructural features. The impact direction is the same in Figs. 10–12.

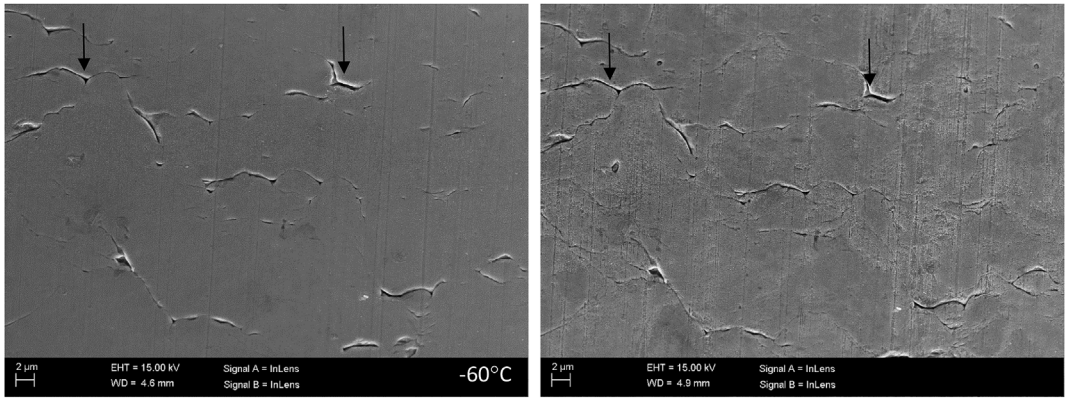

a) b)

Fig. 11. SEM images from the S355 steel tested at −60 °C showing wear close to the tip of the impact mark a) unetched and b) etched from the same area. The arrows indicate some of the opened grain boundaries.

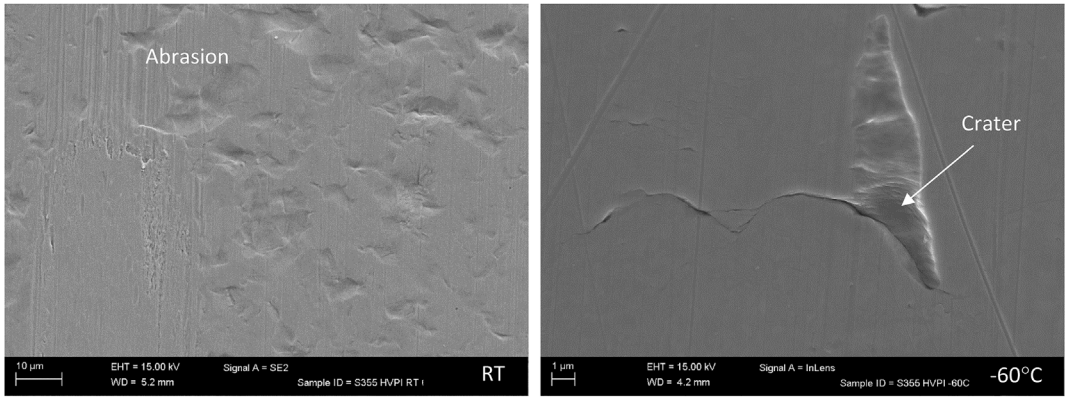

a) b)

Fig. 12. SEM images from the S355 steel showing a) the microstructure at the center of the impact mark at RT, and b) wear close to the tip of the impact mark at −60 °C.

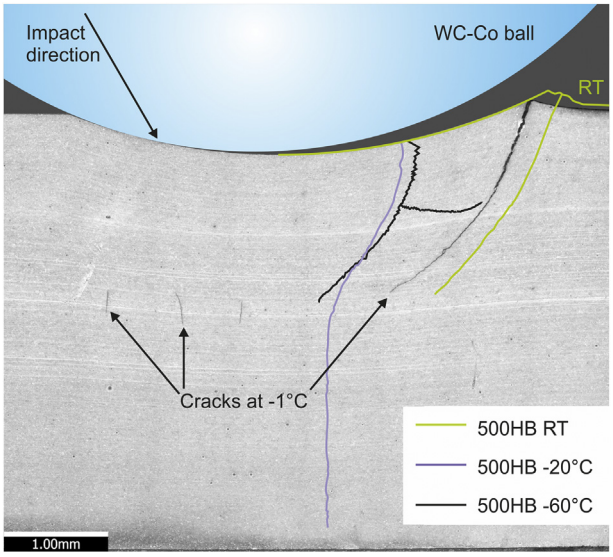

Fig. 13. Optical micrograph showing the cross section of an impact mark in the 500HB steel tested at −1 °C, and the formation of cracks in the 500 H B steel at various temperatures.

Fig. 12a. Moreover, clear adhesion marks and scratches were observed on the impact mark surfaces at room temperature, and cracking-induced wear started to happen already at −20 °C, with wear particles up to 20 µm in size being detached from the surface. Fig. 12b illustrates a typical wear damage in a S355 sample tested at −60 °C.

There was no visible difference between the impact mark surfaces of the 500HB samples tested at +1 °C and −1 °C. This means that the ice formed on the sample surface did not have a significant effect on the impact response of the sample. The opening of the martensite laths was visible at both temperatures in the center areas of the impact marks.

3.2.2. Cross section study

The cross sections revealed that only the 500HB samples had experienced extensive cracking during the impacts. Both subsurface cracks as well as cracks extending to the surface were observed over the entire studied temperature range. Fig. 13, which combines single cross-section images from samples tested at four temperatures, shows that in the 500HB samples tested at lower temperatures the cracks were positioned inside the impact mark area rather than at the top of the pile-up ridge, as in the samples impacted at RT and around 0 °C. In the samples tested at 1 °C and −1 °C, short transgranular cracks had also

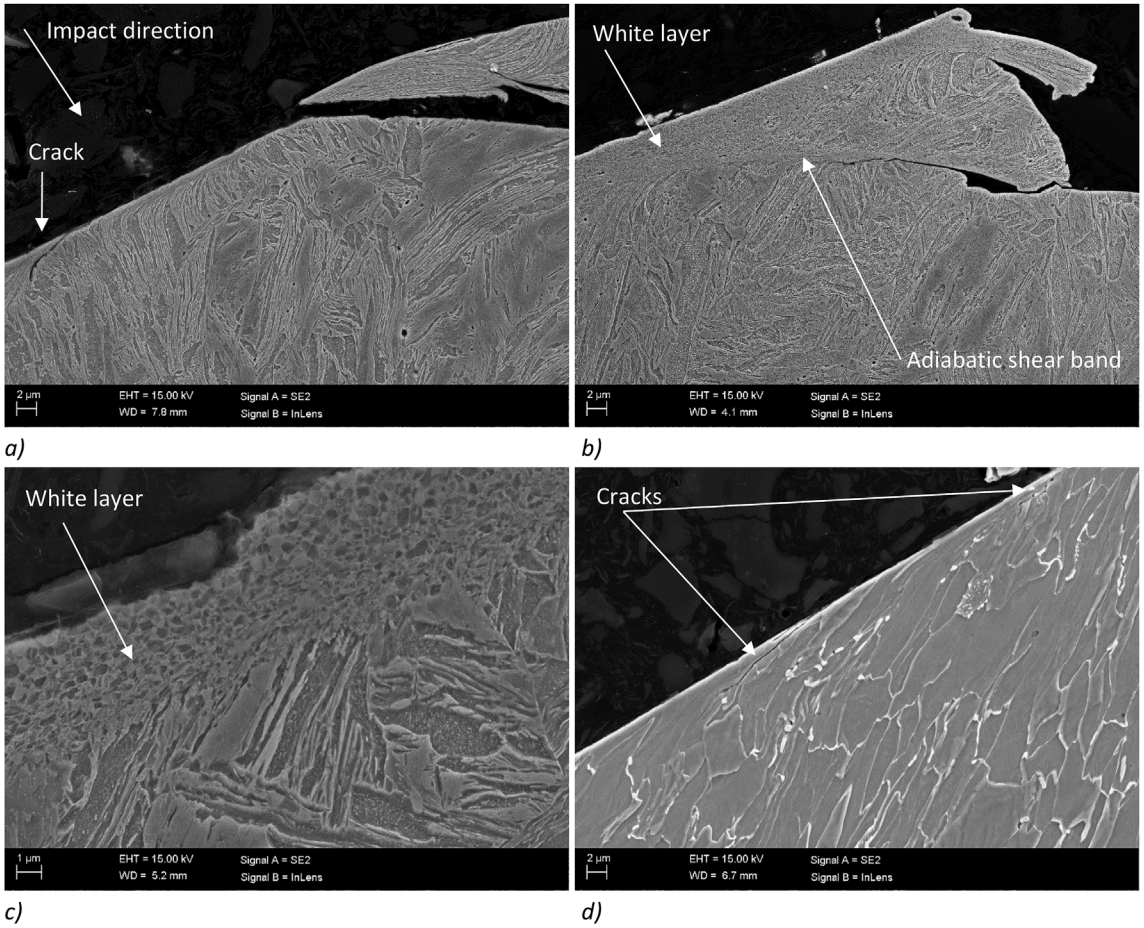

Fig. 14. SEM images of the cross sections of the impact mark ridges of a) 400HB and b, c) 500HB steels tested at −60 °C and d) S355 steel tested at −20 °C. The impact direction is the same in all images.

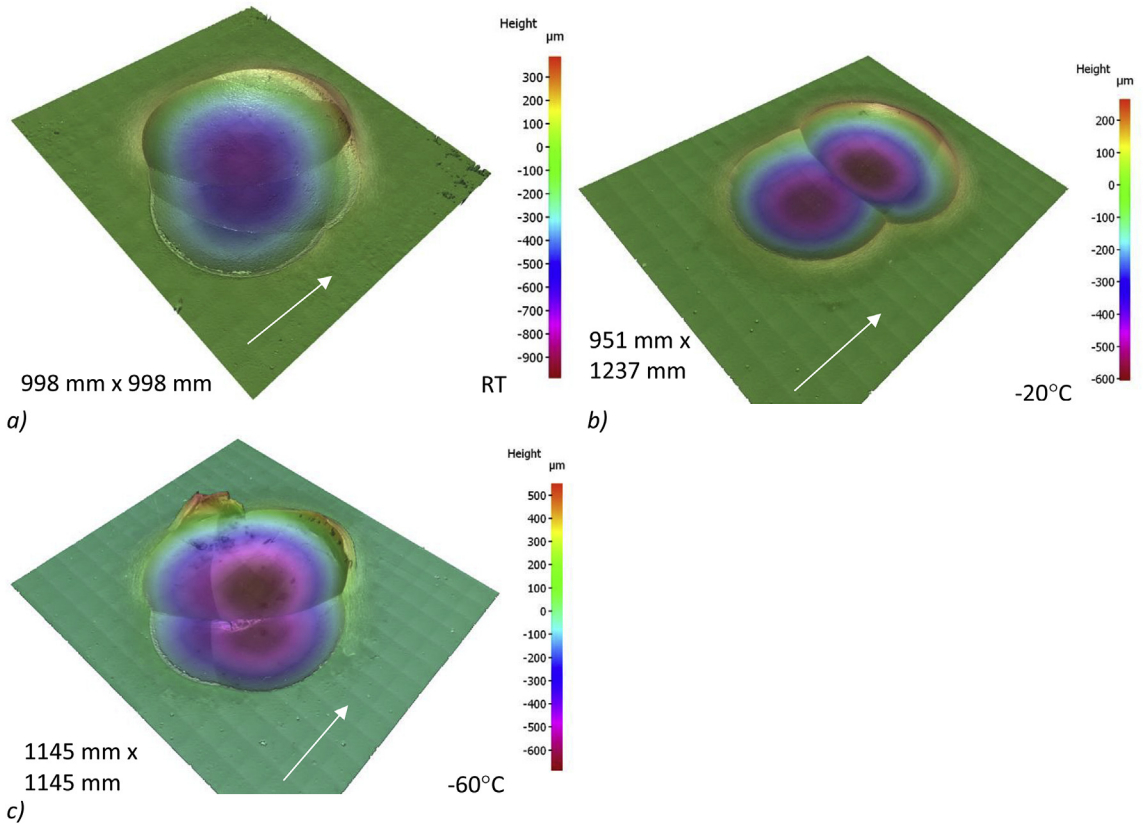

Fig. 15. 3D profiles of five partially overlapping impact marks in the 500HB steel tested at a) room temperature, b) −20 °C, and c) −60 °C. The arrows indicate the impact direction.

formed in the centerline of the impact zone. Moreover, the deformation of the steel was visible down to 3 mm below the surface as seen in Fig. 13.

Fig. 14a and b illustrate the deformation and cracking in the ridge tip areas in the 400HB and 500 H B samples tested at −60 °C. In the 400HB steel, the cracks were formed in the so-called white layer or a thin shear band layer in the surface region of about 100 µm from the tip of the ridge. In the 500HB steel, the slightly cracked white layer extended down to 300 µm from the top of the impact mark, i.e., further than seen in Fig. 14b. Fig. 14c shows the very fine microstructure of the white layer formed in the 500HB steel. The thickness of the white layer was about 6 µm. Moreover, an adiabatic shear band was formed in the shear localization area at the tip of the ridge, and the sample was fractured along it.

In the 400HB samples tested under subzero conditions, also small intergranular cracks were formed in the pile-up region, the shape and size of which was changing with temperature, as was seen already in Fig. 9 c and e. In the samples impacted at room temperature, the lip extended wider and with a smoother shape in comparison to the lips formed at lower temperatures. The same change was seen also in the 500 H B steel samples.

In the cross-sections of the S355 samples, small single subsurface cracks parallel to the impact mark surfaces with a length of approximately 100 µm were detected in the samples tested below 0 °C. Moreover, there were smaller cracks close to the tip of the impact mark (Fig. 14d). The impact marks were so deep that small bulges were visible also on the rear side of the 4 mm steel plates.

3.3. Characterization of multiple impacts

Some of the 500HB steel samples were impacted multiple times in order to see the effect of repeated impacting on the deformation of the surfaces. Even though the HVPI device is quite precise, the individual impact marks did not fully coincide, as seen in Fig. 15. Nevertheless, the differences between the samples tested at different temperatures were found to increase markedly, as seen in Fig. 16, which presents some typical features of the overlapping impact marks. At room temperature, the forming craters were only plastically deformed and no cracking was observed. Moreover, the multiple impacted surfaces contained signs of abrasion similar to the single impact marks. At −20 °C, some cracks were already formed, but at −60 °C the crack formation was severe and the steel surface started to fracture in a brittle manner. The largest fracture on the edge of the impact area was almost 2 mm long, as seen in Fig. 16d.

Although cracking on the surfaces was barely visible, especially on samples tested at room temperature, the cross-sections of the samples

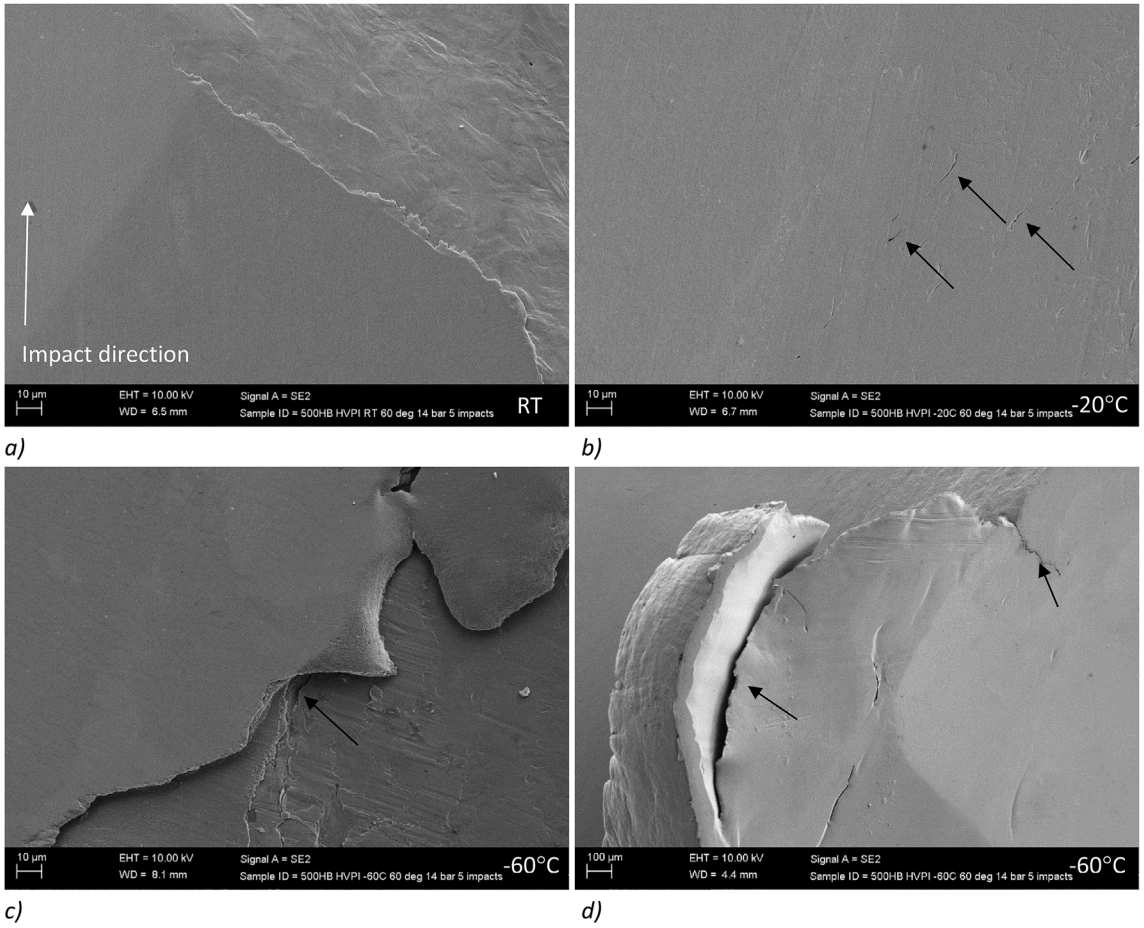

Fig. 16. SEM images of the 500HB steel samples showing some typical features of overlapping impact marks from tests conducted at a) RT, b) −20 °C, and c, d) −60 °C. The black arrows indicate examples of cracking sites. The impact direction is the same in all images.

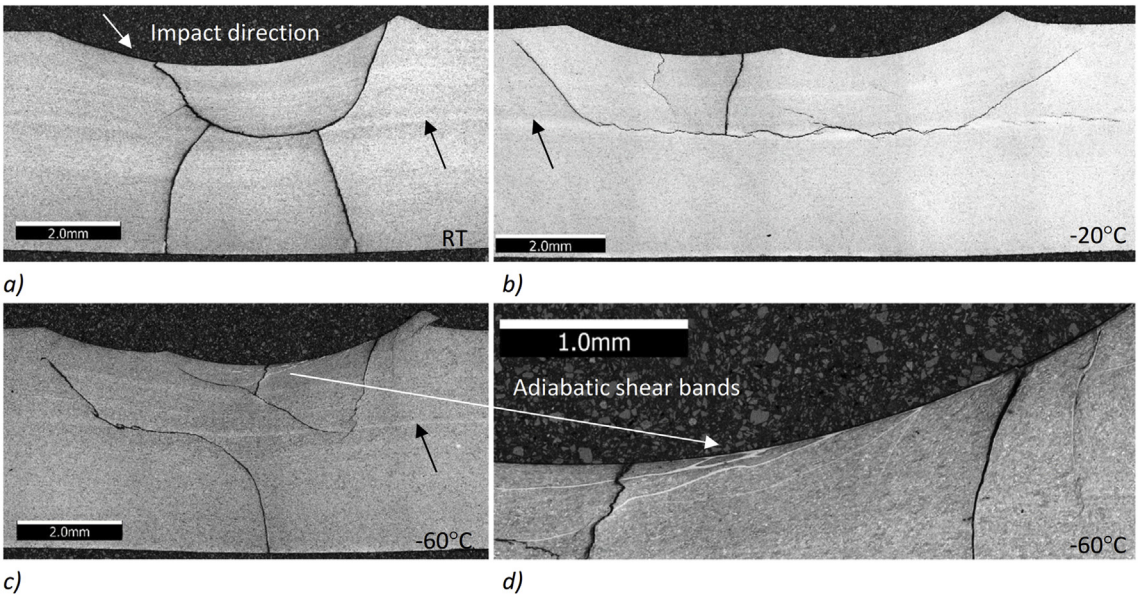

Fig. 17. Optical micrographs of the cross-sections of five partially overlapping impact marks in the 500HB steel tested at a) room temperature, b) −20 °C, and c) −60 °C with d) adiabatic shear bands indicated by the white arrow. The black arrows indicate the centerline segregation. The impact direction is the same in all images.

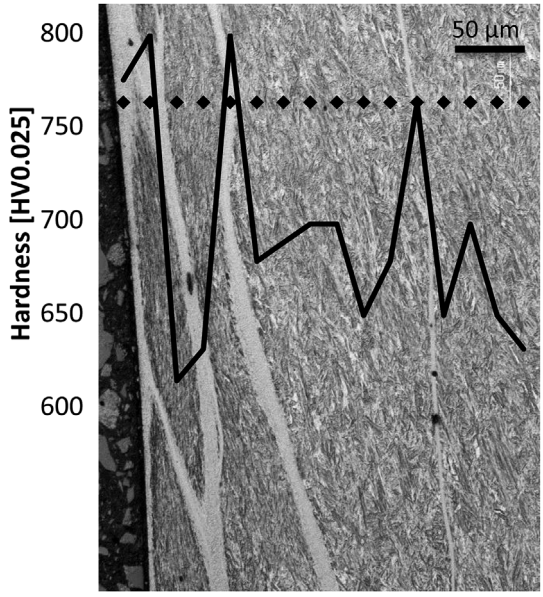

Fig. 18. Optical micrograph of the adiabatic shear bands formed in the 500HB steel at −60 °C. The hardness profile was measured from the diamond marker locations.

revealed severe cracking in all samples, as disclosed by Fig. 17. The largest cracks followed the centerline segregation, which is seen as a lighter line in the etched cross-section of the steel plate. In the centerline the steel hardness was quite high, 688 ± 13 $HV_{0.1}$, while the average hardness of the plate was 506.5 ± 6.5 HV_{10}.

Only at the testing temperature of −60 °C, a significant number of adiabatic shear bands (ASB) were formed. Fig. 18 presents a typical example of the adiabatic shear bands with a hardness profile, the mean hardness of the thick adiabatic shear bands being 787 ± 14 $HV_{0.025}$. At −60 °C, the thickness of a single ASB was typically under 15 µm. At −20 °C, just a couple of thin, less than 5 µm thick ASBs were observed.

3.4. Results of the FE simulation of HVPI

Fig. 19 shows the typical sequence of events when a spherical projectile hits a steel plate, as simulated by the Abaqus/Explicit Finite Element software. In the beginning of the contact, the projectile deforms the target plastically at the point of impact and starts to create a crater on the surface by displacing the material in front of it (b-d). When the projectile starts to bounce back (e-f), it leaves behind a lip of material at the exit point. A close-up of the impact crater at the end of the simulation is shown in Fig. 19g.

One of the advantages of the numerical modeling is that it can provide us with a good estimate of the force(s) acting on the steel surface during the impact, which is quite difficult to experimentally measure (although such experiments with the HVPI device have in fact already been done [18]). Fig. 20 shows the simulated time history of the contact force during an impact of a WC-Co projectile on a 500HB steel target at the speed of 110 m/s at −60 °C. It can be seen that the contact duration of the impact is about 37 µs, and the peak force is 32.5 kN. The evolution of the impact crater during the impact is illustrated in Fig. 21.

The Abaqus model was validated by comparing the simulated profiles of the impact craters taken along their centerline both in the longitudinal and transverse directions with the 3D profilometer results. As Fig. 22 illustrates, the FE simulation is able to reproduce quite well the plastic deformation related to the ploughing process during the impact. The maximum depth of the craters were especially well predicted by the simulations for all studied steels at all studied temperatures. The lengths and widths of the craters were also closely similar in the experiments and simulations. However, the height of the lip at the end of the crater was always over-estimated in the simulations. One reason for this discrepancy evidently is that in the real experiments some material is always lost through chip formation, as seen for example in Fig. 14, while there is no element deletion or damage included in the model to take account of such events. However, the observed discrepancy appears to be too large to be explained only by missing chip formation in the model. Another possible reason could be the missing ASB formation in the model, affecting the hardening behavior and size of the forming lip.

4. Discussion

Detailed knowledge of the behavior of steels at subzero temperatures enhances the material selection especially for the Arctic environments. In general, the properties known to improve the wear resistance, such as hardness and strength, should be as high as possible while retaining sufficient ductility to minimize the risk of a catastrophic (brittle) failure. In the current tests, the dimensions of the impact marks decreased with the increasing ultimate tensile strength and decreasing temperature. Fig. 23 illustrates the quite linear correlation between the measured impact mark dimensions and the strength of the steels at the applied test temperatures.

The increased strength with decreasing temperature was found to induce the formation of adiabatic shear bands in the martensitic steel samples impacted at −60 °C. The nanostructured ASB layers prove that the steel had been deformed above the critical strain rate of the steel [33]. The formation of the adiabatic shear bands also seems to facilitate the crack formation especially in the case of multiple impacts, as seen in Fig. 24 and also reported in many earlier studies [21,23,24,34]. According to Kim et al. [34], in the Charpy impact tests the ASBs follow the maximum shear stress planes, and the results of the current multiple impact tests indicate the same. Moreover, Kim et al. [34] noted that tempering of the steel at 600 °C producing martensitic structure with high carbide volume prevented the formation of ASBs in dynamically compressed samples. Thus, it is possible to develop steels that are less prone to form ASB's. Fig. 24a shows that in addition to the cracked subsurface ASBs, a thin white layer was formed on the impact surface of the samples tested at −60 °C. Fig. 24b also reveals the nanostructure of the ASB layer. Lindroos et al. [18] reported cracking of the ASB layers in martensitic steels already during single impacts, but the multiple impacts used in this work probably further enhanced the effect. Similar cracked ASBs are formed also in the actual impact wear conditions, as recently reported by Abbasi et al. [23] for the steel scrap shear blades,

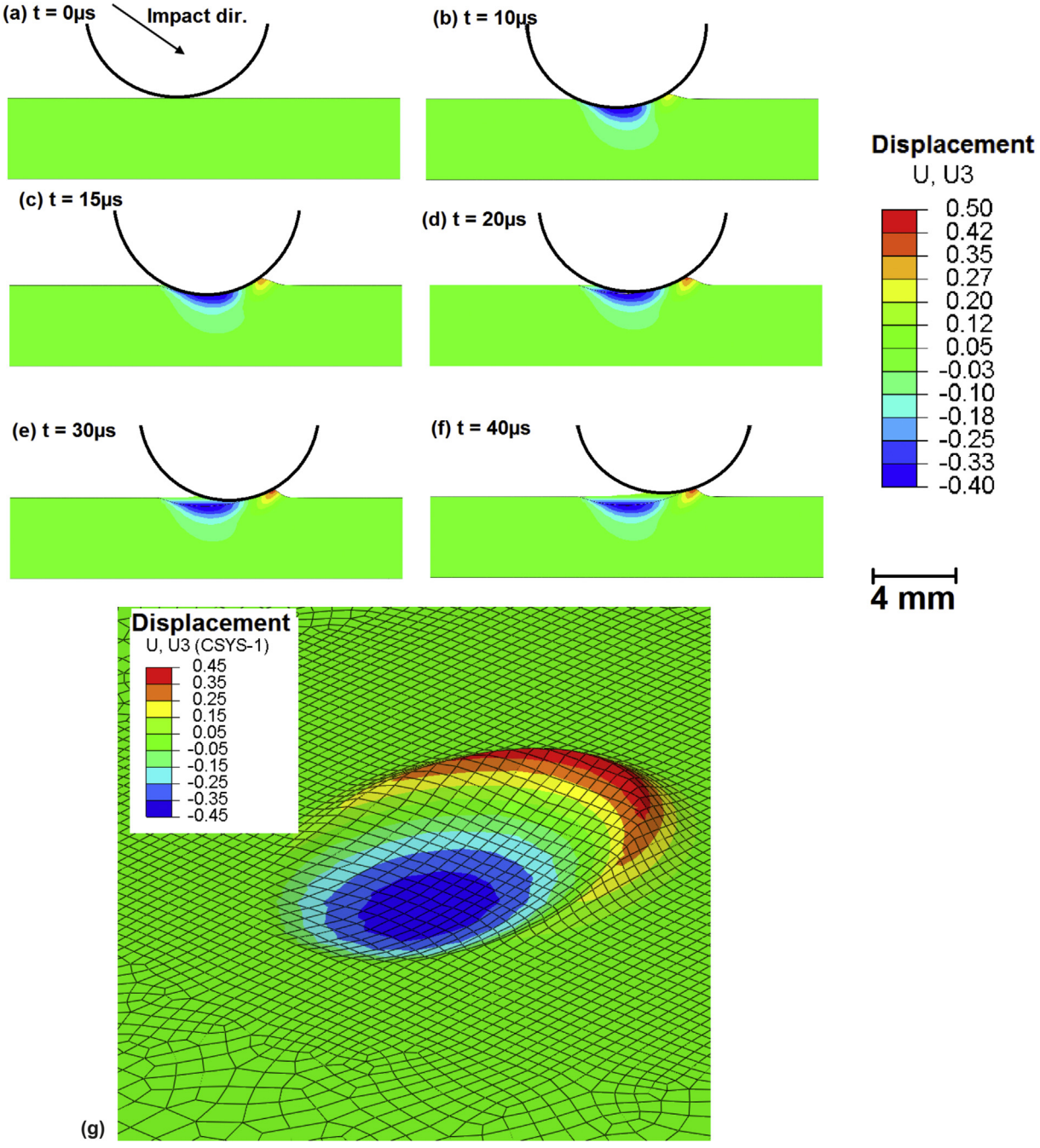

Fig. 19. Typical simulated sequence of events during a high-speed impact of a ball with a tilted steel plate sample.

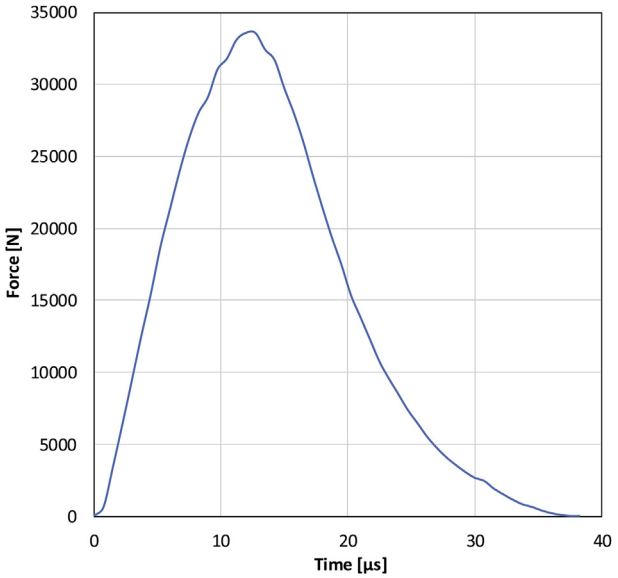

Fig. 20. Force-time history of the impact on a 500HB steel target at the speed of 110 m/s at −60 °C.

where ASBs were formed both on the wear surface as well as in the subsurface similar to the multiple impact tests of this work. Although the surface study showed cracking only at −60 °C, all multiple impacted samples were severely cracked, as observed in the cross-sectional studies. However, as the impacts had visibly bent the steel plates, it is also possible that the cracking had partly occurred only during cutting of the microscopy specimens, when the residual stresses formed during impacting had been released.

However, not all the cracks were initiated by the adiabatic shear bands, and especially in the 500HB steel, also 'ordinary' subsurface cracking occurred at all testing temperatures both in single and multiple impact tests. Similar behavior could also be observed in the FE simulated impacts, even though the model does not take account of the adiabatic effects or particular features of the microstructure. Fig. 25 shows that the cross-section of the simulated target contains a high concentration of shear strains in the same region where the cracks were observed in the physical experiments (Fig. 13). It is recommended that the temperature effects due deformation heating, including the formation of ASBs, would be included in the further modeling schemes of the HVPI tests. The addition of appropriate failure criteria would also increase the accuracy of the simulations markedly. Therefore, FE analysis with modified Johnson Cook model that includes temperature and strain rate dependency, as well as toughness of the material measured from Charpy tests to capture the energy absorption behavior, is proposed for future study.

In the RT tests, the impact marks showed clear indications of both adhesion and abrasion (Fig. 9 a and b). Although the impact angle was steep, 60°, the WC-Co ball ploughed the steel surfaces and even some WC particles were embedded to the steel. However, when the test temperature was decreased, the contact surfaces showed mainly marks of abrasion in the form of linear scratches and the amount of adhesion marks diminished (Fig. 9 c–f). In the tests close to 0 °C, the thick ice layer formed on the sample surface due to ambient humidity seemed to have essentially no effect on the dimensions of the impact marks. This could be explained by the melting of the ice layer formed on the sample immediately when the impactor hits the steel surface [15].

At subzero temperatures, the small surface cracks in the top part of the impact marks led to material removal from the surface of all tested steels. This cracking was not caused by adiabatic shear bands, because the white layers were formed only at the very tips of the ridges, and these cracks were found a bit further away from those areas. In the center of the impact marks, the microstructure of the martensitic steels was clearly visible at subzero temperatures. Apparently, polishing of the samples before testing already revealed the microstructure of the steels, i.e. slightly highlighted the harder phases. Then the deformation due to the impact further opened the structure between the laths, the lath packets, and the grain boundaries. These features have multiple orientations in the martensitic structure [31,35], and under deformation at subzero temperatures, they start to lose their structural integrity. Thus, the presented images appear to reveal the first steps towards a more detrimental failure during impact loading. In the further studies, it would be interesting to study the evolution of the failure by characterization of the impacts marks after every impact in the multiple impact tests.

5. Conclusions

The effects of subzero temperatures on the response of three steels to single and multiple oblique angle impacts were studied. From the

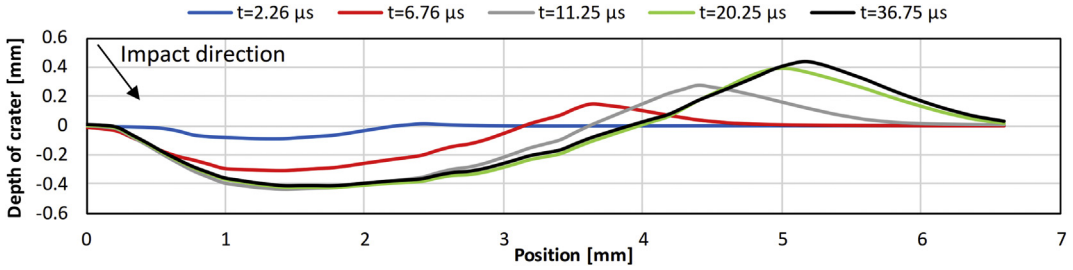

Fig. 21. Evolution of the impact crater during an impact on the 500HB steel at −60 °C.

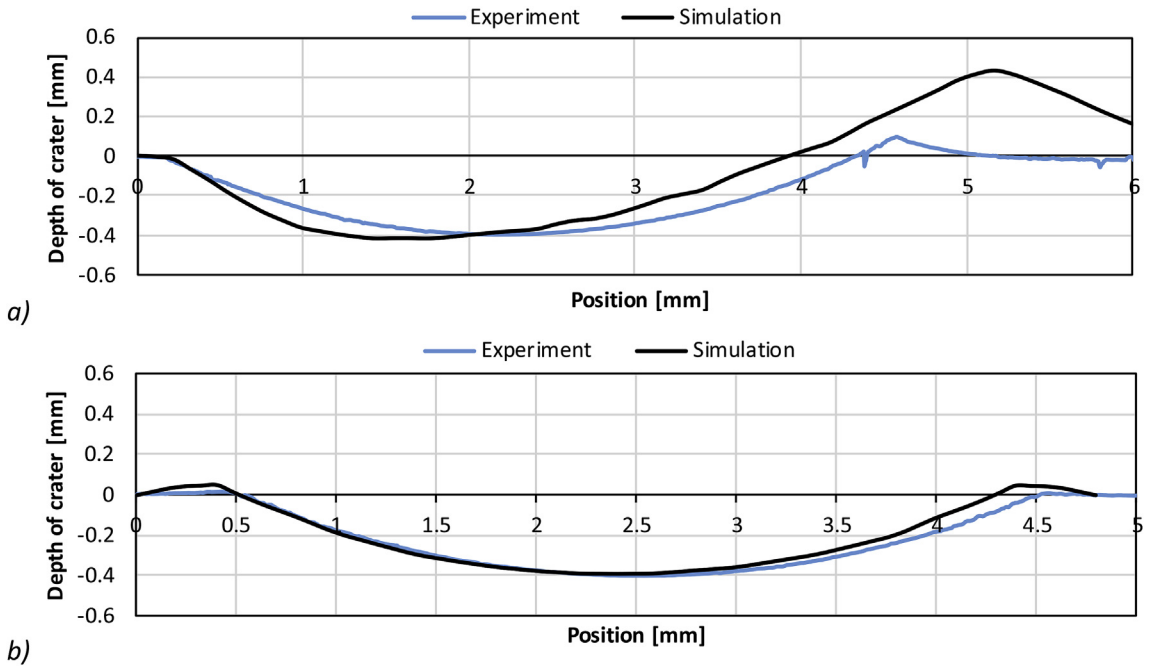

Fig. 22. Comparison of the experimental and simulated crater profiles in a) longitudinal and b) transverse directions for a 500HB steel impact tested at −60 °C.

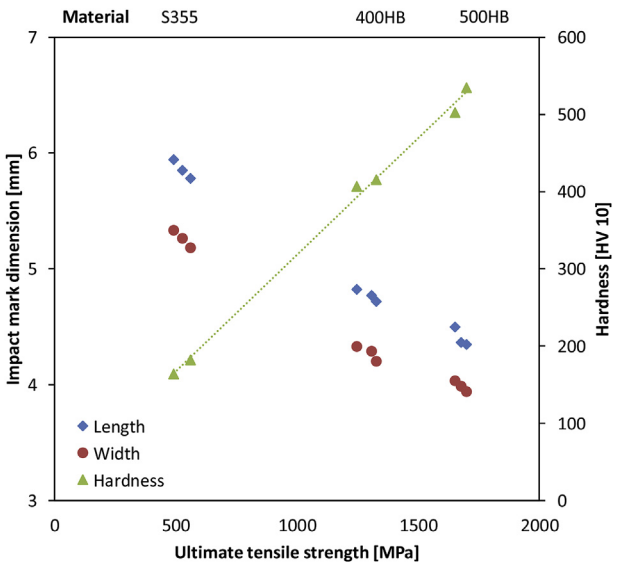

Fig. 23. Measured length and width of the impact marks and hardness vs. ultimate tensile strength of the tested steels at the applied test temperatures.

results, the following conclusions could be drawn:

- At temperatures from RT down to −60 °C, the degree of deformation of the studied steels in single impacts correlate well with the ultimate tensile strength of the steels.
- In martensitic steels, decreasing temperatures promote the formation of adiabatic shear bands.
- During multiple impacts at −60 °C, ample formation of subsurface adiabatic shear bands facilitates the initiation of cracking.
- In single impact tests at subzero temperatures, cracking along various microstructural features, such as grain boundaries and martensite laths, leads to material removal in all tested steels near the tip of the impact mark. Moreover, plastic deformation initiates the opening of the martensite laths at the bottom of the impact marks.
- The high velocity particle impactor with liquid nitrogen cooling was proven an excellent test system for controlled oblique angle impact wear tests at low temperatures, complementing the data collected by other mechanical testing systems.
- A Finite Element model with a simple elastic-plastic material law was capable of reproducing the plastic deformation and crater formation observed in the steel targets during high-speed impacts.

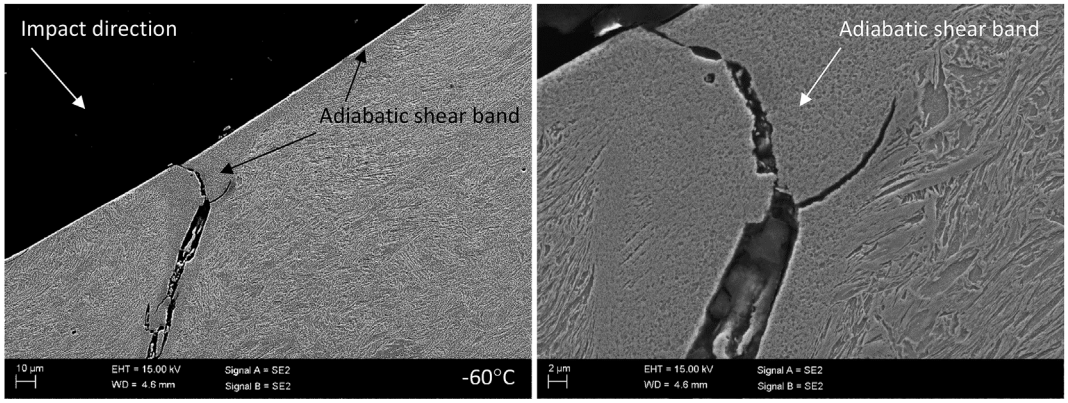

Fig. 24. SEM images of the cross-sections of five partially overlapping impact marks in the 500HB steel tested at −60 °C, showing cracks following the path of adiabatic shear bands (b enlarged from a).

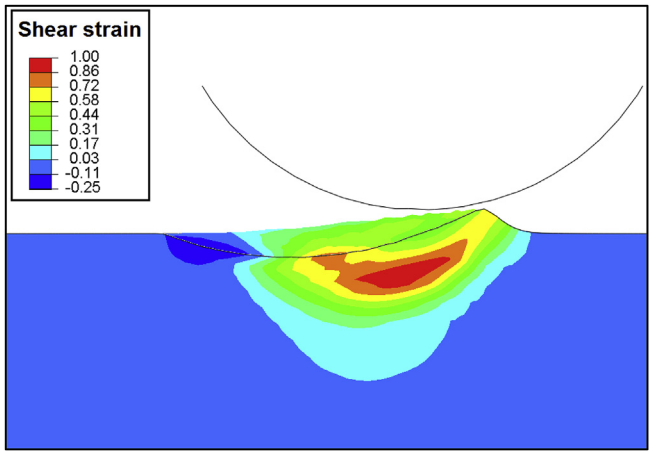

Fig. 25. Cross-sectional view of shear strain distribution in the 500HB steel target after an impact at 110 m/s at −60 °C, revealing high subsurface stresses. The thin black line indicates the bottom of the impact mark at the plane of the cross-section.

Acknowledgements

This work was done within the DIMECC BSA (Breakthrough Steels and Applications) Programme. We gratefully acknowledge the financial support from the Finnish Funding Agency for Innovation (Tekes) and the participating companies.

Appendix A. Supplementary data

Supplementary data related to this article can be found at https://doi.org/10.1016/j.bbrc.2016.12.032.

References

[1] Zlotnikov D. Mining in the extreme. Cim Mag 2012:50–6http://issuu.com/cim-icm_publications/docs/aug12_finald_lr.
[2] Epstein EJ. The rise and fall of diamonds. Smashwords; 2011.
[3] Harris MD, Grogg WJ, Akoma A, Hayes BJ, Reidy RF, Imhoff EF, et al. Revisiting (some of) the lasting impacts of the liberty ships via a metallurgical analysis of rivets from the SS "John W. Brown,". JOM (J Occup Med) 2015;67:2965–75. https://doi.org/10.1007/s11837-015-1668-1.
[4] Layus P, Kah P, Ryabov V, Martikainen J. Evaluation of applicability of thick E500 TMCP and F500W QT steel plates for Arctic service. Int J Mech Mater Eng 2016;11:4. https://doi.org/10.1186/s40712-016-0057-z.
[5] Yan J-B, Xie J. Experimental studies on mechanical properties of steel reinforcements under cryogenic temperatures. Construct Build Mater 2017;151:661–72. https://doi.org/10.1016/j.conbuildmat.2017.06.123.
[6] Yan JB, Liew JYR, Zhang MH, Wang JY. Mechanical properties of normal strength mild steel and high strength steel S690 in low temperature relevant to Arctic environment. Mater Des 2014;61:150–9. https://doi.org/10.1016/j.matdes.2014.04.057.
[7] Layus P, Kah P, Martikainen J, Pirinen M, Khlushova E, Ilyin A. European and Russian metals for arctic offshore structures. Proc Twenty-Third Int Offshore Polar Eng 2013;9:242–9.
[8] SFS-EN ISO 148-1. Metallic materials. Charpy pendulum impact test. Part 1 : test method, 2009, 30. 2009.
[9] ASTM. E208 - 17e1 Standard Test Method for Conducting Drop-Weight Test to Determine Nil-Ductility Transition Temperature of Ferritic Steels. 2017. p. 14. https://doi.org/10.1520/E0208-17E01.
[10] Hokka M, Kuokkala V-T, Curtze S, Vuoristo T, Apostol M. Characterization of strain rate and temperature dependent mechanical behaviour of TWIP steels. J Phys IV Fr 2006;134:1301–6. https://doi.org/10.1051/jp4:2006134197.
[11] Hokka M, Curtze S, Kuokkala V-T. Tensile HSB testing of sheet steels at different temperatures. Proc. 2007 SEM Ann. Conf. Expo. Exp. Appl. Mech. 2007. paper 250.
[12] Curtze S, Kuokkala VT, Hokka M, Peura P. Deformation behavior of TRIP and DP steels in tension at different temperatures over a wide range of strain rates. Mater Sci Eng 2009;507:124–31. https://doi.org/10.1016/j.msea.2008.11.050.
[13] Subramonian B, Basu B. Development of a high-speed cryogenic tribometer: design concept and experimental results. Mater Sci Eng 2006;415:72–9. https://doi.org/10.1016/J.MSEA.2005.09.086.
[14] Basu B, Mukhopadhyay A, Mishra A, Sarkar J. Does thermal conductivity play a role in sliding wear of metals in cryogenic environment? J Tribol Asme 2010;132:1–5. https://doi.org/10.1115/1.4002503.
[15] Lyu Y, Bergseth E, Olofsson U. Open system tribology and influence of weather condition. Sci Rep 2016;6. https://doi.org/10.1038/srep32455.
[16] Ma L, Shi LB, Guo J, Liu QY, Wang WJ. On the wear and damage characteristics of rail material under low temperature environment condition. Wear 2018;394–395:149–58. https://doi.org/10.1016/J.WEAR.2017.10.011.
[17] Ratia V, Lindroos M, Valtonen K, Apostol M, Kuokkala V. Impact behavior of martensitic steel at low temperatures. Nord. Conf. Proc. Hämeenlinna: VTT; 2016. p. 1–9.
[18] Lindroos M, Apostol M, Kuokkala V-T, Laukkanen A, Valtonen K, Holmberg K, et al. Experimental study on the behavior of wear resistant steels under high velocity single particle impacts. Int J Impact Eng 2015;78:114–27. https://doi.org/10.1016/j.ijimpeng.2014.12.002.
[19] Hossain R, Pahlevani F, Witteveen E, Banerjee A, Joe B, Prusty BG, et al. Hybrid structure of white layer in high carbon steel - formation mechanism and its properties. Sci Rep 2017;7:1–12. https://doi.org/10.1038/s41598-017-13749-7.
[20] Odeshi AG, Bassim MN. Evolution of adiabatic shear bands in a dual-phase steel at very high strain rates. Mater Sci Eng 2008;488:235–40. https://doi.org/10.1016/j.msea.2007.11.021.
[21] Boakye-Yiadom S, Bassim MN. Effect of prior heat treatment on the dynamic impact behavior of 4340 steel and formation of adiabatic shear bands. Mater Sci Eng 2011;528:8700–8. https://doi.org/10.1016/j.msea.2011.08.036.
[22] Nikas GK. Modeling dark and white layer formation on elastohydrodynamically lubricated steel surfaces by thermomechanical indentation or abrasion by metallic particles. J Tribol 2015;137:031504. https://doi.org/10.1115/1.4029944.
[23] Abbasi E, Luo Q, Owens D. Case study: wear mechanisms of NiCrVMo-steel and CrB-steel scrap shear blades. Wear 2018;398–399:29–40. https://doi.org/10.1016/j.wear.2017.11.014.
[24] Zhang B, Shen W, Liu Y, Tang X, Wang Y. Microstructures of surface white layer and internal white adiabatic shear band. Wear 1997;211:164–8. https://doi.org/10.1016/S0043-1648(97)00099-9.
[25] Fang L, Cen Q, Sun K, Liu W, Zhang X, Huang Z. FEM computation of groove ridge and Monte Carlo simulation in two-body abrasive wear. Wear 2005;258:265–74. https://doi.org/10.1016/J.WEAR.2004.09.024.
[26] Kivikytö-Reponen P, Laukkanen A, Apostol M, Waudby R, Andersson T, Helle A, et al. Modelling and testing of elastomer impact deformation under high strain rates. Tribol Mater Surface Interfac 2014. https://doi.org/10.1179/1751584X14Y.

0000000067.
[27] Arias A, Rodríguez-Martínez JA, Rusinek A. Numerical simulations of impact behaviour of thin steel plates subjected to cylindrical, conical and hemispherical non-deformable projectiles. Eng Fract Mech 2008;75:1635–56. https://doi.org/10.1016/j.engfracmech.2007.06.005.
[28] Iqbal MA, Senthil K, Madhu V, Gupta NK. Oblique impact on single, layered and spaced mild steel targets by 7.62 AP projectiles. Int J Impact Eng 2017;110:26–38. https://doi.org/10.1016/j.ijimpeng.2017.04.011.
[29] Cho S, Truong DD, Shin HK. International Journal of Impact Engineering Repeated lateral impacts on steel beams at room and sub-zero temperatures. Int J Impact Eng 2014;72:75–84. https://doi.org/10.1016/j.ijimpeng.2014.05.010.
[30] Apostol M, Kuokkala V-T, Laukkanen A, Holmberg K, Waudby R, Lindroos M. High velocity particle impactor – modeling and experimental verification of impact wear tests. World tribol. Congr., torino, Italy. 2013. p. 1–4.
[31] Lindroos M, Ratia V, Apostol M, Valtonen K, Laukkanen A, Molnar W, et al. The effect of impact conditions on the wear and deformation behavior of wear resistant steels. Wear 2015;328–329:197–205. https://doi.org/10.1016/j.wear.2015.02.032.
[32] Woldman M, Van Der Heide E, Tinga T, Masen MA. A finite element approach to modeling abrasive wear modes. Tribol Trans 2017;60:711–8. https://doi.org/10.1080/10402004.2016.1206647.
[33] Xu Y, Meyers MA. Nanostructural and microstructural aspects of shear localization at high-strain rates for materials. Adiabatic shear localization 2012. p. 111–71. https://doi.org/10.1016/B978-0-08-097781-2.00003-4.
[34] Kim H, Park J, Kang M, Lee S. Interpretation of Charpy impact energy characteristics by microstructural evolution of dynamically compressed specimens in three tempered martensitic steels. Mater Sci Eng 2016;649:57–67. https://doi.org/10.1016/j.msea.2015.09.099.
[35] Ratia V, Rojacz H, Terva J, Valtonen K, Badisch E, Kuokkala V-T. Effect of multiple impacts on the deformation of wear-resistant steels. Tribol Lett 2015;57. https://doi.org/10.1007/s11249-014-0460-7.

Publication V

Ville Oksanen, Kati Valtonen, Peter Andersson, Antti Vaajoki, Anssi Laukkanen, Kenneth Holmberg, and Veli-Tapani Kuokkala

Comparison of laboratory rolling-sliding wear tests with in-service wear of nodular cast iron rollers against wire ropes

Wear 340-341 (2015) pp. 73-81

Wear 340-341 (2015) 73–81

Contents lists available at ScienceDirect

Wear

journal homepage: www.elsevier.com/locate/wear

Comparison of laboratory rolling–sliding wear tests with in-service wear of nodular cast iron rollers against wire ropes

V. Oksanen [a,*], K. Valtonen [a], P. Andersson [b], A. Vaajoki [b], A. Laukkanen [b], K. Holmberg [b], V.T. Kuokkala [a]

[a] Tampere University of Technology, Department of Materials Science, Tampere Wear Center, P.O. Box 589, FI-33101 Tampere, Finland
[b] VTT Technical Research Centre of Finland, P.O.Box 1000, FI-02044 Espoo, Finland

ARTICLE INFO

Article history:
Received 6 October 2014
Received in revised form
25 June 2015
Accepted 12 July 2015
Available online 20 July 2015

Keywords:
Nodular cast iron
Contact mechanics
Rolling–sliding
Rolling contact fatigue
Wear testing
Wire rope

ABSTRACT

The present work describes the wear behaviour of nodular cast iron in rolling–sliding contact with steel wire ropes and steel wires in laboratory and in-service conditions. In each of the studied examples, the wear had proceeded through a surface fatigue process, in which inter-nodular crack propagation and simultaneous deformation in a thin sub-surface zone had resulted in the formation of ferrous scales consisting of material from the metal matrix of the cast iron. The scale layers of the wear surface were oriented towards the direction of the sliding component of the motion, and the spalling of the scales was identified as the dominating mechanism for material removal from the wear surface. The initiation behaviour of the inter-nodular cracks was analysed by crack measurements and statistical analysis of the depths and initiation angles of the cracks in relation to the wear surface. The initiation depths of the cracks increased with increasing contact pressure. Roller samples from in-service and from the component wear tests showed closely similar distributions of the crack depths and crack initiation angles. The sample from the twin-disc test showed aspects of cracking behaviour that were typical of both the rolling and the sliding direction of the roller samples.

1. Introduction

Wire rope drives are all around us, in lifting equipment, cable cars, cable railways, funiculars, just to mention some of the applications. A rope drive comprises a wire rope and one or several rollers, over which the wire rope is bent during operation. The wire rope is built up from a large number of steel wires wound together to a complex structure, which carries loads in the length direction while being laterally flexible. The most widely used wire material in rope drives is a high-strength non-alloyed carbon steel with a pearlitic microstructure [1].

The wire rope is traditionally the most critical component in a wire rope drive, because the breakage of the wire rope usually is an issue of both economical and safety-related relevance. Cable breakages can occur for instance due to fretting wear and fatigue at poorly lubricated wires of a cable, or due to abrasive wear [1]. For this reason, the tribological research on wire rope drives has so far mainly focused on the wire rope [2–5], while the rollers have gained rather limited attention.

Recent studies on the wear of rollers of wire rope drives are mainly limited to steel and polymer roller materials [6–8], while the literature available on the wear of nodular cast iron in contact with steel mainly covers other applications than wire rope drives [9–13].

Oksanen and co-workers [14] have previously described the wear behaviour of power-transmitting drive cast iron rollers in rolling–sliding contact with steel wire ropes in different contact pressure ranges and with sliding ratios of 0.02% and 2.0% in the rolling direction and pure sliding perpendicularly to the rolling motion. The wear proceeded by simultaneous processes of crack growth from the graphite nodules diagonally towards the wear surface, and deformation of the material towards the net sliding direction, which was affected by the value of the sliding ratio in the rolling direction. The crack growth and deformation resulted in the formation of deformation tongues in the net sliding direction. Under normal or increased contact pressures, the material removal proceeded through the cracking-off of small fragments from the edges of the deformation tongues. Increased contact pressure activated a multi-directional crack growth diagonally towards the wear surface, and led to the removal of large surface fatigue spalls.

In this study, the wear behaviour of nodular cast iron components in contact with steel wire ropes and wires in different

* Corresponding author.
E-mail address: ville.t.oksanen@tut.fi (V. Oksanen).

http://dx.doi.org/10.1016/j.wear.2015.07.006
0043-1648/

conditions was characterized by microscopy and statistically analysed in terms of cracks caused during the wear processes. Grooved rollers made from nodular cast iron had operated in contact with steel wire ropes under bi-directional rolling motion in the running direction of the rope and sliding motion in a direction perpendicular to the rolling motion. An in-service roller sample, two component wear test roller samples, and an unused roller sample with an as-machined groove were characterized. A twin-disc test was performed with unidirectional rolling–sliding motion against a steel-wire-coated disc. The statistical analysis of the fatigue wear cracks can be utilised in the validation of the similarity of the wear behaviour of in-service samples and wear test samples, and in the adjustment of wear test parameters.

2. Materials and methods

2.1. Materials

The grooved rollers and the cast iron disc sample for the twin-disc test had been produced from nodular cast iron EN-GJS-700-2, which comprises of spherical graphite precipitations in an almost fully pearlitic iron matrix. The minimum standard tensile strength was 700 MPa and the minimum standard elongation 2%. Table 1 presents the median hardness of the cast iron samples. The wire rope grooves in the roller samples had been produced by turning with form-cutting tools.

The rollers had operated against wire ropes with a diameter of 8 mm and a tensile strength grade of 2160 N/mm^2. The wire rope construction consisted of 8 × 19 regular left lay Seale outer strands and a steel wire rope core. The wires of the wire ropes, as well as the wire used in twin-disc tests, had been drawn from unalloyed pearlitic steel with a carbon content of about 0.6%, according to the manufacturers. The wire used in the twin-disc tests had an ultimate tensile strength of 1700 N/mm^2 and a hardness of 456 HV_5 with a standard deviation of ± 6 HV_5, as determined by a median obtained from ten indentations on each of three longitudinal cross-sections.

2.2. Testing conditions

The grooved rollers had operated under contact with wire ropes under specific rope forces and bi-directional rolling motion. Fig. 1 illustrates the contact geometry of the wire rope in the roller groove. The contact between the roller and the wire rope consists of numerous small contact areas. As the wear of the wire rope proceeds, the contact points evolve into lens-like ovals.

Two of the roller samples had operated in two tests in component test equipment used for life-time testing of wire ropes. Fig. 2 illustrates the test set up. The wire rope was run by the drive roller in a regularly changing bi-directional running motion with a running distance of approximately 1.0 m per full cycle, or 0.5 m per running direction. The wire rope ran over three freely rotating invert rollers. The middle invert roller was the one chosen for characterization in the present work. To prevent sliding, the wire rope had been secured to the drive roller, and the ends of the wire rope had been attached to each other with rope wedge sockets. In the wear tests, the applied loads, and consequently the rope forces, were kept constant. The fleet angle, i.e., the deflection angle between the radial plane of the roller and the axis of the wire rope exiting or entering the groove, was 0° in the present wear tests.

The two wear-test roller samples had operated in five life-time tests with similar wire ropes. Before each test, the wire rope had been lubricated with an additive-free paraffinic vaseline (petrolatum) with a kinematic viscosity of 80 mm^2/s when heated to a temperature of 100 °C. One of the roller samples had been tested with a rope force of 10 kN for a duration of 639,198 running cycles, and the other one with 15 kN and 309,969 running cycles. In addition, an unused as-machined roller sample was characterized for comparison.

Table 1
Median hardness of the cast iron samples.

Sample	Hardness HBW 1/30	Standard deviation [± HBW 1/30]
Unused roller	285	6
In-service roller	268	7
Test roller 10 kN	277	4
Test roller 15 kN	277	2
Twin-disc	272	5

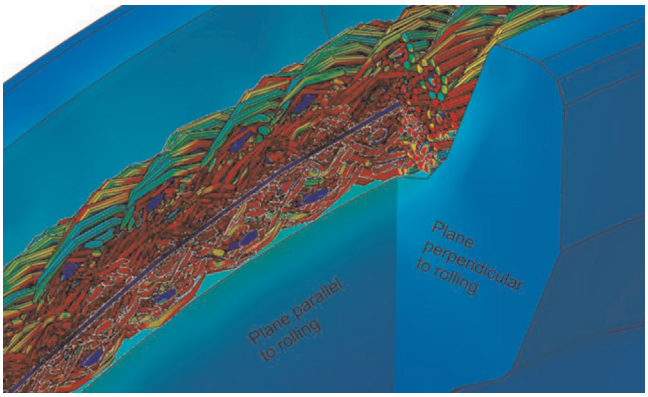

Fig. 1. Modelled image of the contact between the present type of roller and the wire rope, and the cross-sectional planes, along which the roller samples were characterized.

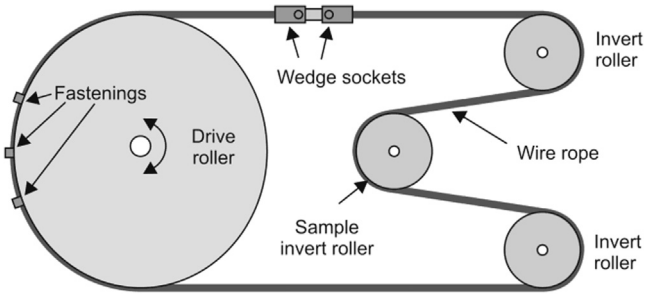

Fig. 2. Schematic of the component wear test setup. The middle invert rollers from the two tests were characterized in this study.

The in-service roller sample had operated as one of two invert rollers in a hoist system consisting of a rope drum, two load-carrying invert rollers, and an equalizing roller between the invert rollers. Both ends of the wire rope had been fastened in the rope drum. The invert roller sample had operated under a variable load, an intermittently changing running direction, and a varying fleet angle, for approximately 400–500 h. The wire rope of the in-service machinery had been lubricated with paraffinic vaseline before commissioning, but most likely not during the service life.

Due to the free rotation of the roller and the almost equally large rope forces on both sides of the roller, the sliding between the roller and the wire rope in the running direction had been negligible both during the in-service operation and in the component wear tests.

The twin-disc test was carried out with a cast iron disc in rolling–sliding contact with a steel wire of 1.4 mm in diameter wrapped as a spiral around a grooved steel disc. Fig. 3 presents a schematic of the contact in the initial stage of the test. The cast iron disc had an initial diameter of 50 mm and a radius of

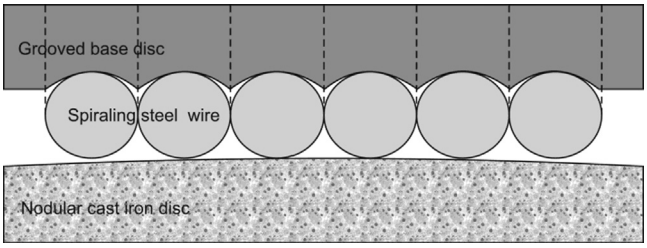

Fig. 3. Schematic of the twin-disc test at the initial stage of the wear process, showing the cross-section of the contact between the cast iron and the steel wire discs in a plane perpendicular to the rolling direction.

curvature of 100 mm in the axial direction. The steel-wire-coated disc had an initial circumference of 50 mm. In the twin-disc test, the normal force was 500 N and the initial circumferential velocities were 3.0 m/s for the cast iron disc and 2.94 m/s for the steel-wire-coated disc, corresponding to a slip-ratio of 0.2% in the contact. Initially, due to the curvature of the cast iron disc in the direction of its axis, contacts between the steel wire and the cast iron discs occurred on only two points. The number of contacts increased as the wear process proceeded. Due to diameter changes caused by wear, the circumferential velocities and the sliding ratio changed during the test. The duration of the test was 48 h, during which the tribosystem was lubricated automatically with a total of 1.0 g of paraffinic vaseline (petrolatum) with a drop point of approximately 80 °C and a kinematic viscosity of 20 mm^2/s when heated to a temperature of 100 °C.

2.3. Post-test analysis methods

The samples were characterized both qualitatively and quantitatively. Qualitative characterization of the microstructure and wear behaviour was performed by inspecting the worn surfaces and cross-sections of the samples using an optical microscope and a Philips XL30 scanning electron microscope (SEM). The characterized cross-sectional planes of the roller components are presented in Fig. 1. The sectional samples were prepared so that the sample planes were closely parallel to the tangent of the wear surface. The sectional samples of the roller components in the plane parallel to the rolling direction were prepared so that the cross-section in the rolling direction was located at the groove bottom. The cross-sectional twin-disc samples were produced so that the sample plane was at the midpoint of the disc axis.

Quantitative characterization of the worn surfaces of the nodular cast iron samples was conducted by measurement of the depths and initiation angles of wear cracks in relation to the surface of the component. The measurements were performed by computer assisted optical microscopy of the cross-sectional samples, on 171 μm long and 128 μm wide image fields, using a magnification factor of 10^3. Fig. 4 illustrates the measurement procedure for single cracks. The crack depth h was determined as the distance between the general surface line in the image area and the probable initiation point of the crack.

The initiation angle α of a crack was defined as the angle between the general surface line and a straight line that begun from the probable initiation point of the crack and followed the crack line for as long as the crack was linear. Cracks extending towards the wear surface were given positive values and, consequently, cracks oriented inwards obtained negative values. In the case of the unused roller sample and the twin-disc sample, the cracks oriented towards the direction of the motion of the contact, i.e., the direction of the sliding motion of the machining tool or the steel wire disc on the surface of the nodular cast iron component, were given angles $-90°…0°…90°$. In the case of the roller components, the rolling motion had a changing direction, and one of the rolling directions was arbitrarily chosen to have the initiation angle values $-90°…0°…90°$. The angles $-90°…\pm180°…90°$ then represented the cracks oriented towards the other rolling direction. The measurement uncertainty of the angles caused by the microscope system was $\pm1°$.

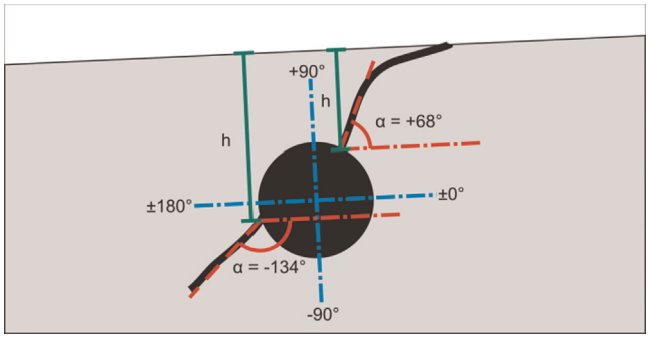

Fig. 4. Schematic illustration of the definitions used for the depths and initiation angles (α) of the cracks. The dash–dot lines indicate the vertical and horizontal axes in relation to the general surface line, and the dashed lines indicate the initial angles of the cracks.

Table 2
The number of analysed cracks for each sample and cross-section plane used in the statistical analysis.

Plane	Unused roller	In-service roller	Test roller 10 kN	Test roller 15 kN	Twin-disc
Parallel to rolling	79	341	232	188	239
Perpendicular to rolling	–	291	174	144	–

The measurement of the crack initiation angles was slightly inaccurate, because most of the cracks were somewhat curved. This was caused by the nonlinear crack propagation paths and by curvedness caused by the plastic deformation of the wear surface.

The crack depths and initiation angles in the roller samples were measured in both the inspected planes, i.e., in the plane parallel to the rolling direction at the groove bottom and in the plane perpendicular to the rolling motion. The measurements of the twin-disc sample were performed in the plane parallel to the rolling–sliding motion, in the middle parts of the disc axis, where the contact pressure had been at its highest. The number of analysed cracks for each sample and cross-section plane in the statistical analysis are given in Table 2.

The measurement data of the depths and initiation angles of the cracks were analysed statistically. Cumulative histograms were defined for the crack depths of each sample, using bins, i.e., discrete interval groups, of 5 μm with relative frequencies. Depths of less than 2 μm were disregarded.

To analyse the initiation angles of the crack, they were presented in circular histograms with relative frequencies having bins of, for example, $-4°$ to $+5°$, $+6°$ to $+15°$, etc. The bins have been labelled $\pm0°$, $+10°$ and so on, for a more convenient presentation of the results.

3. Results

3.1. Unused roller

The as-machined wire-rope groove of the unused roller had a rough surface with bare graphite nodules visible under the microscope. Fig. 5a presents the as-machined surface. Fig. 5b

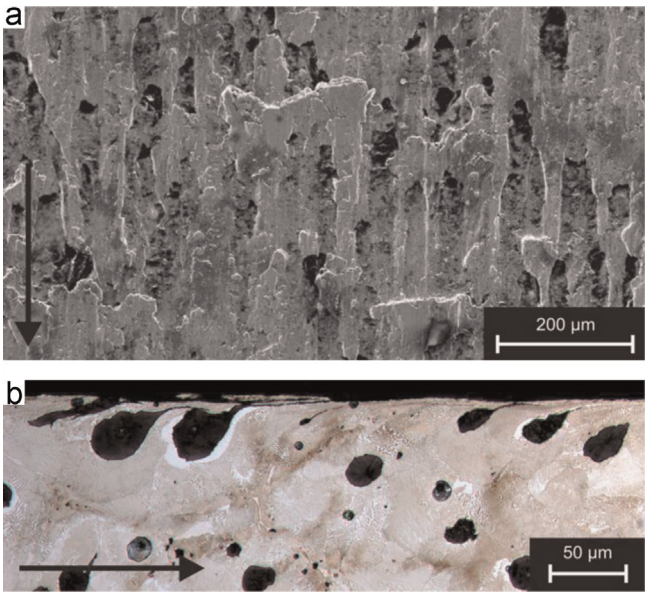

Fig. 5. As-machined groove bottom of the unused roller sample. a) Secondary electron SEM image of the surface. b) Cross-section by light optical microscopy, in parallel with the cutting direction of the machining tool. The cutting direction of the machining tool is indicated by the arrows.

presents a cross-section in the plane parallel to the machining direction, revealing a shallow sub-surface zone, in which the metal matrix has been plastically deformed towards the motion direction of the cutting tool. In the deformed zone, cracks have initiated at the interface of the graphite nodules and the matrix metal. Most of the cracks had an initiation angle that was oriented diagonally towards the surface. In the immediate vicinity of the groove surface, the cracks were curved as following the surface. In addition to the cutting of the material, delamination of the metal matrix above the cracks had played a role in the material removal process.

3.2. *In-service roller*

The in-service roller showed a rather different damage type than did the unused roller. Fig. 6a presents the wear surface at the groove bottom of the in-service roller sample, showing metallic scales and a pit and, in addition, scratches perpendicular to the rolling direction. Small hard particles were present in the surface of the in-service roller sample, as embedded in the metal matrix of the worn surface. The scales were caused by cracks extending to the surface, and had a rather uniform orientation perpendicular to the rolling directions.

Fig. 6b presents a cross-section of the in-service roller in the plane parallel to the rolling directions. The image reveals deformed graphite nodules and cracks in the metal matrix that originate from the interface between the graphite nodules and the metal matrix. The cracks appeared deeper than those in the unused roller component, and, contrary to those in the unused sample, they did not have a uniform orientation but appeared to be distributed quite evenly between the two rolling directions. Networks of inter-nodular cracks had formed at depths of approximately 20 μm or less from the surface. At higher depths from the surface, most of the cracks had not yet interconnected between the graphite nodules.

Fig. 6c shows a cross-section perpendicular to the rolling direction at the groove bottom of the in-service roller, revealing strong deformation of the matrix metal and the graphite nodules with uniform orientation. The cross-sections also revealed cracks originating from the interfaces between the graphite nodules and

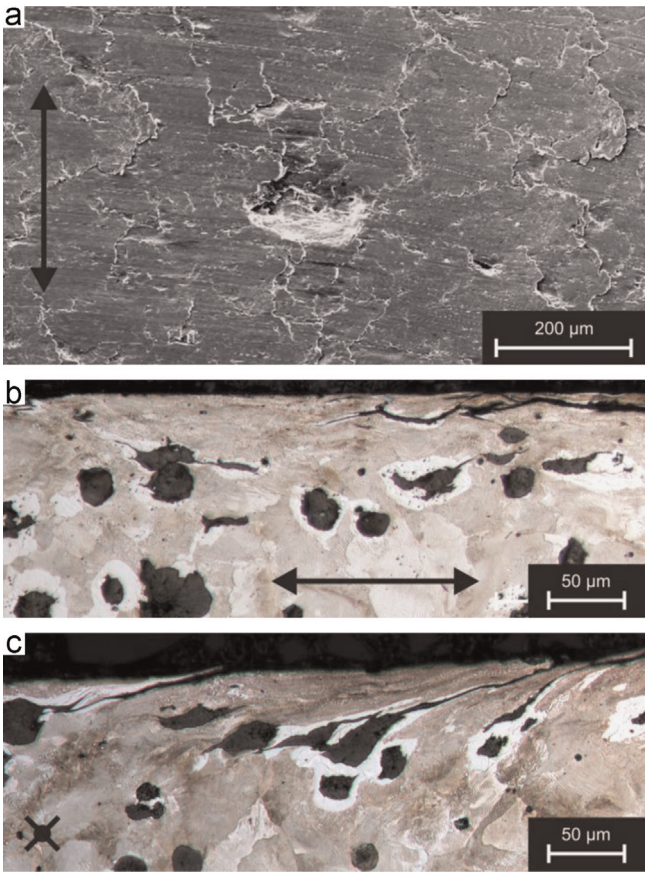

Fig. 6. In-service roller sample; a) worn surface, and cross-sections in planes b) parallel and c) perpendicular to the rolling directions. The rolling directions are indicated in each image.

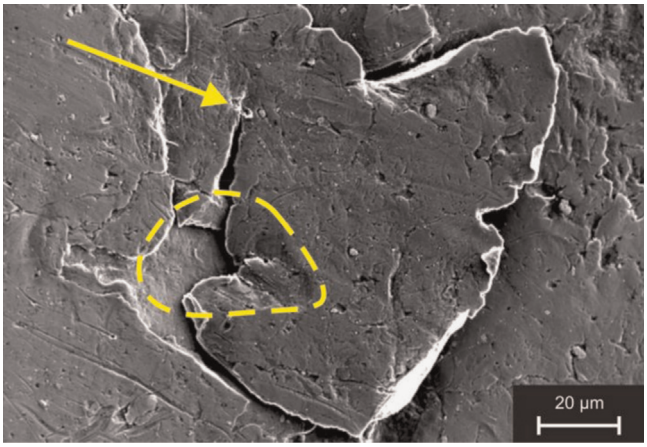

Fig. 7. SEM image of a delaminated fragment on the surface of the in-service roller. The arrow indicates the point to which the final crack had proceeded. The dashed line indicates a pit left by removal of a smaller spall.

the matrix metal. In the plane perpendicular to the rolling directions, the cracks were mostly oriented diagonally towards the wear surface, parallel to the deformation, or deeper into the material in the opposite orientation.

Fig. 7 presents a surface area of the in-service roller with a loosely attached, delaminated fragment of the metal matrix, which, if detached, would have resulted in a surface pit similar to the one shown in Fig. 6a. Deformation tongues had been formed at the loose edge of the delaminated fragment, and the final crack had been propagating at the opposite edge of the delaminated

fragment, as shown by the arrow in Fig. 7. A smaller spall had cracked off from the area indicated by the dashed line. In the rightmost part of the pit inside the dash-lined area, a depression formed by the deformation tongue of the smaller spall can be seen. The leftmost part of the pit consists of intact fracture surface. Pits caused by the removal of large spalls were rather rare in the roller samples. Small, hard particles embedded in the metal matrix are also visible in Fig. 7. EDS analyses showed that the particles consisted of tungsten, carbon and cobalt. The scratches visible in Fig. 6a were most probably caused by hard particles sliding against the groove surface.

3.3. Component wear test rollers

The component wear test results showed, that the increase in the rope force from 10 kN to 15 kN had halved the average life-time of the wire ropes and doubled the average volumetric wear rate of the roller. In this context, the wear rate is equal to the wear volume divided by the force acting on the contact and the distance of motion. At the end of the test sequences comprising the five wire ropes, the wear volumes of the rollers were nearly equal.

The roller sample tested at the 10 kN rope force had a rather smooth wear surface covered by metallic scales oriented uniformly perpendicular to the rolling directions, as presented in Fig. 8a. The wear surface showed scarce pits caused by the removal of scales, but no scratches or embedded hard particles were observed. The cross-sections showed rather similar behaviour to that of the in-service roller sample. Fig. 8b presents a cross-section perpendicular to the direction of rolling revealing cracks, which had a uniform orientation diagonally towards the surface, and similarly oriented strong deformation. In the plane parallel to the rolling direction, the deformation had been weaker, and neither the deformation nor the cracks had a uniform orientation. At depths close to the surface, the internodular cracks had joined and formed networks.

The roller tested with the 15 kN rope force revealed macroscopic imprints at the groove bottom that were corrugated as the result of repeated contacts with the surface wires of the wire rope.

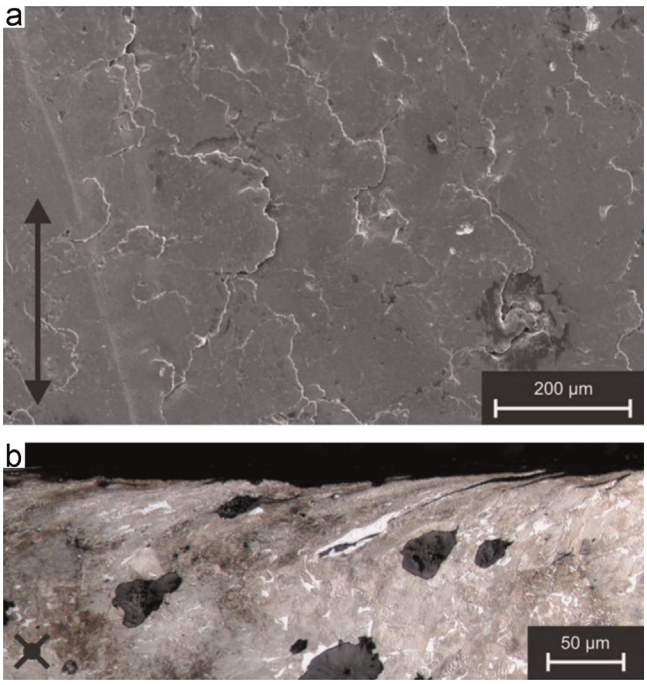

Fig. 8. Roller sample tested at 10 kN rope force; a) wear surface and b) cross-section perpendicular to the direction of rolling. The rolling directions are indicated in each image.

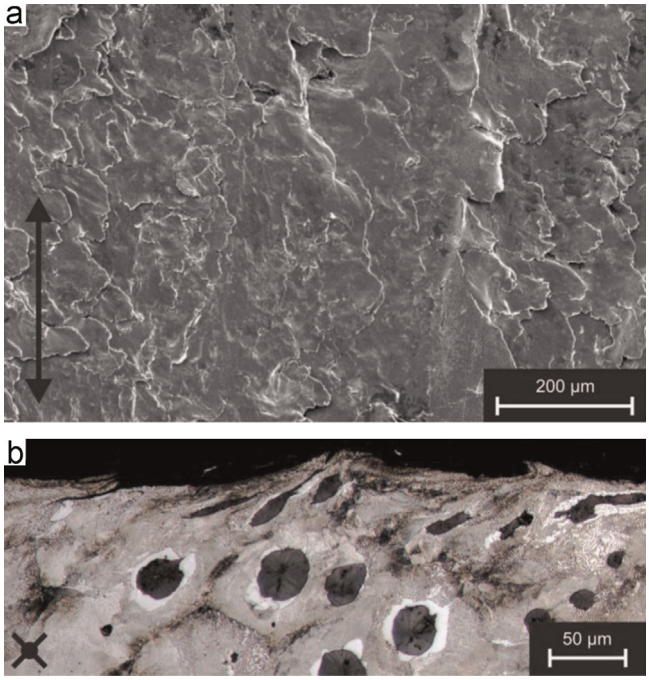

Fig. 9. The roller sample tested with the 15 kN rope force; a) wear surface at a corrugation valley of the groove bottom and b) cross-section perpendicular to the direction of rolling that shows a corrugation peak in the middle of the image. The rolling directions are indicated in each image.

Corrugations are formed when the diameter of the groove is such that the contact between the strands and the roller occur repeatedly at the same point, i.e., the circumference of the groove bottom is close to a multiple of the lay length of the wire rope. On the two other worn roller samples, such conditions had not occurred, or at least not towards the end of the operational life-time, and no corrugation imprints had been formed. In addition to the momentary circumference length of groove bottom of the roller, the corrugation may be promoted by increased load, by increasing the contact pressure and by elongating the wire rope, thus affecting the lay length. The corrugated wear surface contained valleys at the spots where the strands and wires had repeatedly contacted the groove, and peaks between the valleys. Fig. 9a shows a rough wear surface at a corrugation valley. Similarly to those of the other two worn roller samples, the deformation tongues of the roller tested at the 15 kN rope force had a uniform orientation perpendicular to rolling. However, the surface was rougher than those of the other two worn roller samples. Fig. 9b presents a cross-section perpendicular to the direction of rolling. The cross-sectional sample revealed deformation and crack propagation at the corrugation valleys similar to that in the other two roller samples. However, at the corrugation peaks, the deformation was oriented from both directions towards the centre of the peak. The peaks were formed by material pushed away from the contact areas. Scratches or hard particles were not observed in the sample.

3.4. Twin-disc test disc

The twin-disc test sample made from cast iron showed traces of a wear behaviour that was somewhat different from that of the roller samples. Fig. 10a presents a wear surface on the twin-disc test disc sample, which was covered by matrix-related metal scales oriented in parallel to the direction of motion, as well as numerous pits. Fig. 10b shows deformation that is oriented towards the sliding direction and cracks along a plane parallel to the rolling–sliding direction of the twin-disc test disc sample. The

deformation was clearly oriented towards the sliding direction. In the vicinity of the surface, the inter-nodular cracks had intersected and formed long networks. The networks of cracks had a general orientation diagonally towards the surface. The networks of cracks appeared to slightly favour the orientation towards the sliding direction. However, the orientation was not as evident as in the case of the worn roller samples in the plane perpendicular to the direction of rolling. The cracked sub-surface zone in the twin-disc sample reached deeper than the corresponding zones in the roller samples, and the deepest cracks appeared to be unaffected by the deformation. A plane perpendicular to the rolling–sliding direction of the twin-disc sample revealed low deformation of the sub-surface zone and long networks of cracks, oriented in parallel to the surface.

3.5. Statistical analysis

The surface crack depths were characterized for all the present samples. Fig. 11 shows the cumulative frequencies of the surface crack depths as measured from the present samples. The crack depths of the roller samples in the histogram were measured from the groove bottom parallel to the rolling directions.

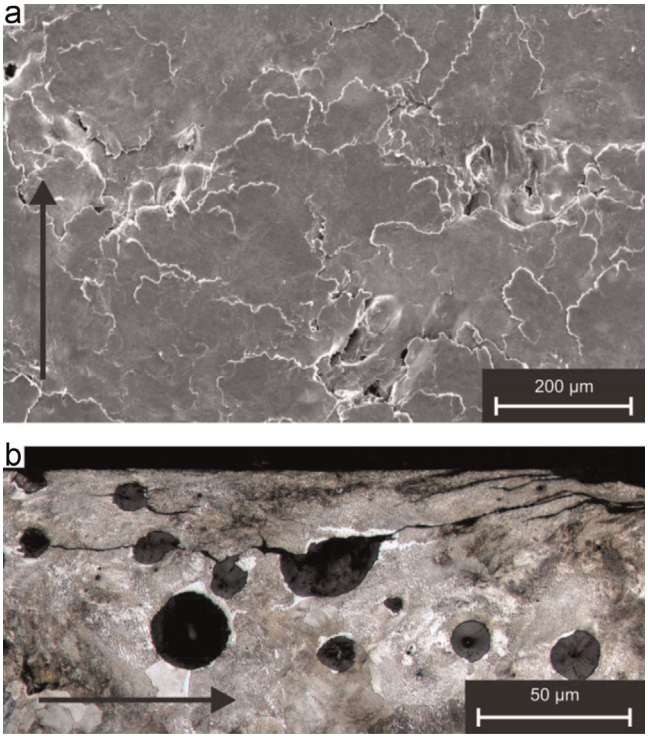

Fig. 10. a) Worn surface and b) a cross-section parallel to the direction of rolling–sliding motion in the twin-disc sample. The arrows indicate the direction of the contact motion and sliding.

Fig. 11 shows that the three worn rollers have very similar distributions of the crack depths. The unused roller sample shows a narrow distribution of the crack depths, with the deepest crack initiating at a depth of 19 µm. The in-service roller and the wear-test roller from the test with the 15 kN rope force have a slightly higher maximum crack depth (approximately 60 µm) than the sample tested with the 10 kN rope force (approx. 50 µm). The twin-disc sample had a somewhat wider crack depth distribution, having the deepest crack initiating at a depth of 77 µm.

Fig. 12 shows the relative frequencies of the crack initiation angles for all four rollers in the plane parallel to the rolling direction, and for those of the twin-disc sample in the plane parallel to the direction of motion. The 0° angle represents the contact motion direction of the twin-disc sample and the cutting tool motion direction in the as-machined roller sample. In the case of the worn roller sample, the angles 0° and ±180° represent the two running directions of the wire-rope. The negative angles represent cracks extending deeper into the sub-surface material from the graphite nodules, and positive angles correspondingly those extending towards the wear surface. The peak in the curve of the as-machined roller sample are extended to 20% in the angle bins of +20° and +30°.

Fig. 12 shows that the unused roller sample had an evident preference of crack initiation orientation towards the machining direction. Approximately one-half of the machining cracks had initial angles of 10°…30° in relation to the cutting tool motion direction. A smaller peak in the crack distribution occurred at almost opposite angles (−170°…−160°), which represented the cracks oriented deeper into the material from graphite nodules, which were already part of the machining surface and were partially cut.

Each of the worn roller samples had an approximately symmetrical distribution of crack initiation angles in relation to the two rolling directions. Fig. 12 indicates that the cracks initiating towards both rolling direction have clear peaks at angles of +10°…+20° and +170°…+160°. These orientations represent +10°…+20° angles in relation to the surface line in the two opposite rolling directions. Furthermore, the cracks with negative angles, i.e., those that were oriented deeper into the material, had quite symmetrical distributions when considering the two rolling directions.

The twin-disc sample showed a somewhat similar distribution of crack initiation angles as did the worn rollers. Similarly to the roller samples, the twin-disc sample had high distributions at +10°…+20° and +170° angle bins. However, it also had a high distribution at −170°…±180° angle, which is not present in the roller samples.

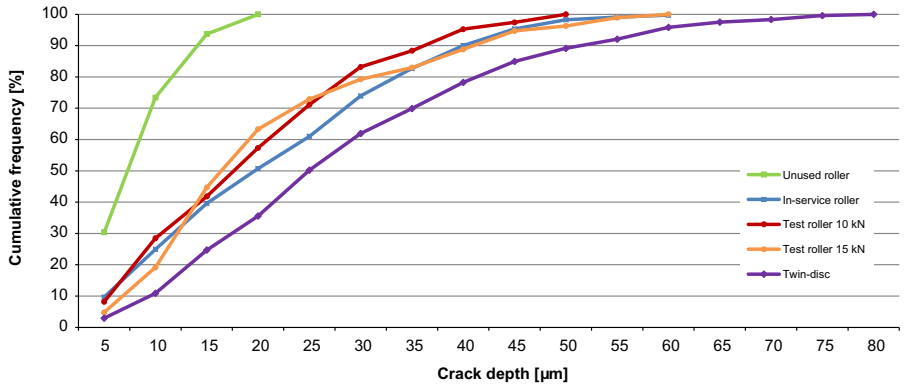

Fig. 11. Cumulative histogram of the crack depths. Each point in the graph represents the cumulative percentage of the cracks extending to the corresponding depth bin.

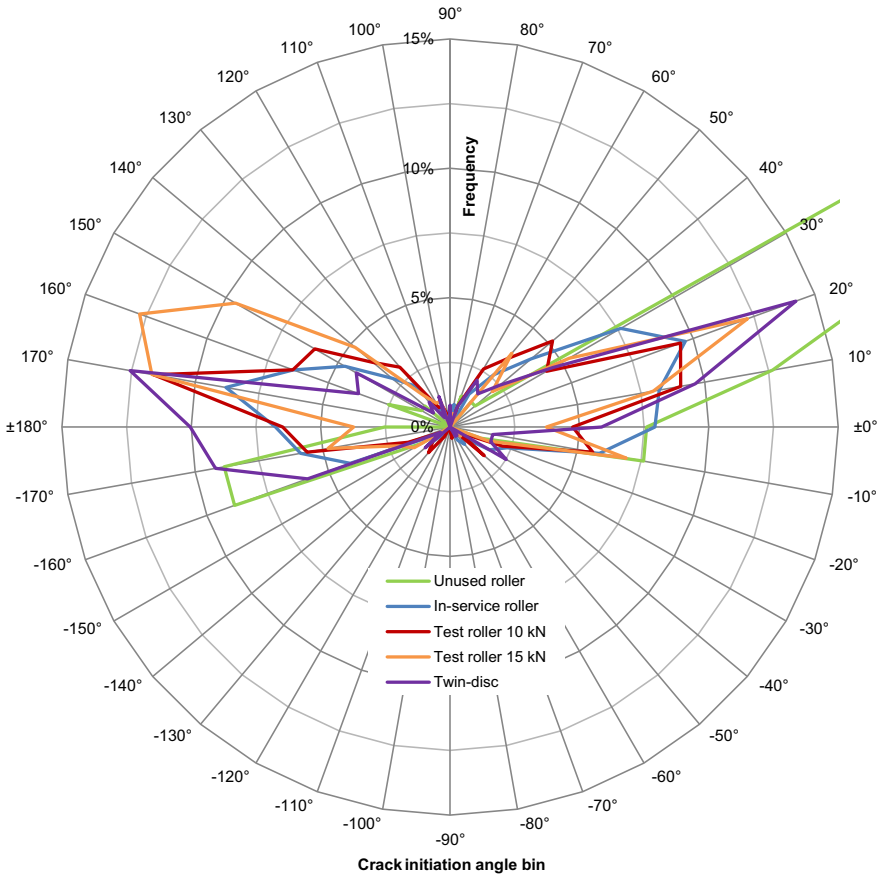

Fig. 12. Histograms of initial crack angles in the plane parallel to the direction of rolling motion.

Fig. 13 represents the initiation angles of the cracks in the surface zones of the worn roller samples, in the plane perpendicular to the rolling direction. The curve of the twin-disc sample is the same as in Fig. 12, i.e., in the plane parallel to the contact motion. Each worn roller sample showed a distribution peak at the angles of $+20°…+30°$ in relation to the surface in the direction of the deformation, and another peak at the angle bin of $-170°$, representing cracks that extended deeper into the material in the direction opposite to the deformation.

Again, the distribution of the twin-disc sample in the plane parallel to the motion shows rather similar behaviour to that of the roller samples, having high distribution at the angles of $+20°$ and $-170°$. However, the roller samples did not have a peak at $+170°$ in the plane perpendicular to rolling.

4. Discussion

4.1. Analysis of the wear mechanism

The wear behaviour appeared similar in each of the worn roller samples. The roller samples showed deformation tongues oriented perpendicularly to the direction of rolling. However, the roller sample tested with the 15 kN rope force had experienced corrugation and had consequently a rougher surface than had the other roller samples.

The wear process of the nodular cast iron samples had proceeded mainly through rolling contact fatigue under rolling–sliding conditions. Cracks had initiated at the interfaces of the graphite nodules and propagated inter-nodularly through the metal phase of the cast iron material. On the other hand, the sliding motion had induced plastic deformation of the material in the subsurface region. The cracks extending to the surface enabled strong deformation, which resulted in the formation of scale-like deformation tongues on the wear surface.

The material removal proceeded by spalling of the metallic surface scales, as described in the context of Fig. 7. At the initial stage of the formation of the spall, one or multiple cracks had emerged on the surface in the direction of sliding and the two orientations parallel to the rolling direction. The scale formed by these multidirectional cracks was then removed through crack growth between the graphite nodules and the surface in the final undamaged neck of the metal fragment.

In the twin-disc sample, the cracking scales and the deformation tongues were formed in the direction of motion at the contact point, because the direction of motion was uniform. On the other hand, in each of the three worn roller samples, the deformation and the deformation tongues were uniformly oriented in one of the directions perpendicular to the rolling. It can be concluded that the deformation in this direction had to be caused by torsional and bending stresses in the wire ropes, arising in the surface strands and particularly individual surface wires in contact with the roller with respect to transfer of contact stresses. The subsequent surface deformation state due to the locality of the contact is two-dimensional, because slip is prevalent in the direction perpendicular to the direction of rolling. The torsional and bending stresses in the wire rope have caused shear stresses in the subsurface of the roller and, as a result, contact surface sliding in the direction perpendicular to the direction of rolling when the wire rope deforms and accommodates against the higher stiffness roller surface. Despite the lack of significant roller scale wire rope slip, sliding can result from the high contact pressures that subsequently deform the wire rope and particularly the surface strands and wires, thus promoting surface shear and finite sliding. The

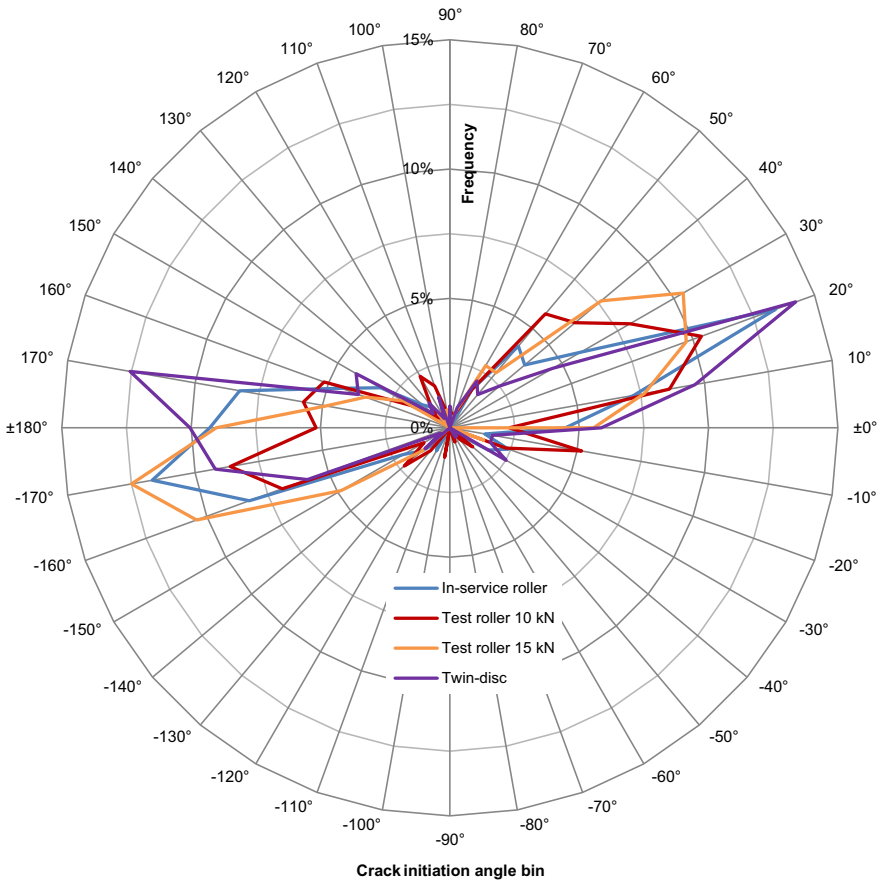

Fig. 13. Histograms of initial crack angles in the plane perpendicular to the rolling directions in the worn roller samples. The histogram for the twin-disc sample is the same as in Fig. 12, i.e., the one parallel to the rolling–sliding direction in the twin-disc test.

scratches caused by the hard particles in the in-service roller sample support the assumption that the stress state has caused sliding between the wire rope and the roller. The sliding rate between the groove and the wire rope could not be determined.

The amount of surface fatigue pits was substantially higher in the twin-disc sample than in the rollers. The high wear rate was caused by the high applied contact pressure, which accelerated the wear process. Moreover, the radial stiffness of the twin-disc arrangement exceeded that of the roller tests, hence the radial forces in the twin-disc test contained larger dynamic components than did the forces in the roller tests and promoted pitting-type surface damage and caused more extensive sub-surface damage due to the deeper penetrating contact stress fields.

Quite similar wear behaviour was observed by Oksanen et al. [14] for drive rollers that had transmitted power to wire ropes at a 0.02% slip rate in the rolling direction. In this case, the contact geometry was different from any of the present ones, and the contact pressure levels were lower. Furthermore, the sliding in the direction perpendicular to the rolling motion was not caused only by the stress state of the wire rope but by the motion of the wire rope when pressed into the gap between the two flanges of the groove. Thus, deformation tongues were oriented towards the groove bottom in both flanges of the groove.

4.2. Statistical analysis of the wear cracks

The statistical analysis of the three worn roller samples showed a consistent wear behaviour. Both the crack depths and the crack initiation angles had closely similar distributions both in the in-service sample and the component wear test samples. The crack orientations were comparable to the surface shear and normal stress–strain states expectable under such surface loading conditions. It can be concluded that the test set up produced realistic wear behaviour of the roller components. The machining damage in the unused roller showed similar elements of surface deformation and cracks initiating from the graphite nodules. Some material removal had occurred by delamination of the material above the cracks initiating from the graphite nodules, which was somewhat similar to the surface fatigue in the worn rollers. However, the material removal in the unused roller occurred mostly by cutting of the matrix metal, and the cracks in the damaged sub-surface were evidently shallower than those in the worn rollers. In other words, the fatigue wear process was more severe than the machining, and the quality of the machining surface did not significantly affect the wear process after the removal of the outermost surface layer by surface fatigue.

The twin-disc test disc sample made from cast iron showed notably higher maximum crack depths than did the roller samples. This was most likely caused by the higher contact pressure level. The distribution of the crack initiation angles of the disc sample in the plane parallel to the rolling–sliding motion showed a complex behaviour that has elements from both sliding and unidirectional rolling. In addition to the partial sliding, the unidirectional contact motion affected the distribution of the initial crack orientations in the twin-disc test sample. However, the wear behaviour of the twin-disc test disc appears to imitate that of the roller samples under the bi-axial contact motion quite well. By decreasing the contact pressure and increasing the sliding ratio, it might be possible to further optimise the wear behaviour simulation ability of the twin-disc test.

In order to obtain a comprehensive understanding of the relation between the behaviour in the twin-disc tests and in the

component operation, a complex modelling approach would be required. The model should be capable of describing both the deformation and wear responses of the twin-disc and wire rope arrangements, using a representative contact model accounting for sliding and frictional responses. Especially the resolution of the wire-rope-affiliated contacts with the required precision is a challenging task. Due to the inherent complexities of the problem, numerical solution would most probably be the best approach. If such an approach can be demonstrated, the models can be utilised to reproduce comparable contact conditions in the wire-rope-operation and in the twin-disc test.

It was not clear if the cracks extending from the graphite nodules deeper into the material had actually initiated with a negative crack initiation angle, or if they had propagated purely from the graphite nodules that were deeper in the material towards those closer to the surface. It was found probable and even highly likely, that the cracks could propagate simultaneously from two nodules and merge in the metal matrix.

5. Conclusions

The present analysis of the wear behaviour of nodular cast iron in contact with steel wire ropes and wires resulted in the following findings:

- The contact fatigue wear proceeds through surface deformation oriented towards the sliding direction and through internodular crack growth. The cracks propagate between the graphite nodules in the orientations are diagonal to the wear surface, towards both the rolling direction and the sliding direction. The propagation of the cracks to the surface, as well as the surface deformation, result in the formation of metallic deformation tongues oriented towards the sliding direction.
- In the roller samples, the sliding direction and consequently the deformation tongues are oriented perpendicular to the rolling directions due to the stress state caused by the torsional and bending stresses in the wire rope.
- Material removal proceeds through the spalling of the deformation tongues by crack growth between the graphite nodules and the surface.
- The distributions of the crack depths and the crack initiation angles are quite similar in the in-service roller and the two wear test rollers. In addition, the wear surfaces are similar particularly on the in-service roller and on the roller from the wear tested performed with 10 kN rope force. Therefore, the test set up employed for the present component wear testing simulates well the in-service conditions.
- The unidirectional sliding–rolling contact in the twin-disc test results in a distribution of the crack initiation angles that has combined aspects of the behaviour in the rolling and sliding directions of the roller samples.
- Increased contact pressure and radial stiffness increase the maximum crack initiation depth and promote pitting-type surface fatigue.
- By adjusting the contact pressure and the sliding ratio in the twin-disc test, the wear behaviour can be optimised to better simulate the contact between a roller and a wire rope.

Acknowledgements

This study was carried out in the Friction and Energy project, which was part of the extensive FIMECC DEMAPP programme funded by Tekes - the Finnish Funding Agency for Innovation (1111/31/10), and the participating companies. The authors are grateful to the other project partners for the roller wear testing and the samples for the present study, and for fruitful discussions during the project.

References

[1] K. Feyrer, Wire ropes – tension, endurance, reliability, Springer-Verlag, Germany, 2007.
[2] A. Cruzado, M. Hartelt, R. Wäsche, M.A. Urchegui, X. Gómez, Fretting wear of thin steel wires. Part 1: influence of contact pressure, Wear 268 (2010) 1409–1416.
[3] A. Cruzado, M. Hartelt, R. Wäsche, M.A. Urchegui, X. Gómez, Fretting wear of thin steel wires. Part 2: influence of crossing angle, Wear 273 (2011) 60–69.
[4] I.M.L. Ridge, C.R. Chaplin, J. Zheng, Effect of degradation and impaired quality on wire rope bending over sheave fatigue endurance, Eng. Fail. Anal. 8 (2001) 173–187.
[5] A. Cruzado, M.A. Urchegui, X. Gómez, Finite element modeling of fretting wear scars in the thin steel wires: application in crossed cylinder arrangements, Wear 318 (2014) 98–105.
[6] M.G. Hamblin, G.W. Stachowiak, Environmental and sheave material effects on the wear of roping wire and sheave, Tribol. Int. 28 (1995) 307–315.
[7] Jung-Buk Ryu, Seock-Sam Kim, Young-Hun Chae, A fundamental study of the tribological characteristics of sheave steel against a wire rope, Key Eng. Mater. 297–300 (2005) 1382–1387.
[8] J.B. Ryu, S.S. Kim, Y.H. Chae, Wear mechanisms map proposal of crane sheave steel materials, J. Mod. Phys. B 20 (2006) 4401–4406.
[9] M. Beltowksi, P.J. Blau, J. Qu, Wear of spheroidal graphite cast irons for tractor drive train components, Wear 267 (2009) 1752–1756.
[10] M. Ben Tkaya, S. Mezlini, M. El Mansori, H. Zahouani, On some tribological effects of graphite nodules in wear mechanism of SG cast iron: finite element and experimental analysis, Wear 267 (2009) 535–539.
[11] H.R. Abedi, A. Fareghi, H. Saghafian, S.H. Kheirandish, Sliding wear behaviour of a ferritic–pearlitic ductile cast iron with different nodule count, Wear 268 (2010) 622–628.
[12] Q. Luo, J. Xie, Y. Song, Effects of microstructures on the abrasive wear behaviour of spheroidal cast iron, Wear 184 (1995) 1–10.
[13] K. Yıldızlı, M.B. Karamış, F. Nair, Erosion mechanisms of nodular and gray cast irons at different impact angles, Wear 261 (2006) 622–633.
[14] V. Oksanen, P. Andersson, K. Valtonen, K. Holmberg, V.T. Kuokkala, Characterization of the wear of nodular cast iron rollers in contact with wire ropes, Wear 308 (2013) 199–205.

Tampereen teknillinen yliopisto
PL 527
33101 Tampere

Tampere University of Technology
P.O.B. 527
FI-33101 Tampere, Finland

ISBN 978-952-15-4228-2
ISSN 1459-2045